2018-11-01

Characterizing Interfacial Bonds in Hybrid Metal AM Structures

John Ross Linn
Brigham Young University

Characterizing Interfacial Bonds in Hybrid Metal AM Structures

John Ross Linn

A thesis submitted to the faculty of
Brigham Young University
in partial fulfillment of the requirements for the degree of

Master of Science

Jason M. Weaver, Chair
Michael P. Miles
Yuri Hovanski

School of Technology

Brigham Young University

ABSTRACT

Characterizing Interfacial Bonds in Hybrid Metal AM Structures

John Ross Linn
School of Technology, BYU
Master of Science

The capabilities of various metal Additive Manufacturing (AM) processes, such as Powder Bed Fusion – Laser (PBF-L) and Direct Energy Deposition (DED) are increasing such that it is becoming ever more common to use them in industrial applications. The ability to print atop a substrate broadens that scope of applications. There is ongoing research regarding the mechanical properties of additively processed materials, but little regarding the interaction between additive material and its substrate. An understanding of the mechanical and performance properties of the AM/substrate interface is imperative. This paper describes a study of the strength properties of AM/substrate interfaces, with respect to torsion and tension, and compares them to their fully wrought and fully additive counterparts. PBF-L and DED are used to produce tensile and torsion test specimens of two different materials, SS316L and M300 steels. This provides sufficient variety in testing for a confident analysis to be made.

Keywords: additive, AM, PBF-L, DED, substrate, interface, bond, tensile, tension, torsion, hybrid, wrought, SS316L, M300 mechanical properties, John Linn

ACKNOWLEDGEMENTS

First, I would like to extend my gratitude to Brigham Young University, and more especially the School of Technology. My undergraduate and graduate experiences have been influential for me in great ways. The mentorship, support, and funding I have received has been vital. I thank my graduate committee for their wisdom, guidance, and excitement regarding this research. The fascination which has grown within me for this topic came in large part from that excitement and knowledge which they have.

I extend appreciation to Robert Smith at Qualified Rapid Products for providing AM parts from his state-of-the-art PBF-L machines. To Jason Jones and Peter-Jon Solomon at Hybrid Manufacturing Technologies, who in the spirit of research provided most of the samples used in this work at a substantial discount, I am so grateful. All these men were a privilege to work with, and their shared expertise was valuable in my design process.

My parents, Larry and Jean Linn, are to be recognized and thanked in great measure. They have ceaselessly provided me with encouragement and support in furthering my education, as well as in all other opportunities that I have ever desired to pursue.

Finally, for my sweet wife, Jane, I offer my most heartfelt gratitude. My pursuit of a graduate degree, like any other lofty goal that I aspire to, was made in large part with her as much of my inspiration. She supported me completely, while not only carrying our first son, William, but also completing her own master's degree in Computer Science on the opposite side of campus. Thank you, my love, for shining brightly and providing inspiration for me and all others that surround you.

TABLE OF CONTENTS

LIST OF TABLES

LIST OF FIGURES

1 INTRODUCTION

1.1 The Problem

There is a great amount of waste in the metal product fabrication and tooling industry. Many products and tools are machined from large blocks of metal, leaving behind piles of chips and smaller blocks to be recycled. Many tools will experience wear rapidly when dealing with higher strength materials, such as titanium, used often in the aerospace industry (Carroll, Palmer, & Beese, 2015). It is generally considered not worth the time or money to repair a metal tool, as it is cheaper to simply replace it. This is especially true when the tool needing replaced is either very simple, thus being easy to mass produce, or very intricate, making it difficult to repair. If these difficulties could be overcome, remanufacturing has the potential to avoid this large waste of resources. Studies have shown that up to 90% of material can be saved through remanufacturing, and that producing new products can require six times the energy of remanufacturing them (Matsumoto, Yang, Martinsen, & Kainuma, 2016). There are various methods used to repair metal products. Metal filled epoxies, mechanical fasteners, and welding techniques are common solutions to repairing parts for continued use. Reworked tools and products tend to have decreased mechanical properties that may influence their performance. They may also lack the precision of the initial product. In many industries the safety standards require mechanical properties that are unattainable through these common reworking processes. A remanufacturing process that provides similar or better mechanical properties than the original

part, while also being time and cost effective, is a current need in the engineering and manufacturing fields.

1.2 AM as a Solution

Additive manufacturing (AM) may be a viable solution to this need. Due to the recent advancements in metal Additive Manufacturing, there is need for qualifying experiments and research to prove its viability. Metal AM parts have been proved to have high strength characteristics, but their behaviors do not match those of traditionally processed metals (Miller, Morris, & Colvin, 2016). This research will provide pertinent knowledge regarding metal AM part behaviors.

Metal additive manufacturing is rapidly moving from simple welding methods into more precise and capable 3D printing methods, such as Powder Bed Fusion-Laser (PBF-L) and Direct Energy Deposition (DED) processes. Rather than being solely used to join metals and other materials together, entire designs can be created from CAD files via 3D printing. There are numerous benefits to producing metal parts additively, rather than by other conventional casting and machining methods. Time, money, and resources can be preserved, while also dramatically increasing design flexibility. This increase in design flexibility can translate directly into improved product performance in many cases (Miller et al., 2016). Custom parts can be fabricated rapidly, from design phase to solid part, in a matter of hours. This research focuses on the remanufacturing capabilities of AM. Utilizing AM as a remanufacturing process, many tools and products could be repaired rather than replaced, saving immense amounts of resources. The mechanical properties of the additively manufactured parts need investigating in order to prove sufficient to withstand the forces experienced in their respective environments. The focus of this

research will not be on the additive portion of such products, but on the interface between a metal additive piece and the substrate onto which it is printed. There has been very little research focusing on the interfacial bond between a metal AM part and a substrate. Validating Metal Additive Manufacturing as a reliable process for repair of metal tools will have massive implications on many industries worldwide.

1.3 Research Purpose

The purpose of this research is to investigate the capabilities of Metal Additive Manufacturing processes, particularly the interface between an AM specimen and a substrate, through various experimentation, tests, measurements and analysis in order to validate the process as a viable option for manufacturing, remanufacture and repair of metal rotary tools and other products.

1.4 Research Questions

There are three main questions being addressed in this work:

1) Regarding mechanical properties, how does the interfacial bond between AM materials and metal substrates compare with stresses experienced in rotary tool applications?
2) How do the mechanical properties of parts printed onto a substrate PBF-L and DED compare to their wrought counterparts?
3) How do the mechanical properties of the hybrid PBF-L interfaces compare with those processed via DED?

1.5 Hypotheses

1) AM/Substrate bonds created via PBF-L processing will be sufficiently strong to withstand stresses common in rotary tool applications. AM/Substrate bonds created via DED processing will also be sufficiently strong to withstand stresses common in rotary tool applications, but the bond strength will be inferior when compared with PBF-L processing.
2) The grain size and structure of AM processed metals will undoubtedly differ from that of wrought metals. This will most likely result in different mechanical properties in the base materials. It is assumed that the additive material will exhibit higher mechanical properties, due to the martensitic microstructure achieved through AM processing (Fatemi, Molaei, Sharifimehr, Shamsaei, & Phan, 2017). The interface between these two differing materials will be a welding point that has mechanical properties similar to the machined or casted metals. The overall part will perform similarly in mechanical testing to the wrought counterpart.
3) The mechanical properties of the AM/Substrate interfaces of PBF-L processed parts will differ slightly from those of DED processed parts. Both will perform as well as their wrought counterparts, but the DED interfaces will have slightly inferior properties than PBF-L due to its lower resolution.

2 LITERATURE REVIEW

2.1 Introduction

Additive manufacturing is a fairly new process, emerging in the last three decades (Frazier, 2014). The recent advancements of metal AM processes are still in their infancy when compared with other traditional processes, such as casting and machining. For this reason, there are many gaps in the research that have yet to be filled in order to validate metal AM processes. One of these gaps in published research is the investigation of AM/Substrate interfaces. No research could be found that studied the mechanical properties of such interfaces. While this increases the significance of the work at hand, it decreases the amount of references with which to compare, contrast, and concur with this work. The majority of the literature cited is regarding metal AM processing capabilities, with a few works that actually step into the scope of hybrid metal AM processing.

2.2 Current State of Metal AM

Additive manufacturing technologies are emerging as a valid industrial process. This is due to the numerous benefits they carry: increased design flexibility, lower footprint, material option flexibility, structurally efficient, rapid design to production time, and much more (Mellor, Hao, & Zhang, 2014). The arguably most significant benefit is that of increased design flexibility. This flexibility comes as a result of removing design restraints formerly imposed by

tooling, such as draft angles in a casting or cutting tool accessibility in machining (Atzeni & Salmi, 2012). The benefits will continue to increase as the technology improves. Another benefit that is a major factor pushing metal AM towards industrial implementation is the capability to manufacture parts at or near the point of use. This compresses or removes many of the common supply chain wait times and complications (Huang, Leu, Mazumder, & Donmez, 2015). The parts ordered can be intricately customized to fit the buyers needs while maintaining a reasonable price. Designs can be changed from part to part without the heavy costs of tooling modifications.

According to ASTM Standard F2792, AM processes can be categorized into two categories, Powder Bed Fusion and Direct Energy Deposition (DebRoy et al., 2018). There are other styles that exist, but they are rarer, and are not the focus of this research. The two processes used to produce the test specimens in this work are PBF-L and DED. Some slight variances in nomenclature exist when speaking of PBF-L and DED machines and processes. The specific machines used for this work were the 400W EOS M280 (for PBF-L) and the Ambit™-dextrous ROMI D800 (for DED), as mentioned in the Methodology section.

2.2.1 PBF-L

PBF-L is an AM process in which the part is produced, layer by layer, onto a platform or substrate which sits in a bed of powdered material. A laser melts a 2-dimensional slice of the 3-dimensional design, and then a blade or roller deposits a new layer of powder over it, so that the next 2D slice can be melted. This is replicated until the entire 3D design has been created. This is all done in an inert atmospheric environment in order to avoid oxidation between layers (Marco & Bianca Maria, 2017). Post processing consists of removing the part from the substrate plate, and removing extra powder and any support structures that were used. Heat treatments and

machining are often used as well, depending on the part requirements. One of the benefits of this process is the high resolution capable. The resolution attained has many factors, such as powder type, grain size, energy density of the beam, laser spot size, velocity, and hatch width. Generally speaking, powder-bed processing can achieve resolutions around 50-100µm (DebRoy et al., 2018). Parts typically fabricated by PBF-L suppliers tend to have high resolution requirements, and are small in size.

There has been research done regarding the effects of energy input levels and cooling rates on the microhardness of various metal alloys, including SS316L (Zuback & DebRoy, 2018). It was determined that the cyclic nature of both PBF-L and DED processes can produce vastly different hardness results, depending on the process parameters. Experimentation showed a cooling rate of 22-764 degrees Centigrade per second when changing processing parameters. This in turn produced hardness variations of 150-368 HV.

Grain sizes can vary greatly when dealing with additive technologies. Once again, the process parameters used have a direct effect on the resulting microstructure (Scipioni Bertoli, MacDonald, & Schoenung, 2019). Directionality of heat flow in AM processing, particularly in PBF-L, results in highly anisotropic microstructures. This will influence material properties and mechanical performance in different directions. Laser power and scan speed are the two primary parameters measured. Introducing higher energy levels decreases the cooling rate, while decreasing the energy level will result in a higher cooling rate. The grains typically increase in length as laser power and scan speed increase. A typical layer thickness used for powder bed processed SS316L is approximately 40 µm (Mower, Long, & A, 2016). Tensile testing of specimens in the work referenced show yield strengths fairly similar to those exhibited in this

work, with wrought SS316L and additive specimens yielding at approximately 350 MPa and 550 MPa respectively.

In other experimentation (Kamath, El-dasher, Gallegos, King, & Sisto, 2014) the optimum processing parameters for producing high density SS316L utilizing powder bed fusion were investigated. The grain size of stainless steel 316L is approximately 42 μm. Utilizing a laser power of 100 W, a spot size of 180 μm, a scan speed of 300 mm/s, and a layer thickness factor of 0.62 yields high density parts (>99 %) with good surface quality. Density tends to increase as layer thickness parameter is decreased. The optimum layer thickness factor obtained was 30 μm. Once again, laser power and scan speed were declared to be the most influential process parameters in achieving material density.

Industrial applications for PBF-L are increasing rapidly. Improving the production rate of powder bed additive technologies is a subject of much research. One investigation (Sun, Tan, Tor, Yeong, & Design, 2016) found that by increasing the laser power to 380 W the scan speed can also be increased, while maintaining material density of greater than 99% and microhardness between 213-220 HV. This can be compared with another study (Yusuf, Chen, Boardman, Yang, & Gao, 2017) which studied specimens of the same material, produced at 200 W and a slower 160 mm/s. These specimens exhibited densities greater than 99%, with microhardness levels between 237-262 HV. While the slower scanning speed and lower power produced higher hardness levels in this case, the rapid production rate produced hardness rates much higher than the wrought counterpart to these SS316L specimens, which are typically ~155 HV.

2.2.2 DED

DED processing has many similarities to PBF-L processing. It utilizes an energy beam, whether laser, electron beam, or other, to melt a powdered material. Layer-by-layer production of 2D slices is utilized to eventually create the 3D product. The main difference is that rather than working with a reservoir, the powder is deposited by in injection system in coordination with the energy beam to form a molten pool along the design path (Everton, Hirsch, Stravroulakis, Leach, & Clare, 2016). This difference allows for increased processing capabilities. Where powder-bed processes are limited to building on strictly horizontal planes, powder-fed systems can work on extremely complex surfaces, such as turbine blades (Jones, McNutt, Tosi, Perry, & Wimpenny, 2012). This makes DED an ideal process for remanufacture and repair of products. The resolution of DED is lower than that of powder-bed processes, usually with millimeter sized melt pools. This in turn increases the achievable deposition rate (DebRoy et al., 2018). With the differences already mentioned it can be noted that one process isn't necessarily better than another. Product design and material requirements will dictate which process is best suited for each situation.

The DED process is ideal for many remanufacturing applications. Research has been done regarding the carbon footprint associated with remanufacturing of turbine blades vs that of producing new blades via conventional methods (Wilson, Piya, Shin, Zhao, & Ramani, 2014). A 45% improvement in carbon footprint was documented, along with a 36% savings in total energy when utilizing DED as a remanufacturing method. In this work, the damaged area of a turbine blade is scanned and a 3D mesh is created, from which a deposition pattern can be formed. SS316L powder was used, which contained grain sizes of 44 µm. The laser spot size was approximately 600 µm. It is worth noting that this spot size is more than three times the size of

the optimum spot size notes for powder bed fusion – laser parameters. The DED processed materials exhibit similar ductility, strength, and life-cycle assessment characteristics to the standard production materials.

There has been work done to investigate how the "Contact Tip to Work Piece" distance affects the bead properties (Nam, Cho, Kim, & Kim, 2018). Distances from 5 mm to 15 mm were tested in 2 mm increments. The closer distances of 5, 7, and 9 mm showed inclusion of pores in the bead. At 11 mm there were few pores visible, but the fusion with the base material began to decrease. At 13 and 15 mm there was visible separation between bead and base material, as negligible fusion occurred between AM material and substrate.

The wattage required in DED processing is much greater than in PBF-L processing. In the same experimentation referenced above regarding nozzle distance there was also an investigation regarding the effect of laser power on AM/substrate fusion. At 500-1000 W there was a lack of fusion experienced. At 1.5-2 kW good fusion was achieved. At 2.5 kW good fusion was achieved, but the bead began to exhibit higher amounts of porosity.

Research has been performed utilizing DED processing of M300 steel alloys (Yao et al., 2018). This research found a positive correlation connecting higher power density to material density. When applying 50-100 J/mm^2 material density typically remained between approximately 98-99%. An increased power density of 180 J/mm^2 resulted in an increased material density of approximately 99.9%. The increased power density is assumed to more fully melt the M300 powdered material, thus improving the resulting solid-state density.

2.3 Rotary Tool Applications

There are numerous applications across many industries in which additive manufacturing can be applied. Rotary tools, such as in friction stir welding (FSW), are an example used in this work. These tools experience traverse forces and torque loads inherent to their function (Arora, Mehta, De, & DebRoy, 2012). The tool pins undertake the majority of these loads, and tend to wear out fairly quickly. Using FSW as an application provides a useful comparison of stresses and forces that may be required of the specimens being interrogated. Utilizing AM technologies to produce FSW tooling has been addressed in other works (Luo, Wang, Chen, & Li, 2015), and is shown to aid with certain aspects of the process, such as tool wear. The torsion and tensile tests included in this work will provided the mechanical data necessary to compare the AM/Substrate interfaces with other common metals used in rotary tool applications.

2.4 Testing Methods

In order to obtain useful data, destructive testing of the samples will be performed. Tensile testing is commonly used to provide mechanical strength data of a material (Davis, 2004). It is especially useful when testing new materials, as it provides a comparison with any other material in the engineering field. There is work being done to characterize AM technologies via simulation (King et al., 2015). When more information is obtained regarding AM/substrate interfaces, perhaps simulation will become a powerful tool in filling in the knowledge gap that currently exists.

3 EXPERIMENTAL DESIGN

3.1 Summary

The experiments performed in this work include torsion tests, tensile tests, and microscopy. Tensile and torsion tests were selected as two of the most fundamental destructive tests which would provide some of the most basic mechanical properties of the specimens. Because these tests are quite common, they provide a vast selection of material performance data from past research with which to make analyses. Microscopy allows a deeper level of analysis and understanding to be reached. By viewing the hybrid interfaces under magnification it allows a comparison to be made between the two additive processes being used. A comparison between additive and wrought material is also useful. Analyzing the grain sizes, structures and geometries, and comparing them with the standard, aids in determining the causes of failures, or lack thereof. This, in turn, provides more evidence needed to validate AM technologies and processes.

3.2 Methodology

3.2.1 Metals

The metal selection process began with two considerations: 1) what metals are most commonly used for additive manufacturing, and 2) what metals are available. In order to keep

the research scope manageable, the number of metals was limited to two. Originally the two selected were stainless steel and aluminum. One of the two suppliers did not work with aluminum powders, due to their explosive properties. After discussing with the suppliers, it was decided that a Maraging steel would be the second metal. SS316L and M300 were selected. The amount of each metal purchased is detailed below. Due to the expensive nature of M300 powder, M300 specimens were only ordered from the DED supplier, while SS316L specimens were ordered from both DED and PBF-L suppliers.

There are three different specimen types per metal type: fully additive, hybrid (AM/Substrate), and fully wrought.

The following was ordered from the DED supplier, which utilized the Ambit™-dextrous ROMI D800:

1) SS316L:
    - One fully additive block -- 0.5" x 2.25" x 3.0"
    - One hybrid material block -- 1.0" x 2.25" x 1.5" (atop a 1.0" x 2.25" x 1.5" substrate block of SS316L)
2) M300:
    - One fully additive block -- 0.5" x 2.25" x 3.0"
    - One hybrid material block -- 1.0" x 2.25" x 1.5" (atop a 1.0" x 2.25" x 1.5" substrate block of M300)

The following image displays all of the DED processed samples (Left to right: Additive M300, Additive SS316L, Hybrid M300, Hybrid SS316L, with the wrought M300 block in the bottom left).

Figure 3-1: Fully Additive and Hybrid SS316L and M300 Samples via DED

The following was ordered from the PBF-L supplier, which utilized the 400W EOS M280:

1) SS316L:
    - One fully additive block -- 0.5" x 2.25" x 3.0"
    - One hybrid material block -- 0.5" x 2.25" x 1.5" (atop a 0.5" x 2.25" x 1.5" substrate block of SS316L)

The supplier keeps most of the details of their parameters proprietary because they invest much in developing them. They provided the energy density used, which was 49 J/mm3.

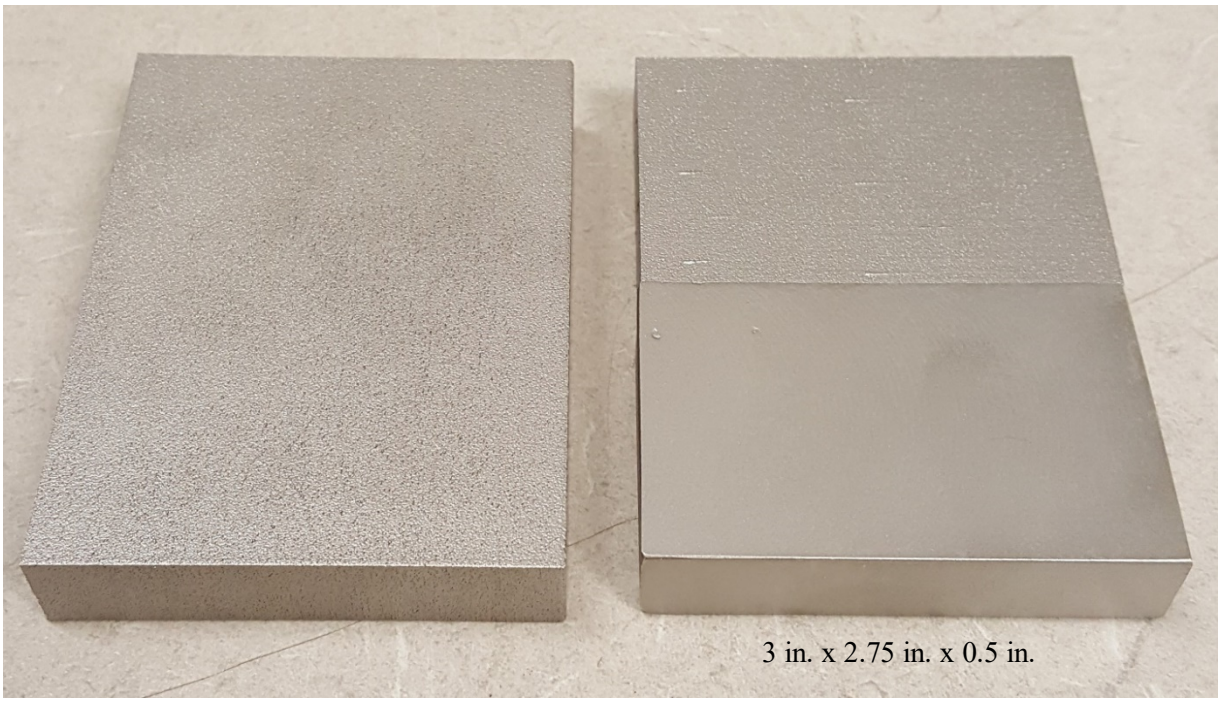

Figure 3-2: SS316L AM and Hybrid Samples via PBF-L

Figure 3-3: View of Specimens in Powder Bed of 400W EOS M280

Fully wrought blocks were purchased from the Precision Machining Lab (SS316L) on campus, and from an online metal supplier (M300).

3.2.2 Experiments

In order to answer the research questions posed, the following experimentation was performed. It involves the creation of test specimens, destructive testing (torsion and tensile), and microscopy.

3.2.2.1 Torsion Testing

Interfacial Bond Strength:

From the hybrid materials purchased, several torsion specimens were cut and machined according to ASTM E8 specifications.

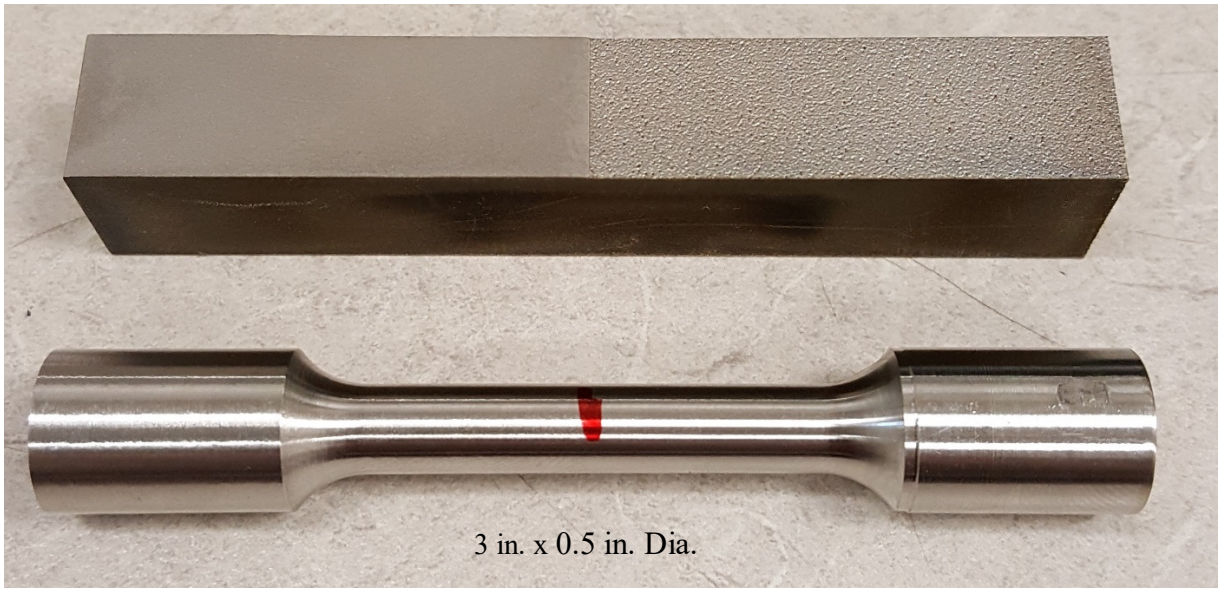

Figure 3-4: Hybrid Torsion Test Specimens Before and After Turning

The machine used to perform both torsion and tensile tests is an Instron, Model 1381 Frame, 8800 Controller. The Instron has both flat and 90-degree diamond shape gripped jaws that were easily switched out for gripping the rectangular tensile specimens and the round torsion

specimens. The maximum torque load of the machine is 10,000 lb-in, with 90-degrees of twist capability. The maximum tensile load of the machine is 20,000 lb (resolution of 2 lb).

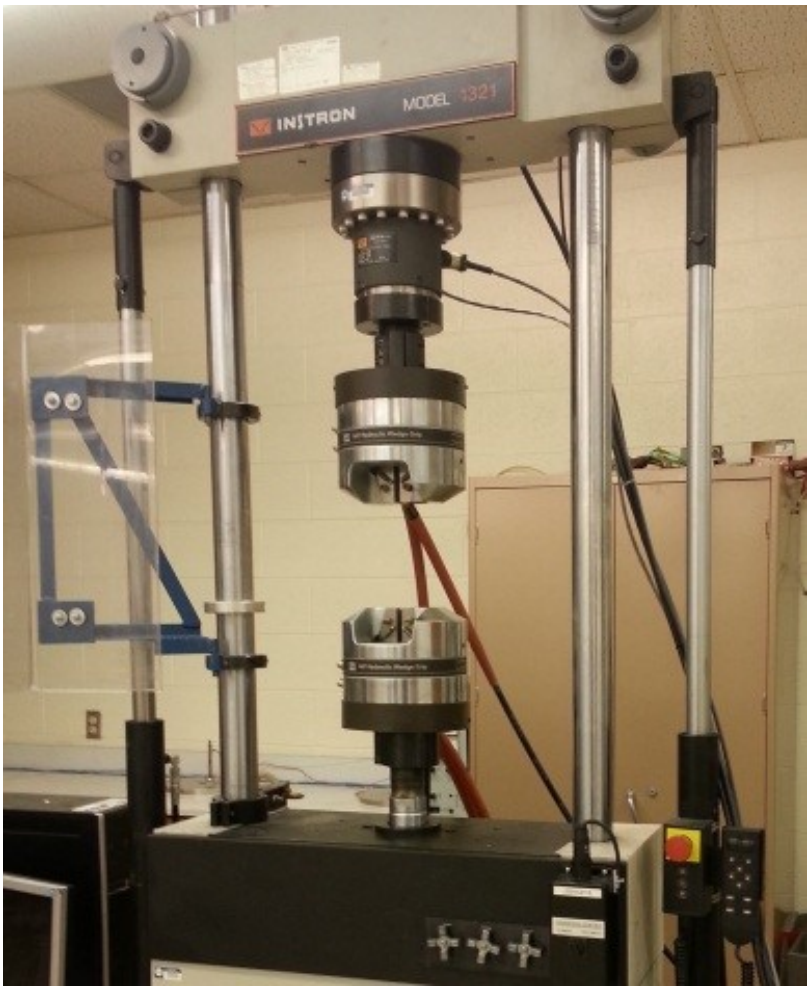

Figure 3-5: Instron Tensile Tester

For each test the specimen is clamped into the lower jaws, using a machinist square to check that it is normal to the jaws. The upper jaws are lowered slowly until surrounding the wide gripping section of the specimen, and then clamped.

Figure 3-6: Torsion Specimen in Instron

For each type of test a specific method was created using WaveMatrixTM, a material testing software. The method parameters used are described below.

Torsion Test:

3) Twist rate of 0.1 degree per second
4) Twist from -45 to +45 degrees (full 90-degree capacity)
5) Data acquisition rate at 10Hz (10 data points per second)
6) Data recorded: Twist (degrees) vs. Torque Load (lb-in)

The experiment method was created in Wave Matrix in order to perform the experiments consistently, and to gather pertinent data. The Wave Matrix software provides useful data (torque load vs. degrees twisted, torque load vs. time) to aid in making observations and drawing conclusions. Pictures were taken of the interfacial breaking point in order to more accurately conclude what was occurring.

Additive Specimen Torsion Strength:

From the fully additive materials purchased, several torsion specimens were cut and machined according to ASTM E8 specifications. These specimens were placed in the same testing parameters as the interfacial test specimens, but for the purpose of investigating the strength of the additive material. The Wave Matrix program provided all of the same feedback as with the interfacial failure tests.

Wrought Metal Torsion Strength:

Torsion specimens of wrought M300 and SS316L were machined according to ASTM E8 specifications. They were placed in the same testing parameters as the previous two types of torsion tests. This provides a good comparison between the performance of the interface, the AM material, and the standard wrought material.

3.2.2.2 Tensile Testing

Interfacial Bond Strength:

From the hybrid materials purchased, several tensile specimens were cut and machined according to ASTM E8 specifications.

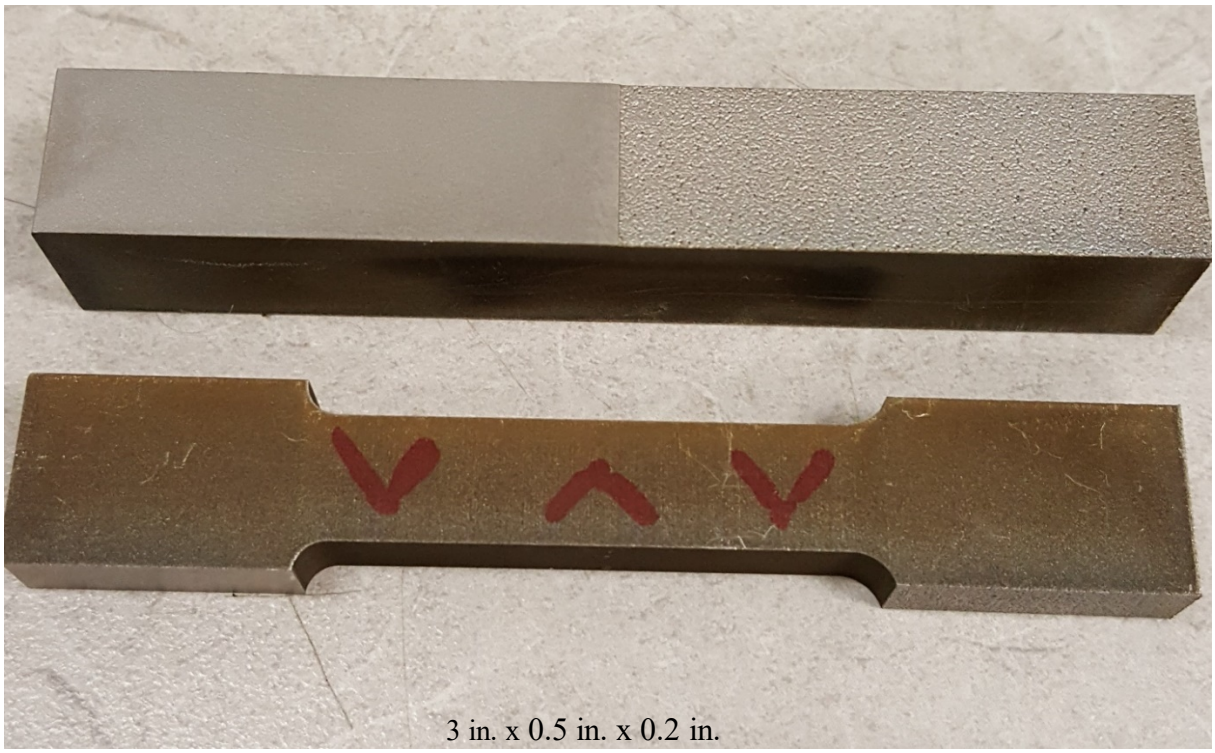

Figure 3-7: Hybrid SS316L Tensile Test Specimen

Using the same Instron on campus, these specimens were pulled to failure using the following method.

Tensile Test:

- Pull rate of 2 inches per minute
- Data acquisition rate at 10Hz
- Data recorded: Load (lb) vs. Distance (in)

Wave Matrix provided useful data for analyzing the performance of the specimens.

Additive Specimen Tensile Strength:

From the fully additive materials purchased, several tensile specimens were cut and machined according to ASTM E8 specifications. These were pulled to failure using the same

testing procedure as the hybrid tensile specimens. This provides a good baseline for the strength of the additive material alone. This can be compared to the wrought and hybrid specimens.

Tensile specimens were machined from the fully wrought materials purchased. These were pulled to failure using the same testing procedure as the other tensile tests performed. This provides a comparison between the tensile performance of the AM/substrate interface, the AM material, and the standard wrought material.

3.2.2.3 Interfacial Bond Characterization

Using the wire EDM machine on campus, cross sectional cuts were taken from hybrid specimens of SS316L from the PBF-L processed sample, and SS316L and M300 steel from the DED processed samples. These cross-sectional slices were mounted in pucks, polished, etched to expose grain boundaries, and viewed microscopically. This allowed for further analysis and insights regarding the performance of these specimens.

The following matrices display the number of each type of test specimens that were created, and how many of each test were performed.

Table 3-1: Testing Matrix for DED Specimens

	DED Specimens						
	Wrought		Additive		Hybrid		
Test Type	SS316L	M300	SS316L	M300	SS316L	M300	Total:
Tensile	3	3	3	3	6	6	24
Torsion	3	3	3	3	6	6	24
Microscopy					1	1	2

Table 3-2: Testing Matrix for PBF-L Specimens

	PBF-L Specimens						
	Wrought		Additive		Hybrid		
Test Type	SS316L	M300	SS316L	M300	SS316L	M300	Total:
Tensile	3		3		3		9
Torsion	3		3		3		9
Microscopy					1		1

3.2.3 Equipment

3.2.3.1 Machining

The specimens tested in this research were all machined on BYU campus in the Crabtree Technology Building machine shop. The large blocks of wrought material were cut to smaller dimensions using a bandsaw. Coolant was applied in order to avoid changing the microstructure during cutting.

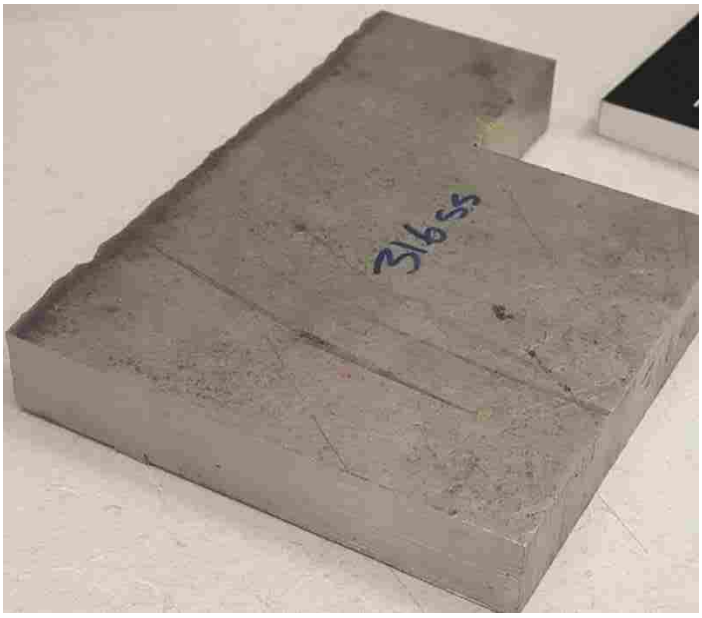

Figure 3-8: SS316L Wrought Stock

A manual mill was then used to machine the wrought blocks to the precise dimensions referenced above. These wrought blocks would be used as the substrate material onto which additive portions would be applied, as well as fully wrought specimens.

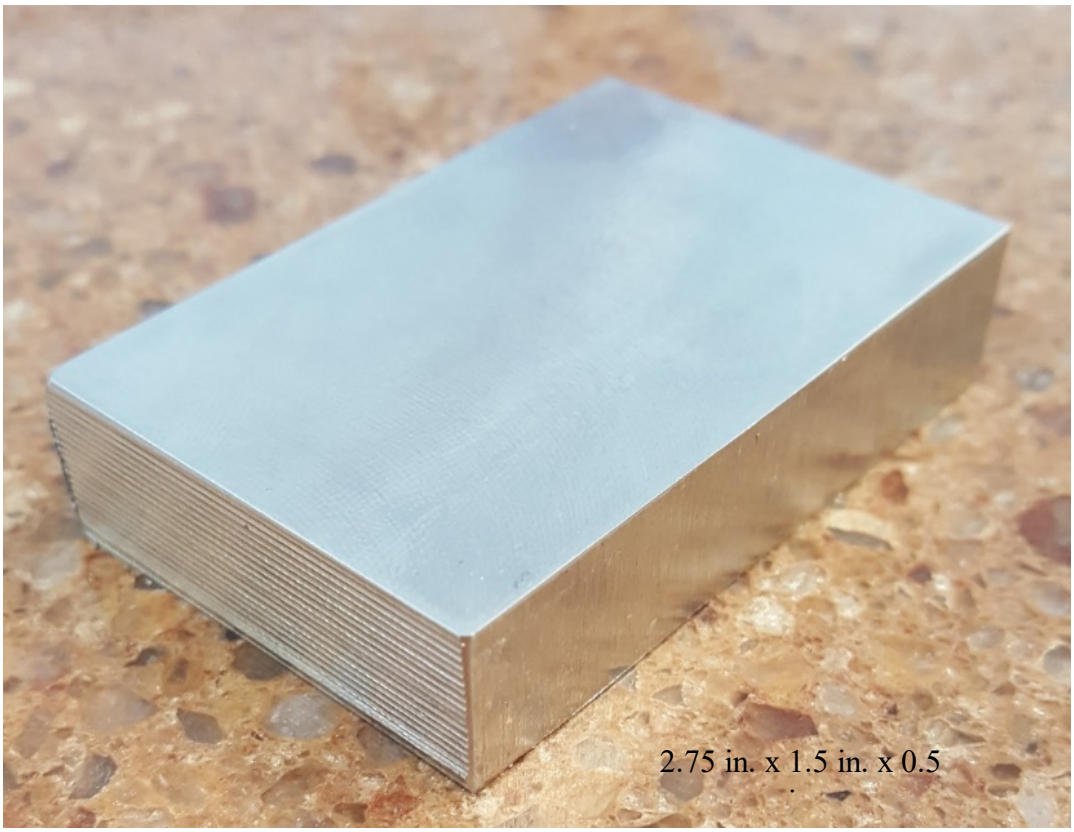

Figure 3-9: SS316L Wrought Stock Ready for AM Processing

A Wire EDM machine was used to cut the fully wrought, hybrid, and fully AM samples into rectangular and square pillars, in preparation for final cuts and machining to be made. Not further machining was required for the tensile specimens. The torsion specimens continued on to manual and CNC lathes in order to turn them to the desired geometry.

Figure 3-10: SS316L Wrought Sample After Wire EDM Cut

The tensile test specimens were all cut to geometry using the Wire EDM machine. Although a time-consuming process, the Wire EDM only requires a 2D design in order to perform the precision cutting operation. Figure 3-4 shows a 2D design of the tensile specimen.

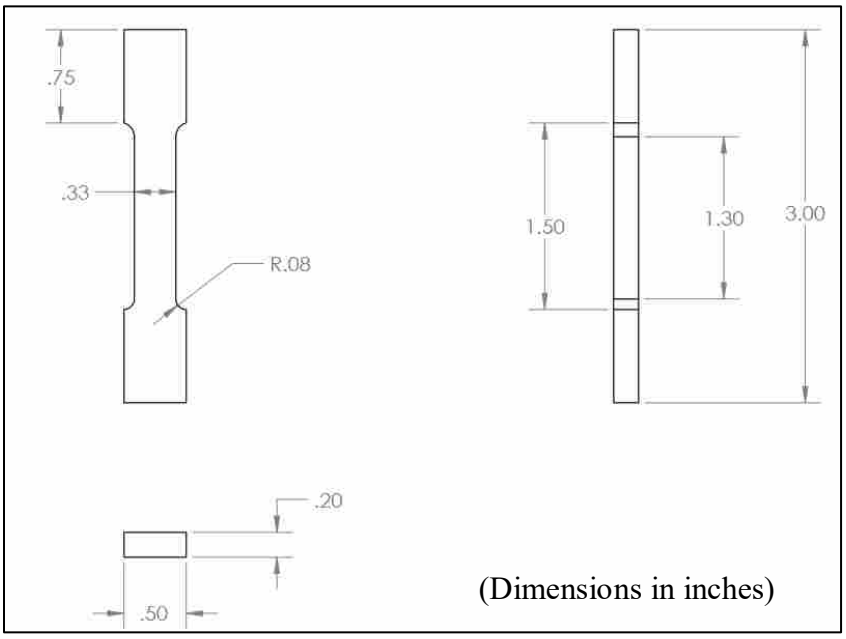

Figure 3-11: Tensile Specimen Design

The torsion specimens required work on both the manual and CNC lathes. Beginning with a 0.5 inch x 0.5 inch x 3.0 inch pillar, a ½ inch square collet is used to load the sample into the manual lathe. One end of the sample is turned down until a radius of no less than 0.45 inches, preferably closer to 0.5 inches is attained, which is enough for gripping in the jaws of the Instron. This may not produce a perfectly round profile, depending on how far down the radius is reduced. The 4-Jaw chuck of the CNC lathe requires only that there are radii to grip. Flats between the radii don't present any complications. The final manual lathe operation is to center drill a hole in the remaining square end, large enough for a lathe center to be applied in the CNC lathe.

The CNC lathe has conversational programming capability. Using the design in Figure 3-5, the profile desired was entered, along with feeds and speeds typical for stainless steel turning.

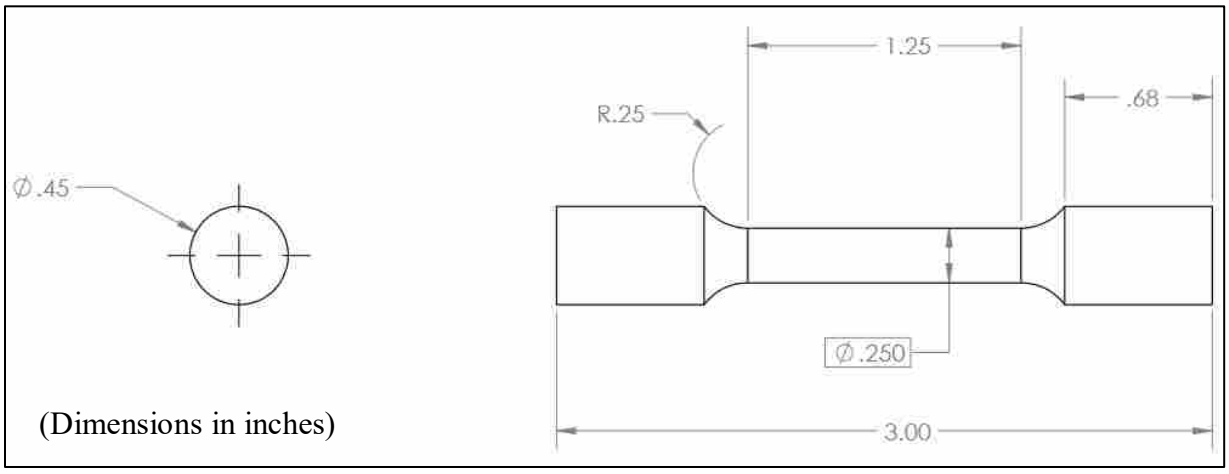

Figure 3-12: Torsion Specimen Design

Each sample was loaded into the 4-jaw chuck, with the lathe center maintaining a true Z-axis.

3.2.3.2 Polishing

The polishing process is quite specific, and following precise methods is important for quality results. The metal samples are first cut on the wire EDM machine to be 1.0625in. x 0.8025in. x 0.625in. The interface in the hybrid samples is directly in the middle of the specimens. They are then placed in a plastic sleeve with mold release, followed by epoxy filling the remainder of the sleeve.

Figure 3-13: Plastic Sleeve for Forming Polishing Specimen Pucks

After a twenty-four-hour cure time the epoxy pucks are removed from the mold, washed, and then grinding begins. Grinding and polishing all take place on a polishing machine. The sandpaper/polishing pads are placed on a round steel plate that is mounted on the machine. In the first stage, 400-grit sandpaper is used. The puck is ground on both sides in order to attain flat, clean surfaces.

Figure 3-14: SS316L Specimen Ready for Polishing

The following procedure is then used for each stage of grinding/polishing:

1) Turn the water on with a stream flowing to the center of the disk.
2) Turn the polishing wheel on, set at 150rpm.
3) By hand, apply the puck with even pressure, specimen side down, slowly moving from the outside of the wheel to the center, and back, repeating for 30 seconds.
4) Rinse specimen with water, dry with compressed air. Check to see that scratch marks are unidirectional.
5) Rotate the puck 90-degrees, and repeat for another 30 seconds.
6) Remove sandpaper/polishing pad, clean the metal base. Apply the next stage sandpaper/polishing pad.

This is done with 600-grit, 800-grit, 1200-grit, and 1200-grit (fine) sand papers. If at any point during inspection there were excessive scratch marks, the process was redone from the beginning stage. After the sandpaper disks are successfully worked through, the following procedure is used:

7) A wool polishing pad is placed on the wheel with a 3-micron diamond paste applied, and wet down with water.
8) At 150rpm, the specimen is polished for 10 minutes, rotating 90-degrees every 2 minutes, slowly moving in and out as previously done.
9) The specimen is rinsed with water, dried with compressed air, and the wool disk is removed, cleaned, and stored.
10) A microfiber disk is then mounted on the clean metal base. 1-micron alumina suspension is generously applied to the polishing disk, and the water is turned on at a slow drip.
11) At 150rpm, the specimen is polished for 10 minutes in the same fashion as with the diamond paste.
12) After cleaning the specimen with water and drying with compressed air, the specimen is inspected. If there are any scratches seen at this point the process is repeated from 800-grit sand paper, depending on the size of the scratches. A mirror finish should be attained at this point.

3.2.3.3 Etching

When the polishing process is successfully completed, the specimens are then etched in order to expose the grain boundaries for microscopic observation. There are various etchant formulas used for different metals and purposes. The one used here is the Carpenter 300 Series Stainless Steel Etchant. This suits the SS316L and M300 specimens. This etchant is composed of:

1) Ferric (Iron III) Chloride – 1.045 grams
2) Cupric Chloride – 0.295 grams
3) Alcohol (Ethanol) – 15 ml

4) Hydrochloric Acid – 15 ml

5) Nitric Acid – 0.738 ml

The listed chemicals are mixed until all solids are dissolved. The specimen is immersed in the etchant for 4 seconds and then immediately sprayed with ethanol for 30 seconds, rinsed with water for 30 seconds, and air dried.

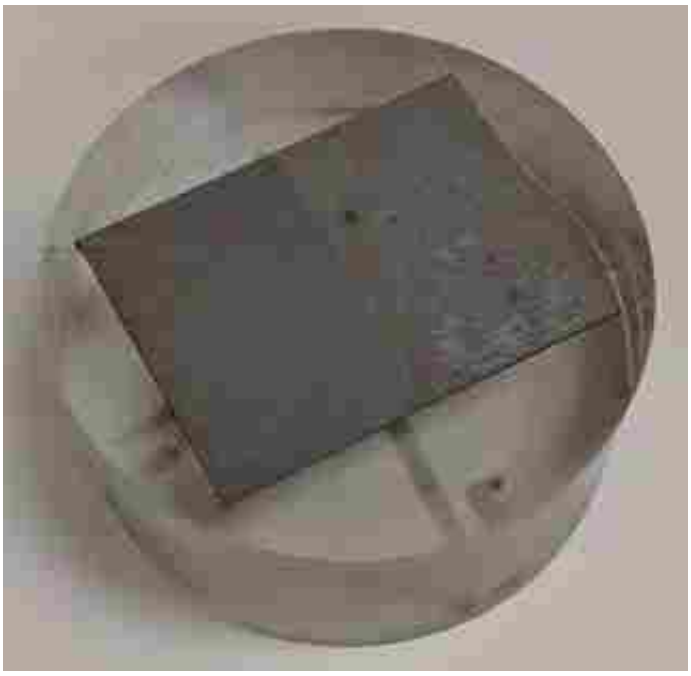

Figure 3-15: An Etched Hybrid SS316L Specimen

3.2.3.4 Microscopy

After etching is completed, the samples are ready for visual analysis via microscopy. Using the correct light contrast, a clear view of the metal grain boundaries can be seen. This allows for a comparison between wrought material, additive material, and the hybrid interface. Screen captures are taken of all three material sections at 32X and 64X magnification.

4 RESEARCH RESULTS AND ANALYSIS

4.1 PBF-L Samples

The first round of tests performed were the PBF-L specimens. The results of these tests are analyzed below. Analysis of the DED specimens is described in Section 4.2. The DED specimens were significantly less expensive, and so the majority of tests performed in this work are from the DED supplier.

4.1.1 Torsion Tests

The stress curves for all torsion tests in this work display the maximum shear stress. This was calculated using the following formula:

$$\tau = T\, r / J \tag{4-1}$$

where τ = shear stress (psi), T = twisting moment (in lb), r = distance from center to stressed surface in the given position (in), and J = Polar Moment of Inertia of Area (in^4).

With regards to the torsion specimens in this work, the polar moment of inertia of the area was calculated using the formula below:

$$J = \pi R^4 / 2 \quad (4\text{-}2)$$
$$= \pi (D / 2)^4 / 2$$
$$= \pi D^4 / 32$$

where D = shaft outside diameter (in).

Below are the results of the wrought and PBF-L processed torsion tests. Only the first test is shown from each category, along with a composite plot displaying all tests of each type. This allows for any variation between like specimens to be shown. All test results can be found in the appendix. It is worth noting that none of the torsion specimens experienced failure, as can be seen in the torque load data, nor did any reach their ultimate tensile strength (UTS).

4.1.1.1 Wrought SS316L Specimens

Of the three initial wrought SS316L specimens, only the data from the first and second are used in this analysis. Specimen 1 was the first test performed, with a twist of 40 degrees. As a 40-degree twist did not reach the UTS of the specimen, the test method was altered for all future tests to twist 90 degrees, which is the limit of the Instron.

It would have been useful to observe a specimen twisted to failure. This was attempted with the third wrought SS316L specimen, by repeatedly resetting the Instron and twisting the specimen in 90-degree increments. It did not reach UTS after 900 degrees of total twist. As the specimen was released and reloaded multiple times, the resulting data is corrupted, and is not part of the analysis.

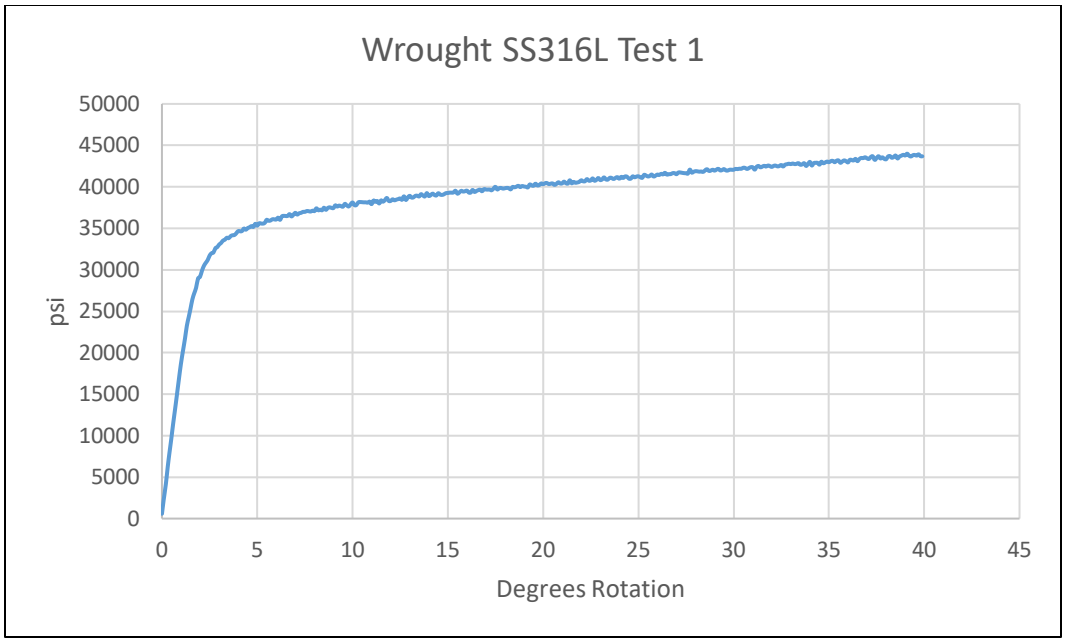

Figure 4-1: Wrought SS316L Torsion Test Curve

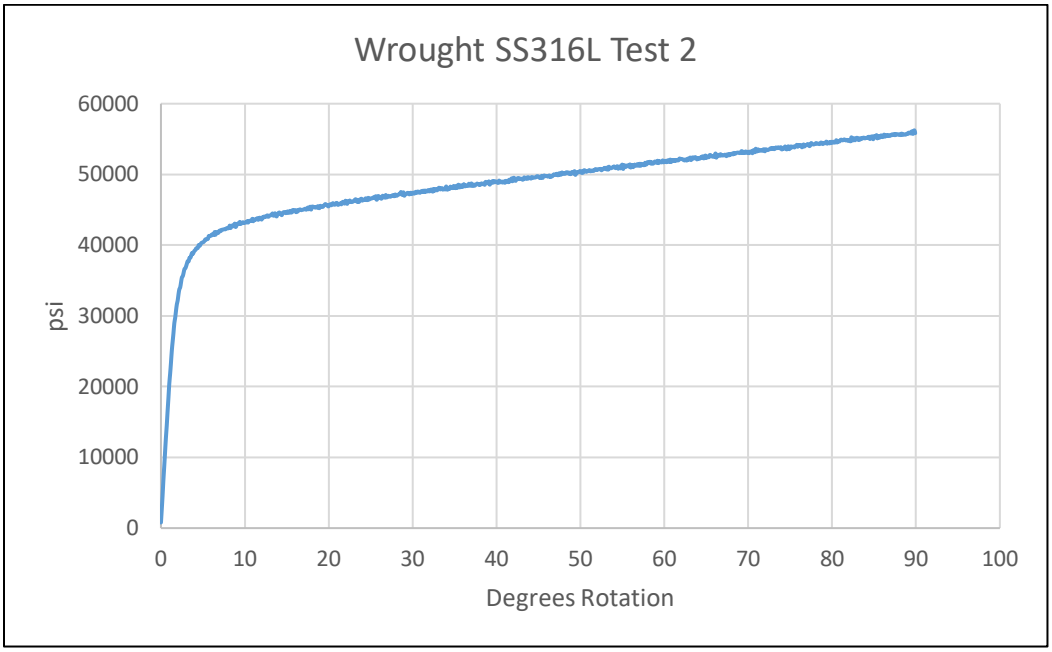

Figure 4-2: Wrought SS316L Torsion Test 2 Curve

An analysis of these test curves suggests that the linear elastic portion of these torsion tests is quite brief. The specimens reach their respective yield points within the first three degrees of

twist. The remaining eighty-seven degrees of twist, all plastic deformation, consists of a linear increase in stress. The results from Specimen 2 show that 90 degrees is still insufficient to reach UTS, which speaks to the highly ductile quality of wrought SS316L. The load at the end of a 90-degree twist reached 56,240 psi.

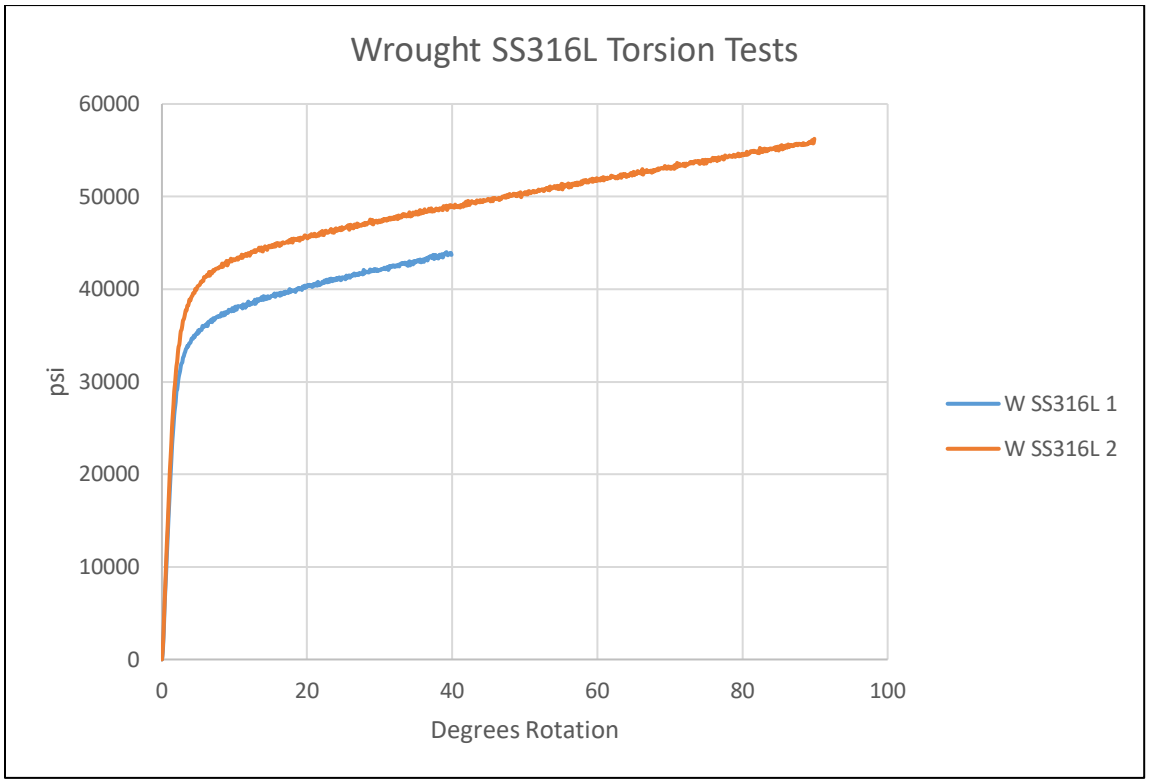

Figure 4-3: Wrought SS316L Torsion Test Curves

4.1.1.2 Fully Additive SS316L Specimens

These three specimens were all twisted 90 degrees. They all performed nearly identically, which speaks well to the integrity and consistency of the PBF-L process. The main difference between the wrought specimens and fully additive specimens is that the yield point of the AM specimens is much higher than the wrought specimens.

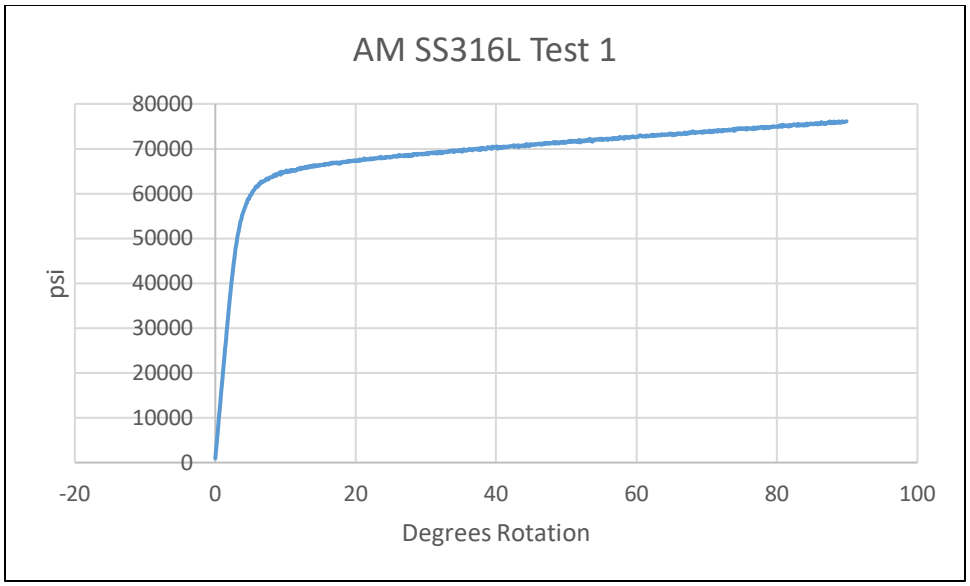

Figure 4-4: Additive SS316L Torsion Test 1 Stress Curve

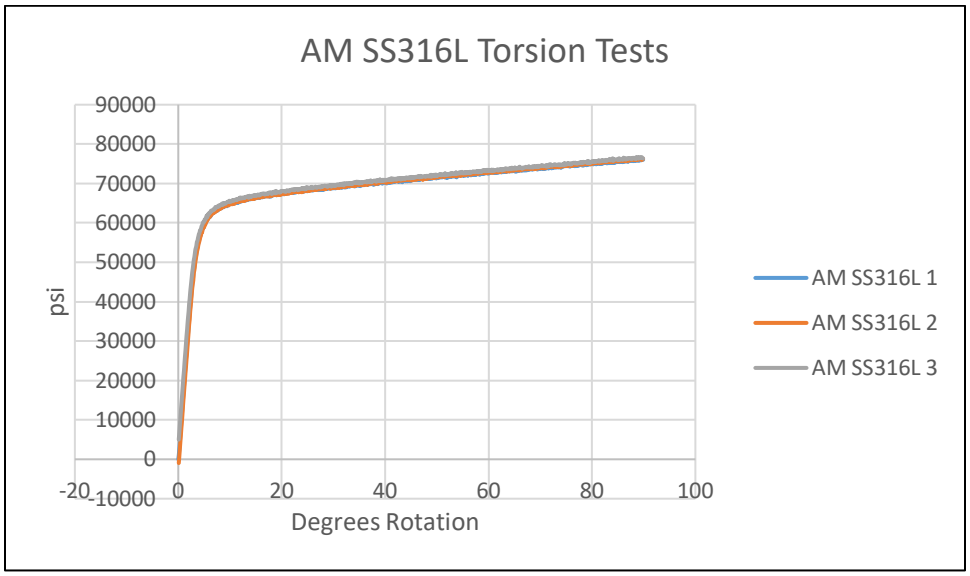

Figure 4-5: PBF-L Additive Torsion Test Curves

The uniformity of the PBF-L processed specimens' performance is quite impressive. The composite chart shows virtually no variation between specimens.

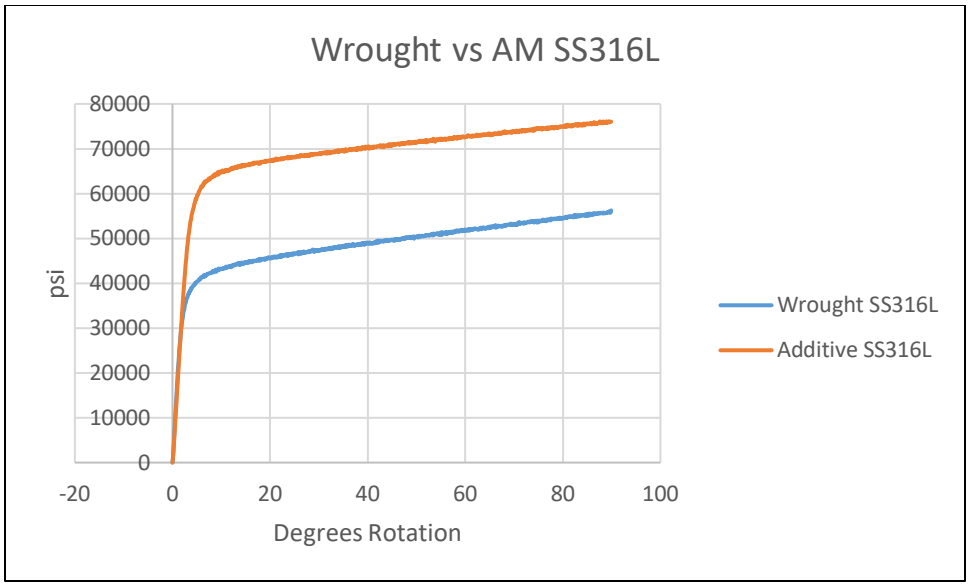

Figure 4-6: Wrought vs PBF-L AM SS316L Torsion Test Curves

An analysis of the test curves suggests that the linear elastic portion of the specimens performed similarly to the wrought specimens, with a slope of approximately 15,000 psi per degree twisted. While the wrought specimens begin yielding at approximately 35,000 psi, the AM pieces reach nearly 65,000 psi before they began to yield. The slope of the plastic deformation region of the AM specimens was virtually identical to that of the wrought specimens, at approximately 175 psi per degree twisted. While the yield point of the PBF-L processed SS316L is much higher than that of the wrought material, it seems that the deformation behavior has remained the same before and after yield. The load at the end of a 90-degree twist reached approximately 77,000 psi. Unit conversions from psi to MPa are provided below in table 4-1.

4.1.1.3 Hybrid SS316L Specimens

The Hybrid (AM/Substrate) specimens were all twisted 90 degrees and performed nearly identically to each other. There are a few significant observations to be made. First, the yield

point of the hybrid specimens was right around 35,000 psi. This correlates perfectly with the yield strength of the wrought specimens above. Beyond that, the maximum stress measured after a 90-degree twist for each was between 52,400 psi and 59,150 psi, which is similar in performance to the wrought specimens.

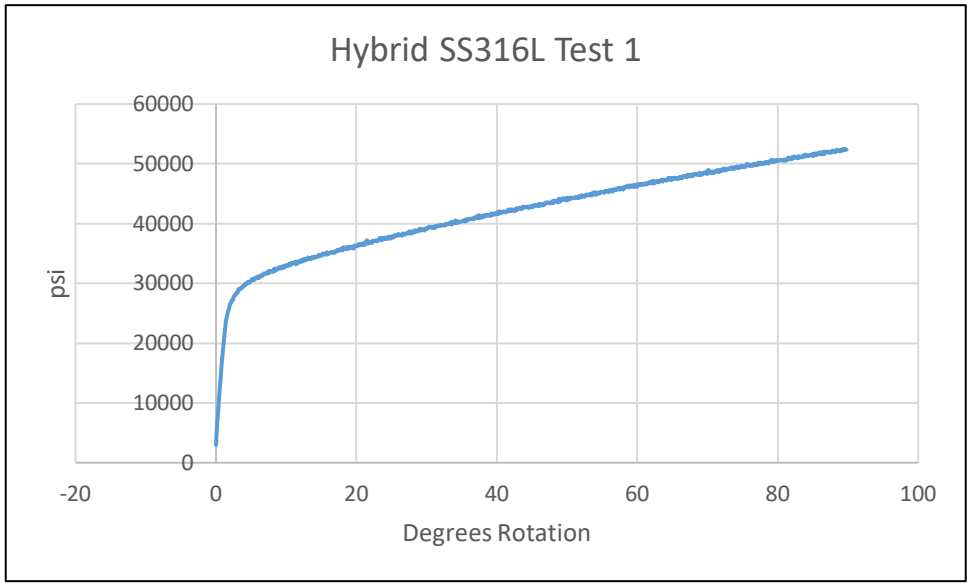

Figure 4-7: Hybrid SS316L Torsion Test 1 Stress Curve

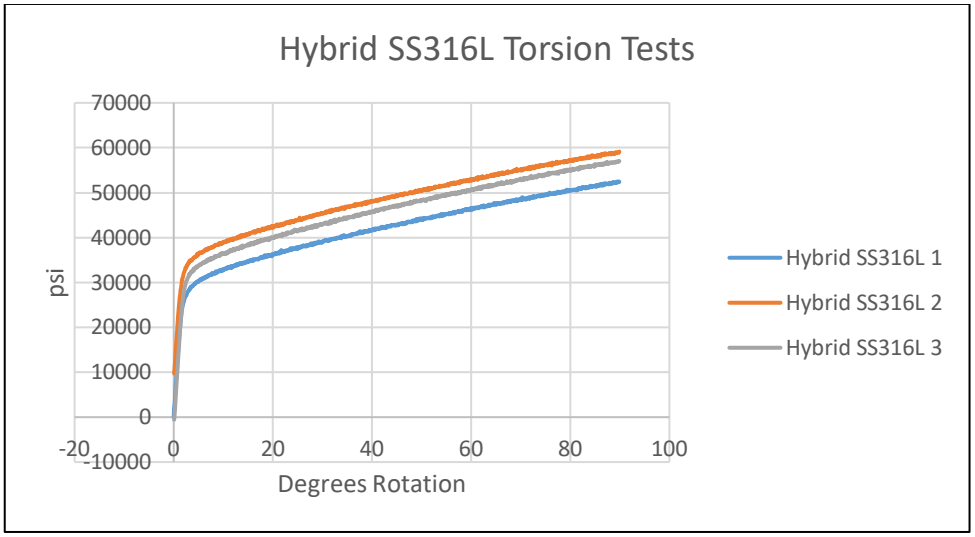

Figure 4-8: Hybrid PBF-L SS316L Torsion Test Curves

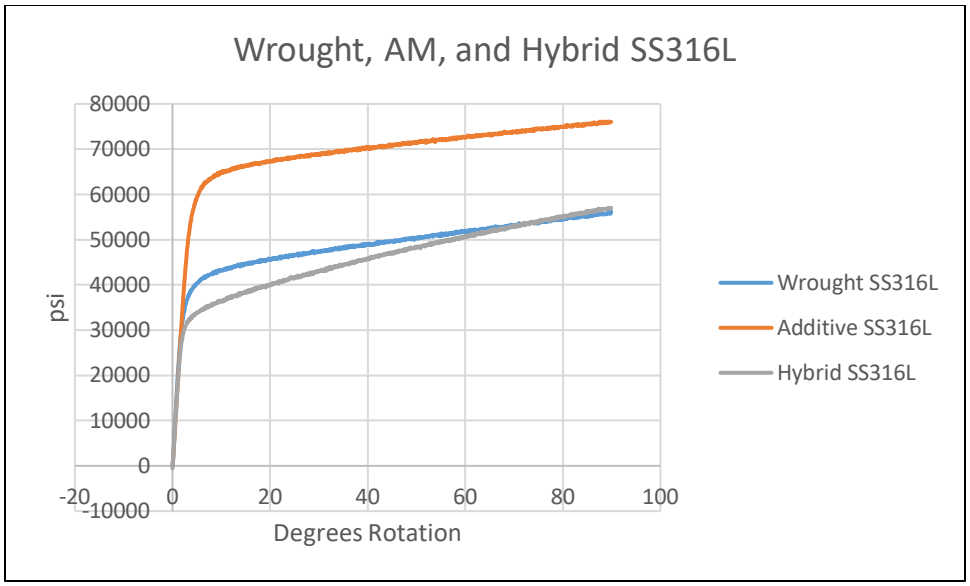

Figure 4-9: Wrought, AM and Hybrid SS316L Torsion Test Curves

An analysis of the data shows that the performance of the hybrid specimens is limited in this case by the mechanical properties of the wrought half of the specimens, while the additive portion remains unaffected. As displayed in the composite plot above, the wrought and hybrid specimens reach their respective yield points and proceed through linear deformation until 90 degrees is reached without ever ascending into the point of yield of the additive material. This initial conclusion is supported from the image of the tested specimen shown below.

Figure 4-10: Hybrid SS316L Torsion Specimen Post Twist

This image clearly displays the deformation that has occurred in the wrought (left) half of the specimen. The red line marks the location of the interface between the substrate and AM portions of the specimen.

The focus of this research is on the performance of the interface. As there were no material failures at the interface, the strength of the interfacial bond in torsion can be analyzed only according to the performance of the hybrid specimen as a whole. For these pieces, that correlates to a maximum stress of 59,148 psi. It is assumed that the interface would have continued on to outperform the wrought section of the specimen. This assumption is made in large part because of the tensile strength of the interface, which is analyzed below. As this will be comparing shear stress to tensile stress, it is not a verified conclusion.

Table 4-1: Average Shear Stress of Wrought, AM, Hybrid SS316L Specimens

	Wrought SS316L	PBF-AM SS316L	Interface SS316L
τ_{yield}	36,000 psi (248 MPa)	65,000 psi (448 MPa)	> 30,000 psi (> 206 MPa)

4.1.2 Tensile Tests

All tensile stresses calculated in this work were done using the following formula:

$$\sigma = F / A \tag{4-3}$$

where σ = stress, F = force applied, and A= cross sectional area of the object.

All strain calculations were done using the following formula:

$$\boldsymbol{\varepsilon = e / l} \tag{4-4}$$

where, $\boldsymbol{\varepsilon}$ = strain, l_o = the original length, extension = $(l\text{-}l_o)$, and l = stretched length.

Below are the results of the wrought and PBF-L processed tensile tests. All of these specimens were pulled to failure. Stress/strain curves for one of each type of specimen is show, along with composite plots for comparison across wrought, AM, and Hybrid specimens. Images of various specimens are provided. The results of the other tests of this type can be found in the appendix.

4.1.2.1 Wrought SS316L Specimens

These three specimens produced normal stress/strain curves. The yield strengths were all fairly similar, at approximately 45,000psi. The elongation at break points showed a slight discrepancy. The first two broke at 63% elongation, which is nominal. The third broke at about 50% elongation, which is less than expected. All specimens showed ultimate tensile strengths of just under 78,000psi.

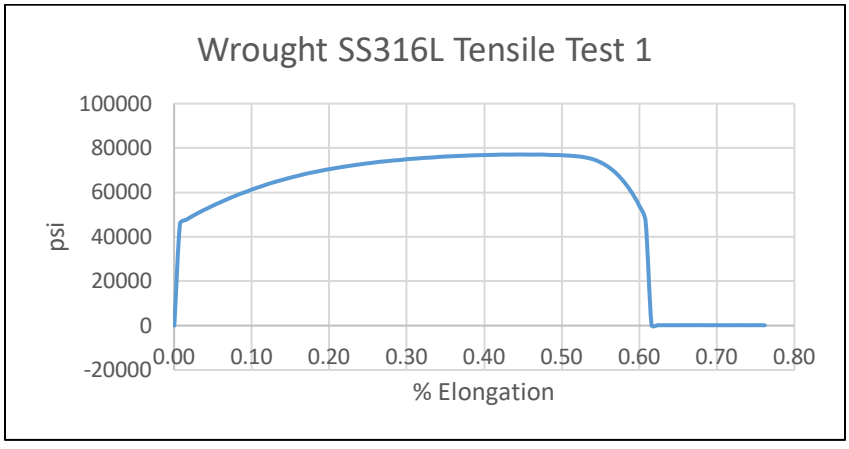

Figure 4-11: Wrought SS316L Tensile Test 1

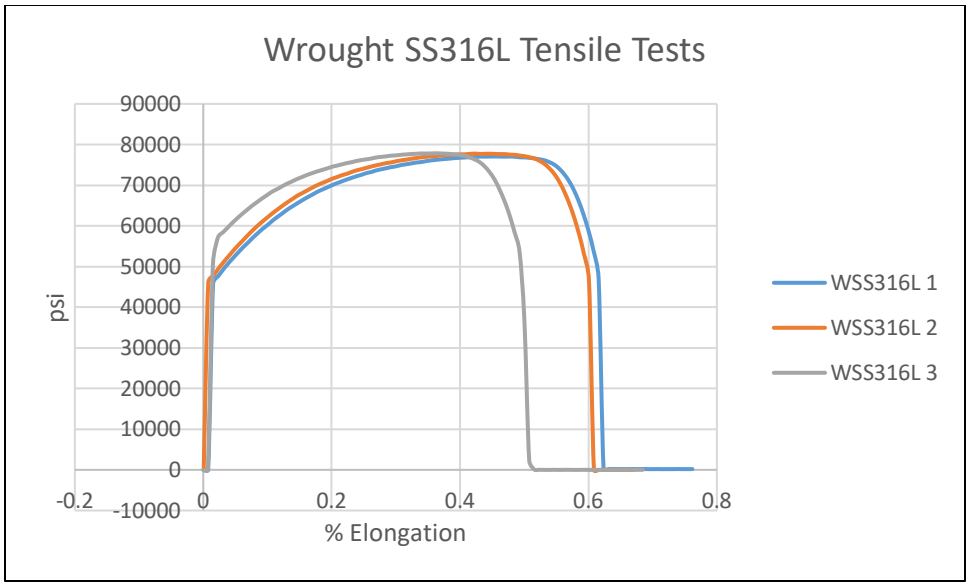

Figure 4-12: Wrought SS316L Tensile Test Curves

An analysis of the stress/strain curves suggests that the wrought SS316L specimens have negligible linear elastic deformation. The second data point (at 0.1 seconds) marks the beginning of yield. After entering plastic deformation, the curves all follow a similar geometry. Stress load continues to increase, but with a negative acceleration, until UTS is reached. After reaching UTS, the curves slope drops dramatically until failure is reached. Failure occurred at approximately the same stress load as the corresponding yield points for each specimen.

4.1.2.2 Fully Additive SS316L Specimens

The three fully additive specimens performed nearly identically. Once again, this shows how consistent and reliable the PBF-L process is. Each of these three specimens displayed a yield strength of 80,000psi, an ultimate strength of 99,000psi, and an elongation at break of 30-33%.

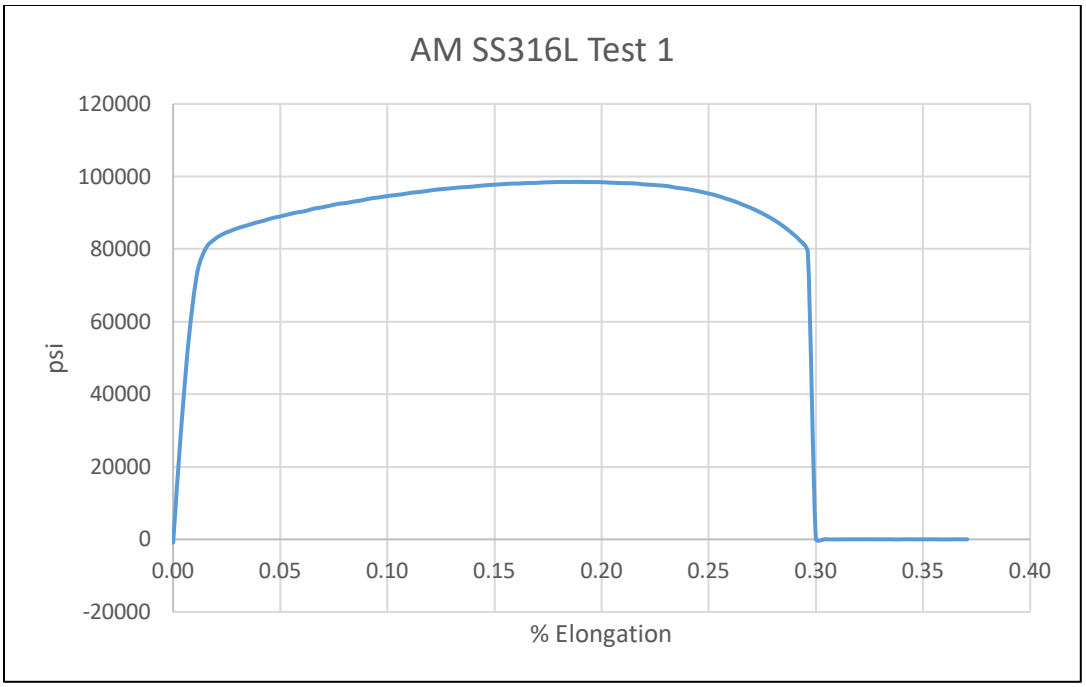

Figure 4-13: Additive SS316L Tensile Test 1

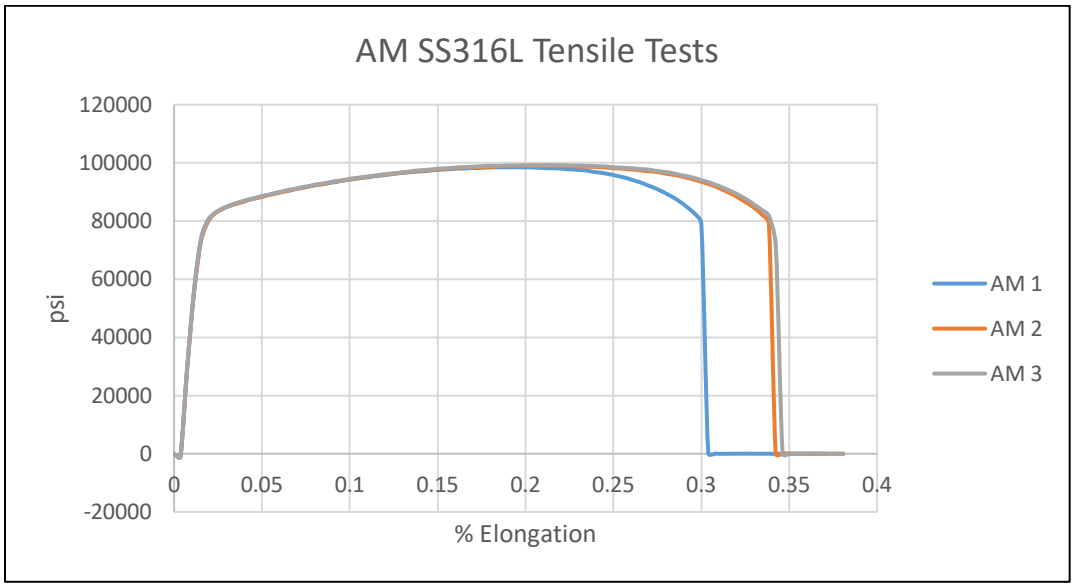

Figure 4-14: Additive SS316L Tensile Test Curves

An analysis of the stress/strain curves suggests that the additive SS316L specimens also experienced negligible linear elastic deformation. However, they did spend 0.3 seconds in this

region before entering yield. The non-linear region of the additive specimens is much shorter, and less curved than the wrought specimens. After yield point, these specimens experienced a 20% rise and drop in stress, as compared with the approximately 44% change experienced by the wrought specimens. Similar to the wrought specimens, the additive curves show failure occurring at the same stress level as the respective yield points.

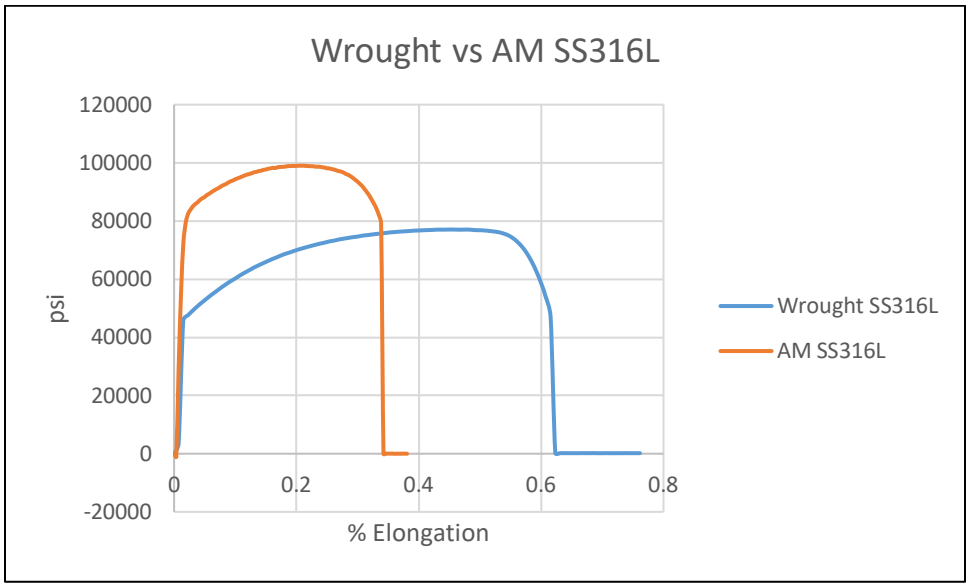

Figure 4-15: Wrought vs AM SS316L Tensile Test Curves

The composite plot above displays well the differences between the wrought and additive specimen performance. An important detail of note is that the UTS of the wrought specimens does not quite reach the yield stress of the additive specimens. This suggests that the hybrid specimens will experience failure either in the wrought region or at the interface.

4.1.2.3 Hybrid SS316L Specimens

The three hybrid specimens all performed nearly identically. Specimen 3 reached UTS at about 71,500 psi, rather than 78,000, but displayed similar curve geometry to that of the other specimens throughout the test. All of the deformation, and the eventual break, took place within the wrought half of the hybrid specimens.

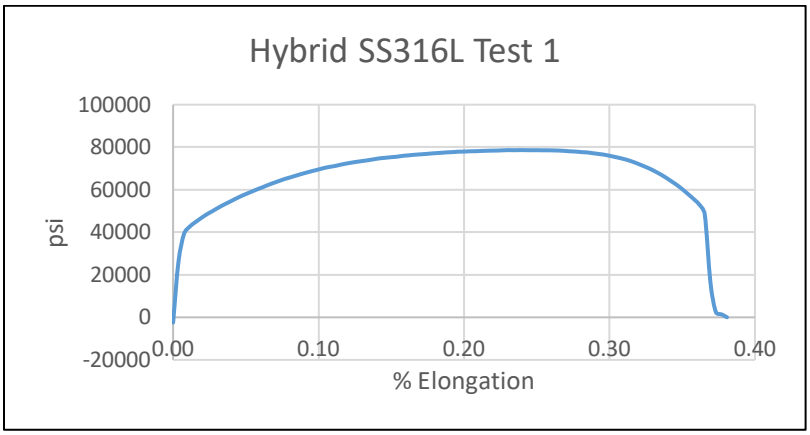

Figure 4-16: Hybrid SS316L Tensile Test 1

The stress strain curves show a performance similar to the wrought specimen curves. The only difference is the percent elongation is just over half that observed in the wrought specimens. As there is exactly half the amount of wrought material in the hybrid specimens compared with the full length, this result is not unexpected. The pulled specimens show no visible deformation in the additive section, as can be seen in the images below.

Figure 4-17: Hybrid SS316L Tensile Specimen Post Test

This is most likely the case because the hybrid tests never reached the yield strength load (~80,000psi) of the additive material. The red markers in this image indicate the interface location. The wrought (left) half of the specimen experienced all of the elongation, while no visible deformation occurred in the additive half.

Figure 4-18: Hybrid SS316L Tensile Specimen Post Test

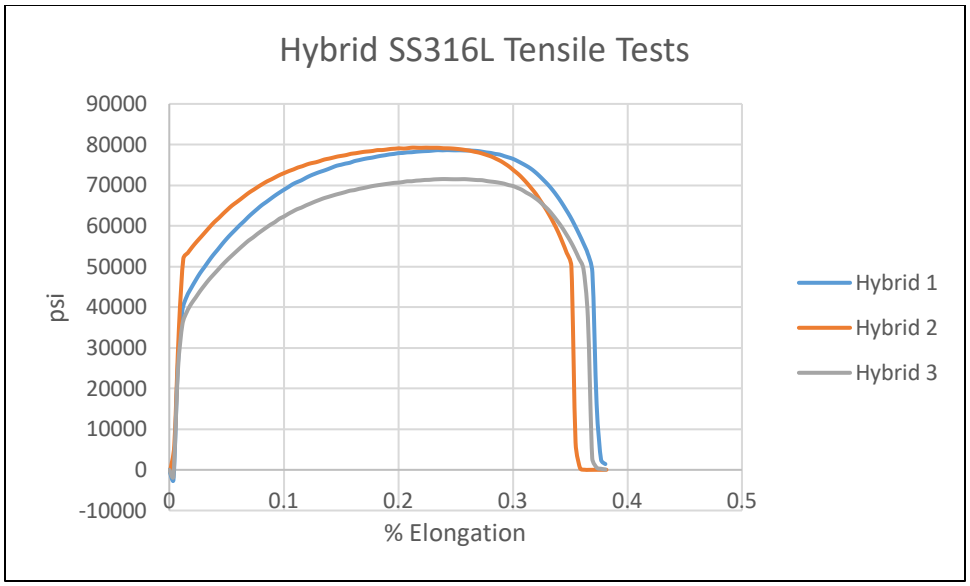

Figure 4-19: Hybrid SS316L Tensile Test Curves

Figure 4-20 displays a comparison of the wrought, additive, and hybrid tensile tests. An analysis of the performance of the interface of the hybrid specimens can be done only according to the maximum stress that the hybrid specimens were able to experience. In this case the interfaces withheld up to 79,000 psi, which is thus the maximum verified tensile stress of the hybrid interface in PBF-L processed SS316L.

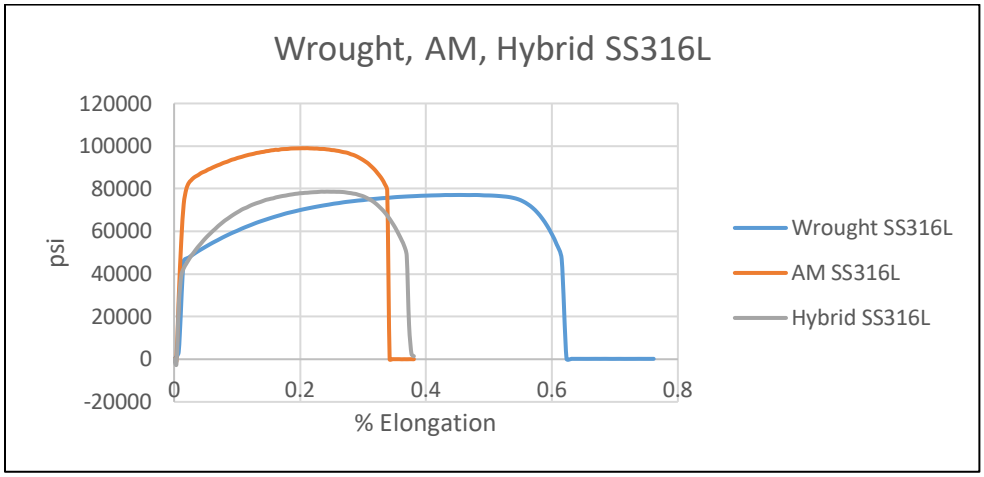

Figure 4-20: Wrought, AM, and Hybrid SS316L Tensile Test Curves

Table 4-2: Average Tensile Stress of Wrought, AM, Hybrid SS316L Specimens

	Wrought SS316L	PBF-AM SS316L	Interface SS316L
σ_{yield}	45,000 psi (310 MPa)	80,000 psi (552 MPa)	> 40,000 psi (> 276 MPa)
$\sigma_{ultimate}$	78,000 psi (538 MPa)	99,000 psi (683 MPa)	> 76,000 psi (> 517 MPa)

4.1.3 Microscopy

From the PBF-L SS316L hybrid block a small specimen was cut, set, polished, etched, and viewed microscopically, as seen in figure 4-21.

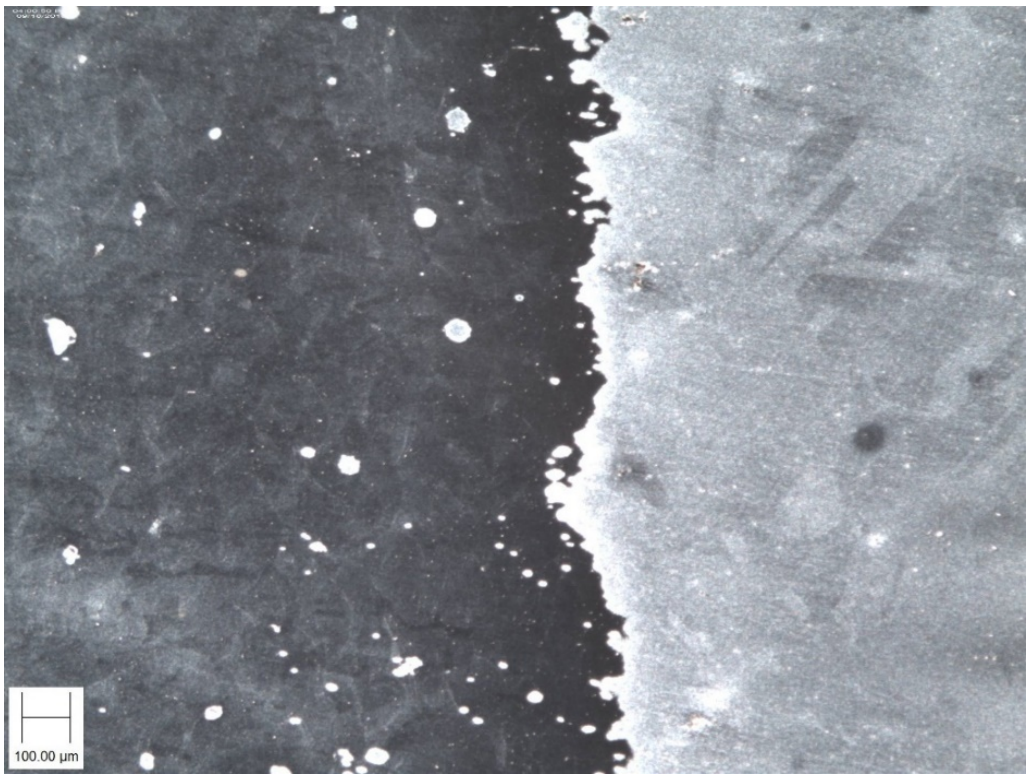

Figure 4-21: Hybrid SS316L PBF-L Interface Under 63X Magnification

From the images captured, it appears that there is good metallurgical bonding between the additive portion and the substrate when using PBF-L processing. The surface of the wrought material was machined to a smooth finish using a manual mill. The flatness of the original surface is more easily seen in Figure 4-55 of the DED processed SS316L hybrid interface. Other than ensure the surface was clean and dry, no further treatment or preparation was performed prior to the additive processing. The amount of additive material penetrating the wrought surface in this image displays the fusion which occurred between AM and substrate materials.

4.2 DED Samples

The DED samples were tested using the same methods as with the PBF-L samples. The only differences are that: 1) there were more DED samples tested than PBF-L samples, and 2) there are two material types, SS316L and M300.

4.2.1 Torsion Tests

4.2.1.1 Wrought M300 Specimens

There were three wrought M300 torsion tests performed in this work. All three of them produced nearly identical testing curves. Figure 4-22 displays the performance of one of these specimens.

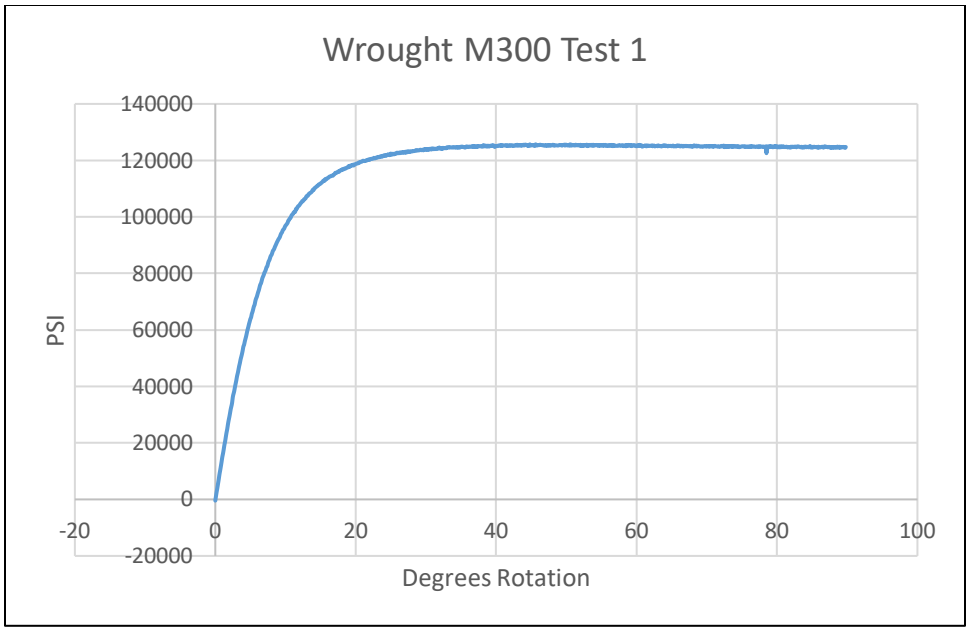

Figure 4-22: Wrought M300 Torsion Test Stress Curves

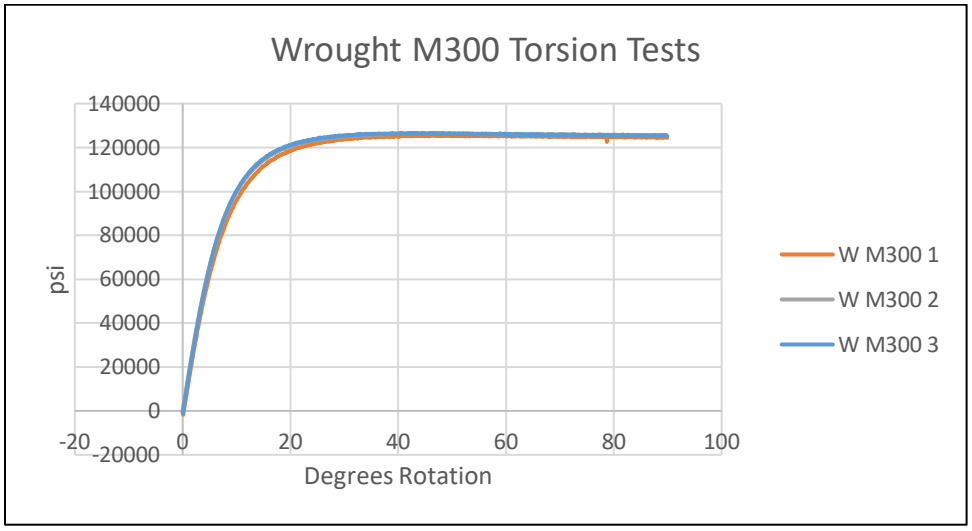

Figure 4-23: Wrought M300 Torsion Test Curves

An analysis of these test curves suggests that wrought M300 performs quite differently than wrought SS316L in torsion. The linear elastic portion of the curves has a lower slope of approximately 10 psi per degree twist. The yield point of these specimens is less distinct. While the slope after yield of the SS316L samples continued to climb linearly, never reaching UTS, the

M300 specimens yield and reach UTS within the first 40 degrees of twist. Following UTS, the curves plateau, with a slight decrease in slope for the remainder of the twist. The wrought M300 samples are much stronger than the wrought SS316L samples in torsion. A comparison of the plateaus of their test curves shows an approximately 65,000 psi difference in strength.

4.2.1.2 Fully Additive M300 Specimens

Three fully additive M300 specimens were processed via DED, machined, and twisted. These specimens performed nearly identically for the first 60 degrees of twist. The end of the test showed discrepancies in behavior. Analysis of Test 1 shows a similar performance to the wrought M300 specimens, with the exception of a 20,000 psi increase in UTS. After reaching UTS, the curve plateaus for the remainder of the twist.

Test 2 and Test 3 follow the same pattern, but the plateaus end just before 70 degrees of twist. At this point these two curves experience a somewhat linear regression of approximately 5,000 psi per degree twist.

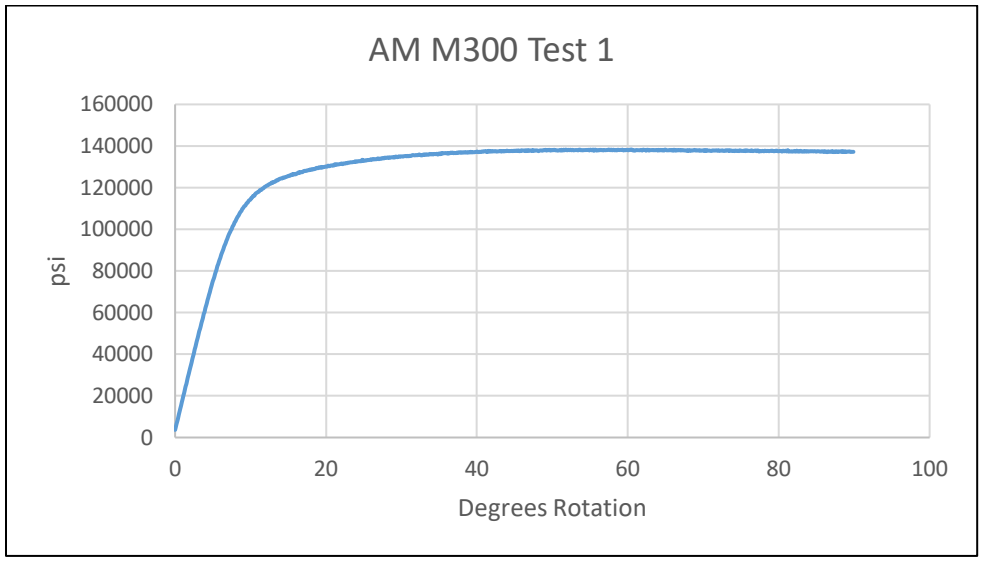

Figure 4-24: Fully Additive DED M300 Torsion Test Curve

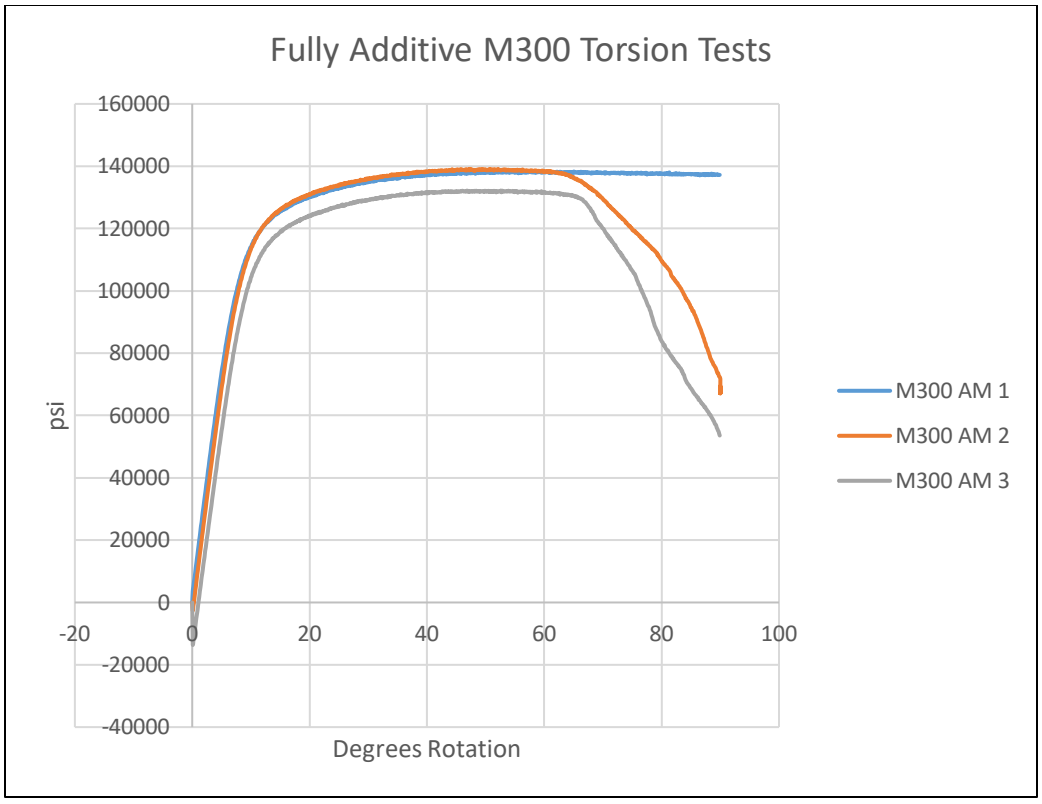

Figure 4-25: Additive M300 Torsion Test Curves

These fully additive M300 specimens withstood torque loads higher than their wrought counterparts. From the curve shown it can be seen that the specimen reached yield strength after the first 10 degrees, at around 122,000 psi. At this point the test curve plateaued at approximately 138,000 psi.

The differences observed between the three AM specimens create an interesting situation when considering the hybrid specimens. The yield strengths of the additive and wrought material will both be reached. The results of the hybrid tests will provide insight as to how the interface will perform when both halves are experiencing deformation.

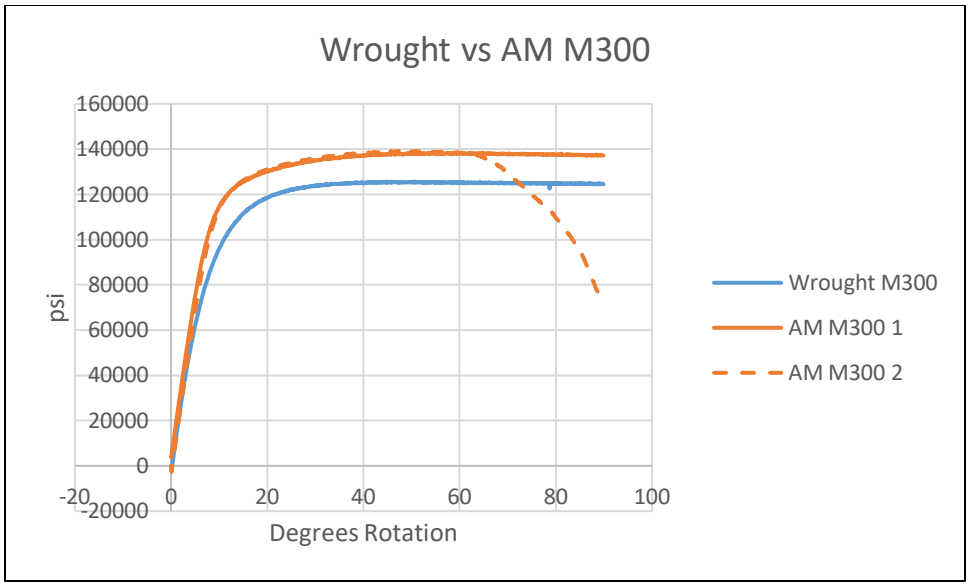

Figure 4-26: Wrought vs AM M300 Torsion Test Curves

The higher strength of the AM material than the wrought is similar to the earlier tests done with powder-bed processed specimens. The additive techniques produce a different grain structure to that of rolled steel, which can be observed in the microscopic images provided. The different grain sizes and structures perform differently when put under stress. As this is not the focus of this research, it will not be investigated, but should be mentioned.

4.2.1.3 Hybrid M300 Specimens

There were six hybrid M300 torsion specimens tested from the DED processed materials. Unfortunately, the first two tests weren't performed to completion due to an equipment malfunction, and the resulting data is corrupted. The curves will be provided in the Appendix, as they do follow a consistent pattern with the four other specimens, but they will not be considered in the analysis.

The following curves display the typical performance of the four hybrid M300 specimens from the DED process.

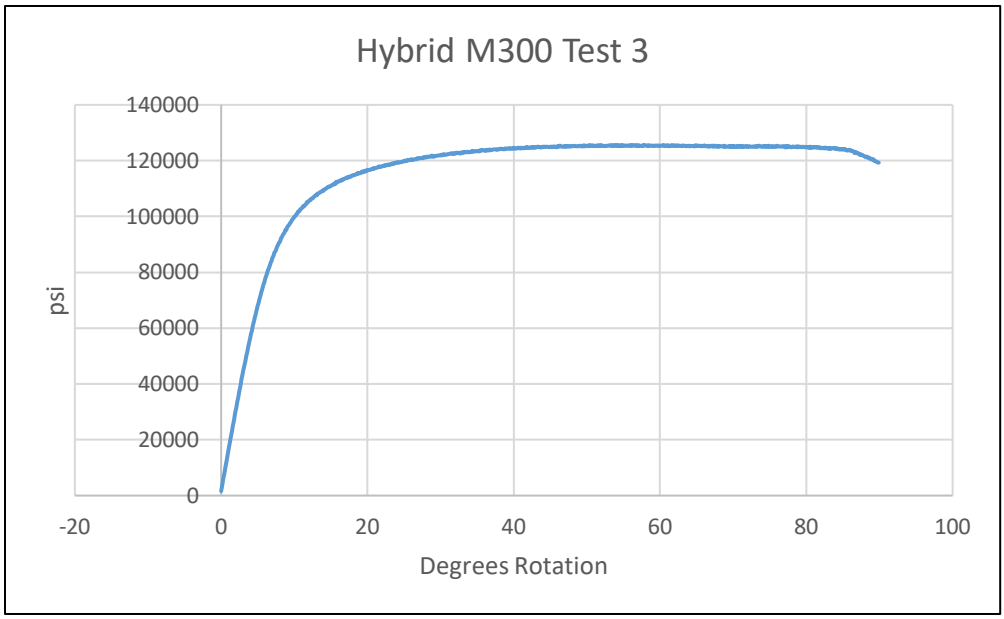

Figure 4-27: Hybrid M300 Torsion Test Curve

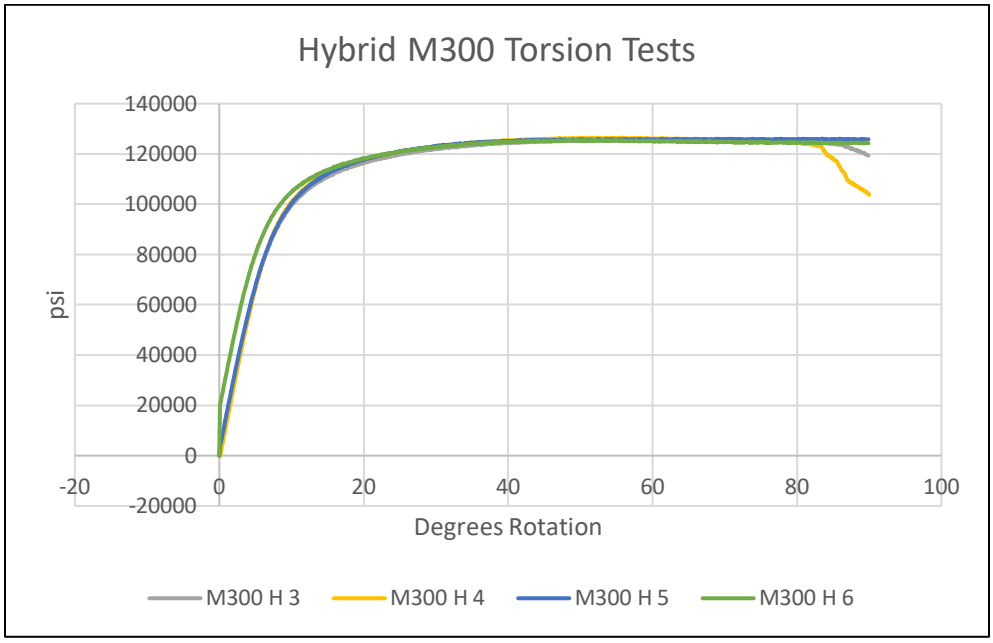

Figure 4-28: Hybrid M300 Torsion Test Curves

An analysis of these curves suggests that the hybrid specimens all performed similarly to their wrought counterparts for the majority of the test. However, at the end of some of the tests a distinct drop takes place. As this is not characteristic of the wrought specimens previously tested, it is assumed that deformation occurred in both the wrought and additive regions of the hybrid specimens. In hybrid specimens 3 and 4, the additive region began experiencing failure. In specimens 5 and 6 it seems that the additive regions did not yet reach failure.

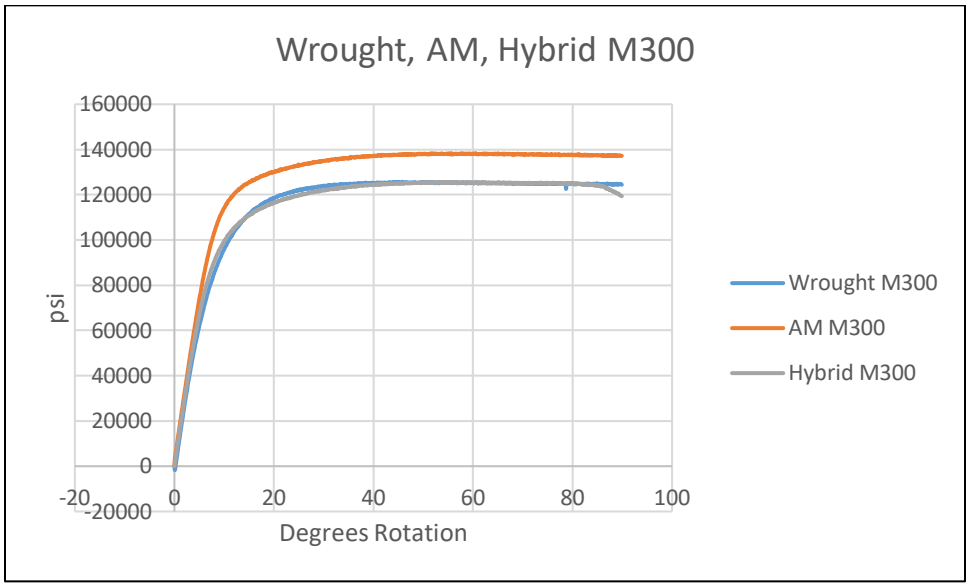

Figure 4-29: Wrought, AM, and Hybrid M300 Torsion Test Curves

A summary of the yield strengths of the wrought, fully additive, and hybrid DED M300 specimens can be found in the table below.

Table 4-3: Average Stresses of DED Processed M300 Torsion Specimens

	Wrought M300	DED-AM M300	Interface M300
τ_{yield}	100,000 psi (690 MPa)	115,000 psi (793 MPa)	100,000 psi (690 MPa)

4.2.1.4 Fully Additive SS316L Specimens

Three fully additive SS316L specimens were produced from the DED process. These were tested under the same parameters as previously described. Each of the tests produced nearly identical test curves, which can be seen in the composite plot below. Figure 4-25 displays the first of the three test curves. Test 2 and 3 can be viewed in the appendix.

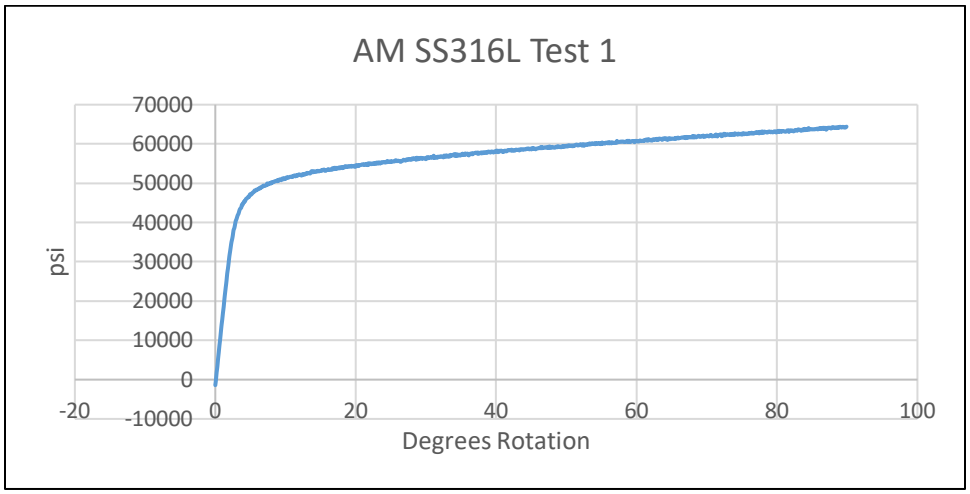

Figure 4-30: Additive SS316L Torsion Test Curve

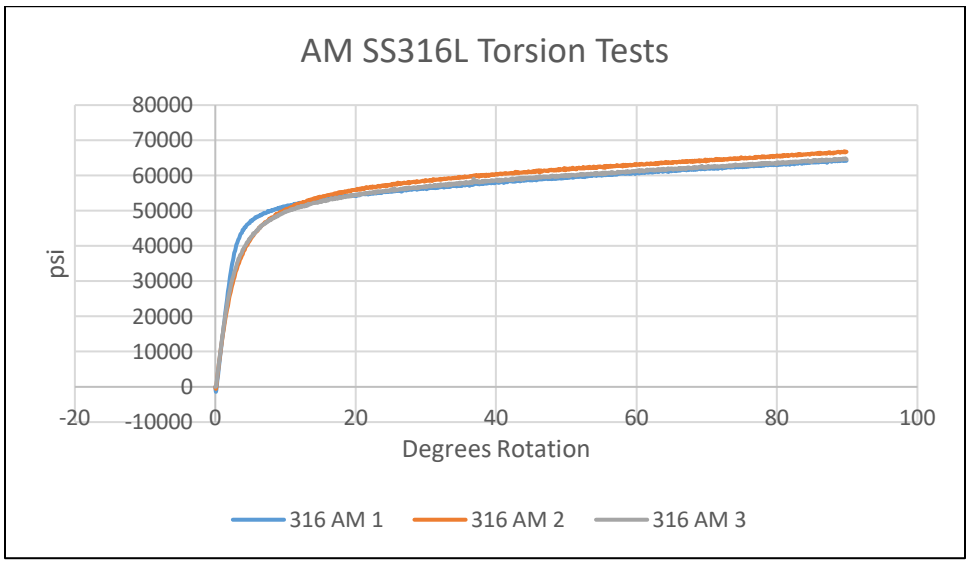

Figure 4-31: AM SS316L Torsion Test Curves

As can be seen from the curve, these specimens experienced a yield point at around 49,000 psi in the first 10 degrees of twist. After this yield point, they continued to resist at a fairly linear rate for the remaining 80 degrees, never reaching UTS. The DED fully additive SS316L torsion curves look very similar to the PBF-L curves. The PBF-L specimens outperformed the DED type by approximately 16,300 psi.

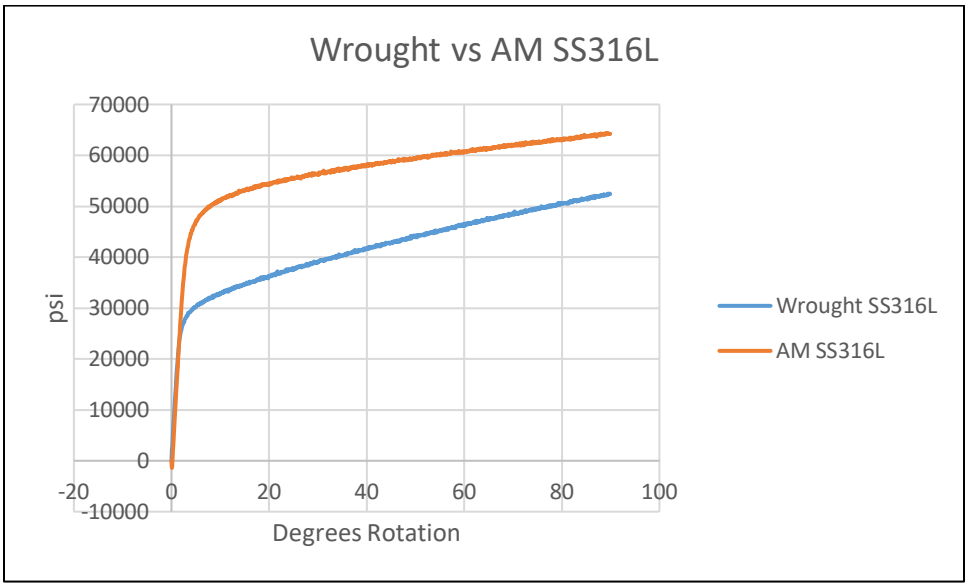

Figure 4-32: Wrought vs AM SS316L Torsion Test Curves

An analysis of these curves suggests that the linear elastic deformation of the additive specimens is similar to that of the wrought specimens, at approximately 15,000 psi per degree twisted. The yield point is much higher, but not quite so high as the PBF-L processed SS316L specimens. The slope of the plastic region is slightly lower than the wrought specimens, at approximately 170 psi per degree twisted. It would be interesting to see if the additive SS316L would begin failing earlier than the wrought material, similar to the results of the M300 specimens. 90 degrees is not sufficient to reach failure in the DED processed SS316L specimens.

4.2.1.5 Hybrid SS316L Specimens

Six hybrid SS316L torsion specimens were created and tested from the DED process. As these specimens also performed fairly similarly to each other, only the first of the six test curves is show below. The rest can be found in the Appendix.

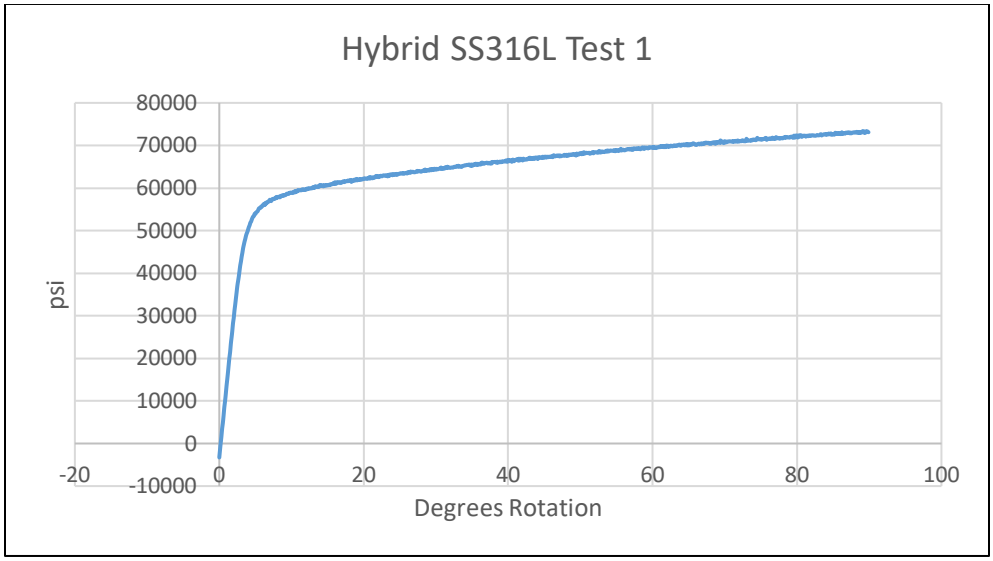

Figure 4-33: Hybrid SS316L Torsion Test Curve

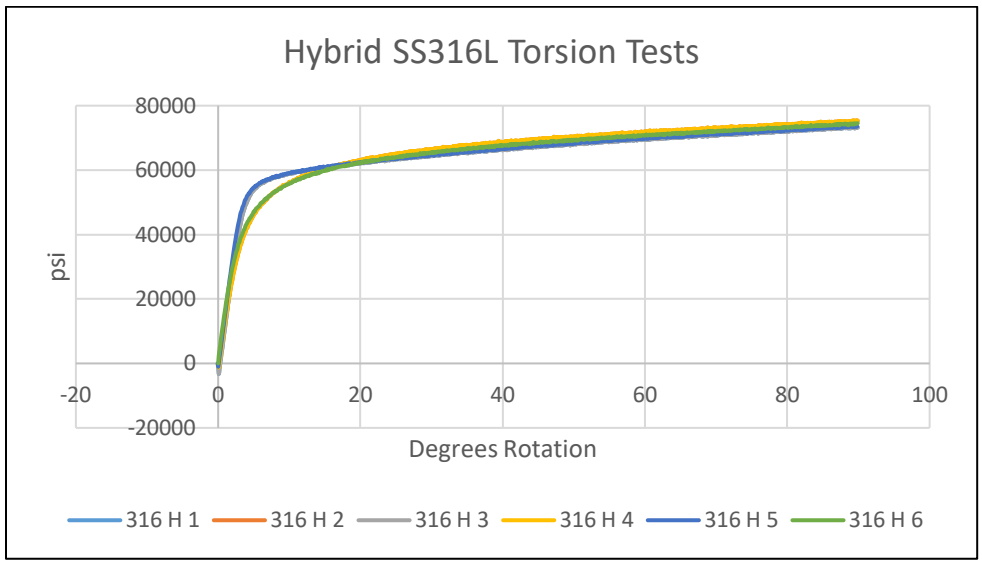

Figure 4-34: Hybrid SS316L Torsion Test Curves

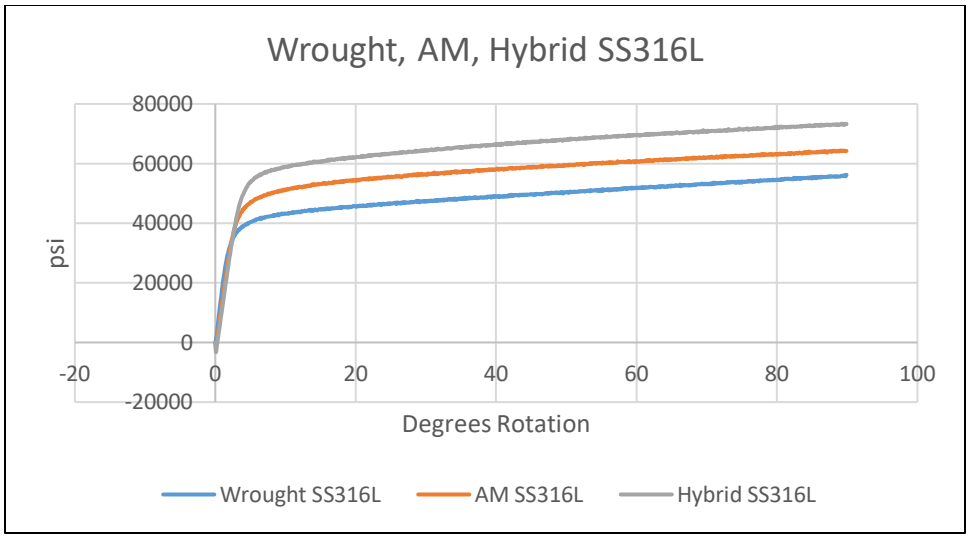

Figure 4-35: Wrought, AM, and Hybrid SS316L Torsion Test Curves

An interesting change occurred with these tests. The previously tested hybrid specimens all followed a similar performance to their corresponding wrought specimen. These hybrid specimens outperformed their wrought and additive counterparts. The reason for this is unknown. In order for this to occur, the wrought material in the hybrid specimen had to surpass its previous yield point by 40%. When considering the performance of the interface, it is known only that it can withstand the torque loads experienced in the test performed. In this case, that would be approximately 73,500 psi, which is above that of the wrought and fully additive SS316L specimens.

A summary of the yield strengths of the wrought, fully additive, and hybrid DED SS316L specimens can be found in the table below.

Table 4-4: Average Stresses of DED Processed SS316L Torsion Specimens

	Wrought SS316L	DED-AM SS316L	Interface SS316L
τ_{yield}	36,000 psi (248 MPa)	50,000 psi (345 MPa)	56,000 psi (386 MPa)

4.2.2 Tensile Tests

4.2.2.1 Wrought M300 Specimens

Three wrought M300 tensile specimens were machined and tested according to the methods already explained. All three of these specimens performed remarkably similar. The stress/strain curve of the first test is shown below. The second and third test curve can be found in the appendix.

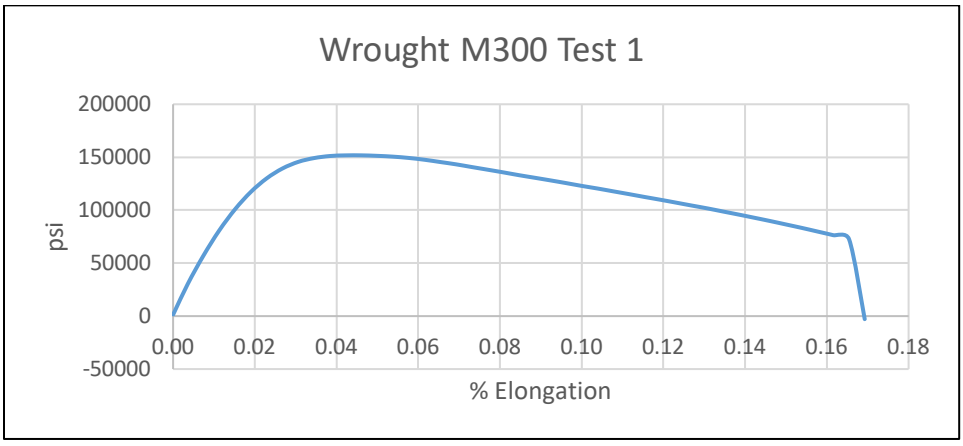

Figure 4-36: Wrought M300 Tensile Test Curve

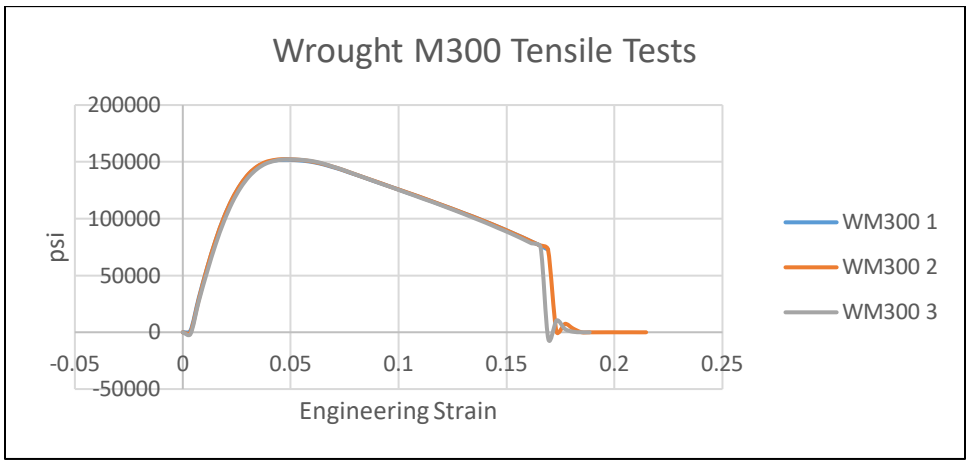

Figure 4-37: Wrought M300 Tensile Test Curves

It is apparent that wrought M300 performs quite differently in tension when compared with wrought SS316L. M300 is much more brittle, and much stronger. Rather than deforming, it takes on a much higher load with very low strain. While SS316L specimens reached strain levels of more than 60%, the M300 specimens all broke at just below 17%. This is typical of wrought M300 material.

An analysis of the curves shows that the linear elastic region has a slope of approximately 65,000 psi per 1% elongation. The yield strength of the wrought M300 specimens is 140,000 psi. After yielding, the curve has a negative slope (-6,000 psi per 1% elongation) that descends linearly for the remainder of the pull until failure occurs at 16.5% elongation.

4.2.2.2 Fully Additive M300 Specimens

Three fully additive M300 tensile specimens were machined and tested using the same procedures previously noted. These tests all performed fairly similarly. The resulting stress/strain curve of the first test is shown below.

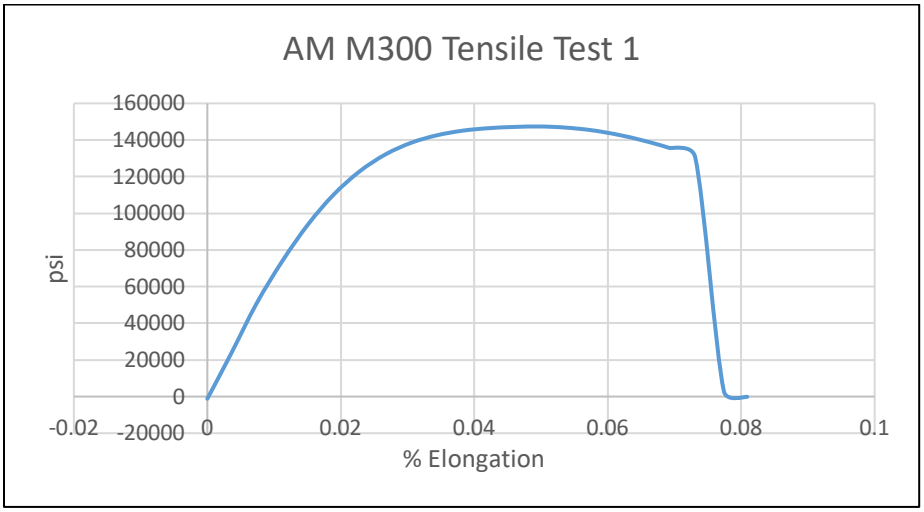

Figure 4-38: Additive M300 Tensile Test Curve

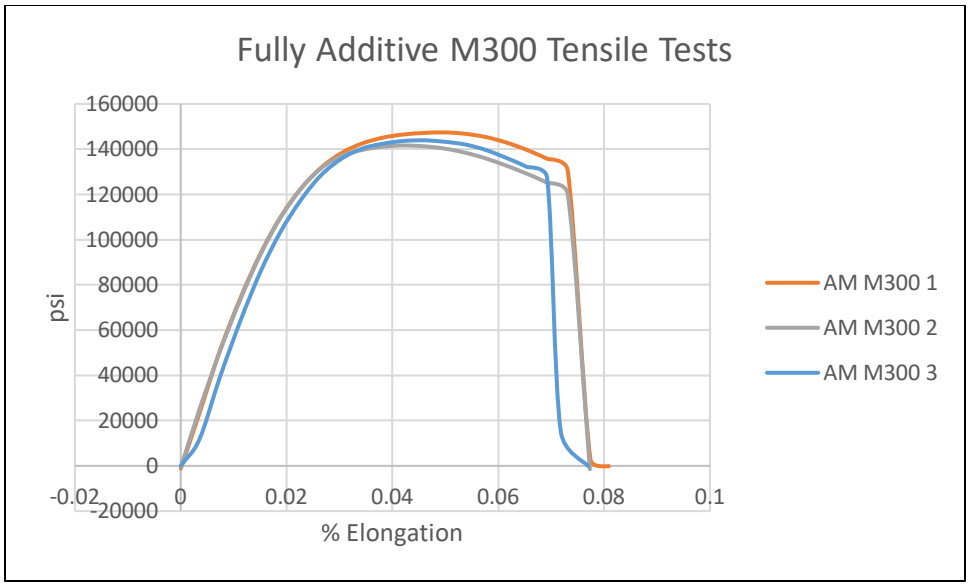

Figure 4-39: Additive M300 Tensile Test Curves

An analysis of the stress/strain curves suggests that the additive M300 specimens performed nearly identically to the wrought specimens in the linear elastic region. The initial slope of the curves is approximately 65,000 psi per 1% elongation.

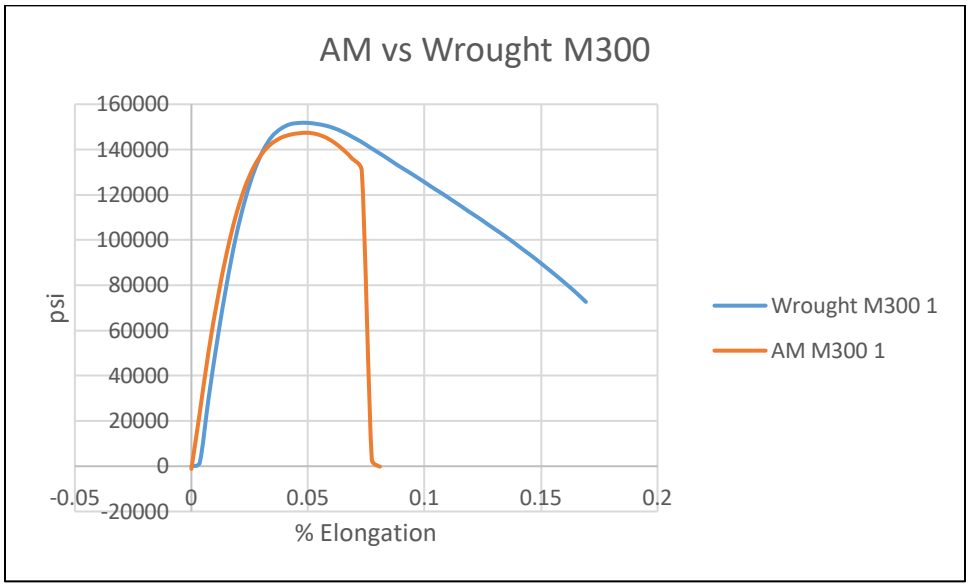

Figure 4-40: Wrought vs AM M300 Tensile Test Curves

An analysis of figure 4-40 shows that while the slopes are nearly the same, there is a slight gap between the two curves, with the AM specimen above the wrought. When the additive specimen begins to yield the two curves cross, after which the additive specimen fails at 7% elongation. The yield strength of the additive specimens is slightly less than the wrought specimens, at approximately 110,000 psi. Because of the very slight differences in performance, it will be interesting to see which pattern the hybrid specimens follow.

The fully additive M300 tensile specimens proved to be far less ductile than even the brittle wrought M300 specimens. They exhibited extremely low strain rates of approximately 6% before breaking. The image below displays the specimen post break.

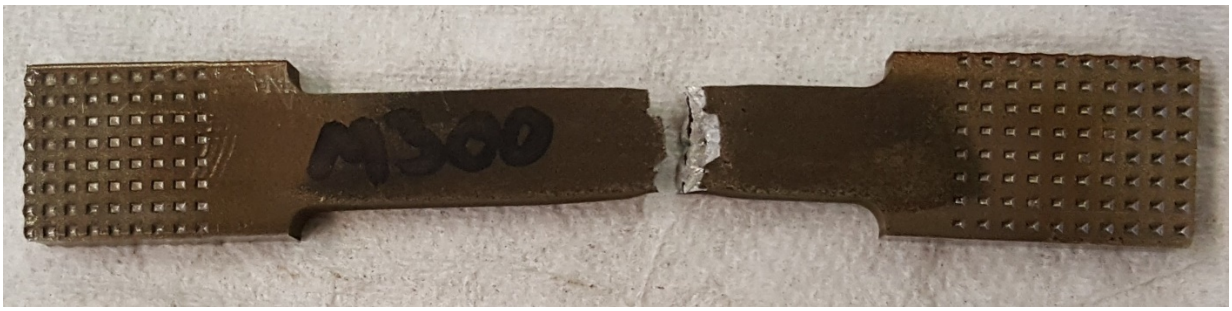

Figure 4-41: Fully Additive DED M300 Tensile Specimen Post Break

A visual observation agrees with the data, in that there was very little strain that occurred before breaking. This could be a contributing factor in the lower yield strength and UTS, when compared with the wrought specimens. It could have been beneficial to perform these tests at a lower rate of pull, and to increase the data acquisition rate. Perhaps the specimens would exhibit different stress capabilities when pulled at a lower rate (Yang, Kang, Kim, Song, & Park, 1999). Such factors are outside the scope of this work.

4.2.2.3 Hybrid M300 Specimens

Six hybrid M300 tensile specimens were fabricated using the DED process, and tested under the same procedures as previously noted. The resulting stress/strain curve of the first test is shown below along with a composite plot of all hybrid M300 tensile tests.

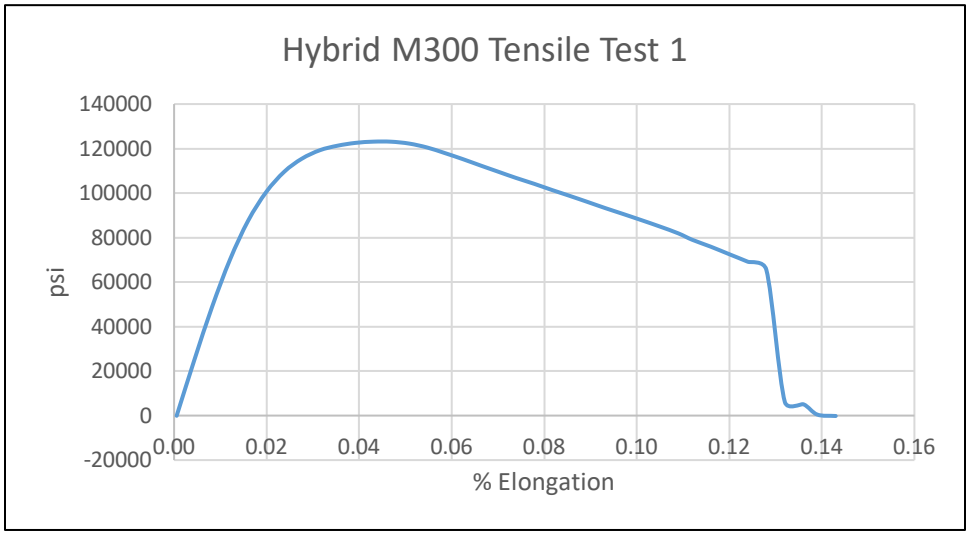

Figure 4-42: Hybrid M300 Tensile Test Curve

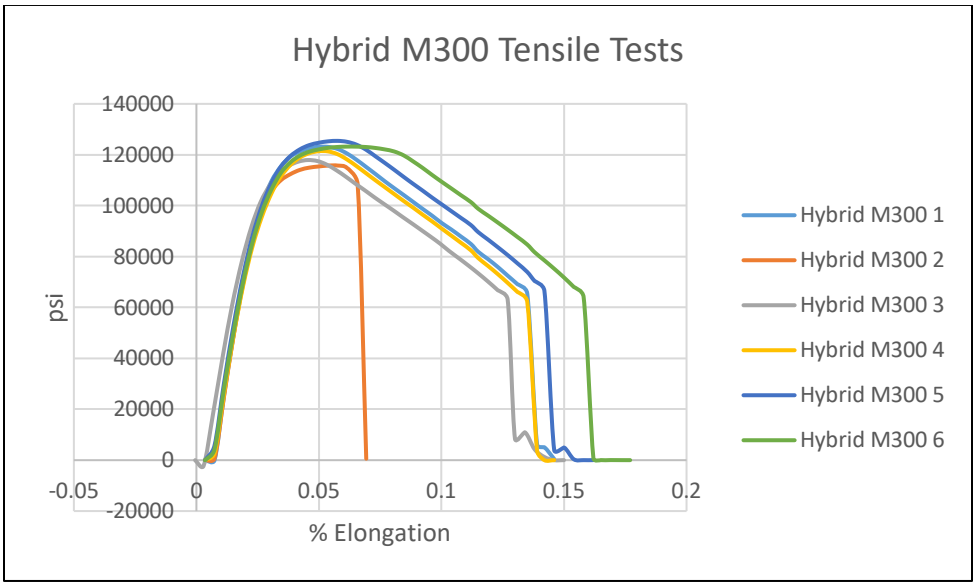

Figure 4-43: Hybrid M300 Tensile Test Curves

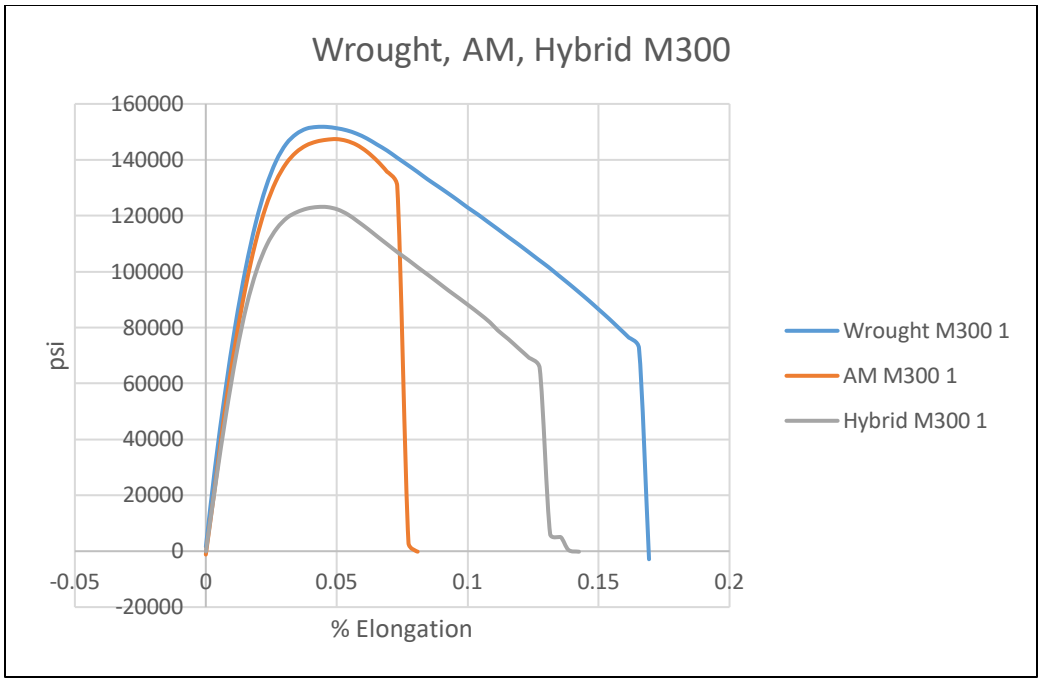

Figure 4-44: Wrought, AM, and Hybrid M300 Tensile Test Curves

An analysis of the curves suggest that the hybrid M300 tensile specimens behave similarly to both the wrought and additive materials, but with a lower yield strength and UTS. As can be observed in figure 4-43, the specimens all failed at different elongations. Test 2 followed the pattern set by the additive specimens, failing at 7% elongation, while the other specimens failed between 13-17% elongation, following the pattern set by the wrought specimens. The specimens exhibited lower UTS as well, at approximately 120,000 psi. As Test 2 failed in the additive portion, and all others failed in the wrought portion, the lower UTS is likely due to the either the decrease in available necking material when compared to the fully wrought and additive specimens, and/or the yielding of both materials simultaneously causing weakened overall tensile stress properties.

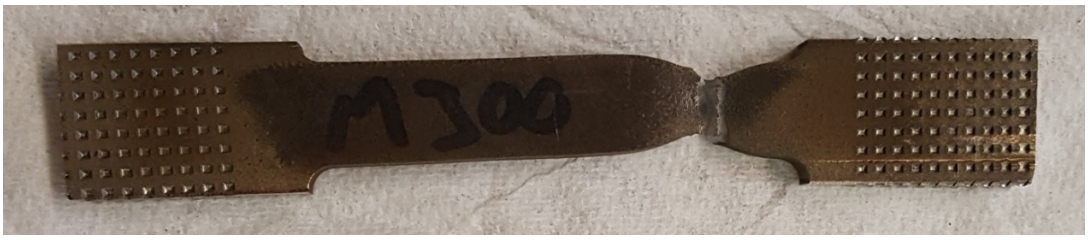

Figure 4-45: Hybrid DED M300 Tensile Test Post Failure

In Figure 4-45 Test 1 can be observed, post failure. The additive portion of the specimen did not experience any deformation. The wrought portion experienced all of the strain, and the eventual break. For Test 2, the opposite situation occurred. All necking and failure occurred in the additive portion. The yield points of the wrought and additive M300 are fairly close together. Because they are so close, this could be a case by case situation that determines which side begins failing first.

The interface between the additive portion and the wrought portion in each of these specimens is performing at the highest stress level recorded in each test. No failures occurred at the interface. The highest recorded stress experienced was by hybrid Test 1, at 147,405 psi.

Table 4-5: Average Stresses of DED Processed M300 Tensile Specimens

	Wrought M300	DED-AM M300	Interface M300
σ_{yield}	120,000 psi (827 MPa)	110,000 psi (758 MPa)	90,000 psi (621 MPa)
$\sigma_{ultimate}$	155,000 psi (1069 MPa)	143,000 psi (986 MPa)	125,000 psi (862 MPa)

4.2.2.4 Fully Additive SS316L Specimens

Three fully additive SS316L tensile specimens were fabricated using the DED process, and tested under the same procedures as previously noted. The stress/strain curves all exhibit a similar geometry. The resulting stress/strain curve of the first test, along with a composite plot of all tests are shown below.

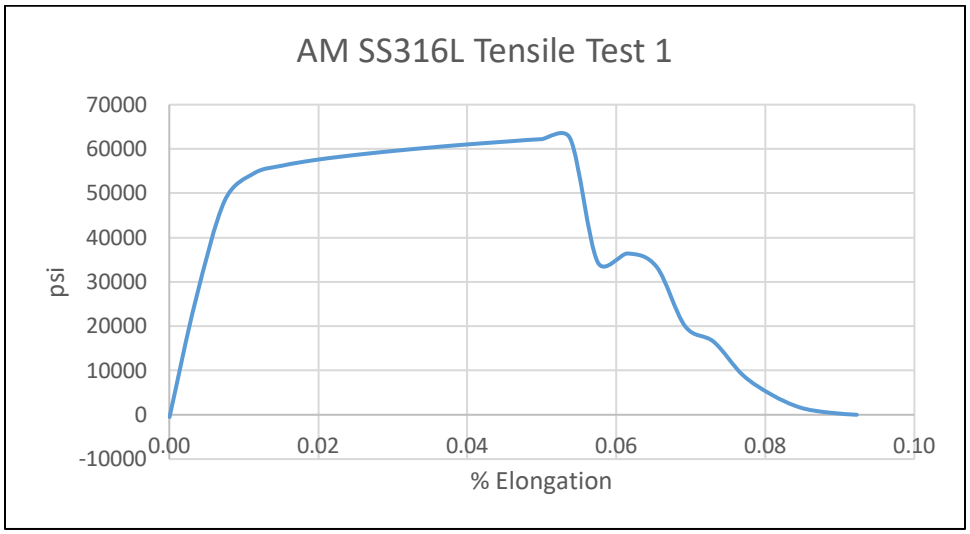

Figure 4-46: AM SS316L Tensile Test Curve

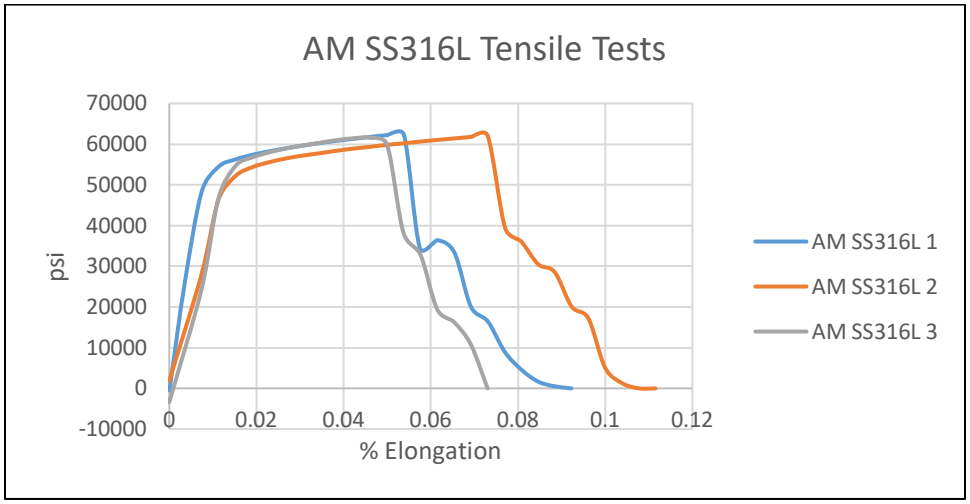

Figure 4-47: Additive SS316L Tensile Test Curves

An analysis of the stress curves suggests that the linear elastic region is similar to that of wrought SS316L tensile tests. The yield point of the additive specimens is higher, at approximately 50,000 psi. The slope following yield is positive, at 1,800 psi per 1% elongation. This linear slope ends abruptly when failure occurs. This is different from the wrought specimens which reach UTS, and then experience a negative slope which decreases gradually until failure.

The most significant difference in these DED processed specimens is the stress pattern that occurs during failure. After reaching UTS the specimen seems to have undergone a series of multiple fractures until ultimately breaking. It could be that the layer-by-layer fabrication of these specimens influenced the way that they failed. Below is an image of the specimen, post break.

Figure 4-48: Fully Additive DED SS316L Tensile Specimen Post Break

On the fractured surface a layered texture can be observed. These layers may have fractured in rapid succession, not all at once, producing a staircase shaped stress/strain curve. This is something that could be investigated further in another experiment. How does deposition layer thickness affect the stress/strain properties? How does it affect the fracture characteristics?

The specimen would likely perform differently if layer orientation were to be normal to direction of pull.

Figure 4-49: Close-up View of Fractured Surface in DED SS316L Tensile 1

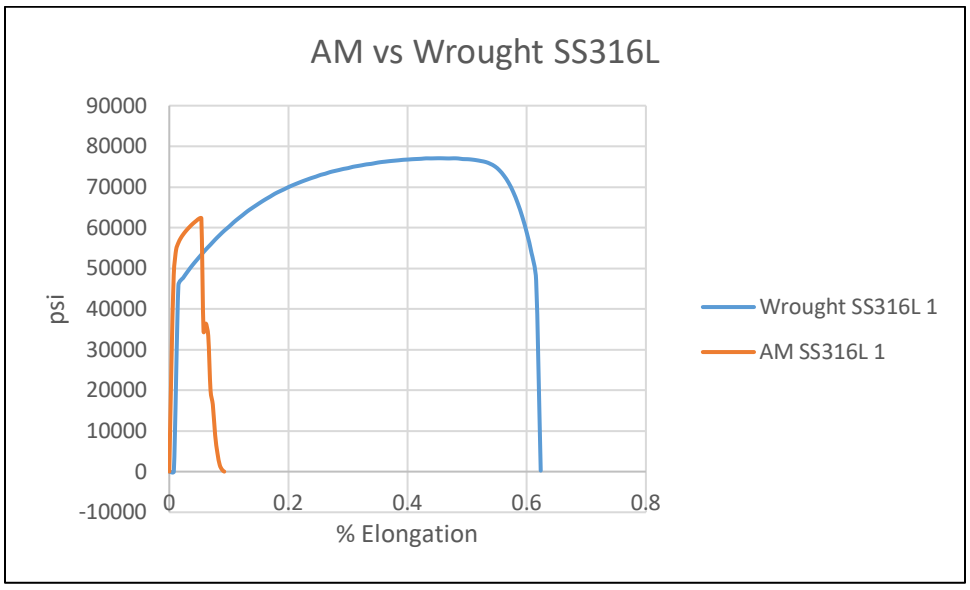

Figure 4-50: Wrought vs AM SS316L Tensile Test Curves

An analysis of Figure 4-50 suggests that, while the wrought SS316L material yields earlier than additive, the UTS is much higher. This will likely show in the hybrid specimens. There will

likely be deformation initially in the wrought portion, followed shortly by deformation and then failure in the additive portion.

4.2.2.5 Hybrid SS316L Specimens

Six hybrid SS316L tensile specimens were fabricated using the DED process, and tested under the same procedures as previously noted. These tests all performed fairly similarly. The resulting stress/strain curve of the first test is shown below. Tests 2-5 are included in a composite plot, and can also be found in the appendix.

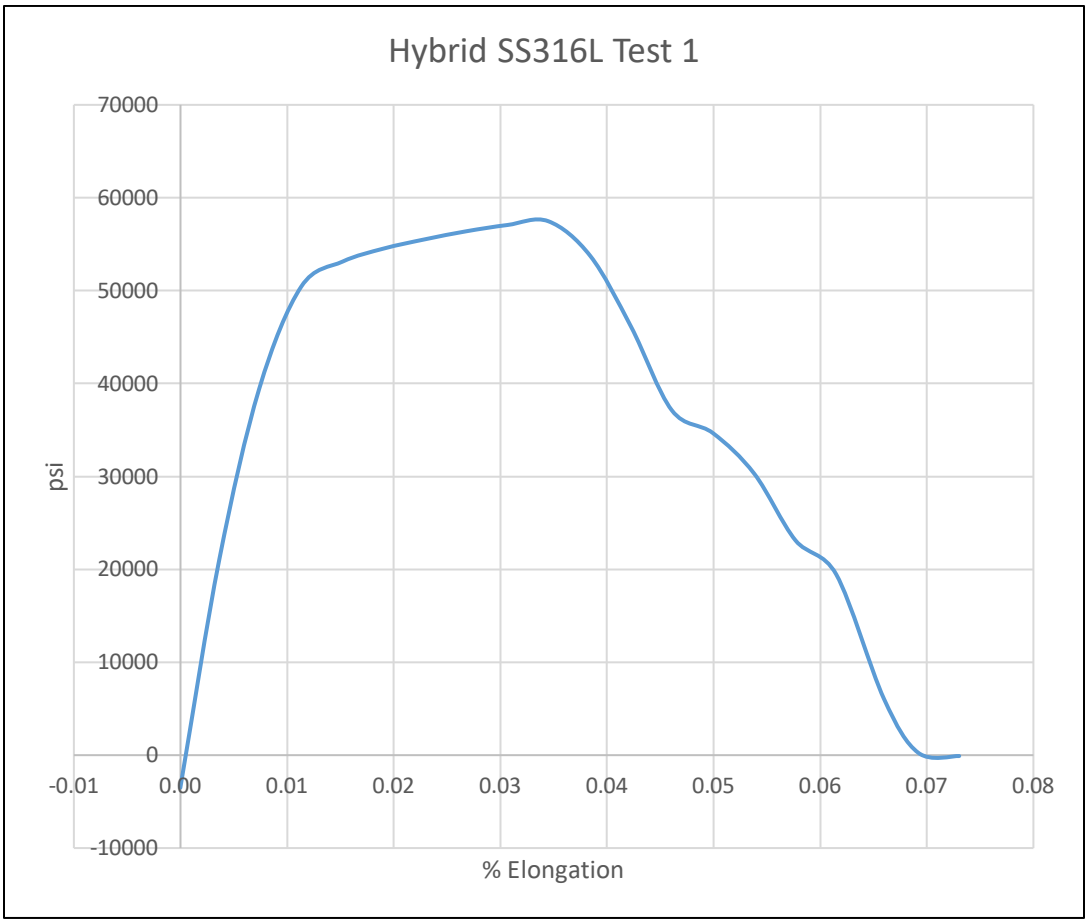

Figure 4-51: Hybrid SS316L Tensile Test Curve

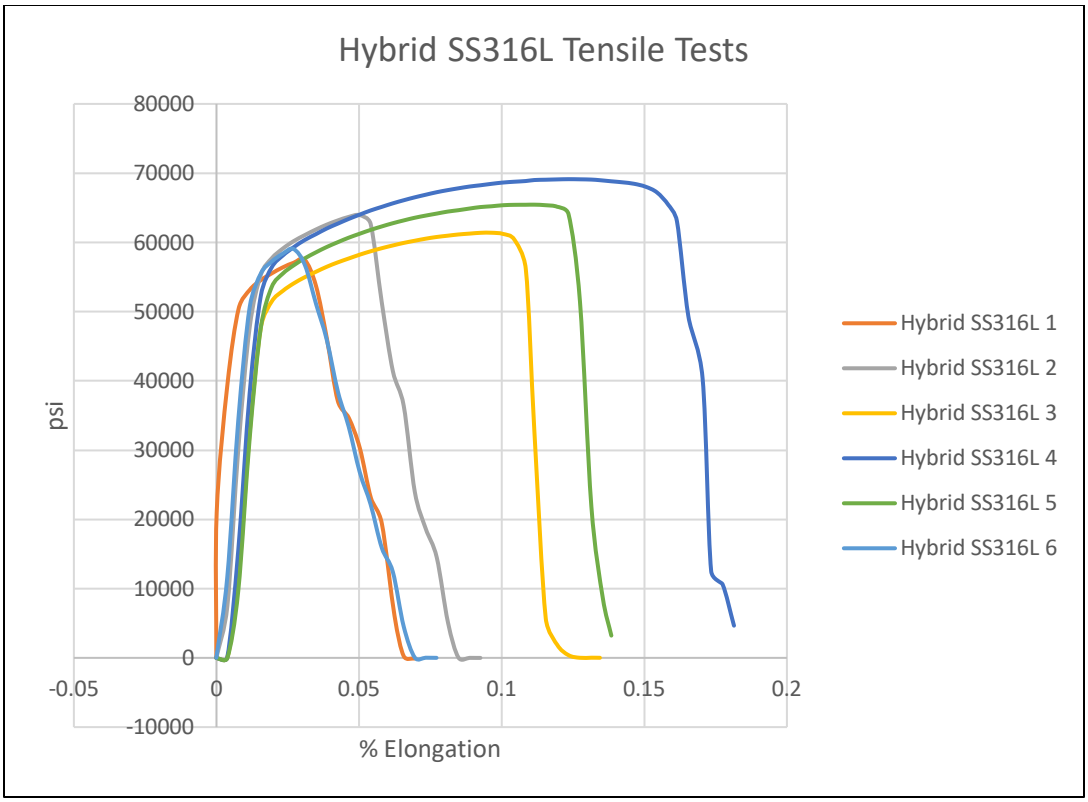

Figure 4-52: Hybrid SS316L Tensile Test Curves

An analysis of these curves suggests that the DED processed hybrid SS316L specimens followed the behavioral patterns of both the wrought SS316L tensile tests and the DED processed fully additive tensile tests. Tests 1, 2, and 6 all matched nearly perfectly with their fully additive counterparts. Tests 3, 4, and 5 seem to have deformed in the wrought region for a certain duration, as can be observed by the greater elongation displayed in Figure 4-52. These specimens ultimately failed in the more brittle additive portion. It is easy to observe the staircase pattern in each of the failures, which is evidence of the DED processed material.

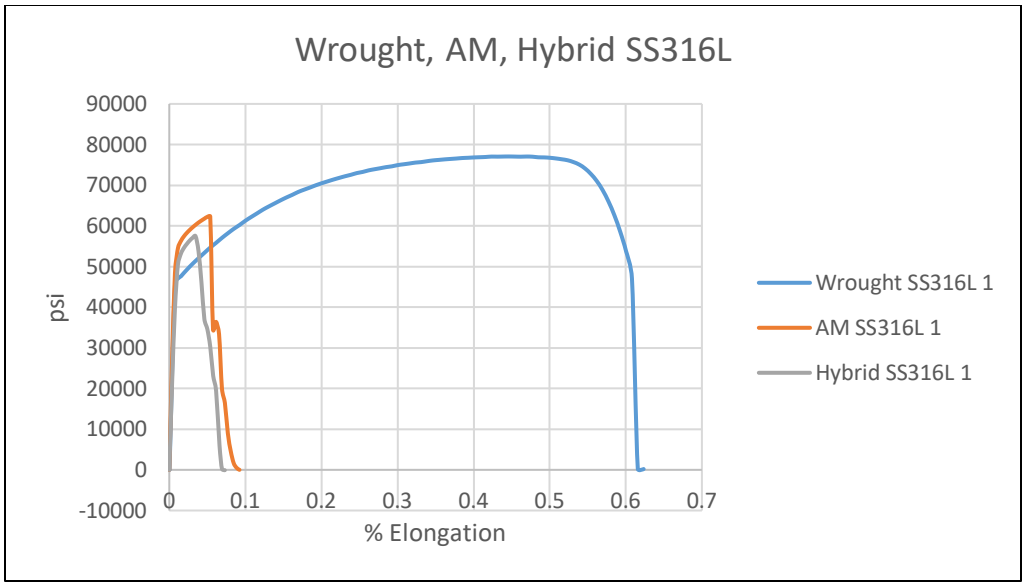

Figure 4-53: Wrought, Am, and Hybrid SS316L Tensile Test Curves

Table 4-6: Average Stresses of DED Processed SS316L Tensile Specimens

	Wrought SS316L	DED-AM SS316L	Interface SS316L
σ_{yield}	45,000 psi (310 MPa)	52,000 psi (359 MPa)	50,000 psi (345 MPa)
$\sigma_{ultimate}$	78,000 psi (538 MPa)	59,000 psi (407 MPa)	65,000 psi (448 MPa)

4.2.3 Microscopy

Sections were cut from the DED processed hybrid SS316L and hybrid M300 material. These were mounted, polished, etched, and viewed microscopically. Images were captured, and are displayed below.

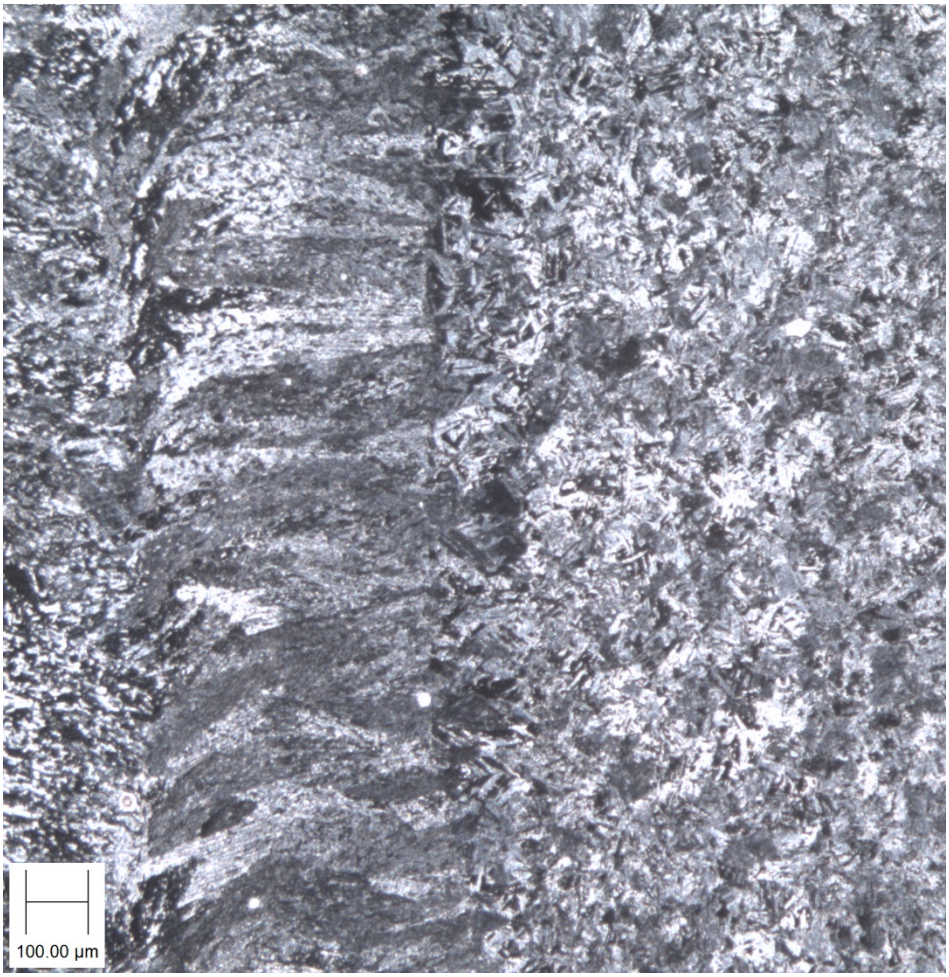

Figure 4-54: DED Hybrid M300 Interface @ 63X

The image above of the DED processed M300 hybrid specimen interface clearly displays the boundary between the two different grain sizes and geometries. The interface shows good metallurgical bonding. No voids are apparent. This is consistent with the performance of the DED processed M300 specimens.

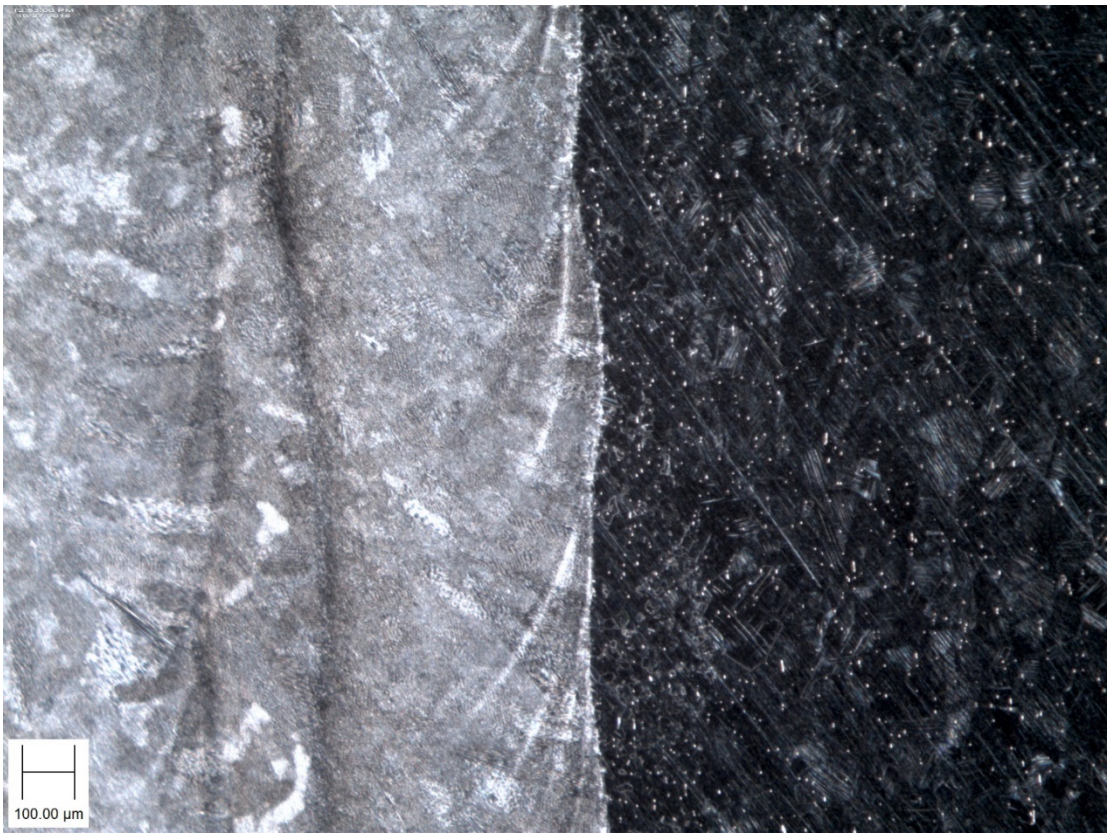

Figure 4-55: DED Hybrid SS316L Interface @ 63X

The image above of the DED processed hybrid SS316L interface has a sharp contrast between the two different processes. On the additive side you can see the deposition layers. The grain sizes and geometries are different when comparing the two processes. The interface has no apparent voids, and appears to have good metallurgical bonding. This is once again consistent with the performance of the DED processed SS316L hybrid specimens.

The surfaces of the wrought SS316L and M300 materials were machined to a smooth finish using a manual mill. Other than ensuring the surfaces were clean and dry, no further treatments or preparations were performed prior to the additive processing.

5 CONCLUSIONS AND RECOMMENDATIONS

Individual analyses of each specimen type have been given, section by section, throughout this paper. This section includes a comparison and analysis between the two additive processes, PBF-L and DED, as well as an overall analysis of the performance of the interface between an additive specimen and its substrate. This will be done by answering the research questions posed in the introduction.

5.1 Conclusions

5.1.1 Research Questions

1) Regarding mechanical properties, how does the interfacial bond between AM materials and metal substrates compare with stresses experienced in rotary tool applications?

There are many factors that go into the material selection of the tools that will be used in FSW processes (Rai, De, Bhadeshia, & DebRoy, 2011). In this work SS316L and M300 steel have been used. Steels of varying alloys and carbon content can be used in FSW processes, and so SS316L and M300 are to be considered a reasonable choice.

Through the mechanical testing performed in this work, it has been validated that the interfacial bond between these additive steels (SS316L and M300) and their corresponding wrought substrates perform as well as the additive material, and perform better than the wrought

material. With this knowledge, it is reasonable to assume that the interface would hold under the stresses experienced in most rotary tool applications, such as FSW.

As tool metals undergo specific treatments, it is unnecessary to compare the metals in this work directly to FSW tooling metals. Performing various treatments on hybrid metal samples in order to investigate more particularly into tooling applications is a good recommendation for future works.

2) How do the mechanical properties of parts printed onto a substrate via PBF-L and DED compare to their wrought counterparts?

In five out of the six hybrid specimen types tested in this work, the result was consistently similar to whichever material exhibited weaker mechanical properties. If the wrought material performed worse than the additive material, the hybrid specimen would follow the behavior of the wrought material. In a few cases where the wrought and additive material performed similarly, the crossover in performance properties would follow the path of least resistance. This was displayed by the DED processed SS316L tensile tests. The hybrid test curves displayed a mix of additive and wrought behaviors.

In the sixth case, however, there is an example of a hybrid specimen forming a synergistic relationship in order to outperform both wrought and additive materials. This occurred with the DED processed SS316L torsion test specimens. The reason for this is unknown. It is possible that the stronger additive material forced the deformation into the wrought SS316L material and caused work hardening to occur, but this is uncertain.

3) How do the mechanical properties of the hybrid PBF-L interfaces compare with those processed via DED?

It is difficult to compare the interfaces produced by these processes through an analysis of the mechanical tests in this work because none of the interfaces experienced failure. In most cases, the interface did not even experience deformation, as all strain occurred in the weaker half of the specimen. The mechanical data collected from the hybrid samples is mainly a result of the stress and strain experienced by the wrought portion of the specimens, with a few exceptions where the wrought and additive materials were similar in mechanical performance. In these instances, it is possible that the interface experienced deformation.

In this work, the two additive processes used were PBF-L and DED. In all of the PBF-L tests, the resulting failures occurred in the wrought material. The DED processed specimens were not always so clear. While most deformation and failures occurred in the wrought material, some specimens (SS316L torsion and SS316L tensile) produced situations where the deformation may have taken place across the interface. In these situations, the interfaces did not experience failure. In the case of the DED processed SS316L torsion specimens, the increase in mechanical performance of the hybrid specimen when compared to wrought and additive materials could potentially be attributed to material interactions through the interface. If this is the case, it only occurs when the wrought and additive materials exhibit similar mechanical properties. This could be why it did not occur in the PBF-L specimens, as the additive SS316L exhibits much higher stress load capability than the wrought SS316L.

A microscopic analysis can be made to compare the interfaces produce by DED and PBF-L. The only sample available from the PBF-L process is SS316L, and so that is the metal used to compare the two interfaces.

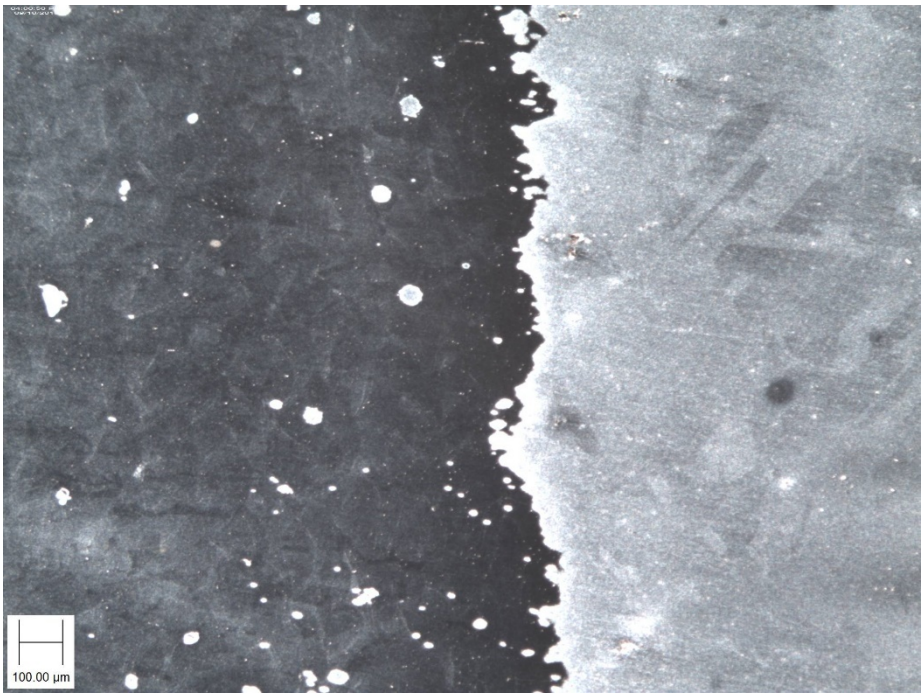

Figure 5-1: PBF-L Processed SS316L AM/Substrate Interface

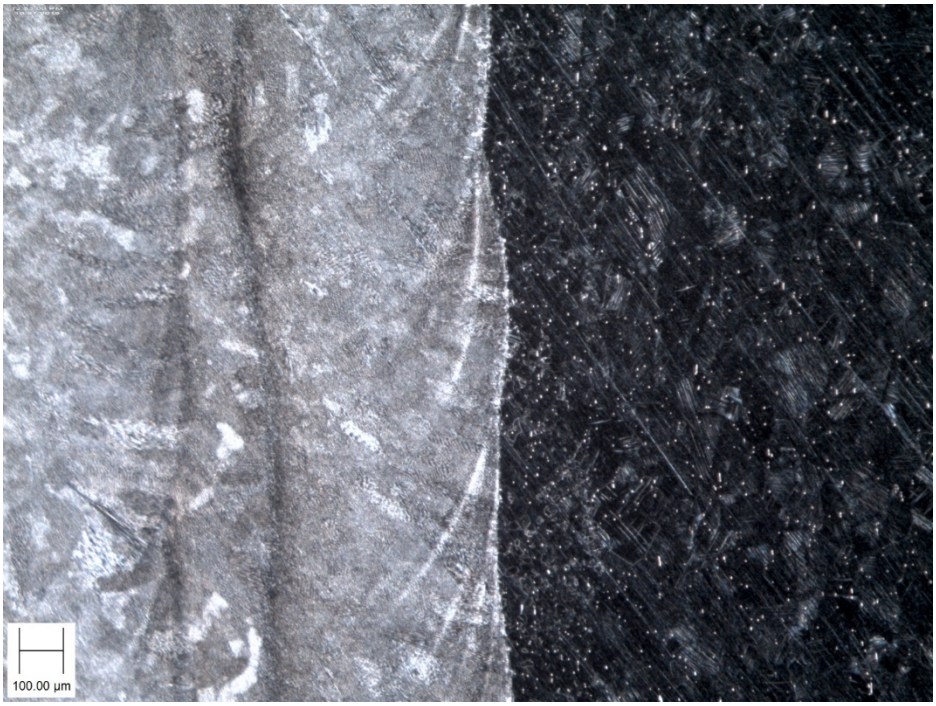

Figure 5-2: DED Processed SS316L AM/Substrate Interface

In the two images above the additive portion is on the left side and the wrought portion is on the right. It is apparent that the PBF-L processed specimen has an interface that merged and mixed together to some extent. Possibly the laser melted the substrate surface slightly as it was melting the AM powder. The DED processed specimen has a very clearly defined boundary between the AM and wrought materials. The molten metal being deposited onto the substrate does not seem to mix like it did in the PBF-L samples.

Whether one of these interfaces will have better mechanical properties than the other is unclear. More experimentation can be done to interrogate these two interface types, such as microhardness tests, EBSD, and Charpy impact tests.

5.2 Recommendations

Additive manufacturing is a rapidly growing field. There is great need for further research and validations in order to produce the foundation of knowledge necessary for many industries to begin adopting and advancing AM technologies.

Due to lack of time and resources, this work was not able to include many desirable experiments.

1) Rotary Beam Fatigue Test

A common test method for testing fatigue of a cylinder under rotation is a rotary beam fatigue test. This would have high relevance towards rotary tool applications.

2) Electron Backscatter Diffraction (EBSD)

The microscopy performed in this experimentation was useful for observing the general bonding condition between additive material and wrought material. EBSD would provide useful

information for characterizing the interface at a deeper level. More information regarding the crystal structures and material phases in the heat affected zone would aid in increasing the understanding of how different AM processes affect substrate surfaces.

3) Surface Finish and Laser/Energy Parameters

Experimenting with various styles of surface finishes on the substrate to see how the bond strength would be affected. Also testing out different deposition or laser parameters, such as power density, deposition/laser pattern, spot size, scan speed, et cetera… to see how each would affect the interface.

REFERENCES

Arora, A., Mehta, M., De, A., & DebRoy, T. (2012). Load bearing capacity of tool pin during friction stir welding. *The International Journal of Advanced Manufacturing Technology, 61*(9), 911-920. doi:10.1007/s00170-011-3759-7

Atzeni, E., & Salmi, A. (2012). Economics of additive manufacturing for end-usable metal parts. *The International Journal of Advanced Manufacturing Technology, 62*(9), 1147-1155. doi:10.1007/s00170-011-3878-1

Carroll, B. E., Palmer, T. A., & Beese, A. M. (2015). Anisotropic tensile behavior of Ti–6Al–4V components fabricated with directed energy deposition additive manufacturing. *Acta Materialia, 87*, 309-320. doi:https://doi.org/10.1016/j.actamat.2014.12.054

Davis, J. R. (2004). *Tensile Testing (2nd Ed.)*. Library of Congress: ASM International.

DebRoy, T., Wei, H. L., Zuback, J. S., Mukherjee, T., Elmer, J. W., Milewski, J. O., . . . Zhang, W. (2018). Additive manufacturing of metallic components – Process, structure and properties. *Progress in Materials Science, 92*, 112-224. doi:https://doi.org/10.1016/j.pmatsci.2017.10.001

Everton, S. K., Hirsch, M., Stravroulakis, P., Leach, R. K., & Clare, A. T. (2016). Review of in-situ process monitoring and in-situ metrology for metal additive manufacturing. *Materials & Design, 95*, 431-445. doi:https://doi.org/10.1016/j.matdes.2016.01.099

Fatemi, A., Molaei, R., Sharifimehr, S., Shamsaei, N., & Phan, N. (2017). Torsional fatigue behavior of wrought and additive manufactured Ti-6Al-4V by powder bed fusion including surface finish effect. *International Journal of Fatigue, 99*, 187-201. doi:https://doi.org/10.1016/j.ijfatigue.2017.03.002

Frazier, W. E. (2014). Metal Additive Manufacturing: A Review. *Journal of Materials Engineering and Performance, 23*(6), 1917-1928. doi:10.1007/s11665-014-0958-z

Huang, Y., Leu, M. C., Mazumder, J., & Donmez, A. (2015). Additive Manufacturing: Current State, Future Potential, Gaps and Needs, and Recommendations. *Journal of Manufacturing Science and Engineering, 137*(1), 014001-014001-014010. doi:10.1115/1.4028725

Jones, J. B., McNutt, P., Tosi, R., Perry, C., & Wimpenny, D. I. (2012). Remanufacture of turbine blades by laser cladding, machining and in-process scanning in a single machine.

Kamath, C., El-dasher, B., Gallegos, G. F., King, W. E., & Sisto, A. J. T. I. J. o. A. M. T. (2014). Density of additively-manufactured, 316L SS parts using laser powder-bed fusion at powers up to 400 W. *74*(1-4), 65-78.

King, W. E., Anderson, A. T., Ferencz, R. M., Hodge, N. E., Kamath, C., Khairallah, S. A., & Rubenchik, A. M. (2015). Laser powder bed fusion additive manufacturing of metals; physics, computational, and materials challenges. *Applied Physics Reviews, 2*(4), 041304. doi:10.1063/1.4937809

Luo, J., Wang, H., Chen, W., & Li, L. (2015). Study on anti-wear property of 3D printed-tools in friction stir welding by numerical and physical experiments. *The International Journal of Advanced Manufacturing Technology, 77*(9), 1781-1791. doi:10.1007/s00170-014-6571-3

Marco, G., & Bianca Maria, C. (2017). Process defects and in situ monitoring methods in metal powder bed fusion: a review. *Measurement Science and Technology, 28*(4), 044005.

Matsumoto, M., Yang, S., Martinsen, K., & Kainuma, Y. (2016). Trends and research challenges in remanufacturing. *International Journal of Precision Engineering and Manufacturing-Green Technology, 3*(1), 129-142. doi:10.1007/s40684-016-0016-4

Mellor, S., Hao, L., & Zhang, D. (2014). Additive manufacturing: A framework for implementation. *International Journal of Production Economics, 149*, 194-201. doi:https://doi.org/10.1016/j.ijpe.2013.07.008

Miller, D., Morris, E., & Colvin, G. (2016). *Metals Additive Manufacturing. Great Promise in Mitigating Shortages but Some Risks Remain*. Retrieved from

Mower, T. M., Long, M. J. J. M. S., & A, E. (2016). Mechanical behavior of additive manufactured, powder-bed laser-fused materials. *651*, 198-213.

Nam, S., Cho, H., Kim, C., & Kim, Y.-M. (2018). Effect of Process Parameters on Deposition Properties of Functionally Graded STS 316/Fe Manufactured by Laser Direct Metal Deposition. *8*(8), 607.

Rai, R., De, A., Bhadeshia, H. K. D. H., & DebRoy, T. (2011). Review: friction stir welding tools. *Science and Technology of Welding and Joining, 16*(4), 325-342. doi:10.1179/1362171811Y.0000000023

Scipioni Bertoli, U., MacDonald, B. E., & Schoenung, J. M. (2019). Stability of cellular microstructure in laser powder bed fusion of 316L stainless steel. *Materials Science and Engineering: A, 739*, 109-117. doi:https://doi.org/10.1016/j.msea.2018.10.051

Sun, Z., Tan, X., Tor, S. B., Yeong, W. Y. J. M., & Design. (2016). Selective laser melting of stainless steel 316L with low porosity and high build rates. *104*, 197-204.

Wilson, J. M., Piya, C., Shin, Y. C., Zhao, F., & Ramani, K. (2014). Remanufacturing of turbine blades by laser direct deposition with its energy and environmental impact analysis. *Journal of Cleaner Production, 80*, 170-178. doi:https://doi.org/10.1016/j.jclepro.2014.05.084

Yang, S., Kang, H., Kim, H., Song, J., & Park, J. (1999). *Influence of loading speed on tensile strength characteristics of high tensile steel.* Paper presented at the ECF13, San Sebastian 2000.

Yao, Y., Huang, Y., Chen, B., Tan, C., Su, Y., Feng, J. J. O., & Technology, L. (2018). Influence of processing parameters and heat treatment on the mechanical properties of 18Ni300 manufactured by laser based directed energy deposition. *105*, 171-179.

Yusuf, S., Chen, Y., Boardman, R., Yang, S., & Gao, N. (2017). Investigation on Porosity and Microhardness of 316L Stainless Steel Fabricated by Selective Laser Melting. *7*(2), 64.

Zuback, J. S., & DebRoy, T. (2018). The Hardness of Additively Manufactured Alloys. *11*(11), 2070.

APPENDIX A. TEST DATA

A.1 Test Data

PBF-L Tests

Torsion Tests

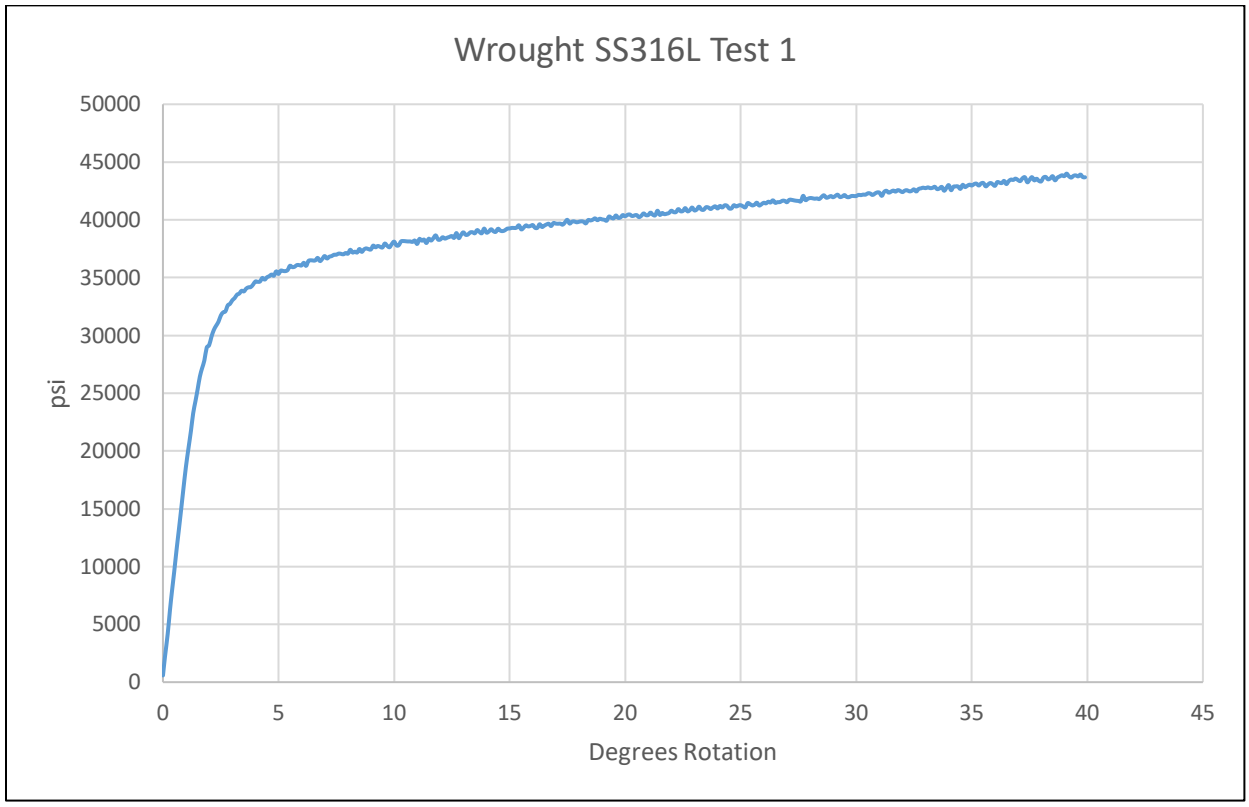

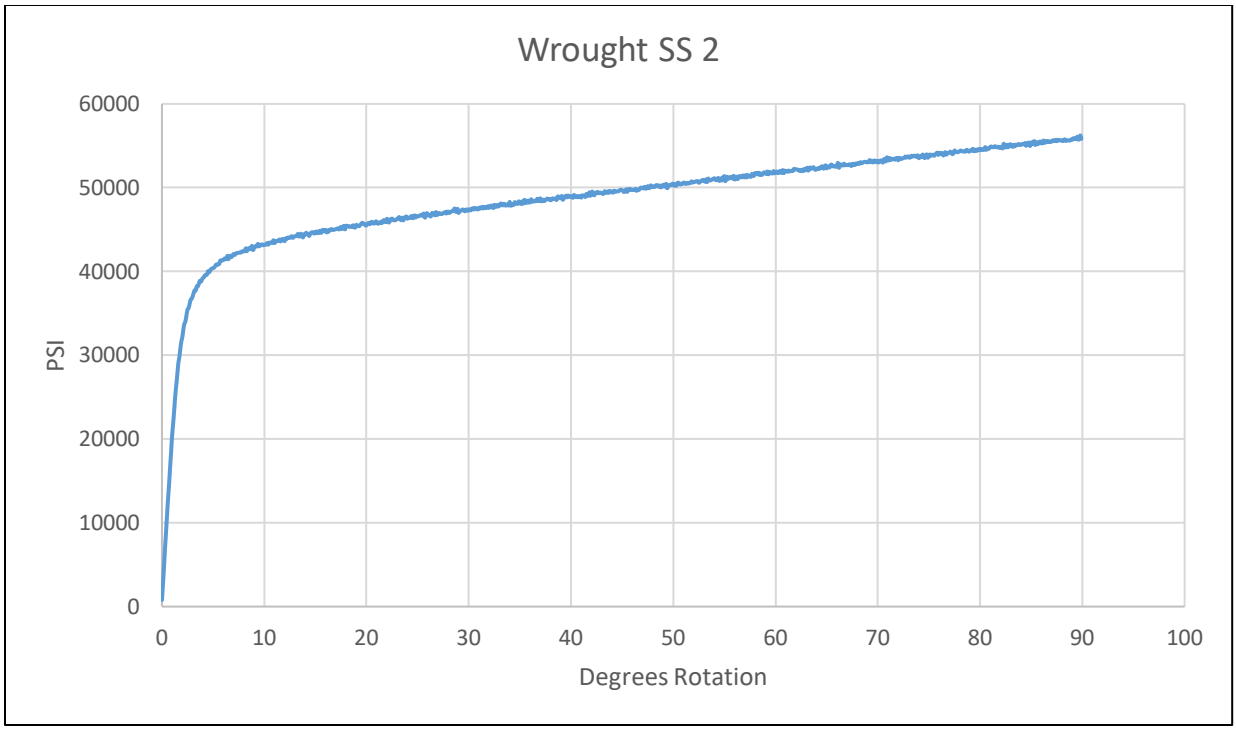
Wrought SS 2
60000
50000
40000
30000
20000
10000
0
PSI
0
10
20
30
40
50
60
70
80
90
100
Degrees Rotation

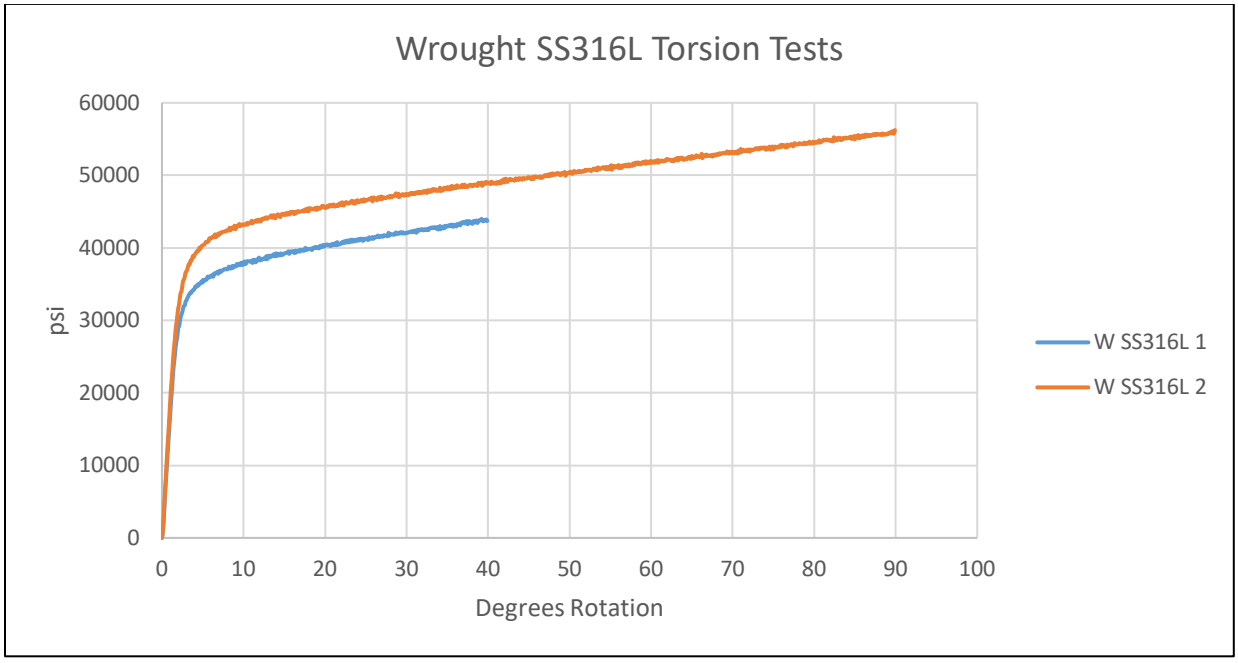
Wrought SS316L Torsion Tests
60000
50000
40000
30000
20000
10000
0
psi
0
10
20
30
40
50
60
70
80
90
100
Degrees Rotation
W SS316L 1
W SS316L 2

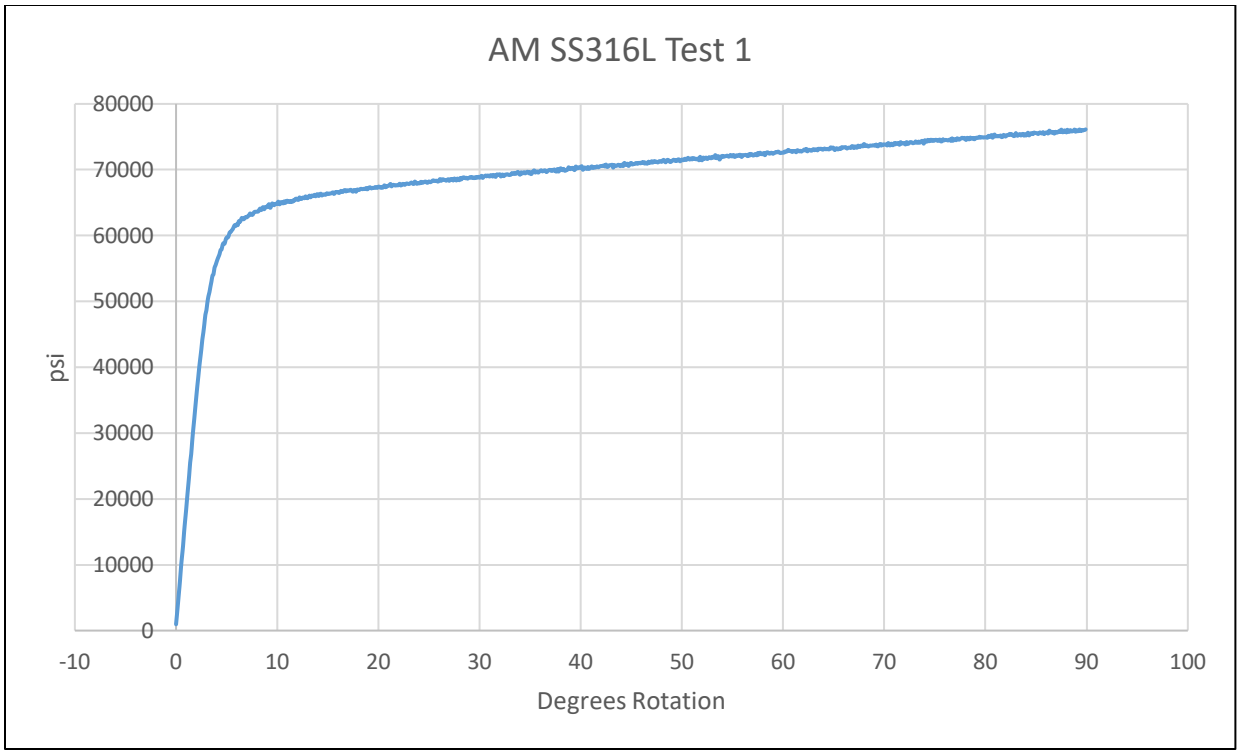
AM SS316L Test 1
80000
70000
60000
50000
40000
30000
20000
10000
0
psi
-10
0
10
20
30
40
50
60
70
80
90
100
Degrees Rotation

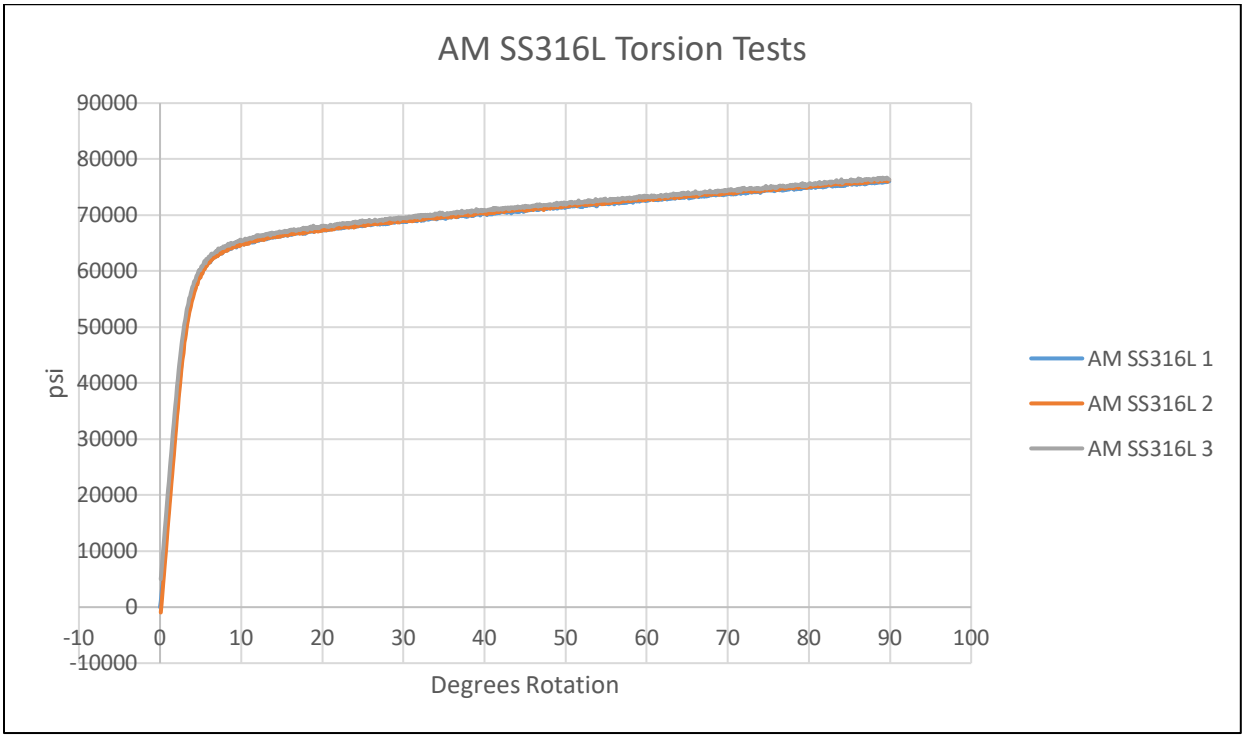
AM SS316L Torsion Tests
90000
80000
70000
60000
50000
40000
30000
20000
10000
0
-10000
psi
-10
0
10
20
30
40
50
60
70
80
90
100
Degrees Rotation
AM SS316L 1
AM SS316L 2
AM SS316L 3

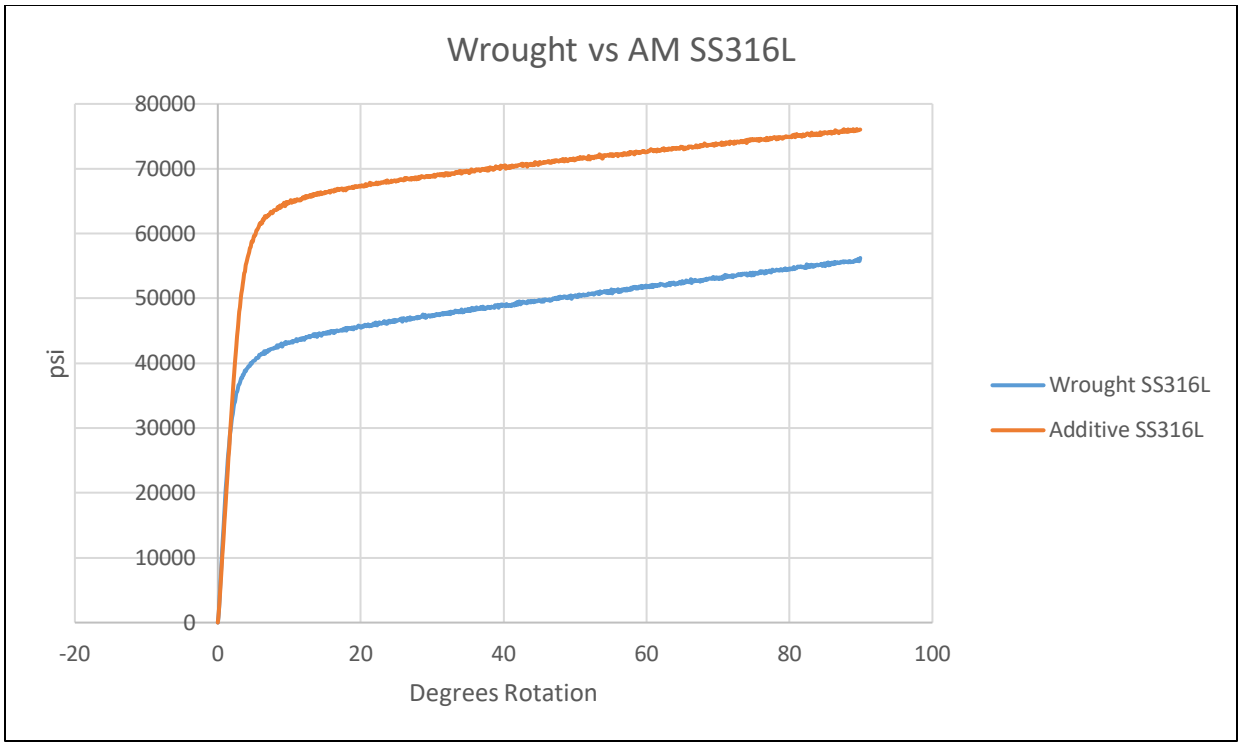
Wrought vs AM SS316L
80000
70000
60000
50000
40000
30000
20000
10000
0
psi
-20
0
20
40
60
80
100
Degrees Rotation
Wrought SS316L
Additive SS316L

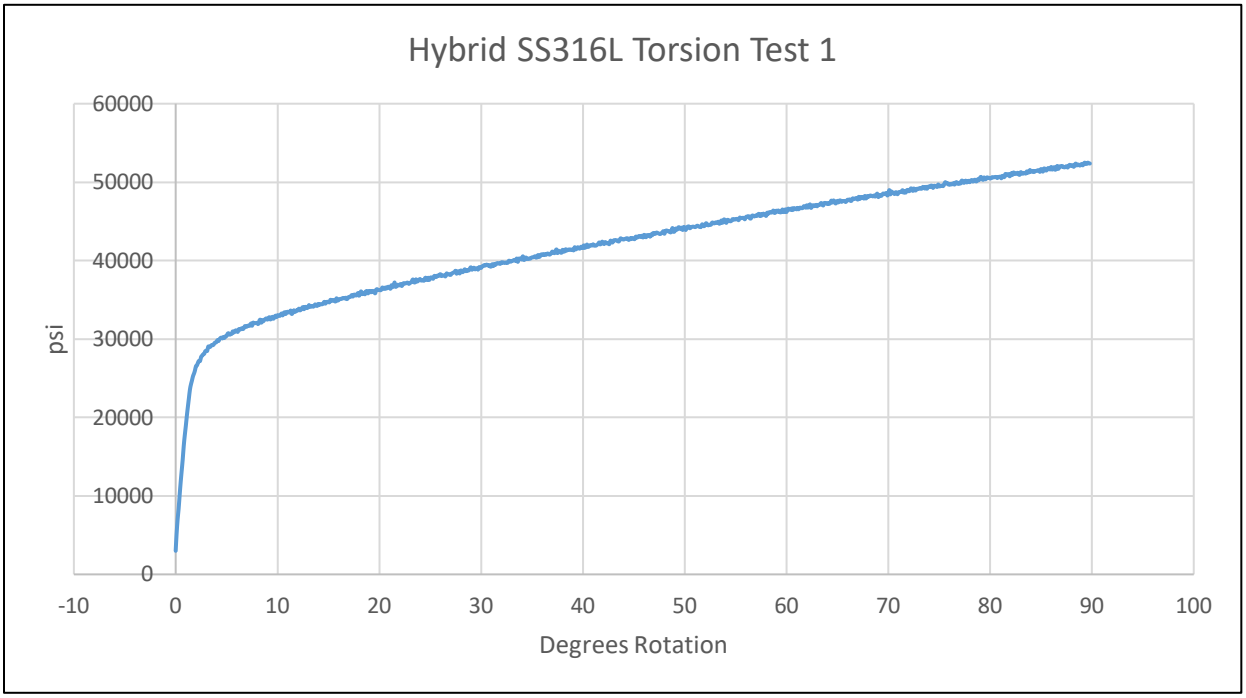
Hybrid SS316L Torsion Test 1
60000
50000
40000
30000
20000
10000
0
psi
-10
0
10
20
30
40
50
60
70
80
90
100
Degrees Rotation

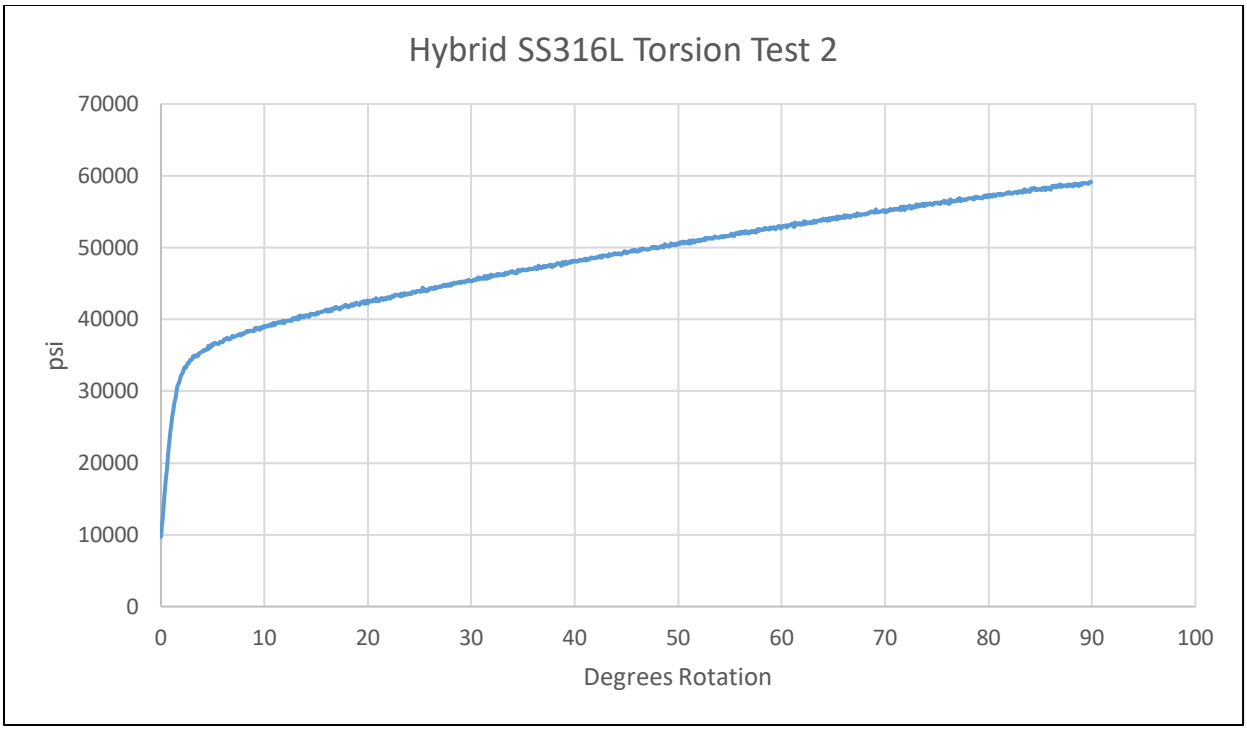
Hybrid SS316L Torsion Test 2
70000
60000
50000
40000
30000
20000
10000
0
psi
0
10
20
30
40
50
60
70
80
90
100
Degrees Rotation

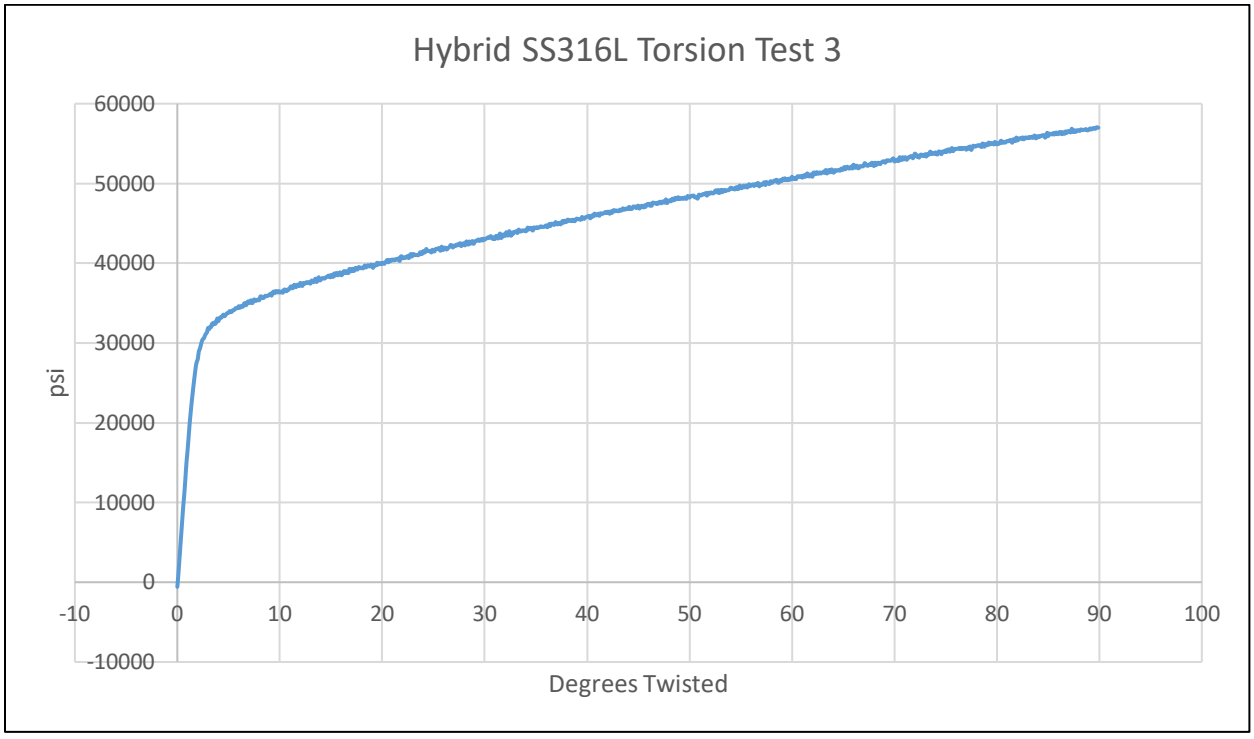
Hybrid SS316L Torsion Test 3
60000
50000
40000
30000
20000
10000
0
-10000
psi
-10
0
10
20
30
40
50
60
70
80
90
100
Degrees Twisted

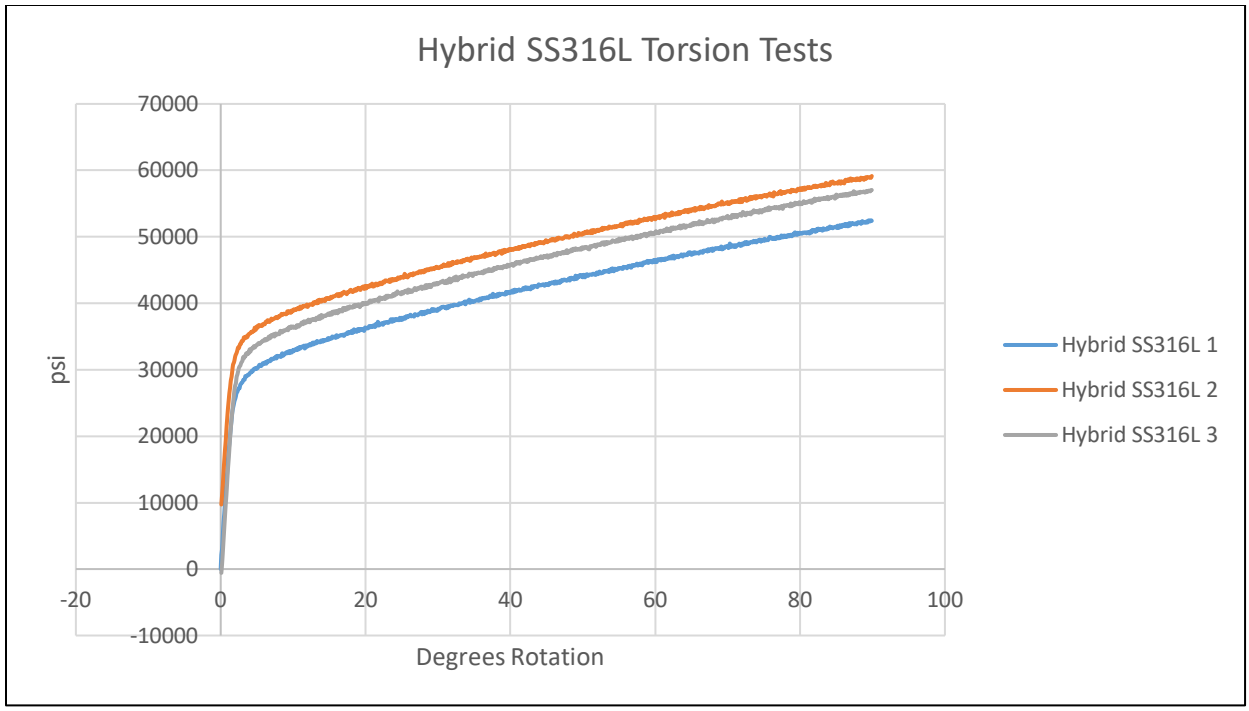
Hybrid SS316L Torsion Tests
70000
60000
50000
40000
30000
20000
10000
0
-10000
psi
-20
0
20
40
60
80
100
Degrees Rotation
Hybrid SS316L 1
Hybrid SS316L 2
Hybrid SS316L 3

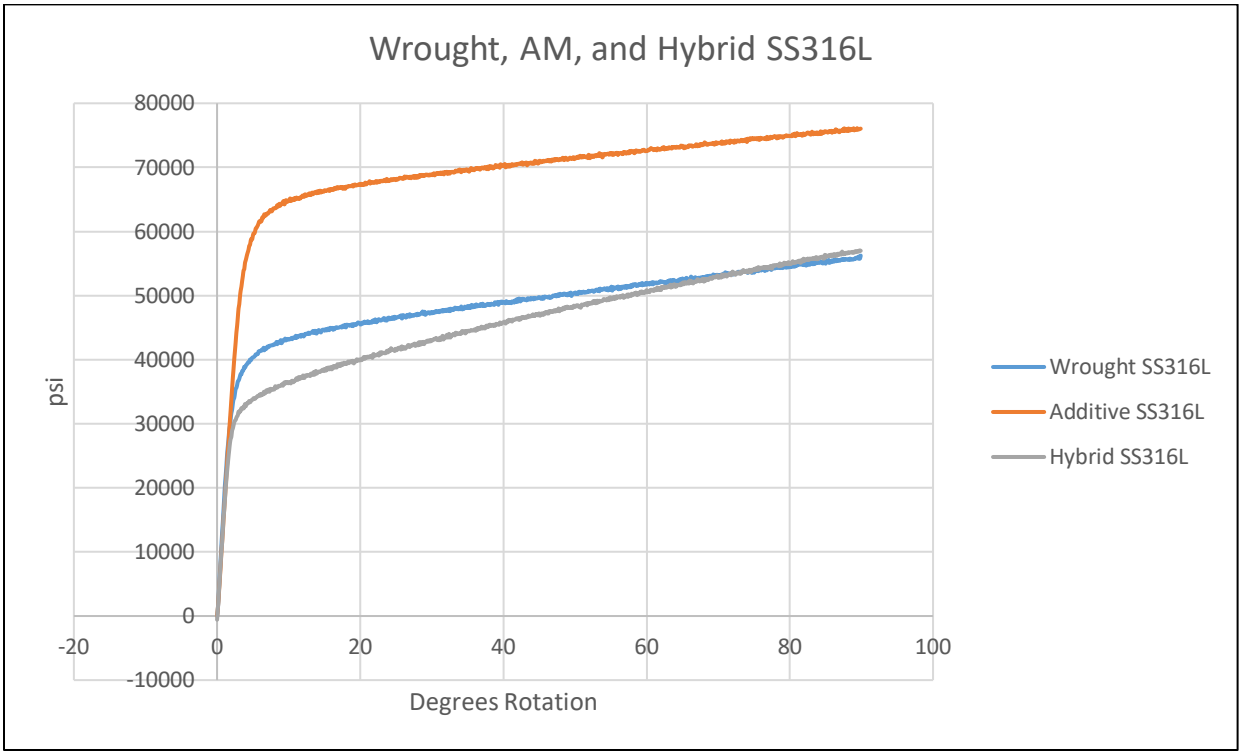
Wrought, AM, and Hybrid SS316L
80000
70000
60000
50000
40000
30000
20000
10000
0
-10000
psi
-20
0
20
40
60
80
100
Degrees Rotation
Wrought SS316L
Additive SS316L
Hybrid SS316L

Tensile Tests

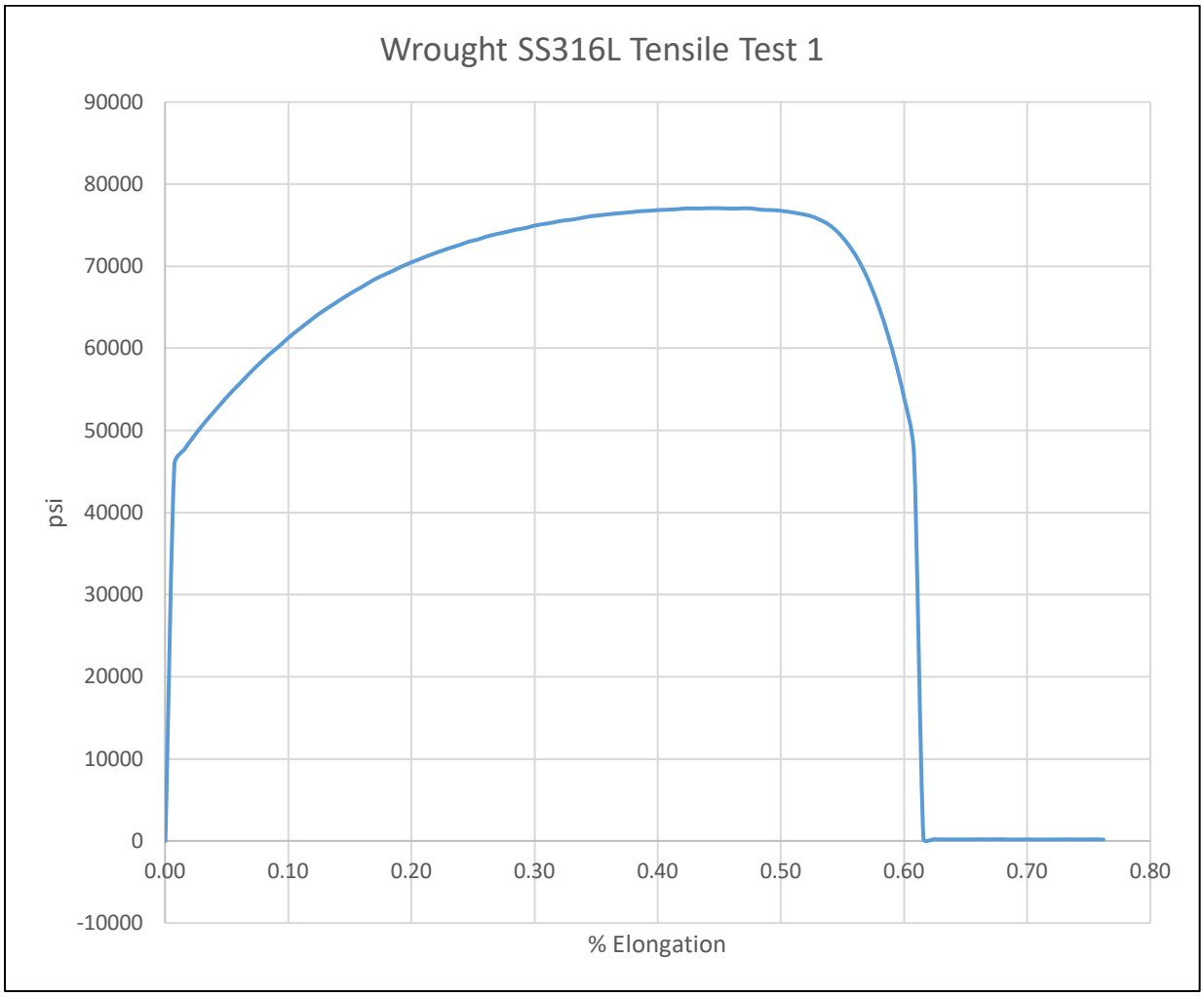

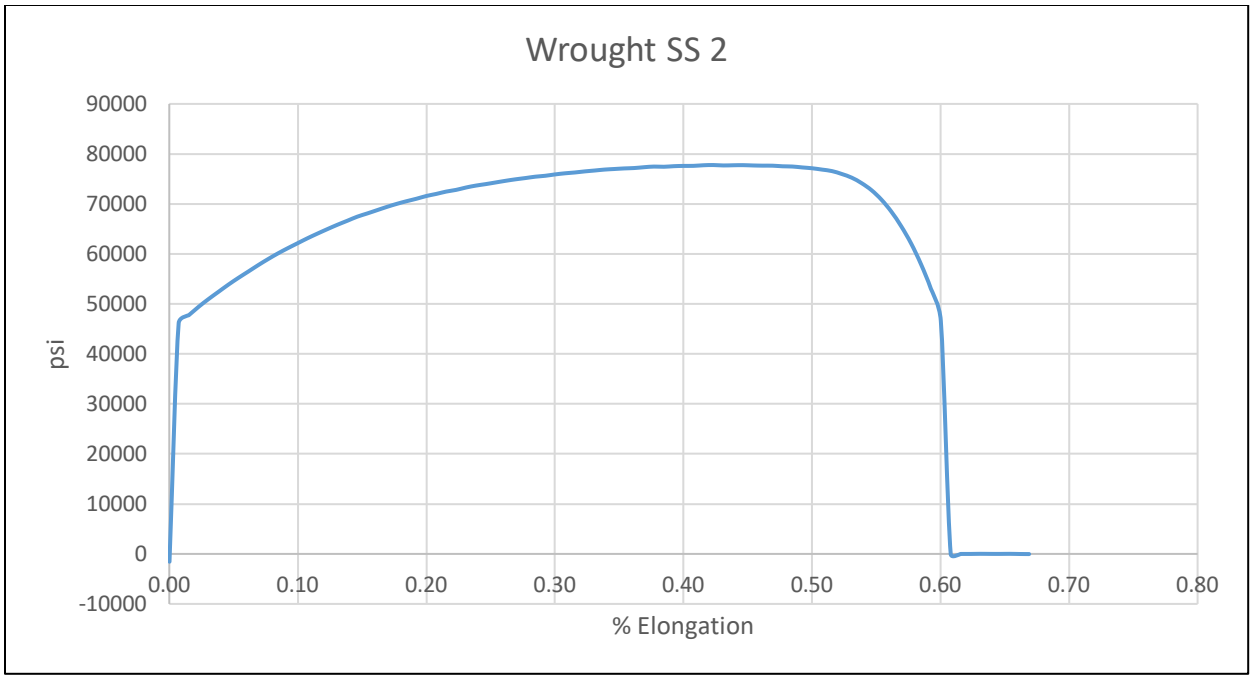
Wrought SS 2
90000
80000
70000
60000
50000
40000
30000
20000
10000
0
-10000
psi
0.00
0.10
0.20
0.30
0.40
0.50
0.60
0.70
0.80
% Elongation

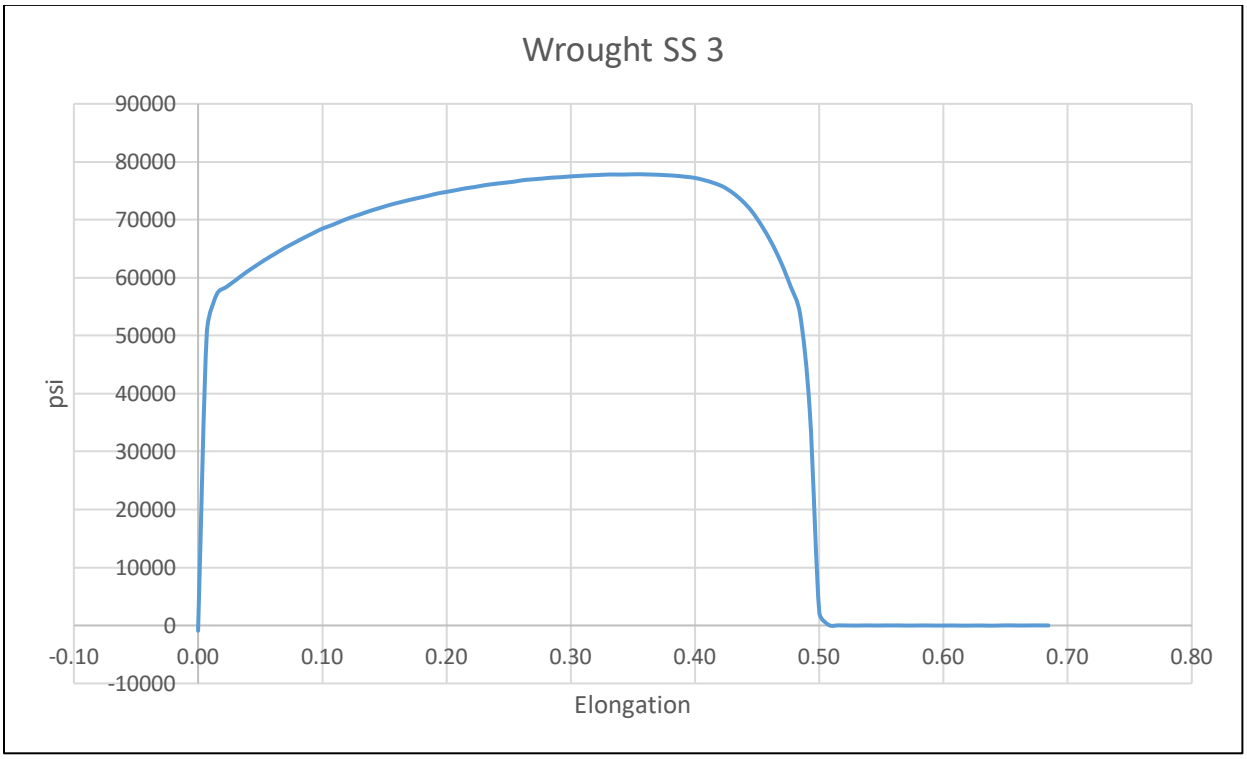
Wrought SS 3
90000
80000
70000
60000
50000
40000
30000
20000
10000
0
-10000
psi
-0.10
0.00
0.10
0.20
0.30
0.40
0.50
0.60
0.70
0.80
Elongation

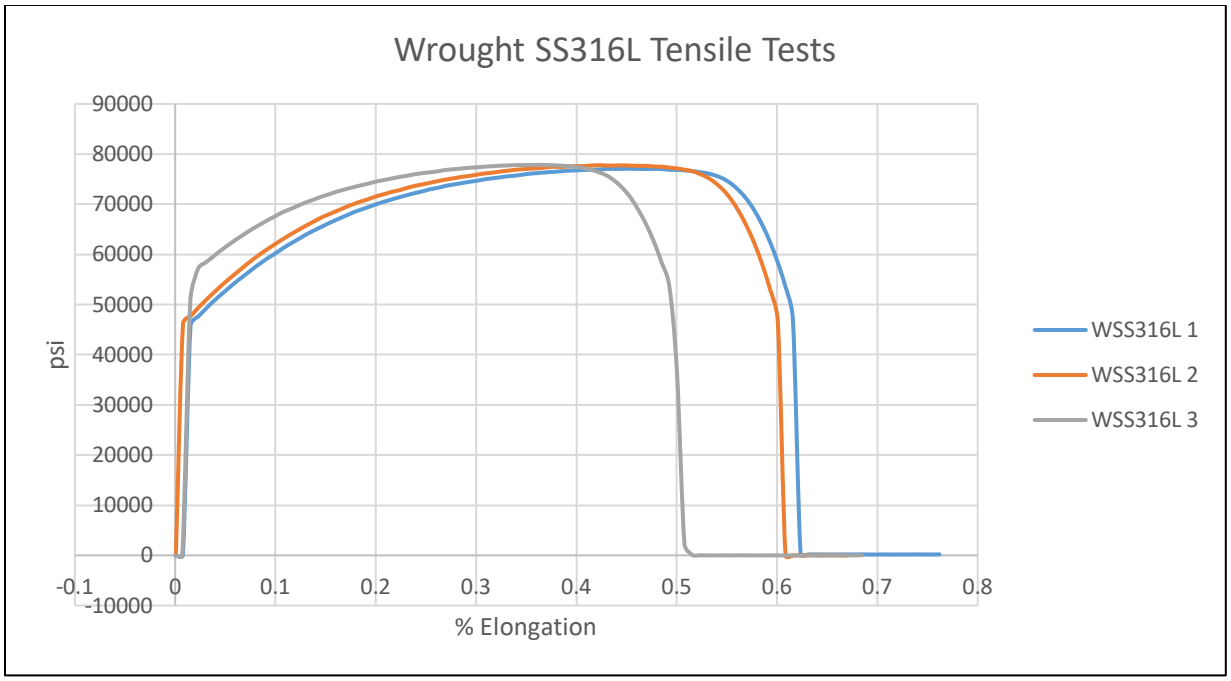
Wrought SS316L Tensile Tests
90000
80000
70000
60000
50000
40000
30000
20000
10000
0
-10000
psi
-0.1
0
0.1
0.2
0.3
0.4
0.5
0.6
0.7
0.8
% Elongation
WSS316L 1
WSS316L 2
WSS316L 3

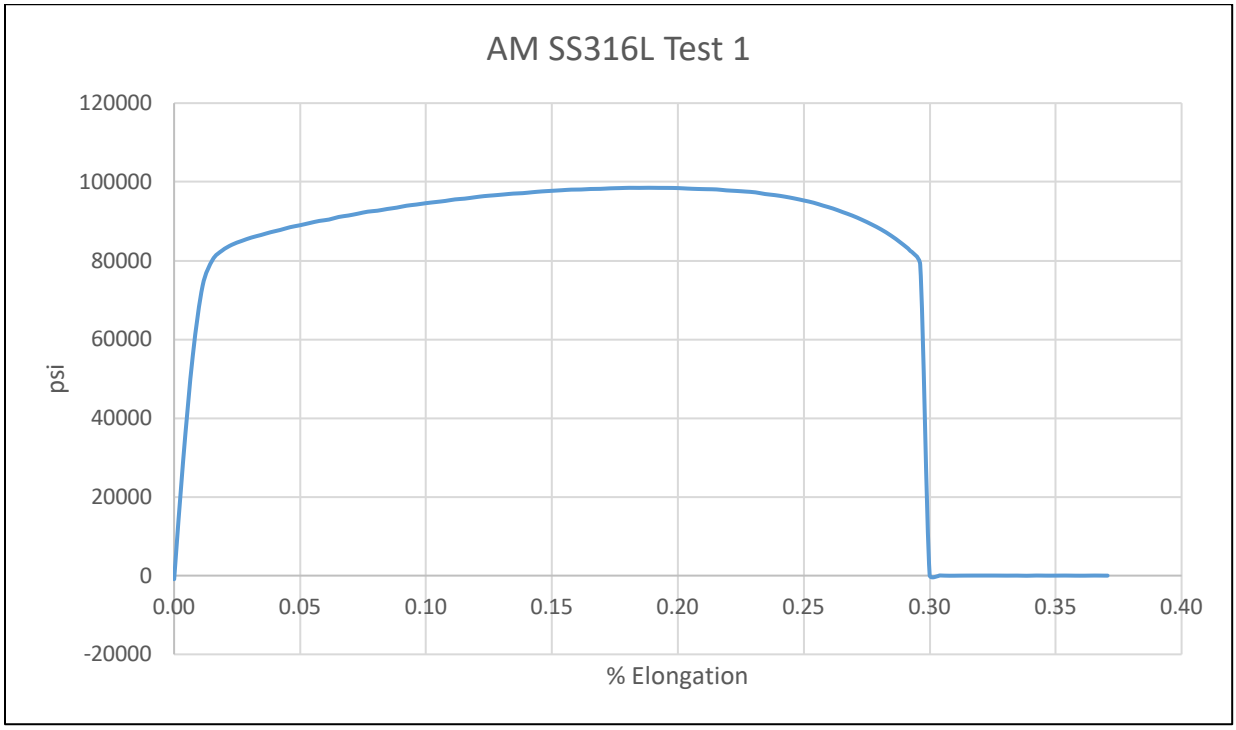
AM SS316L Test 1
120000
100000
80000
60000
40000
20000
0
-20000
psi
0.00
0.05
0.10
0.15
0.20
0.25
0.30
0.35
0.40
% Elongation

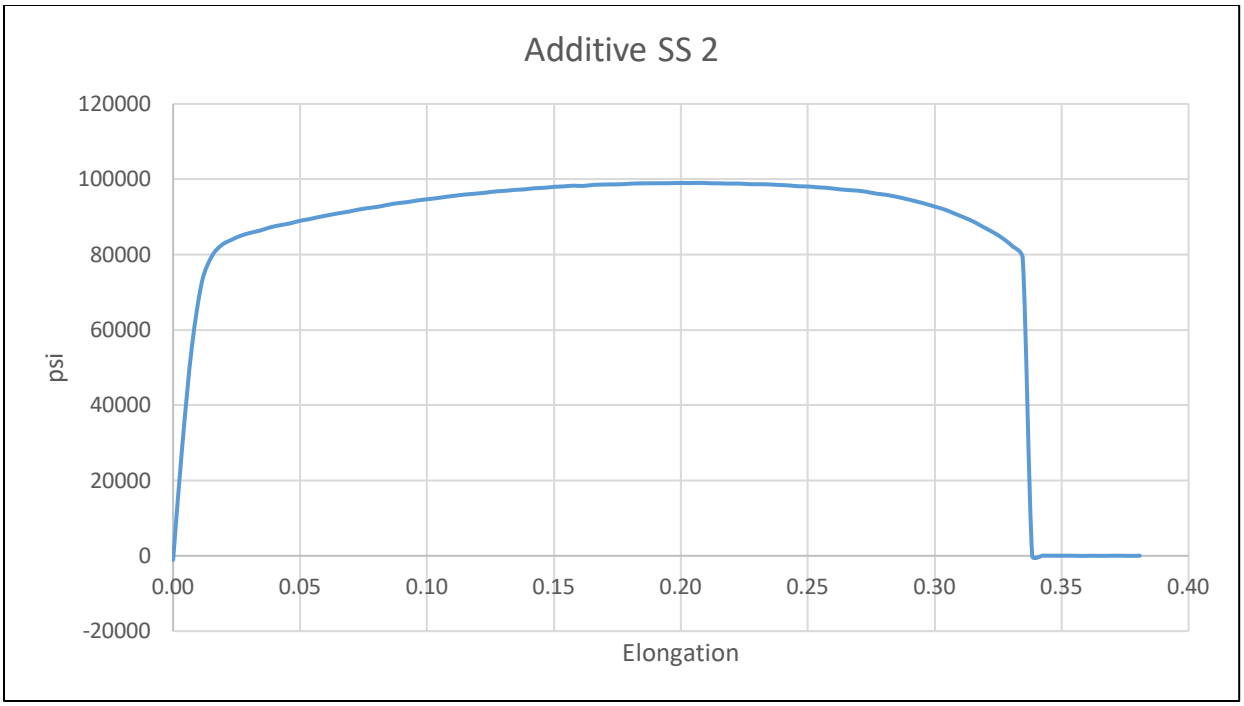
Additive SS 2
120000
100000
80000
60000
40000
20000
0
-20000
psi
0.00
0.05
0.10
0.15
0.20
0.25
0.30
0.35
0.40
Elongation

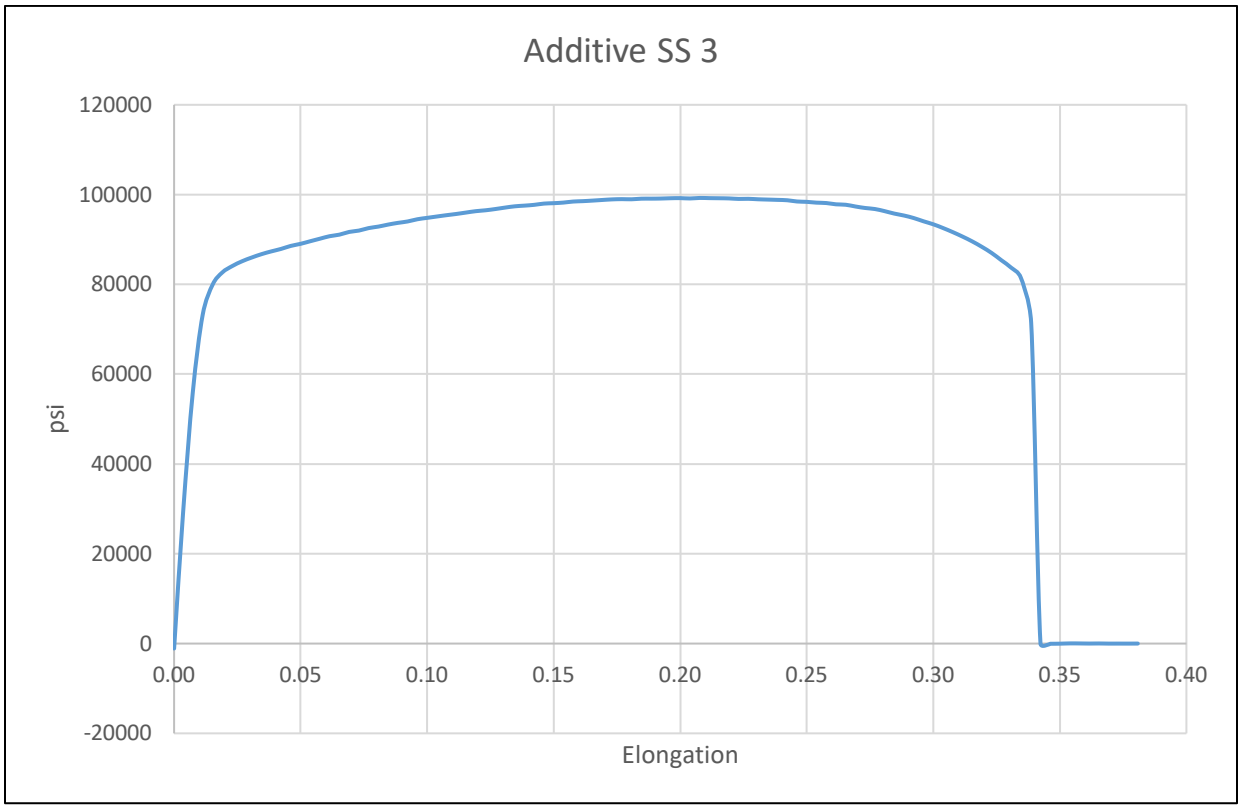
Additive SS 3
120000
100000
80000
60000
40000
20000
0
-20000
psi
0.00
0.05
0.10
0.15
0.20
0.25
0.30
0.35
0.40
Elongation

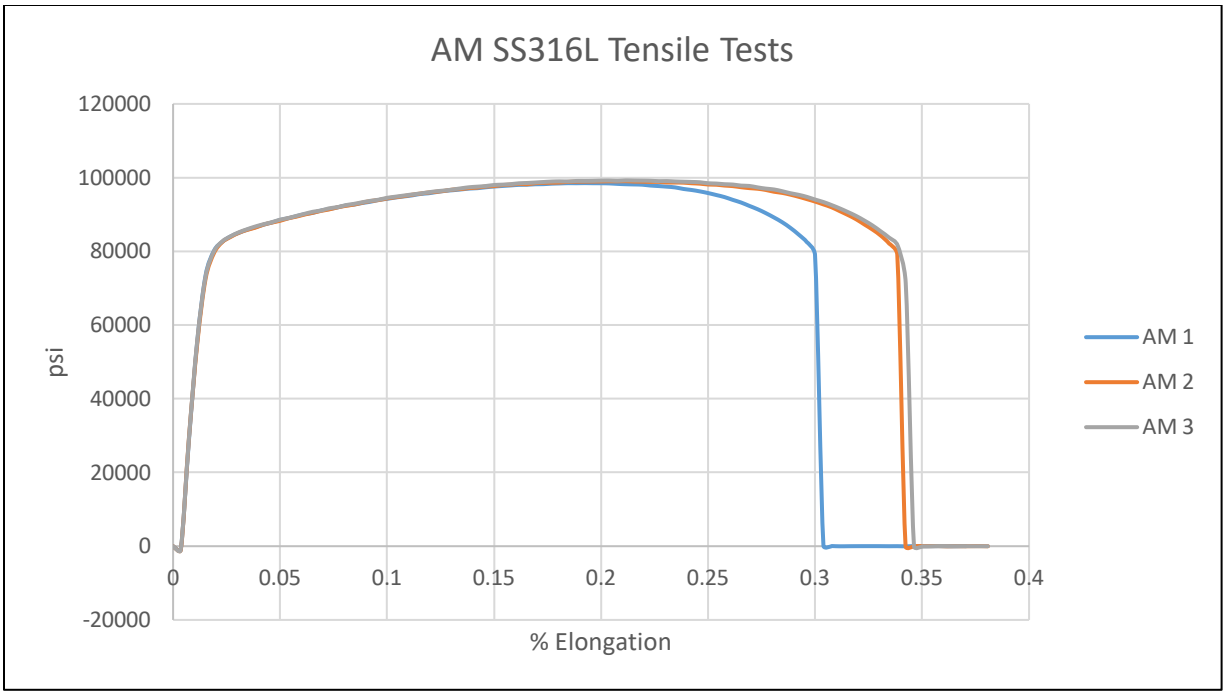
AM SS316L Tensile Tests
120000
100000
80000
60000
40000
20000
0
-20000
psi
0
0.05
0.1
0.15
0.2
0.25
0.3
0.35
0.4
% Elongation
AM 1
AM 2
AM 3

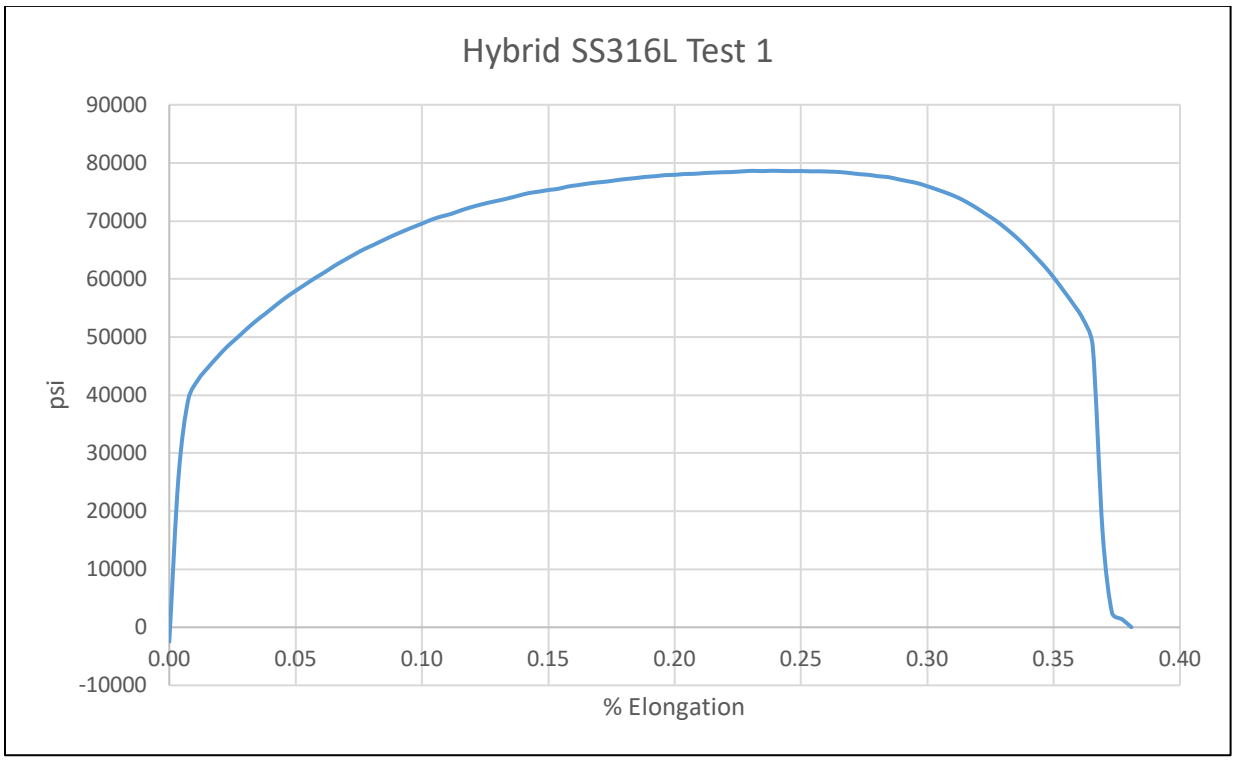
Hybrid SS316L Test 1
90000
80000
70000
60000
50000
40000
30000
20000
10000
0
-10000
psi
0.00
0.05
0.10
0.15
0.20
0.25
0.30
0.35
0.40
% Elongation

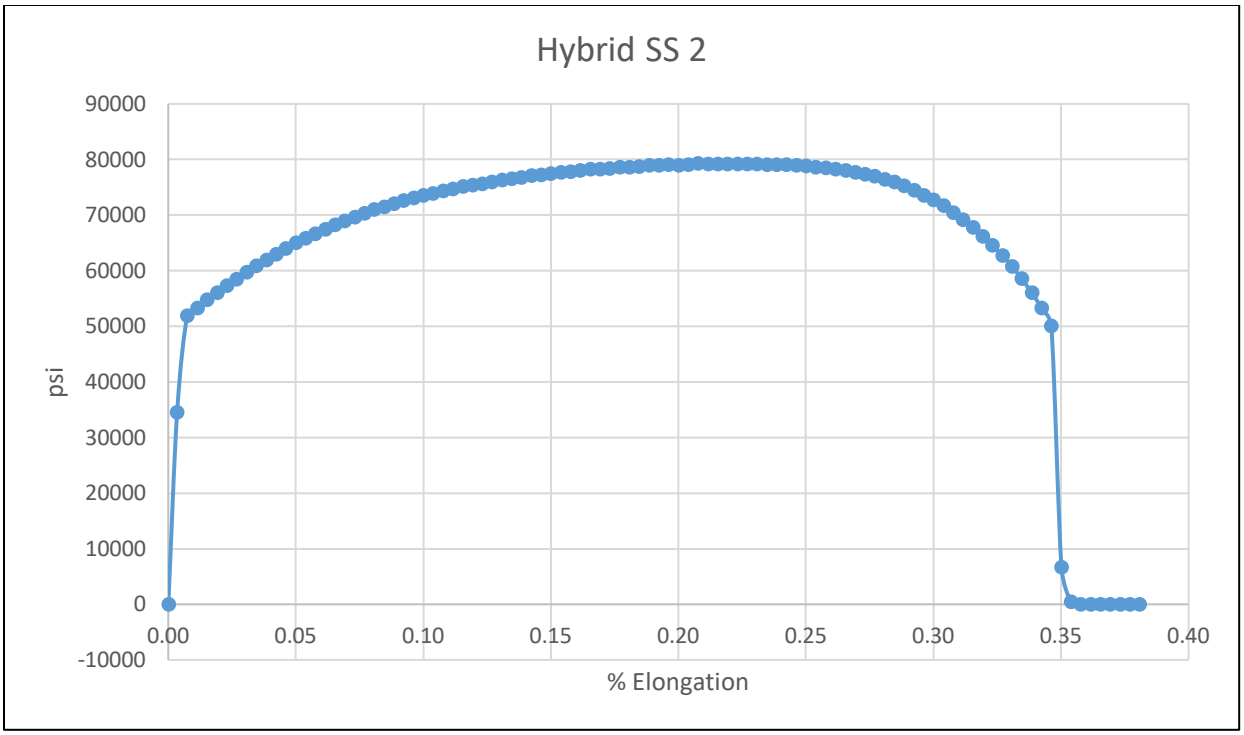
Hybrid SS 2
90000
80000
70000
60000
50000
40000
30000
20000
10000
0
-10000
psi
0.00
0.05
0.10
0.15
0.20
0.25
0.30
0.35
0.40
% Elongation

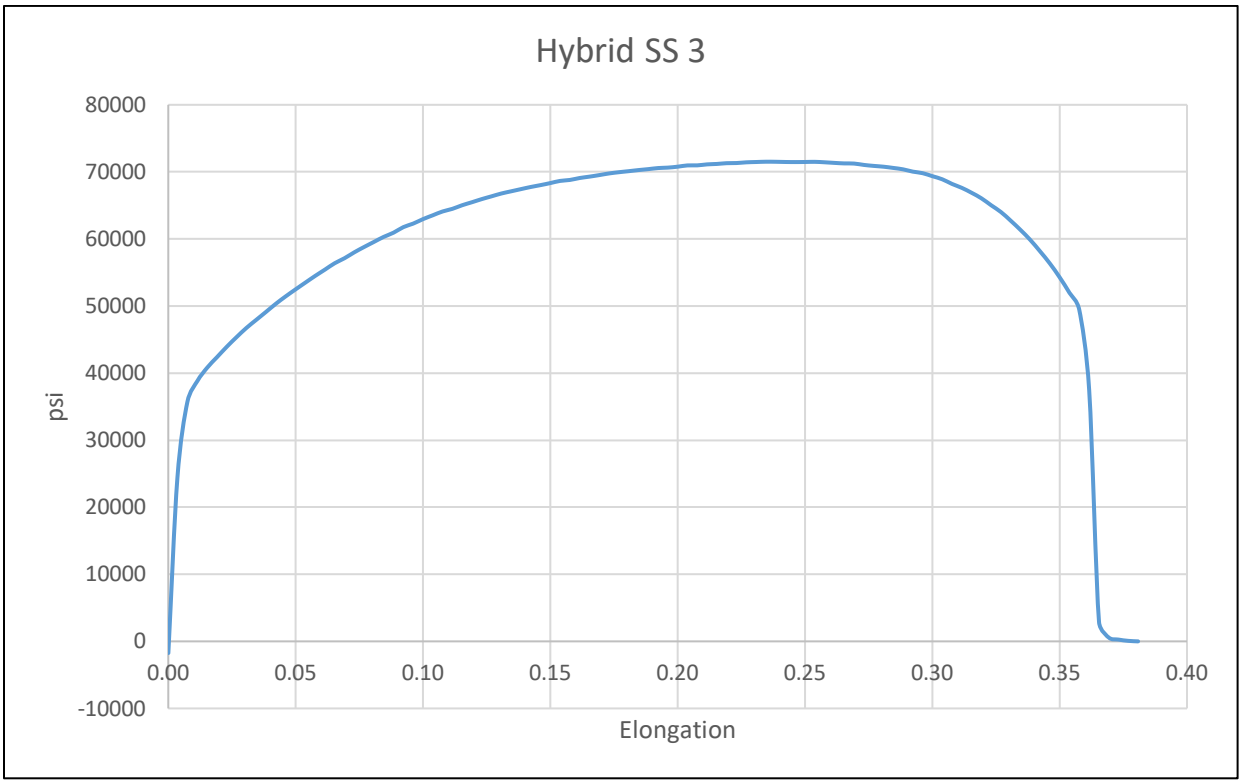
Hybrid SS 3
80000
70000
60000
50000
40000
30000
20000
10000
0
-10000
psi
0.00
0.05
0.10
0.15
0.20
0.25
0.30
0.35
0.40
Elongation

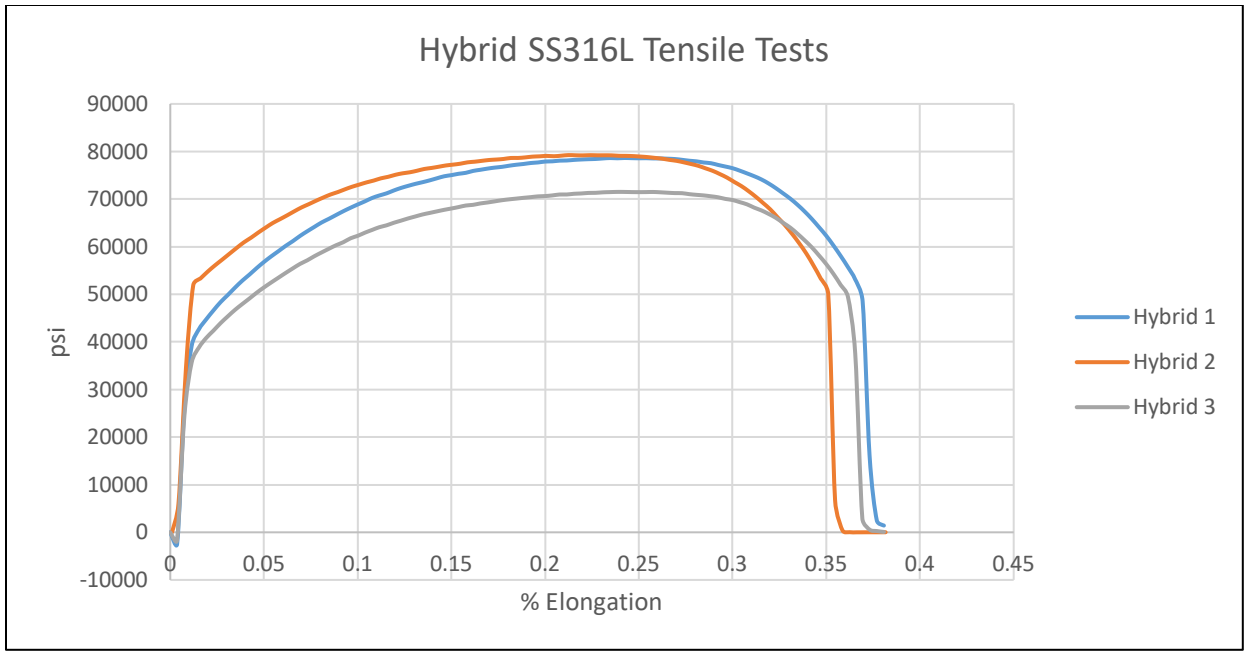
Hybrid SS316L Tensile Tests
90000
80000
70000
60000
50000
40000
30000
20000
10000
0
-10000
psi
0
0.05
0.1
0.15
0.2
0.25
0.3
0.35
0.4
0.45
% Elongation
Hybrid 1
Hybrid 2
Hybrid 3

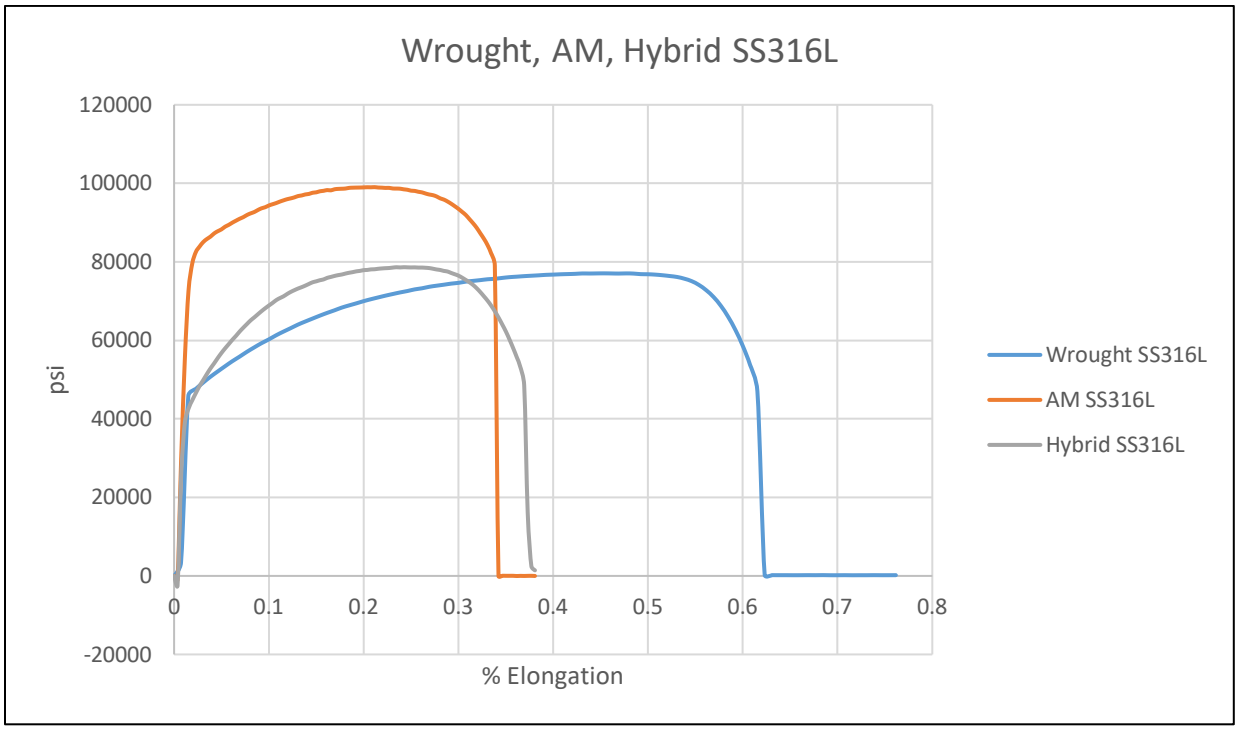
Wrought, AM, Hybrid SS316L
120000
100000
80000
60000
40000
20000
0
-20000
psi
0
0.1
0.2
0.3
0.4
0.5
0.6
0.7
0.8
% Elongation
Wrought SS316L
AM SS316L
Hybrid SS316L

DED Tests

Torsion Tests

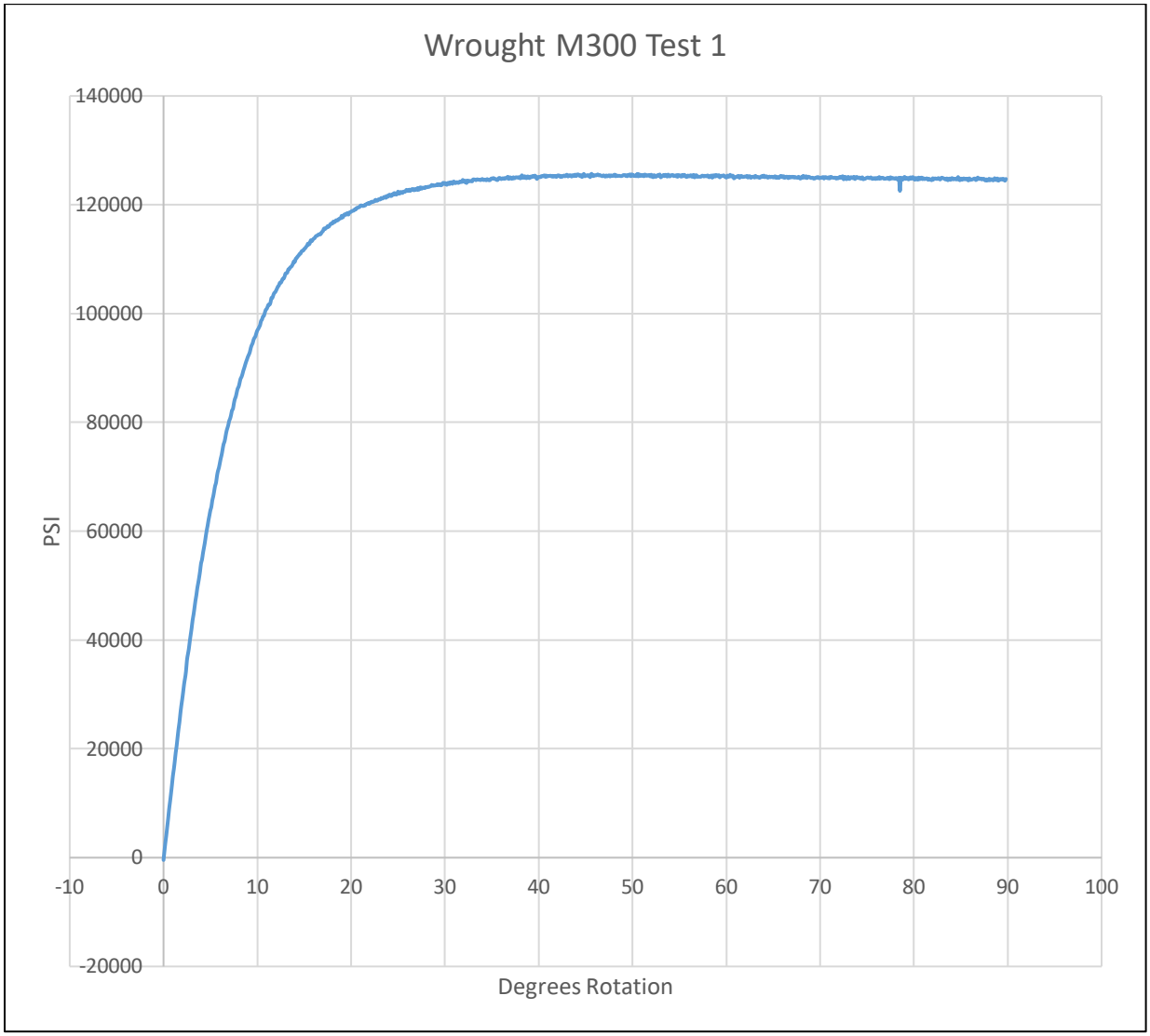

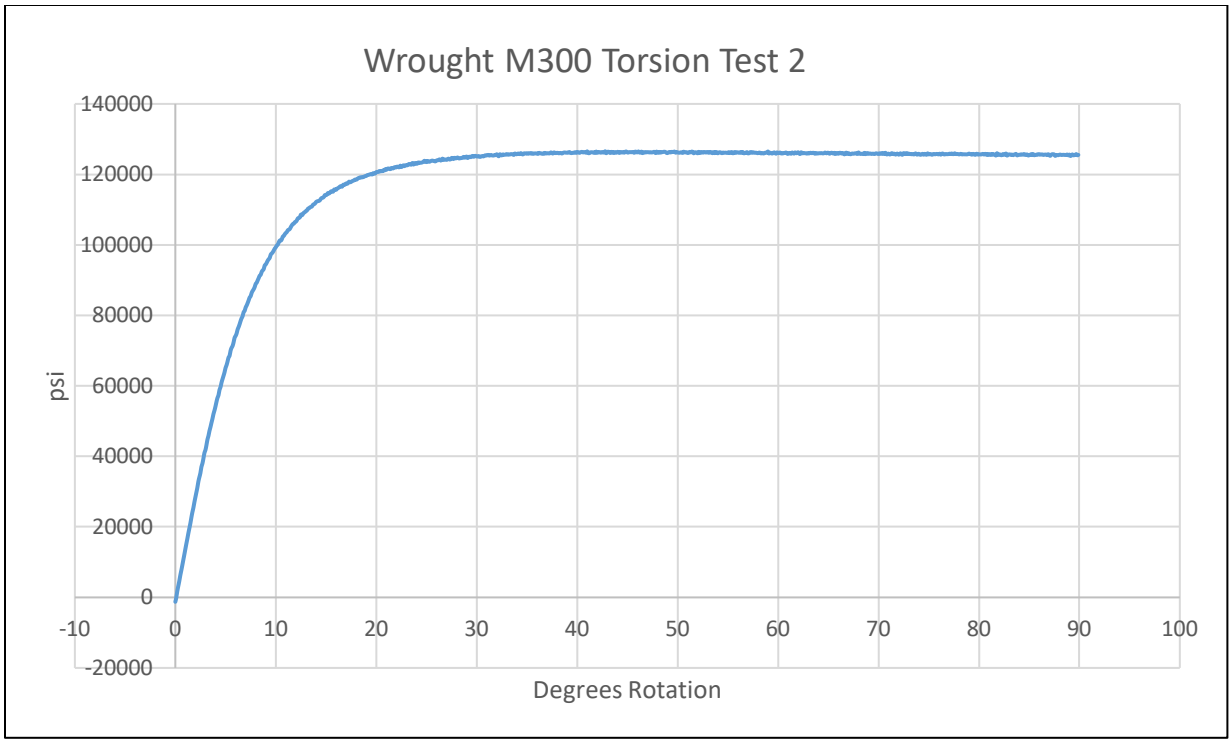
Wrought M300 Torsion Test 2
140000
120000
100000
80000
60000
40000
20000
0
-20000
psi
-10
0
10
20
30
40
50
60
70
80
90
100
Degrees Rotation

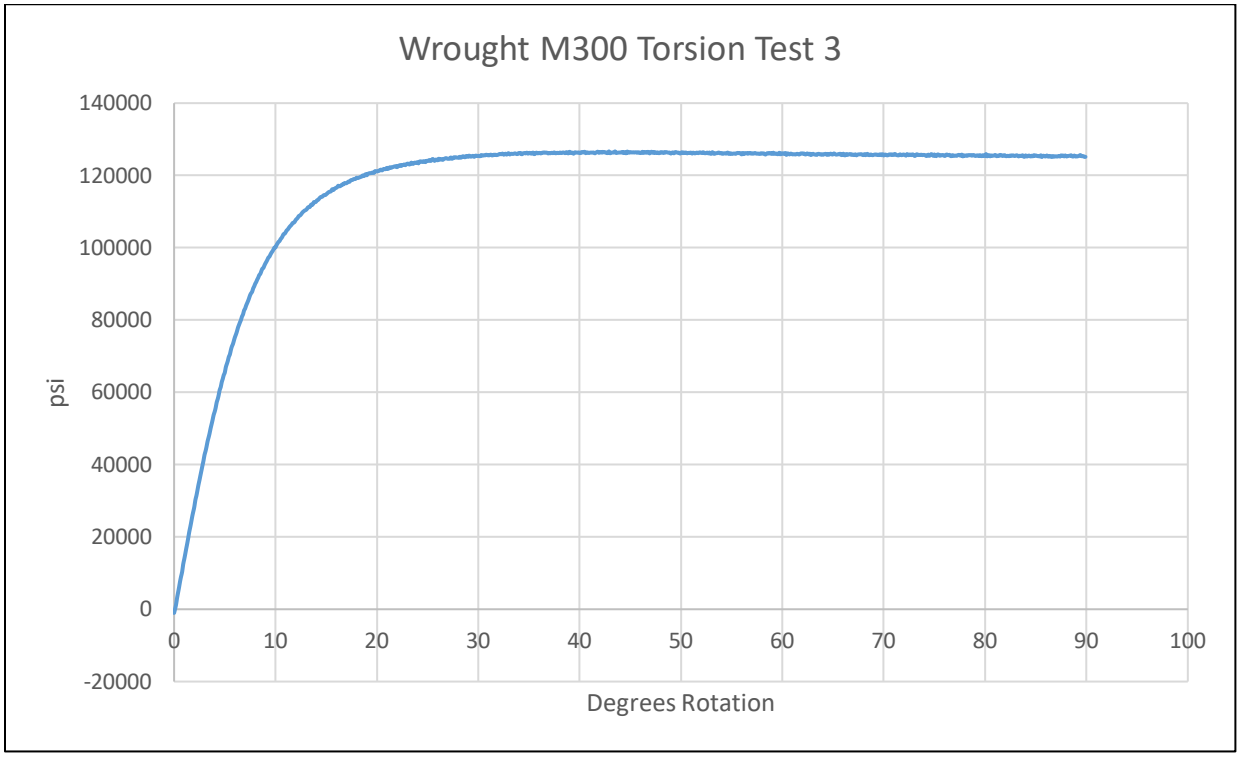
Wrought M300 Torsion Test 3
140000
120000
100000
80000
60000
40000
20000
0
-20000
psi
0
10
20
30
40
50
60
70
80
90
100
Degrees Rotation

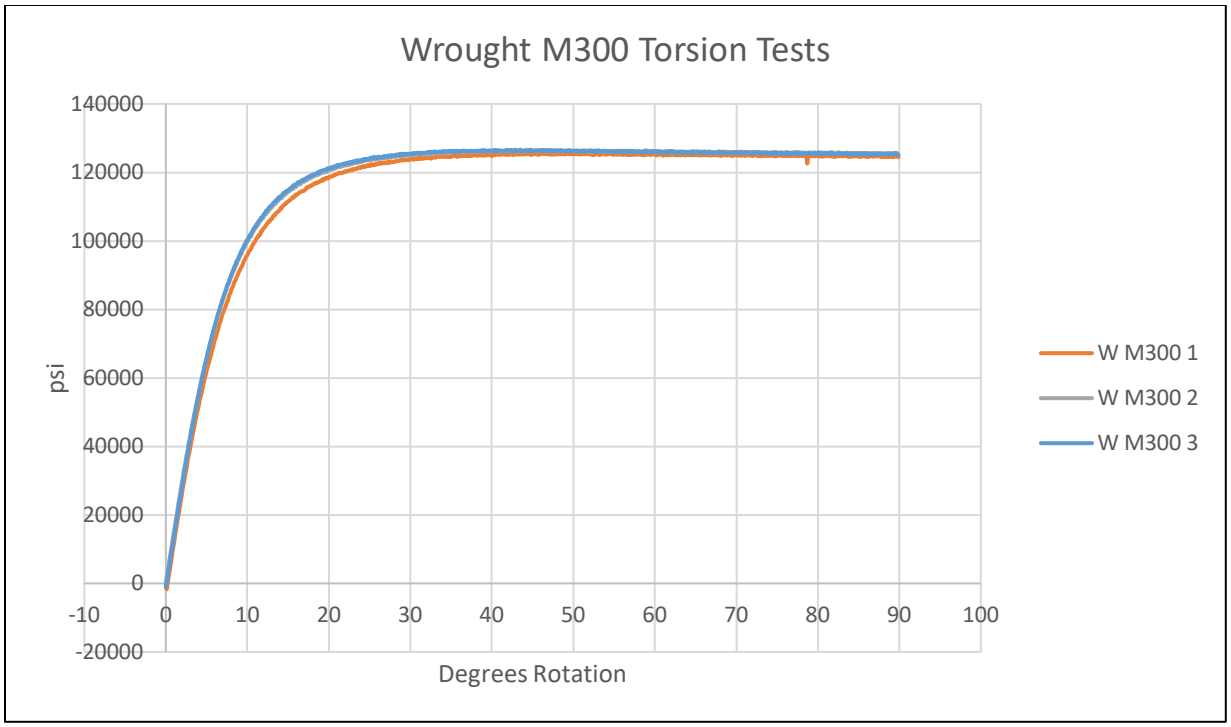
Wrought M300 Torsion Tests
140000
120000
100000
80000
60000
40000
20000
0
-20000
psi
-10
0
10
20
30
40
50
60
70
80
90
100
Degrees Rotation
W M300 1
W M300 2
W M300 3

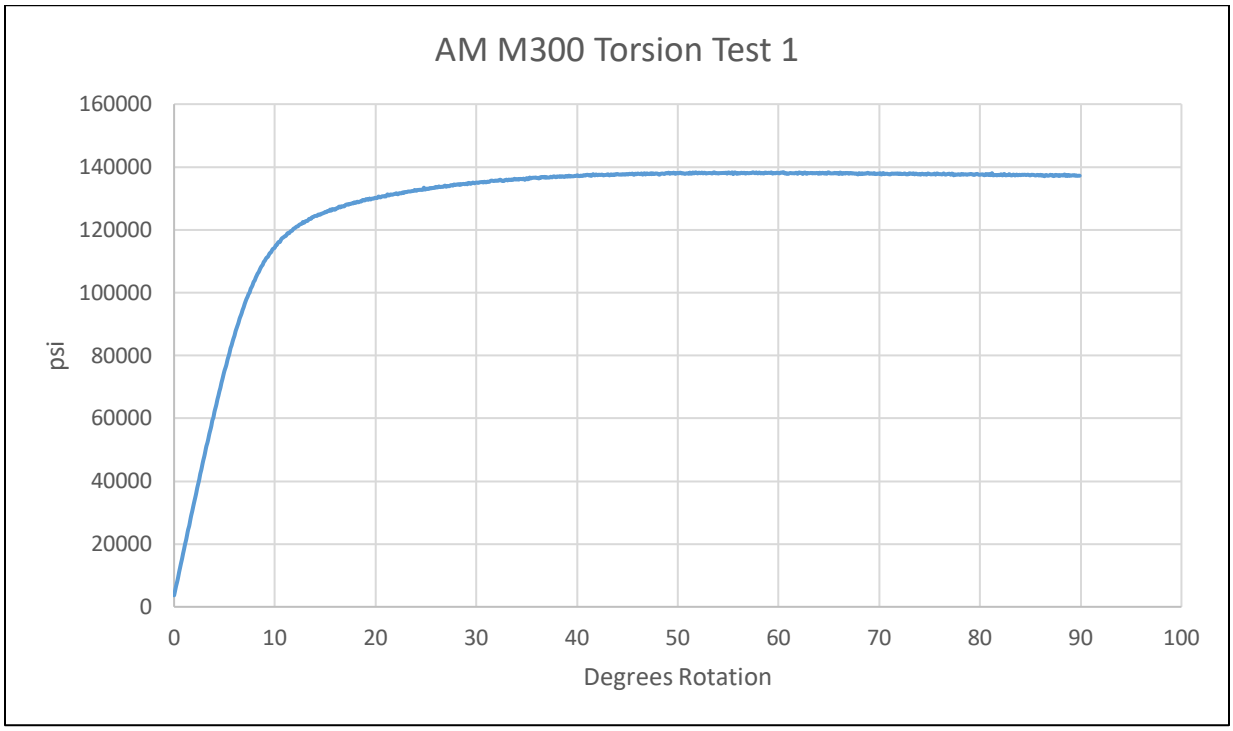
AM M300 Torsion Test 1
160000
140000
120000
100000
80000
60000
40000
20000
0
psi
0
10
20
30
40
50
60
70
80
90
100
Degrees Rotation

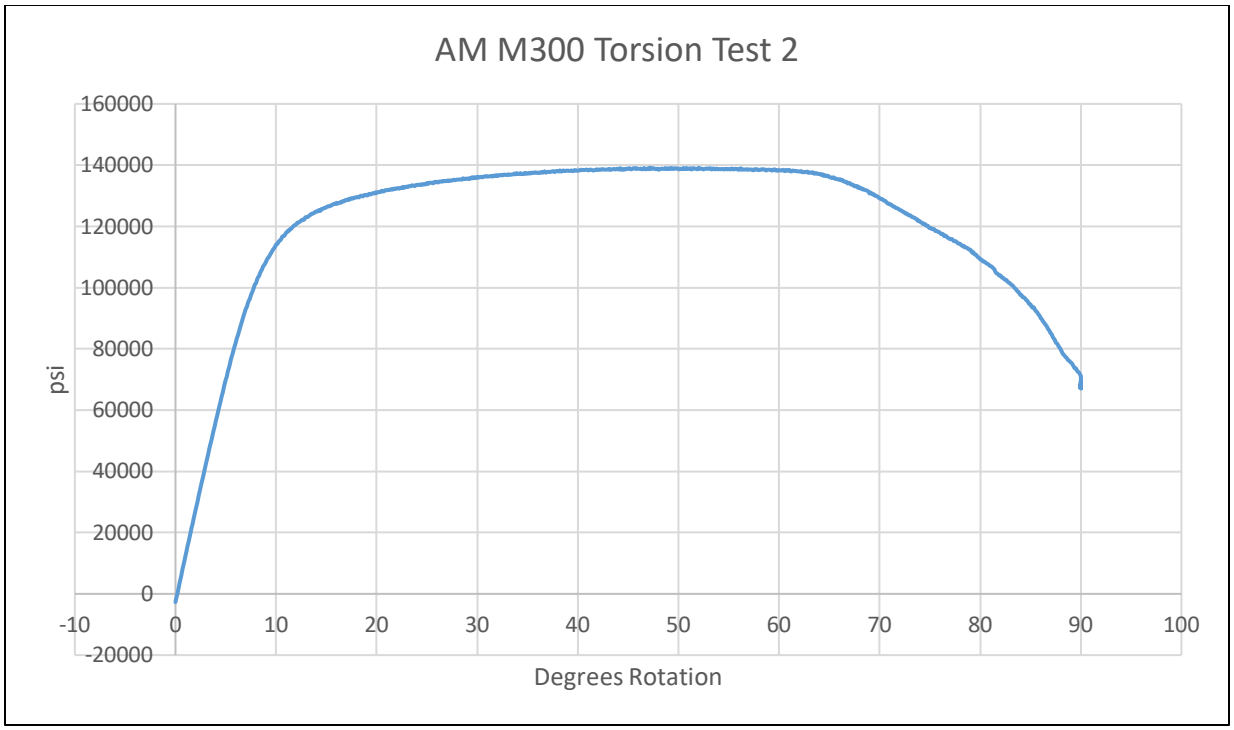
AM M300 Torsion Test 2
160000
140000
120000
100000
80000
60000
40000
20000
0
-20000
psi
-10
0
10
20
30
40
50
60
70
80
90
100
Degrees Rotation

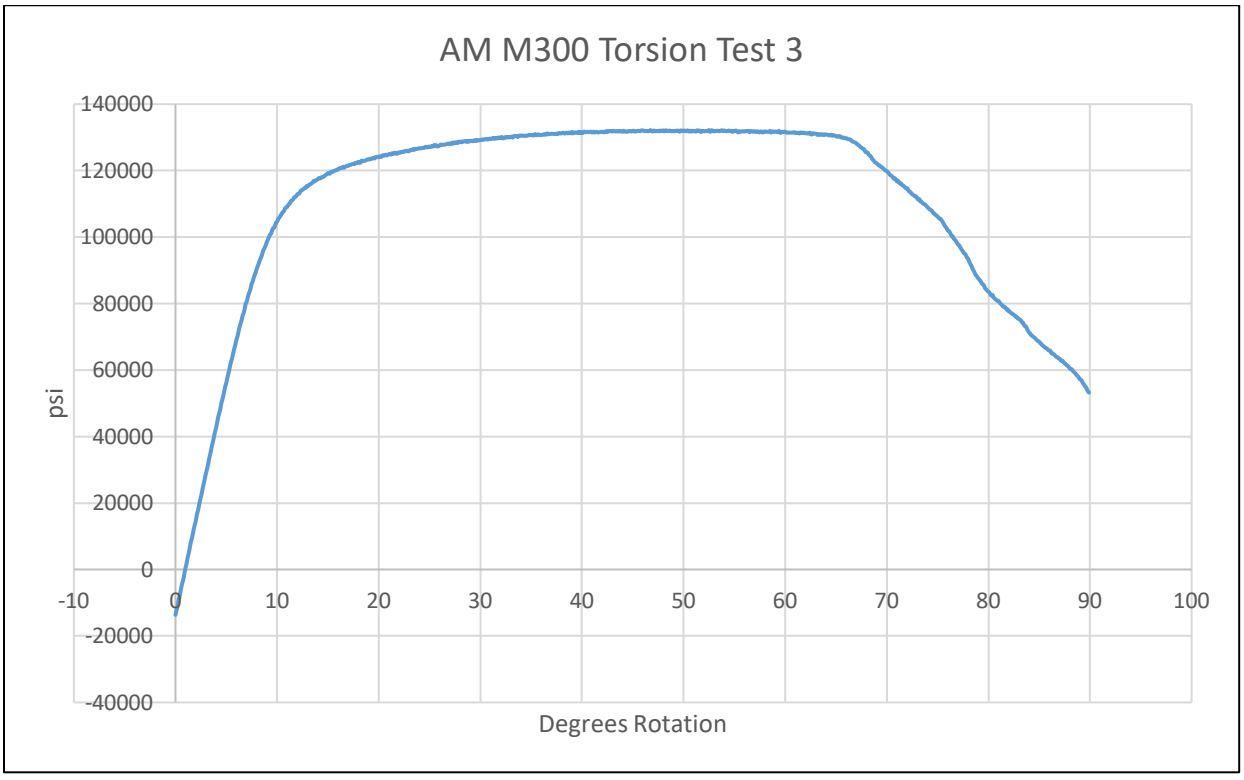
AM M300 Torsion Test 3
140000
120000
100000
80000
60000
40000
20000
0
-20000
-40000
psi
-10
0
10
20
30
40
50
60
70
80
90
100
Degrees Rotation

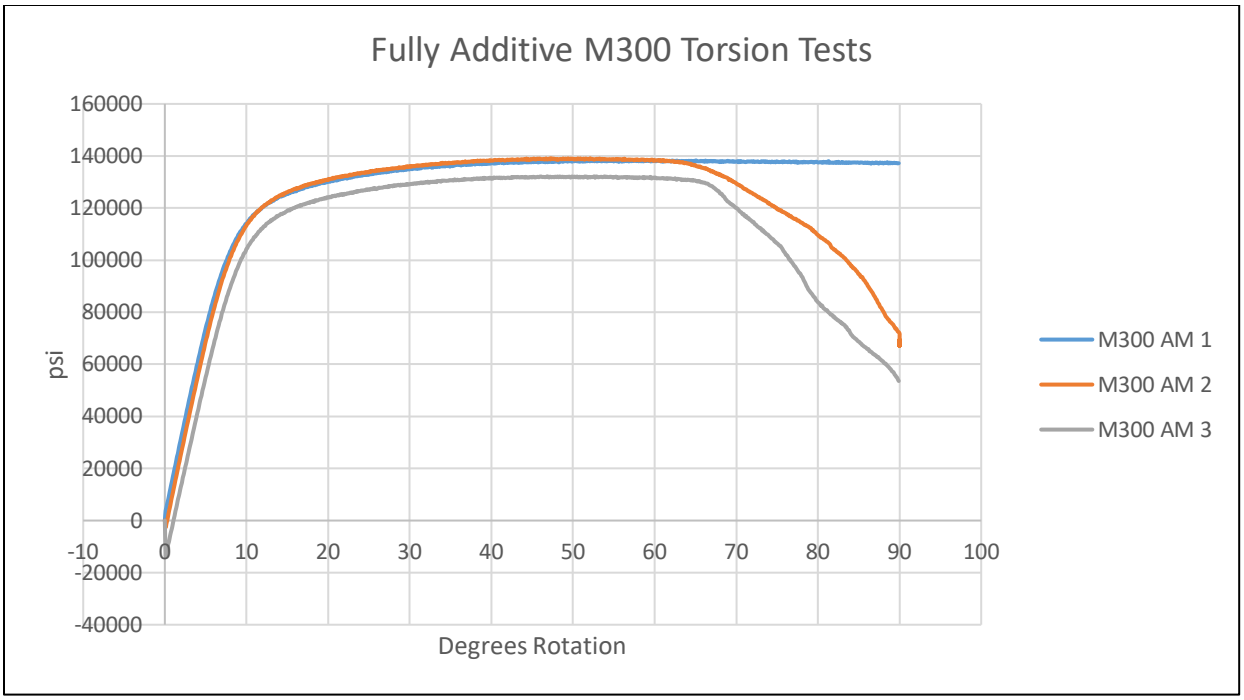
Fully Additive M300 Torsion Tests
160000
140000
120000
100000
80000
60000
40000
20000
0
-20000
-40000
psi
-10
0
10
20
30
40
50
60
70
80
90
100
Degrees Rotation
M300 AM 1
M300 AM 2
M300 AM 3

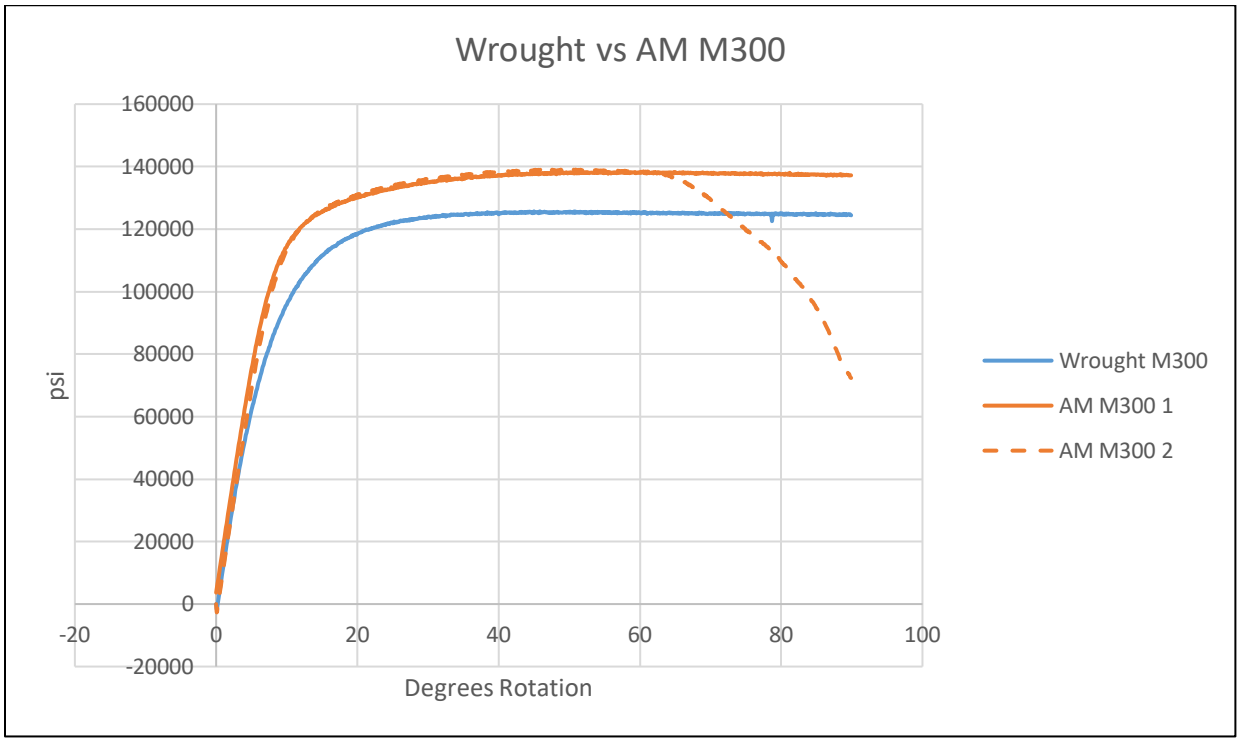
Wrought vs AM M300
160000
140000
120000
100000
80000
60000
40000
20000
0
-20000
psi
-20
0
20
40
60
80
100
Degrees Rotation
Wrought M300
AM M300 1
AM M300 2

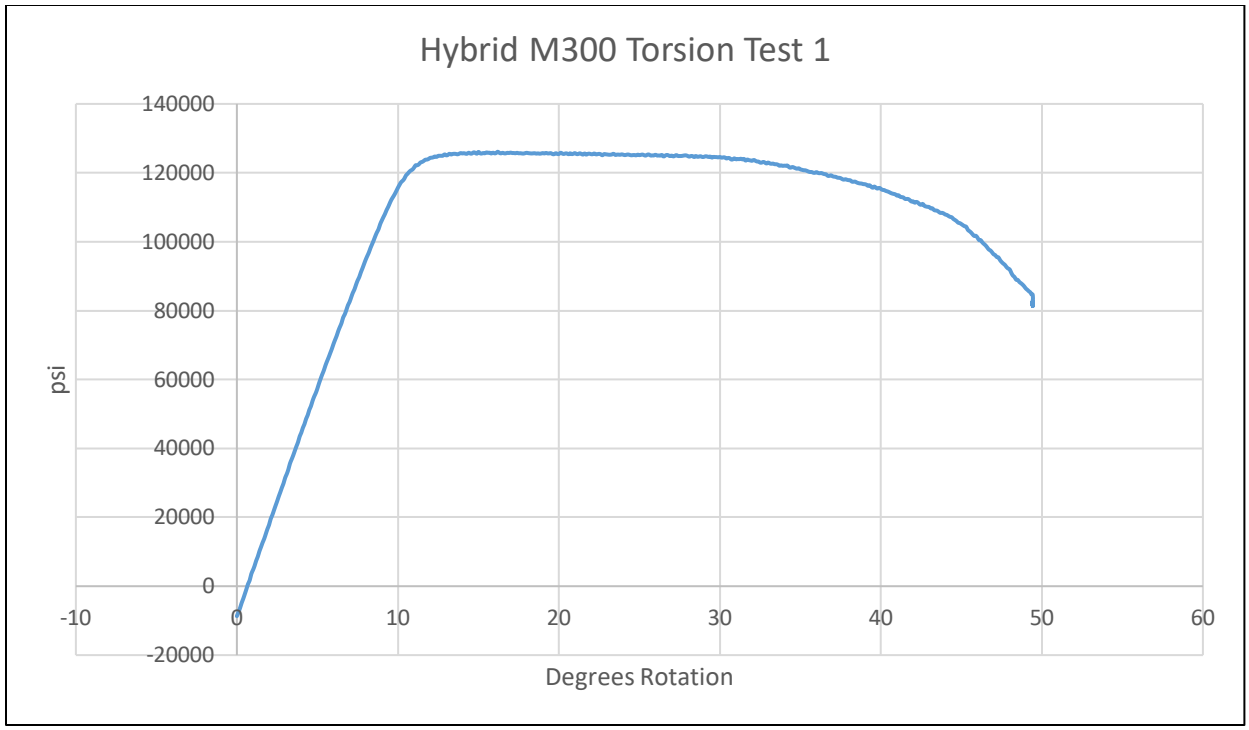
Hybrid M300 Torsion Test 1
140000
120000
100000
80000
60000
40000
20000
0
-20000
psi
-10
0
10
20
30
40
50
60
Degrees Rotation

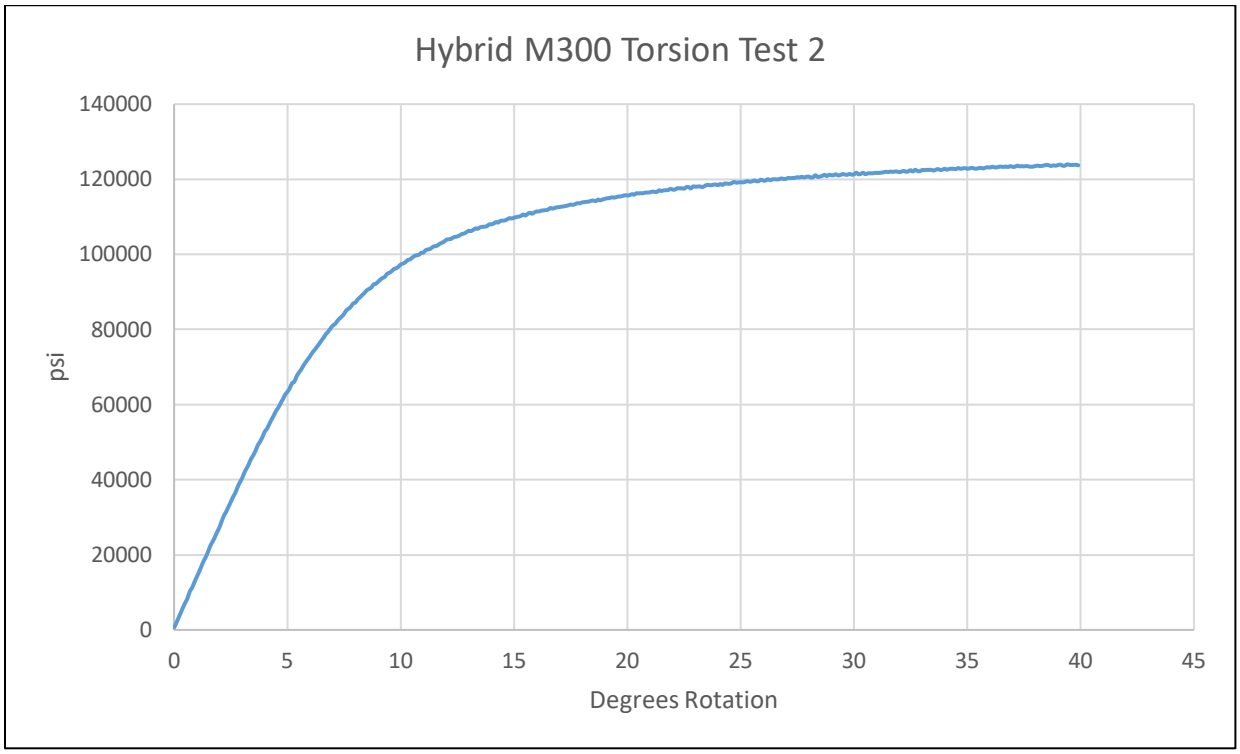
Hybrid M300 Torsion Test 2
140000
120000
100000
80000
60000
40000
20000
0
psi
0
5
10
15
20
25
30
35
40
45
Degrees Rotation

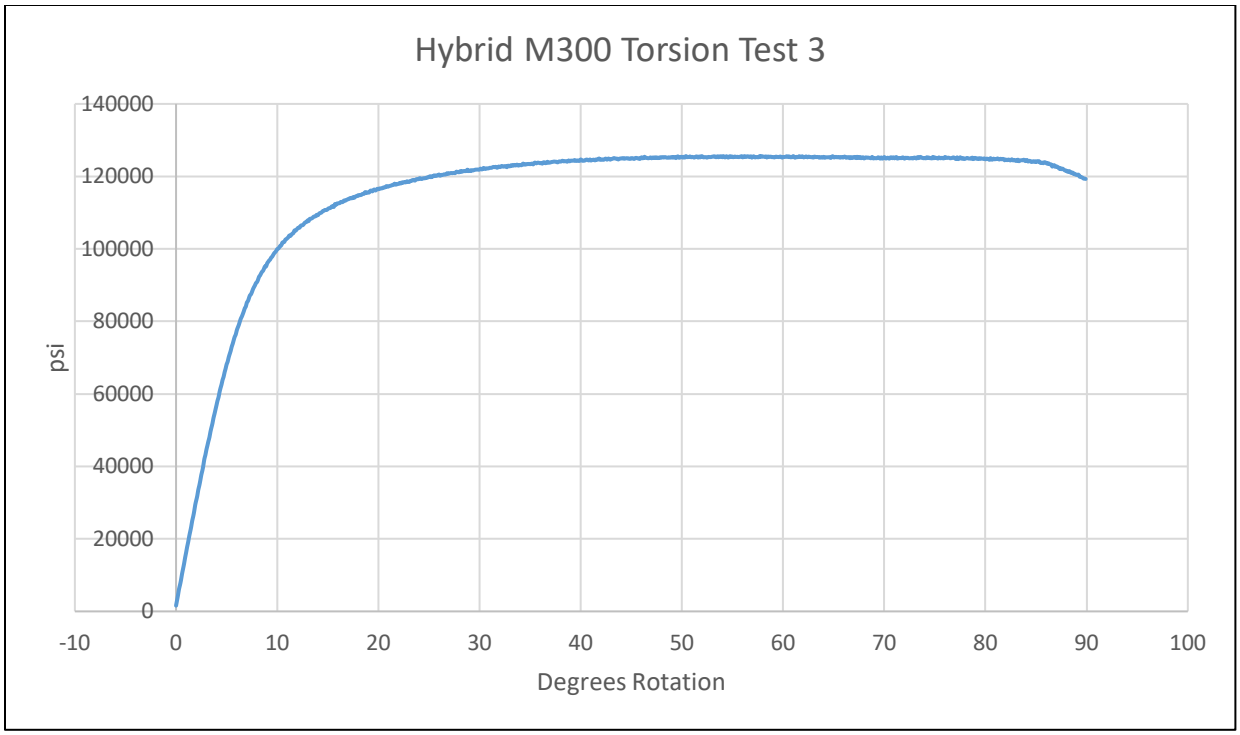
Hybrid M300 Torsion Test 3
140000
120000
100000
80000
60000
40000
20000
0
psi
-10
0
10
20
30
40
50
60
70
80
90
100
Degrees Rotation

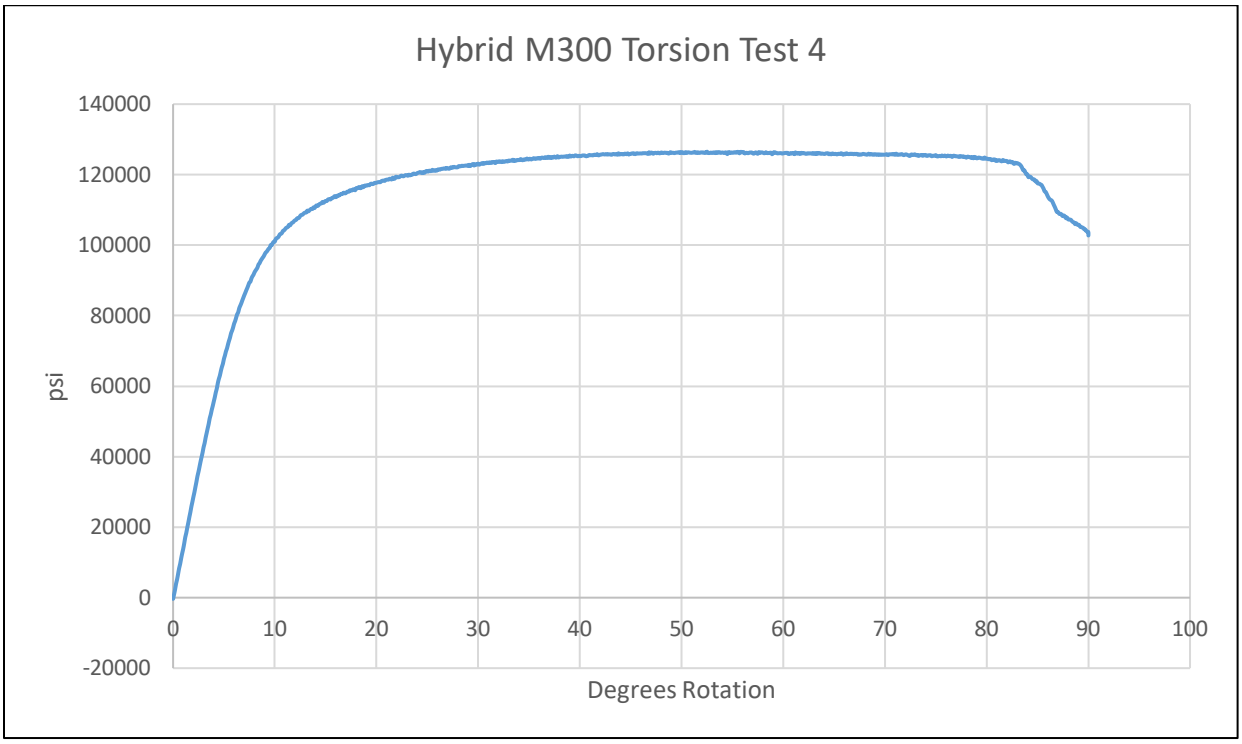
Hybrid M300 Torsion Test 4
140000
120000
100000
80000
60000
40000
20000
0
-20000
psi
0
10
20
30
40
50
60
70
80
90
100
Degrees Rotation

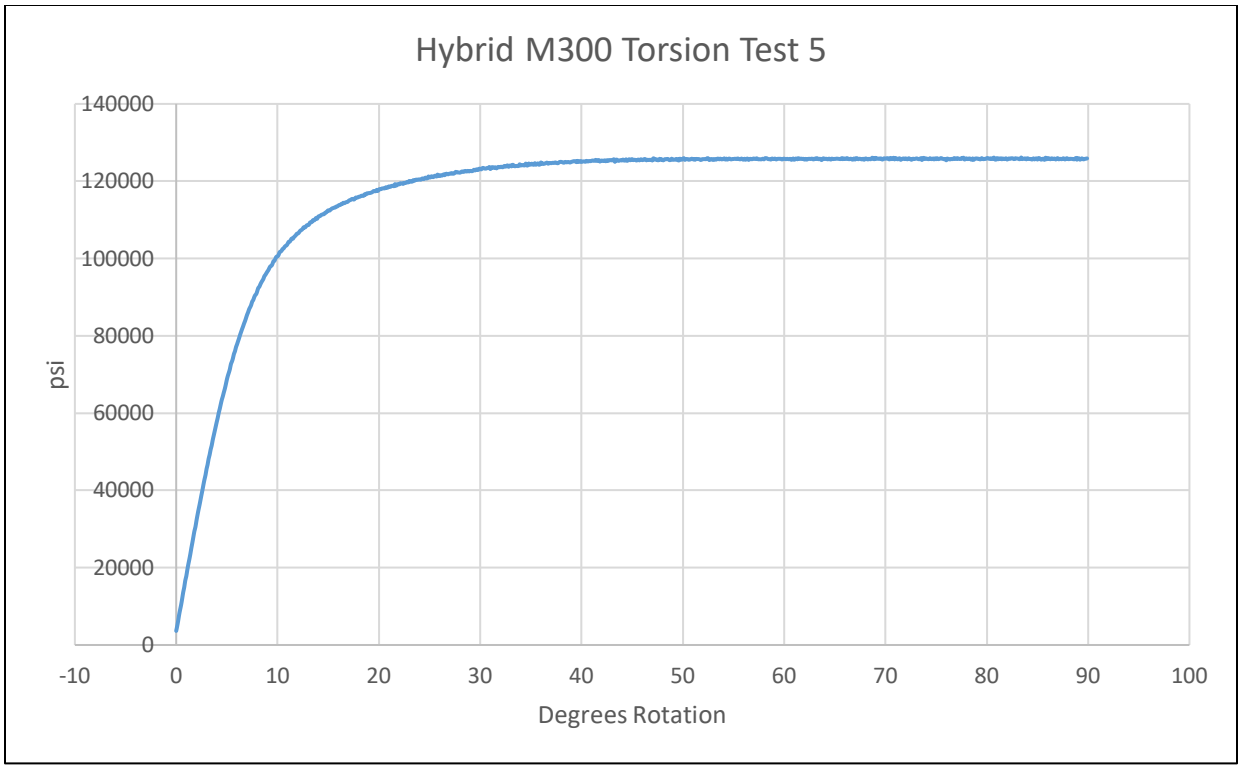
Hybrid M300 Torsion Test 5
140000
120000
100000
80000
60000
40000
20000
0
psi
-10
0
10
20
30
40
50
60
70
80
90
100
Degrees Rotation

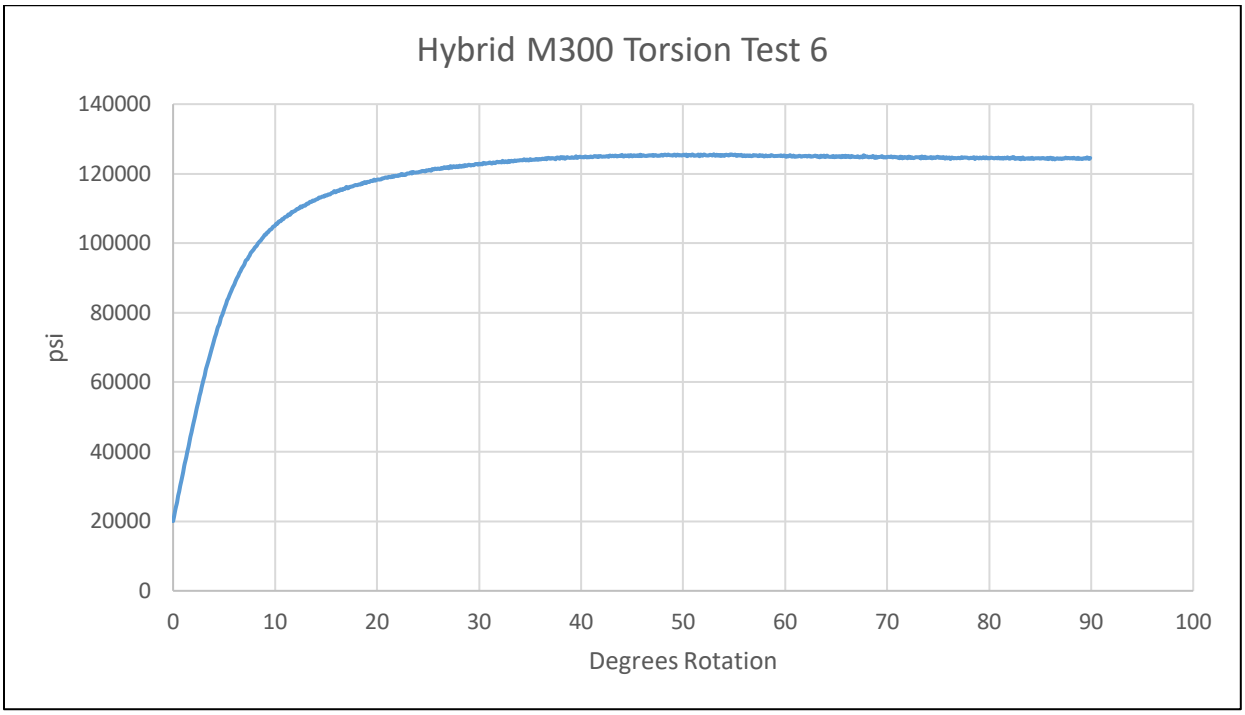
Hybrid M300 Torsion Test 6
140000
120000
100000
80000
60000
40000
20000
0
psi
0
10
20
30
40
50
60
70
80
90
100
Degrees Rotation

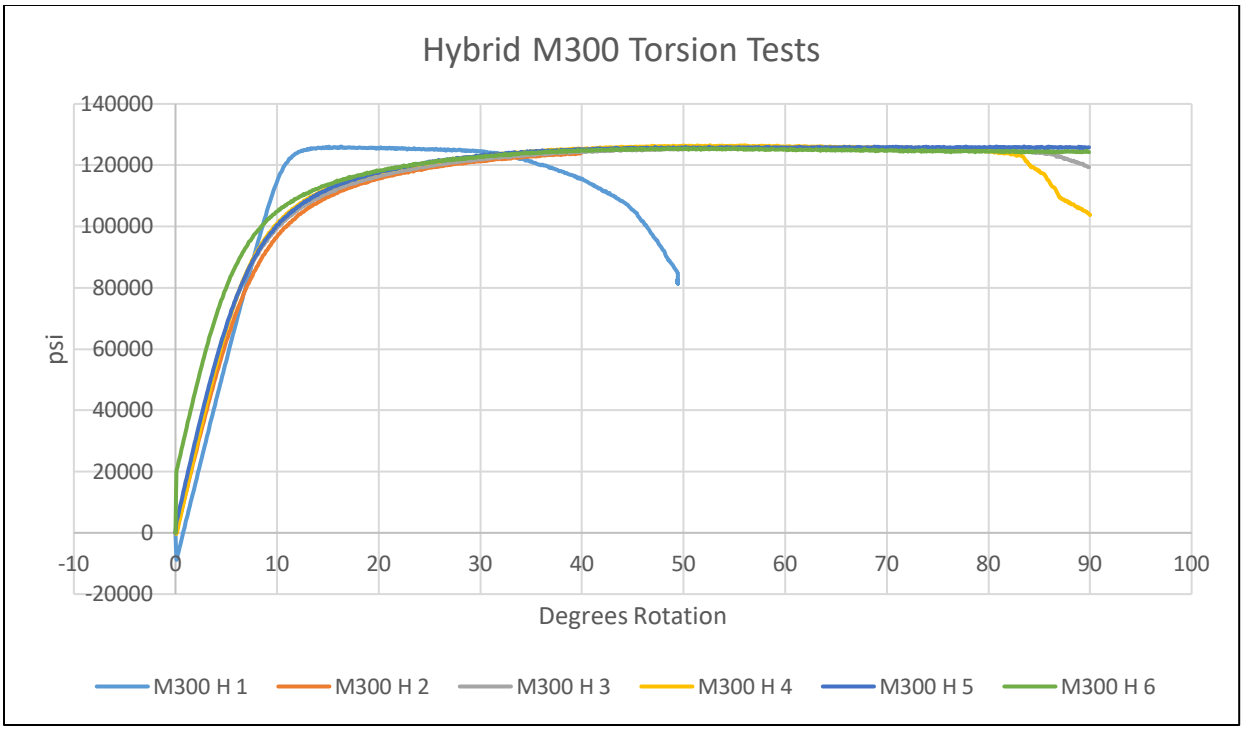
Hybrid M300 Torsion Tests
140000
120000
100000
80000
60000
40000
20000
0
-20000
psi
-10
0
10
20
30
40
50
60
70
80
90
100
Degrees Rotation
M300 H 1
M300 H 2
M300 H 3
M300 H 4
M300 H 5
M300 H 6

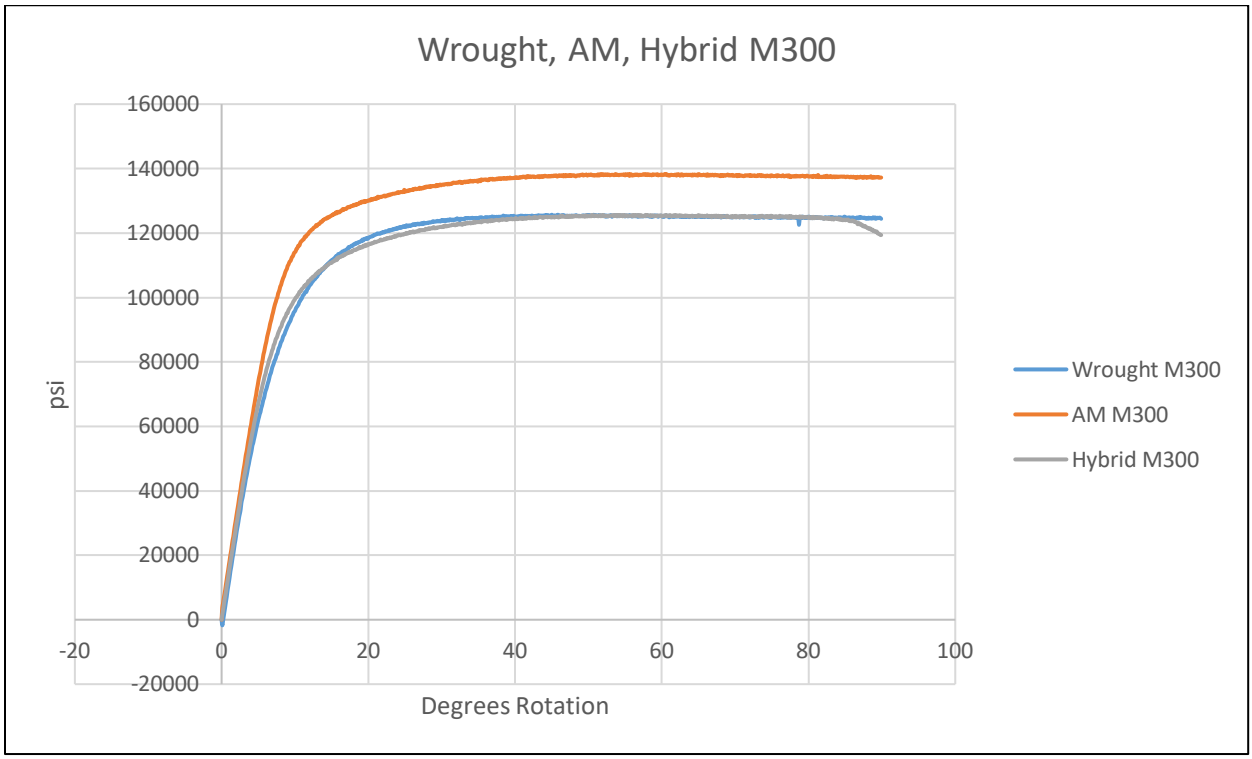
Wrought, AM, Hybrid M300
160000
140000
120000
100000
80000
60000
40000
20000
0
-20000
psi
-20
0
20
40
60
80
100
Degrees Rotation
Wrought M300
AM M300
Hybrid M300

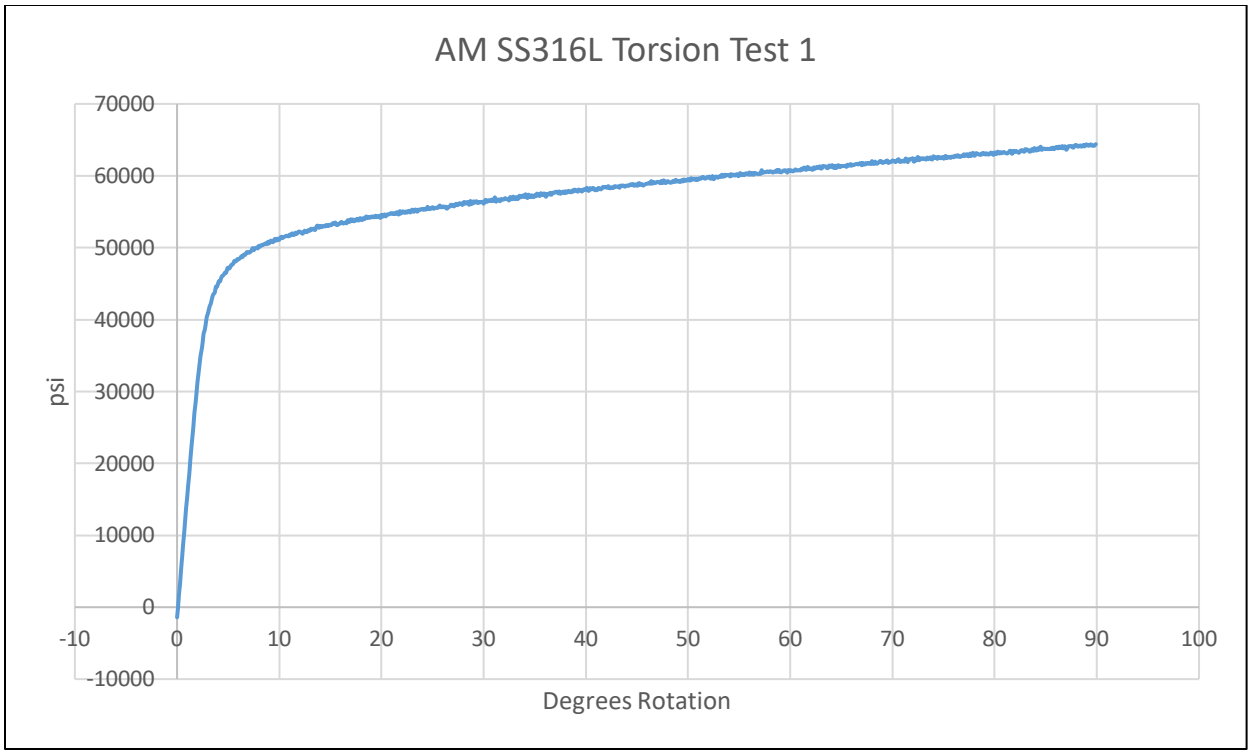
AM SS316L Torsion Test 1
70000
60000
50000
40000
30000
20000
10000
0
-10000
psi
-10
0
10
20
30
40
50
60
70
80
90
100
Degrees Rotation

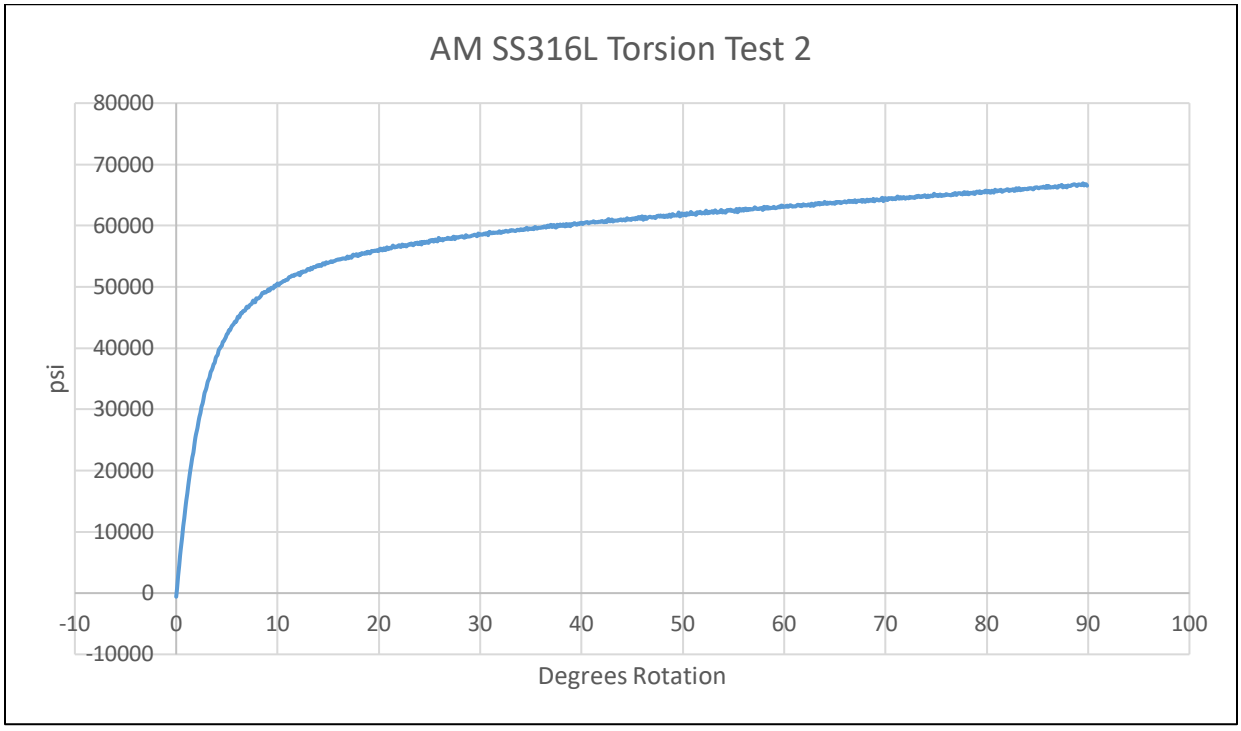
AM SS316L Torsion Test 2
80000
70000
60000
50000
40000
30000
20000
10000
0
-10000
psi
-10
0
10
20
30
40
50
60
70
80
90
100
Degrees Rotation

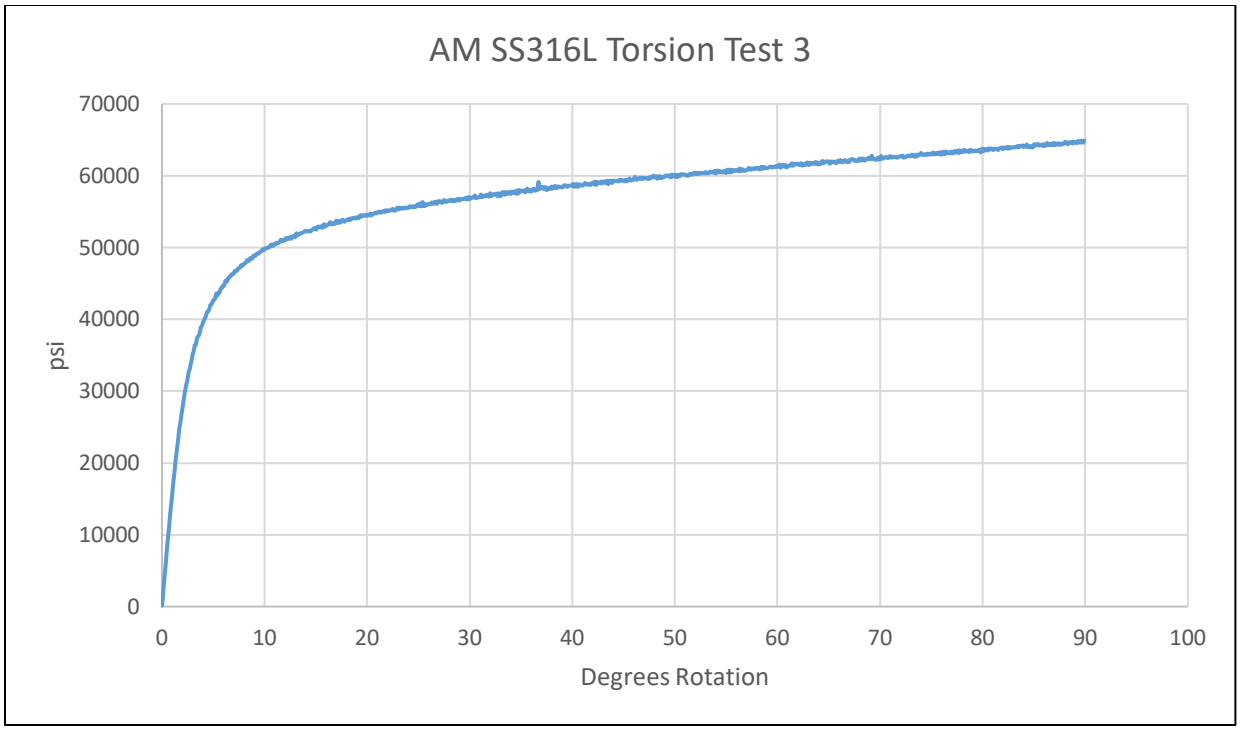
AM SS316L Torsion Test 3
70000
60000
50000
40000
30000
20000
10000
0
psi
0
10
20
30
40
50
60
70
80
90
100
Degrees Rotation

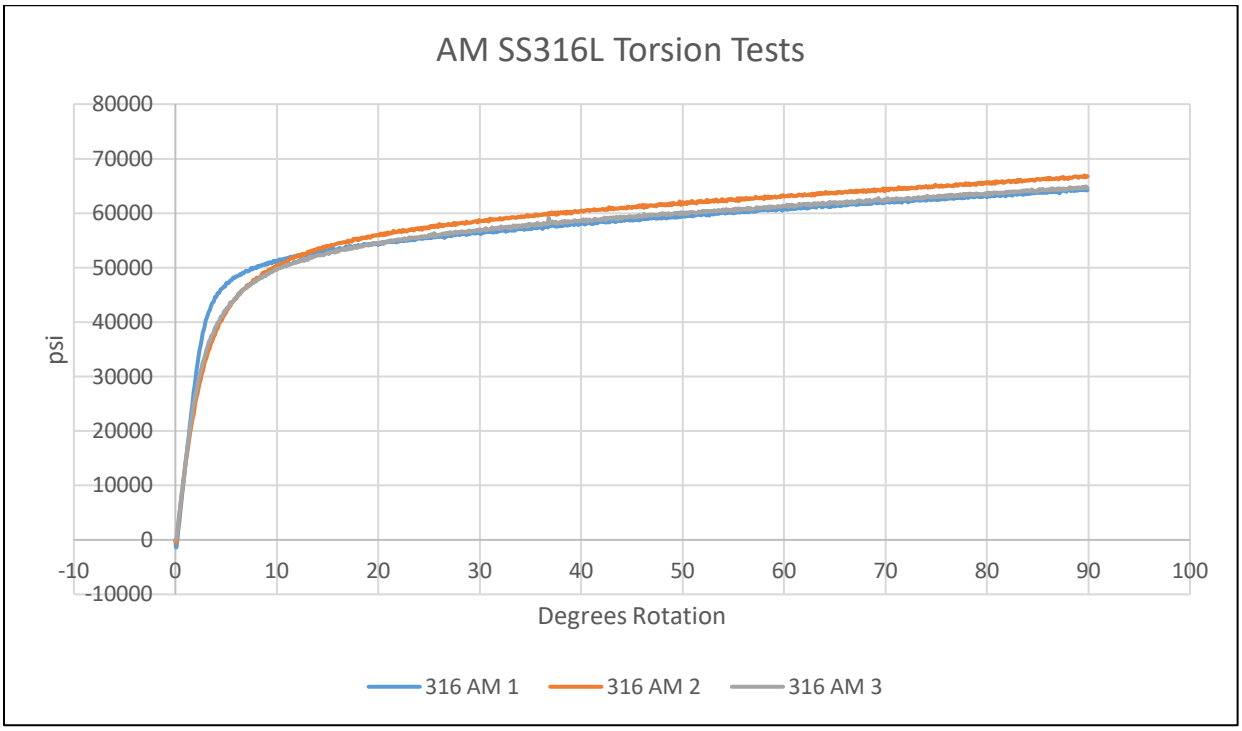
AM SS316L Torsion Tests
80000
70000
60000
50000
40000
30000
20000
10000
0
-10000
psi
-10
0
10
20
30
40
50
60
70
80
90
100
Degrees Rotation
316 AM 1
316 AM 2
316 AM 3

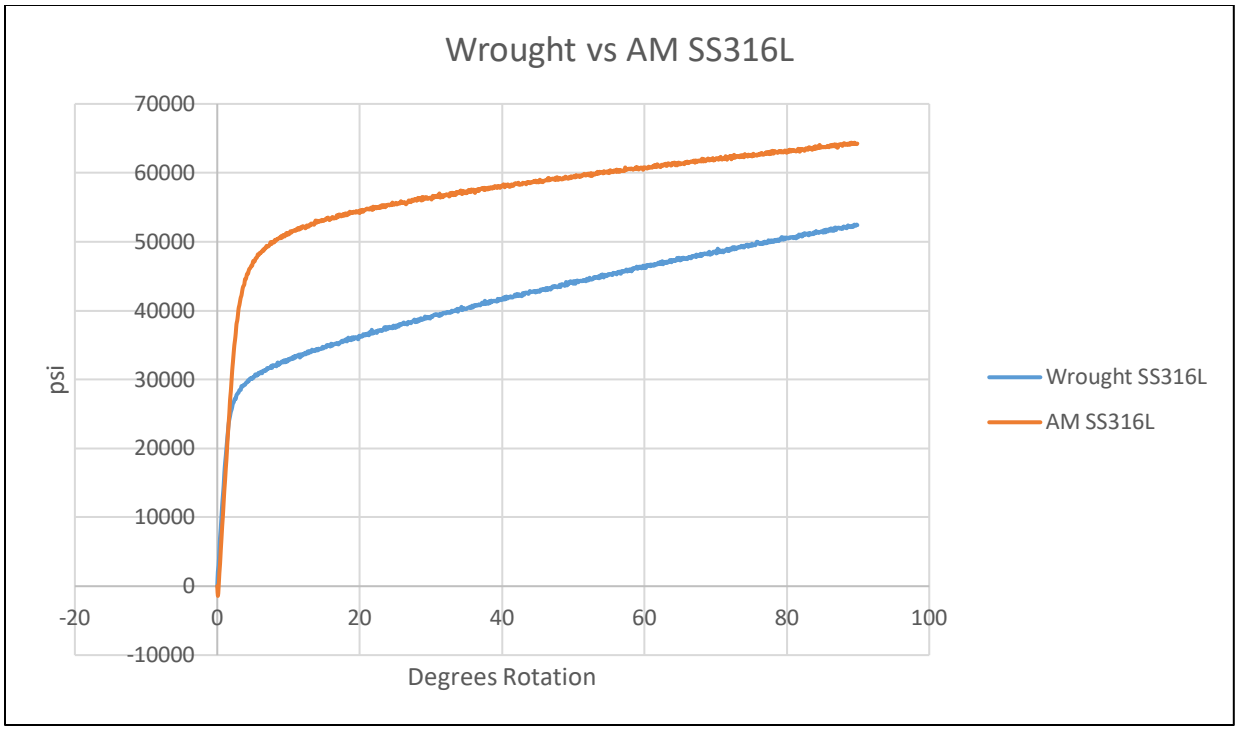
Wrought vs AM SS316L
70000
60000
50000
40000
30000
20000
10000
0
-10000
psi
-20
0
20
40
60
80
100
Degrees Rotation
Wrought SS316L
AM SS316L

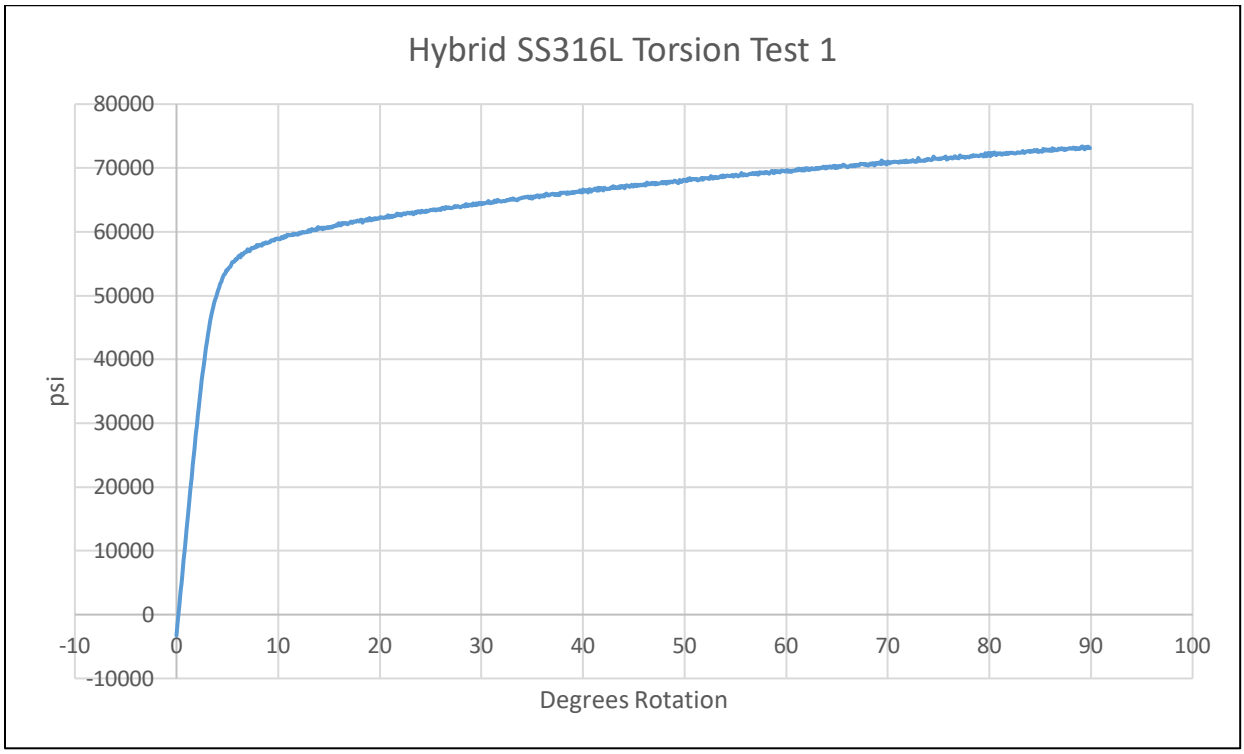
Hybrid SS316L Torsion Test 1
80000
70000
60000
50000
40000
30000
20000
10000
0
-10000
psi
-10
0
10
20
30
40
50
60
70
80
90
100
Degrees Rotation

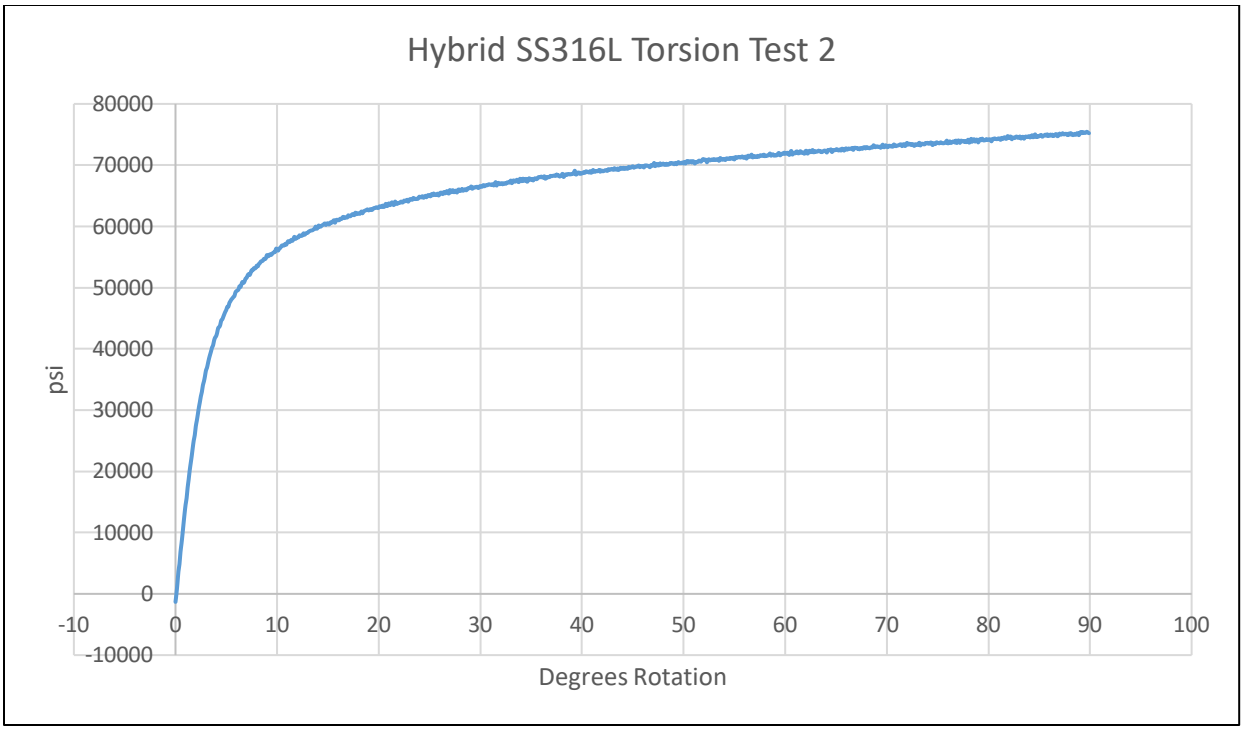
Hybrid SS316L Torsion Test 2
80000
70000
60000
50000
40000
30000
20000
10000
0
-10000
psi
-10
0
10
20
30
40
50
60
70
80
90
100
Degrees Rotation

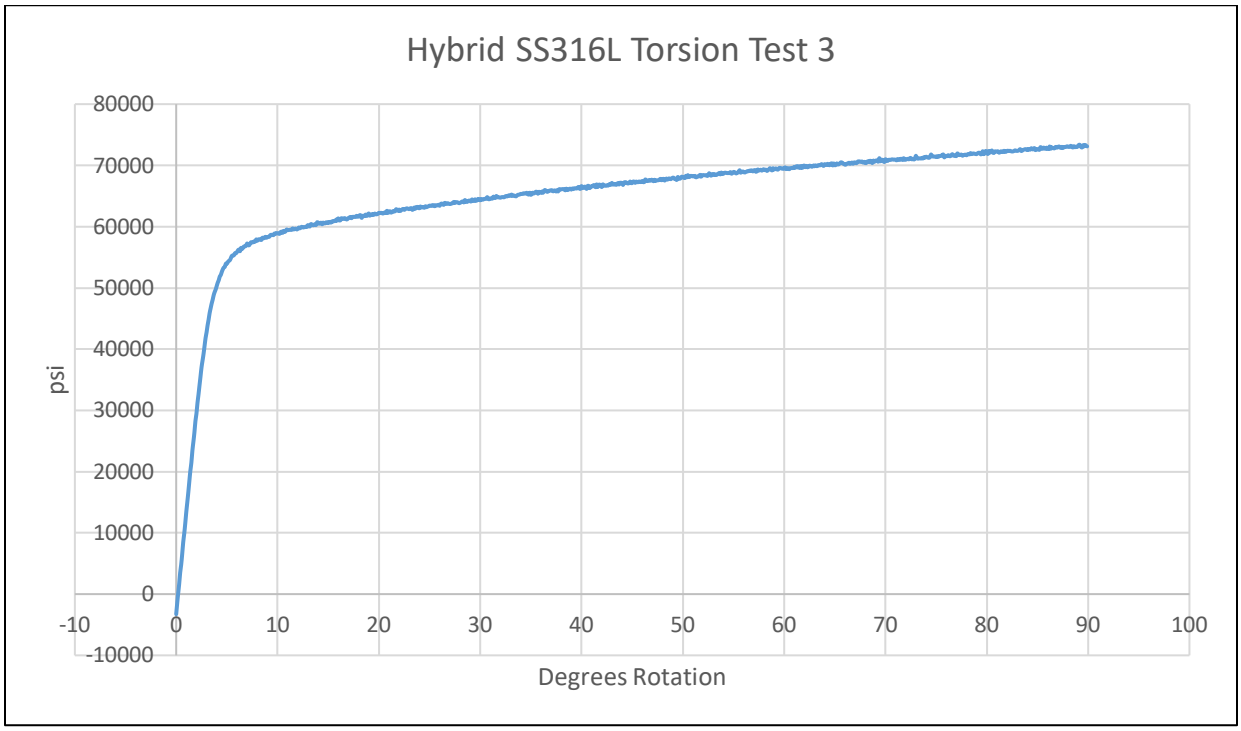
Hybrid SS316L Torsion Test 3
80000
70000
60000
50000
40000
30000
20000
10000
0
-10000
psi
-10
0
10
20
30
40
50
60
70
80
90
100
Degrees Rotation

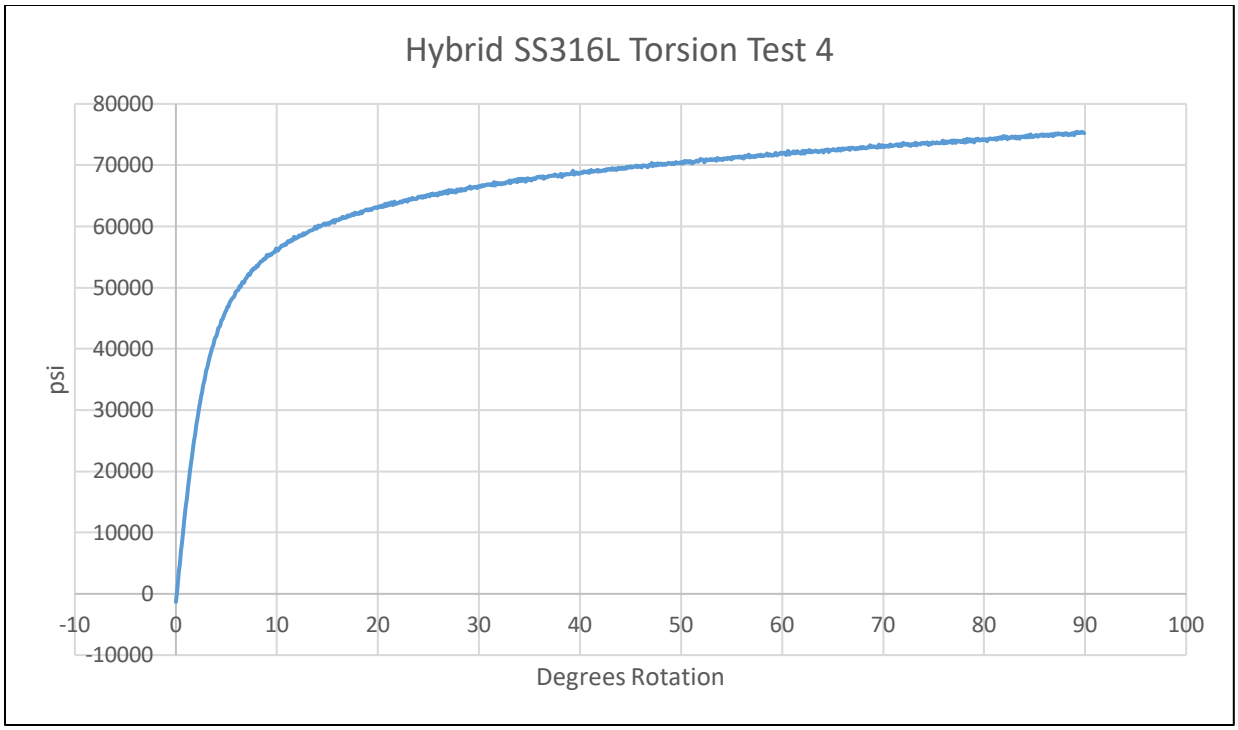
Hybrid SS316L Torsion Test 4
80000
70000
60000
50000
40000
30000
20000
10000
0
-10000
psi
-10
0
10
20
30
40
50
60
70
80
90
100
Degrees Rotation

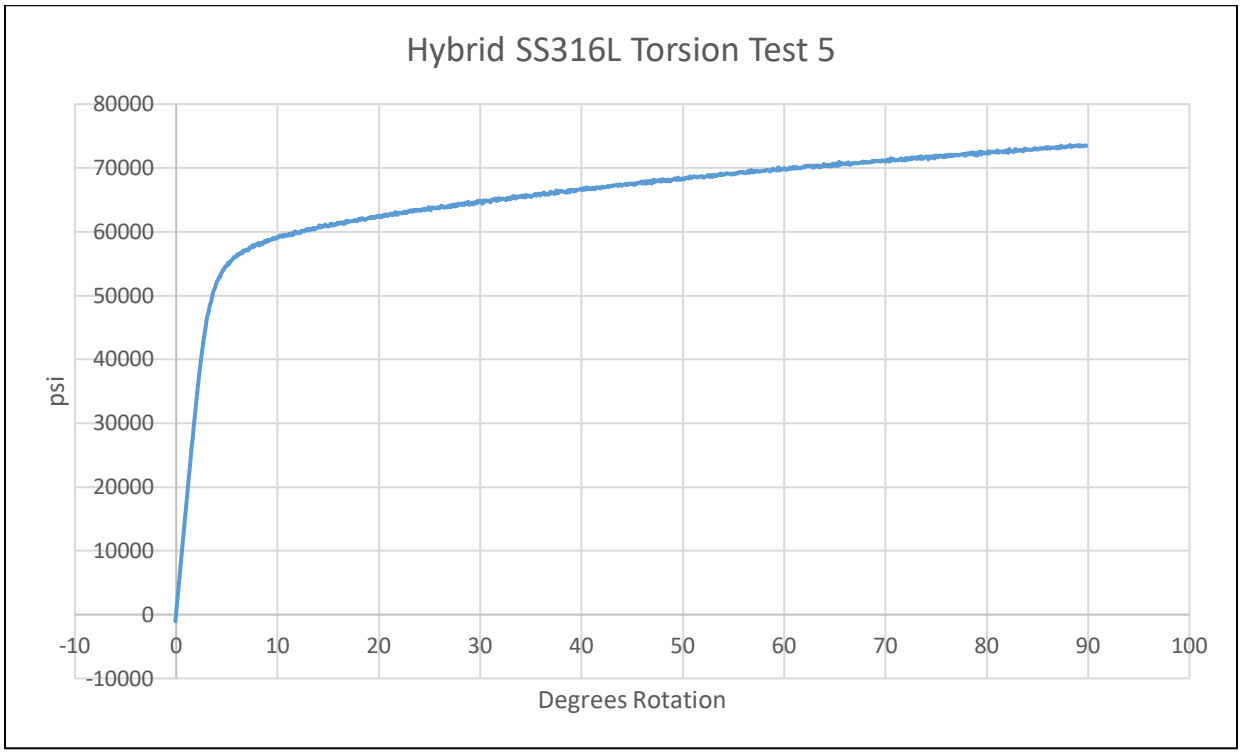
Hybrid SS316L Torsion Test 5
80000
70000
60000
50000
40000
30000
20000
10000
0
-10000
psi
-10
0
10
20
30
40
50
60
70
80
90
100
Degrees Rotation

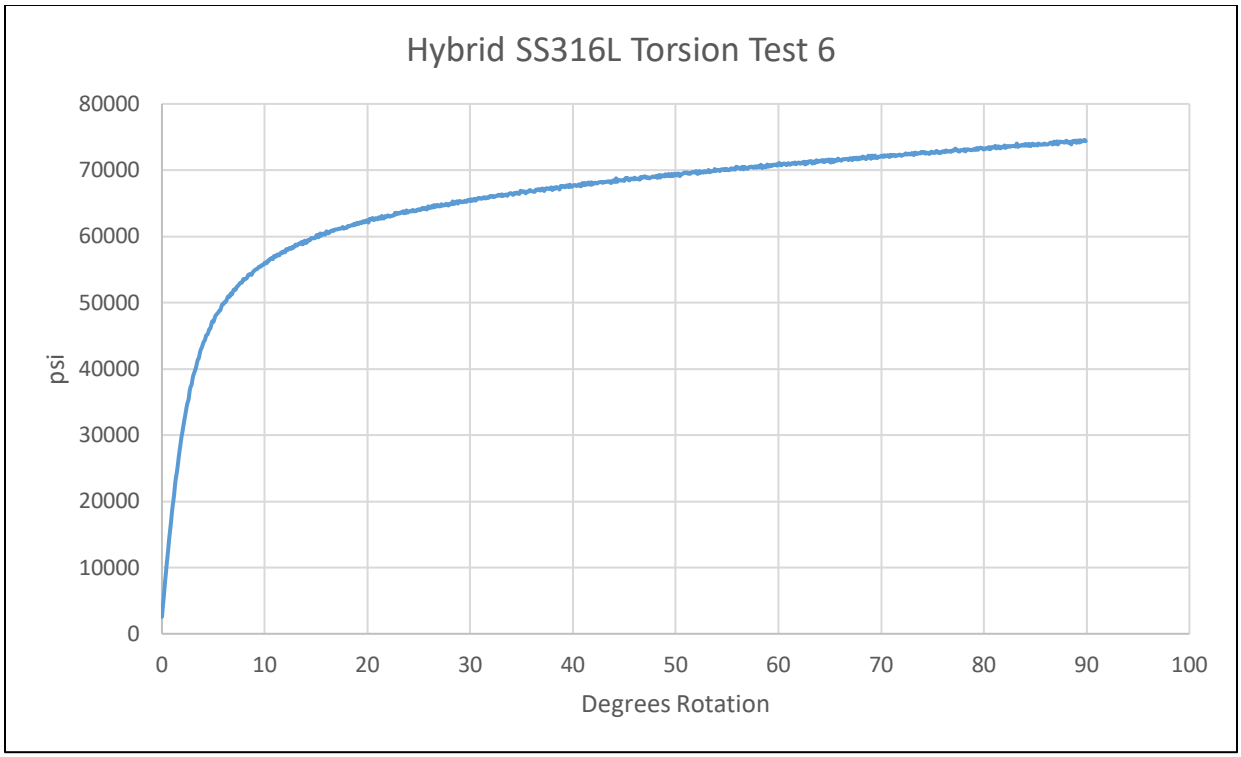
Hybrid SS316L Torsion Test 6
80000
70000
60000
50000
40000
30000
20000
10000
0
psi
0
10
20
30
40
50
60
70
80
90
100
Degrees Rotation

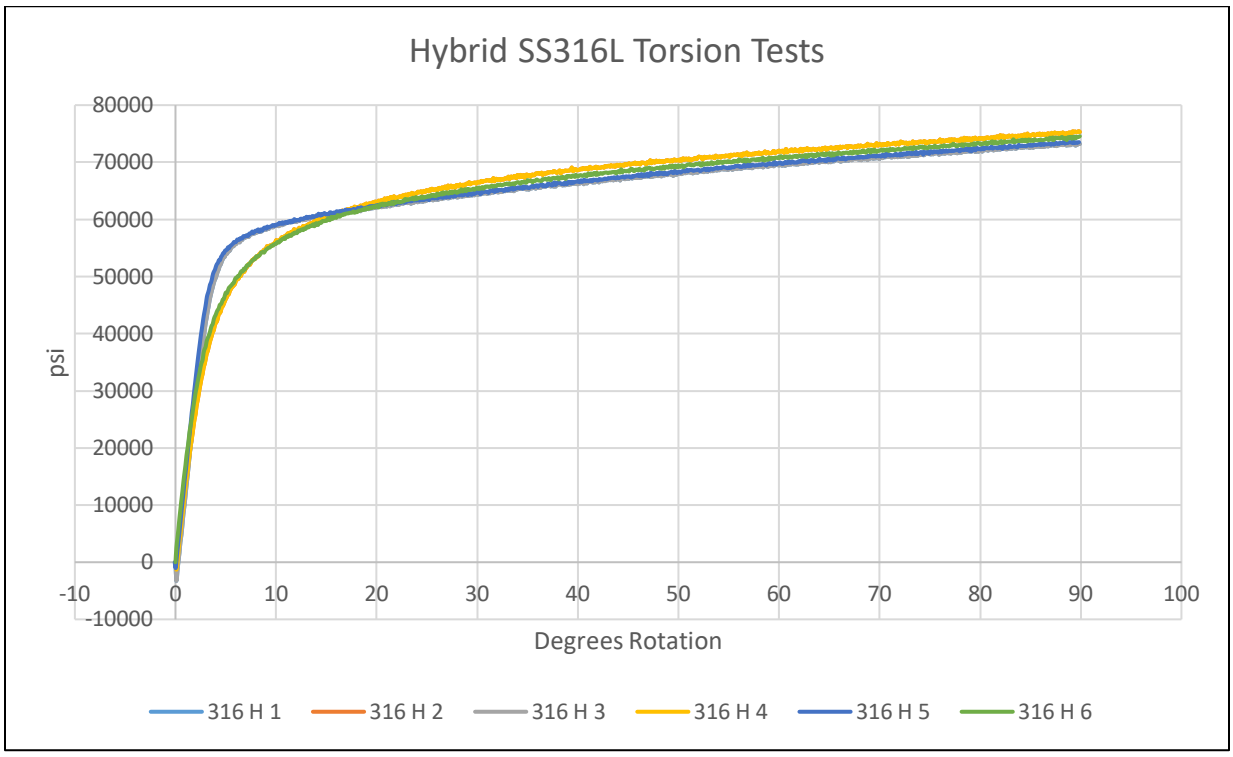
Hybrid SS316L Torsion Tests
80000
70000
60000
50000
40000
30000
20000
10000
0
-10000
psi
-10
0
10
20
30
40
50
60
70
80
90
100
Degrees Rotation
316 H 1
316 H 2
316 H 3
316 H 4
316 H 5
316 H 6

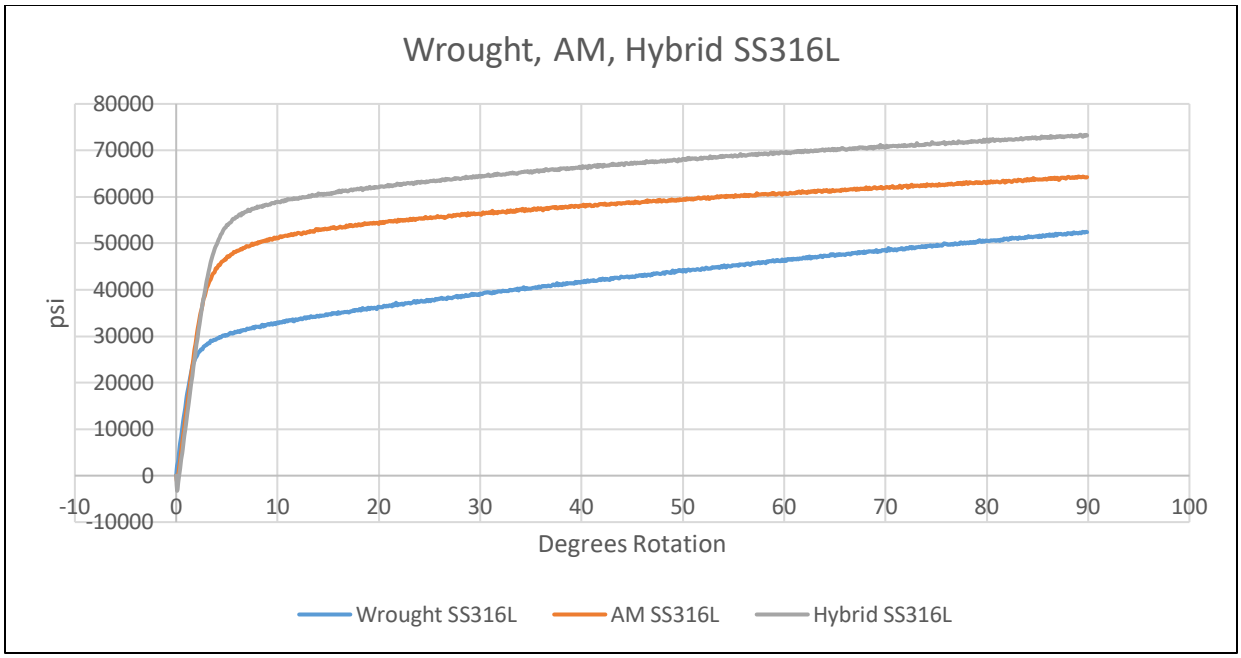

Tensile Tests

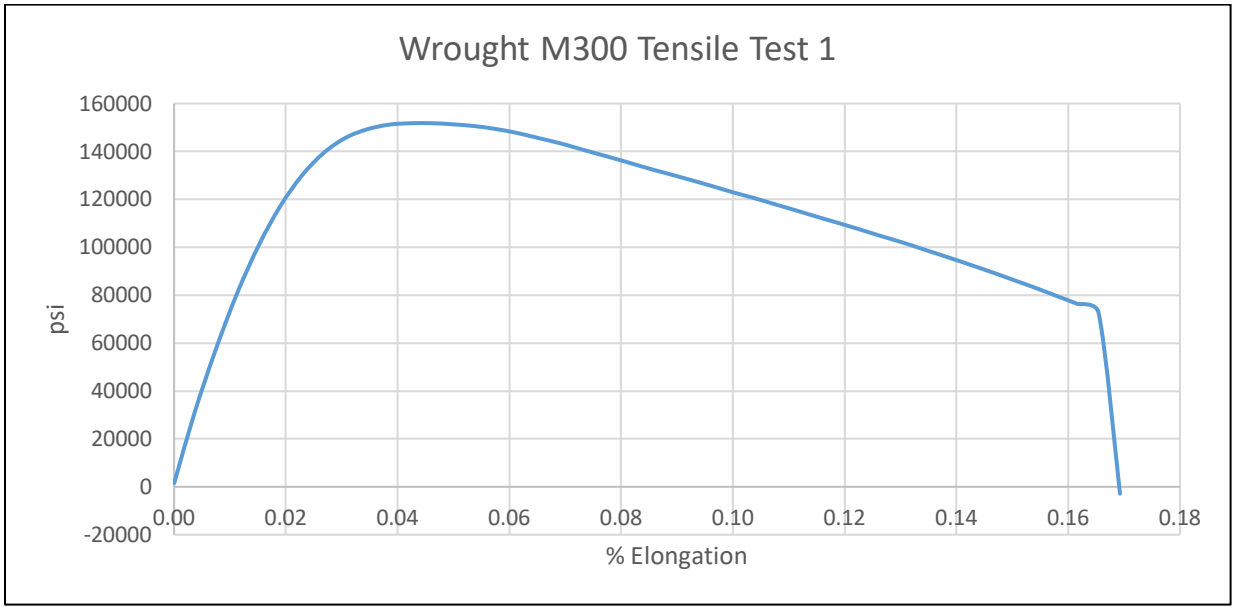

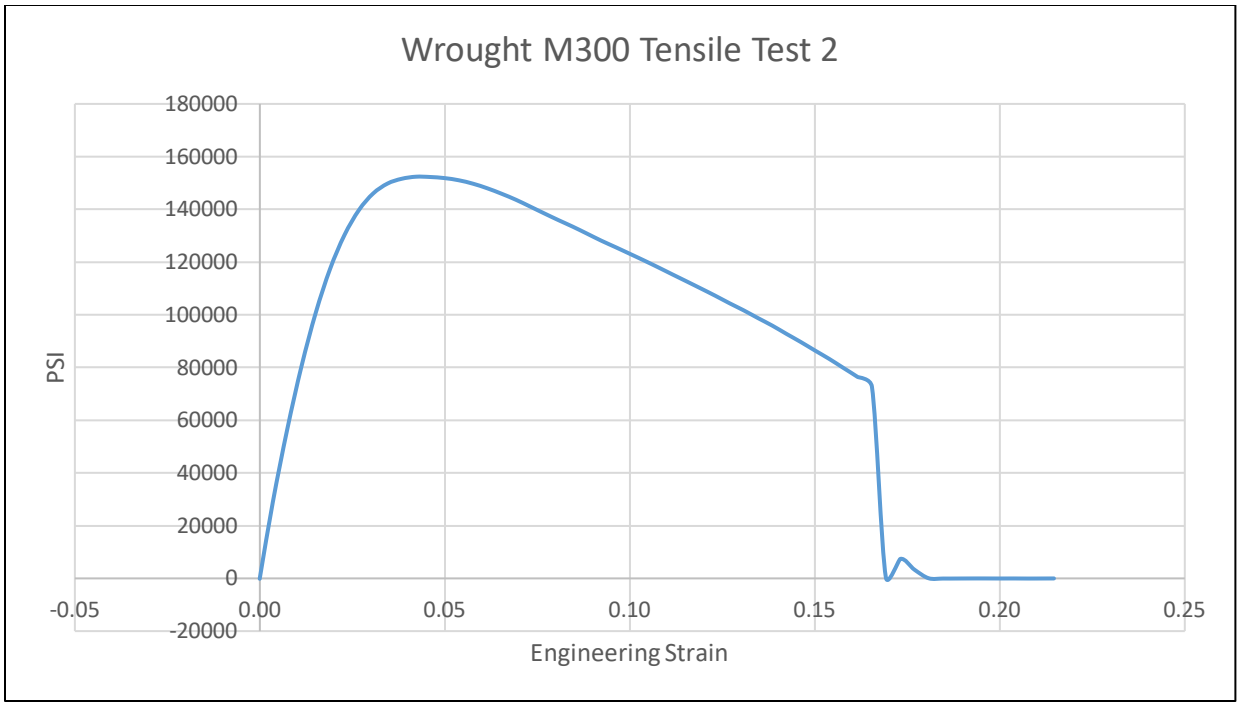
Wrought M300 Tensile Test 2
180000
160000
140000
120000
100000
80000
60000
40000
20000
0
-20000
PSI
-0.05
0.00
0.05
0.10
0.15
0.20
0.25
Engineering Strain

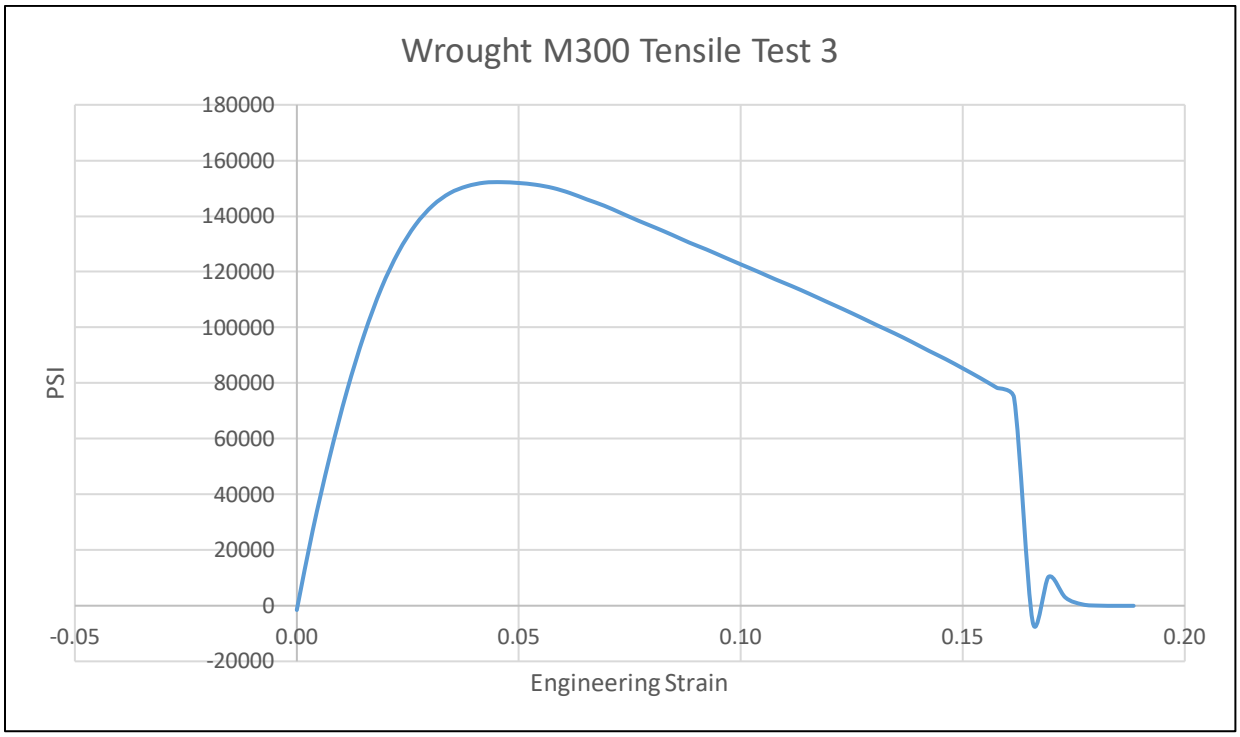
Wrought M300 Tensile Test 3
180000
160000
140000
120000
100000
80000
60000
40000
20000
0
-20000
PSI
-0.05
0.00
0.05
0.10
0.15
0.20
Engineering Strain

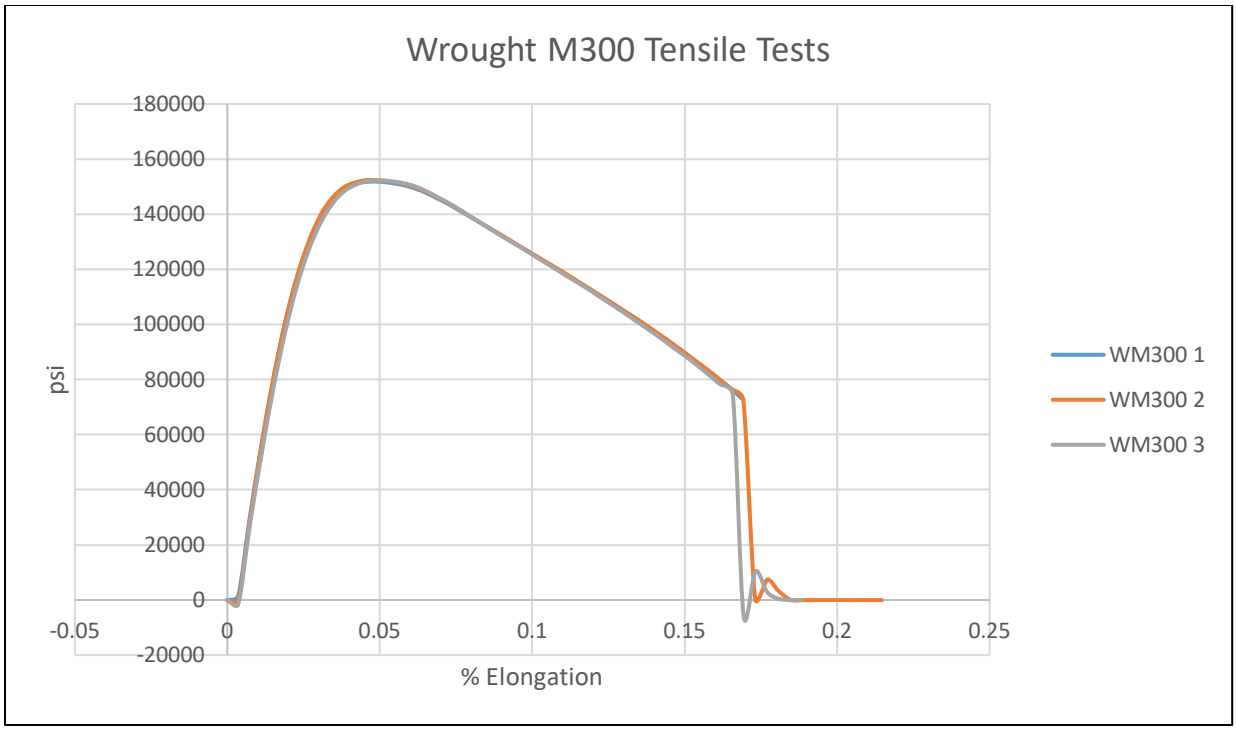
Wrought M300 Tensile Tests
180000
160000
140000
120000
100000
80000
60000
40000
20000
0
-20000
psi
-0.05
0
0.05
0.1
0.15
0.2
0.25
% Elongation
WM300 1
WM300 2
WM300 3

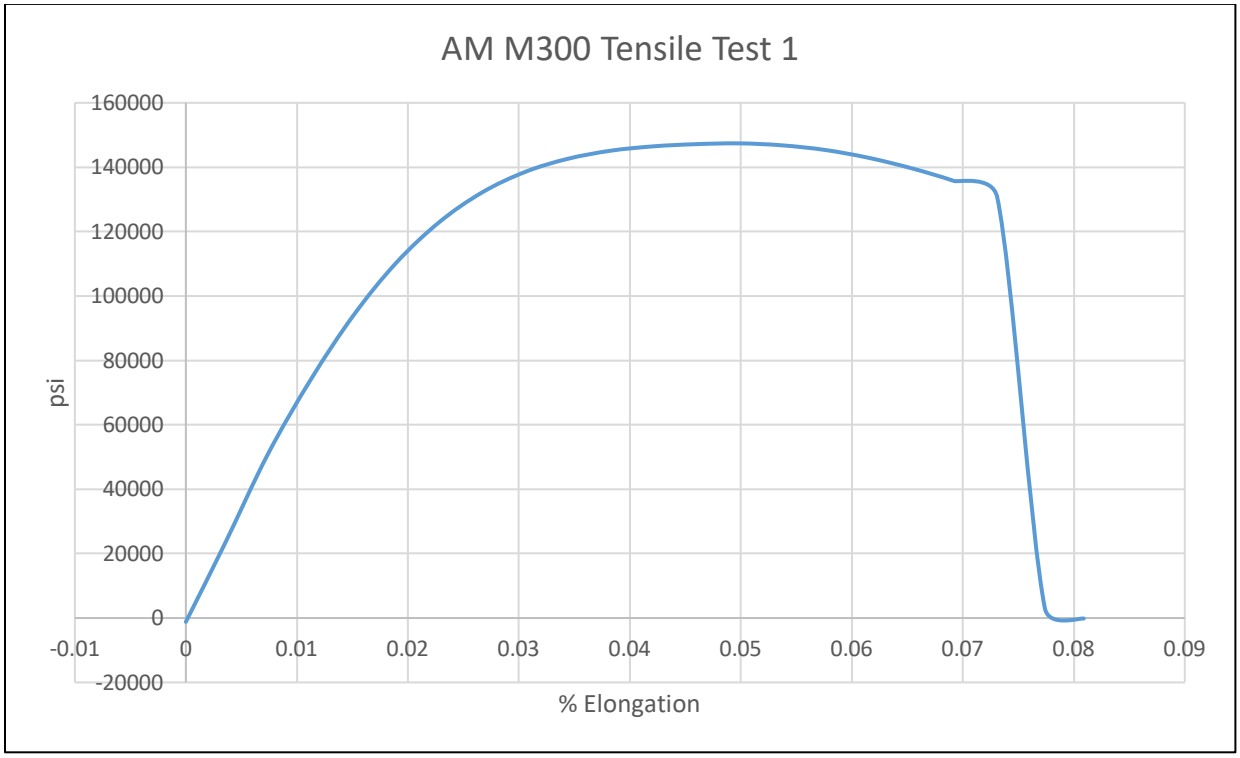
AM M300 Tensile Test 1
160000
140000
120000
100000
80000
60000
40000
20000
0
-20000
psi
-0.01
0
0.01
0.02
0.03
0.04
0.05
0.06
0.07
0.08
0.09
% Elongation

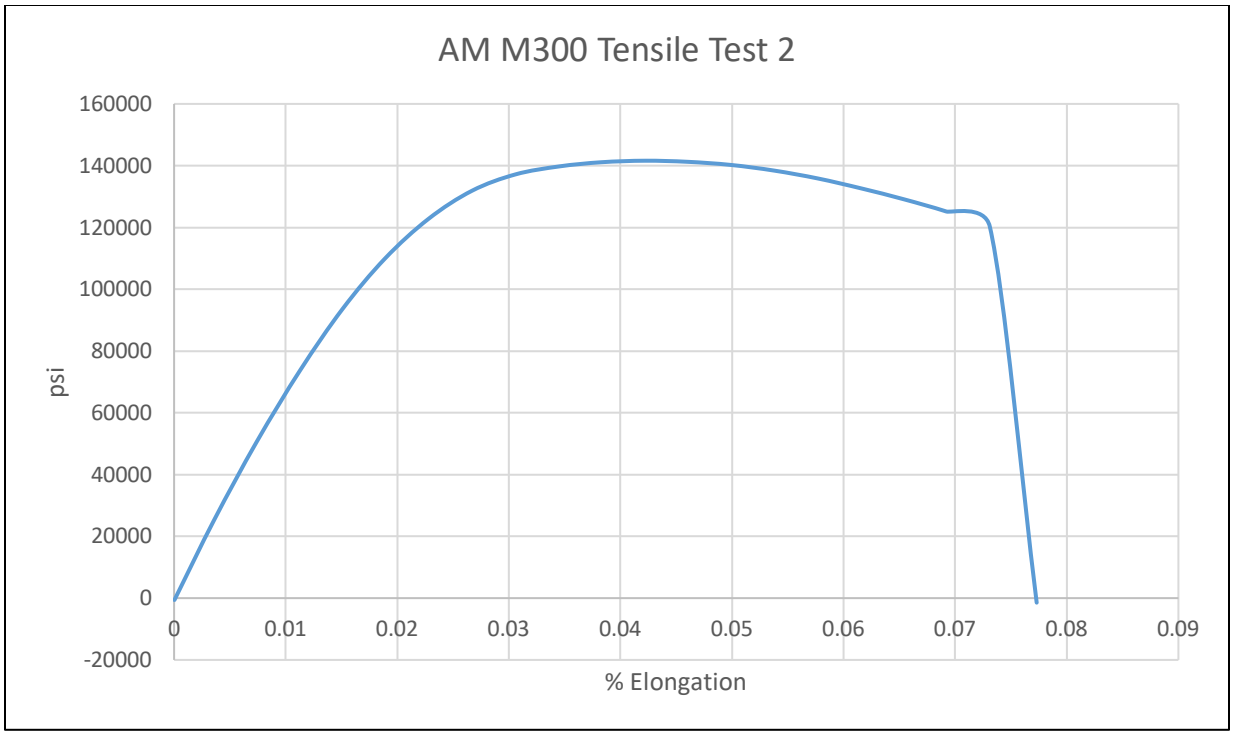
AM M300 Tensile Test 2
160000
140000
120000
100000
80000
60000
40000
20000
0
-20000
psi
0
0.01
0.02
0.03
0.04
0.05
0.06
0.07
0.08
0.09
% Elongation

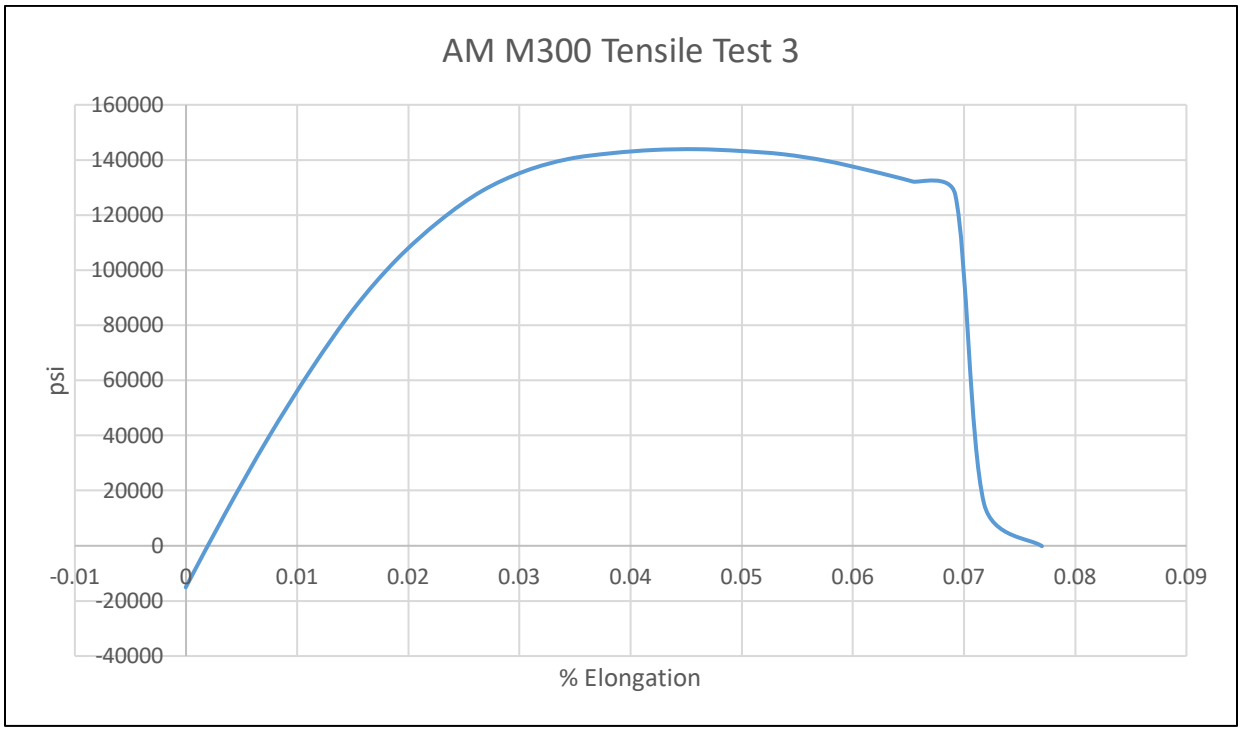
AM M300 Tensile Test 3
160000
140000
120000
100000
80000
60000
40000
20000
0
-20000
-40000
psi
-0.01
0
0.01
0.02
0.03
0.04
0.05
0.06
0.07
0.08
0.09
% Elongation

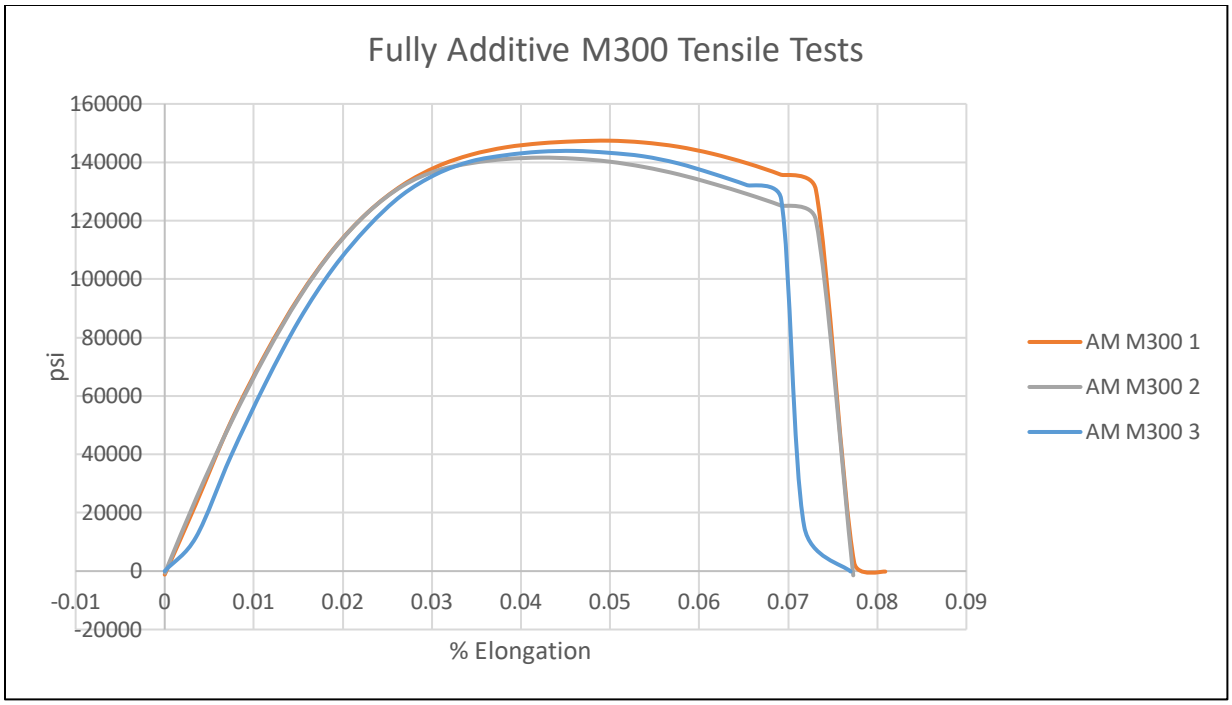
Fully Additive M300 Tensile Tests
160000
140000
120000
100000
80000
60000
40000
20000
0
-20000
psi
-0.01
0
0.01
0.02
0.03
0.04
0.05
0.06
0.07
0.08
0.09
% Elongation
AM M300 1
AM M300 2
AM M300 3

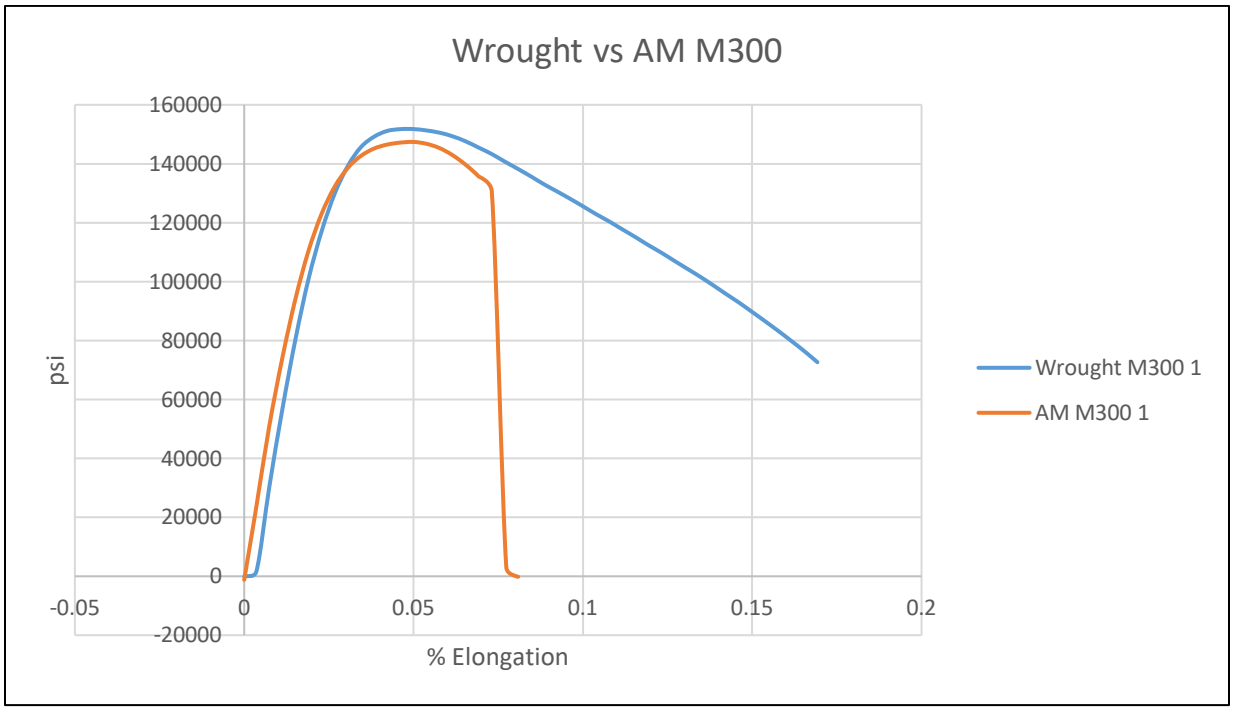
Wrought vs AM M300
160000
140000
120000
100000
80000
60000
40000
20000
0
-20000
psi
-0.05
0
0.05
0.1
0.15
0.2
% Elongation
Wrought M300 1
AM M300 1

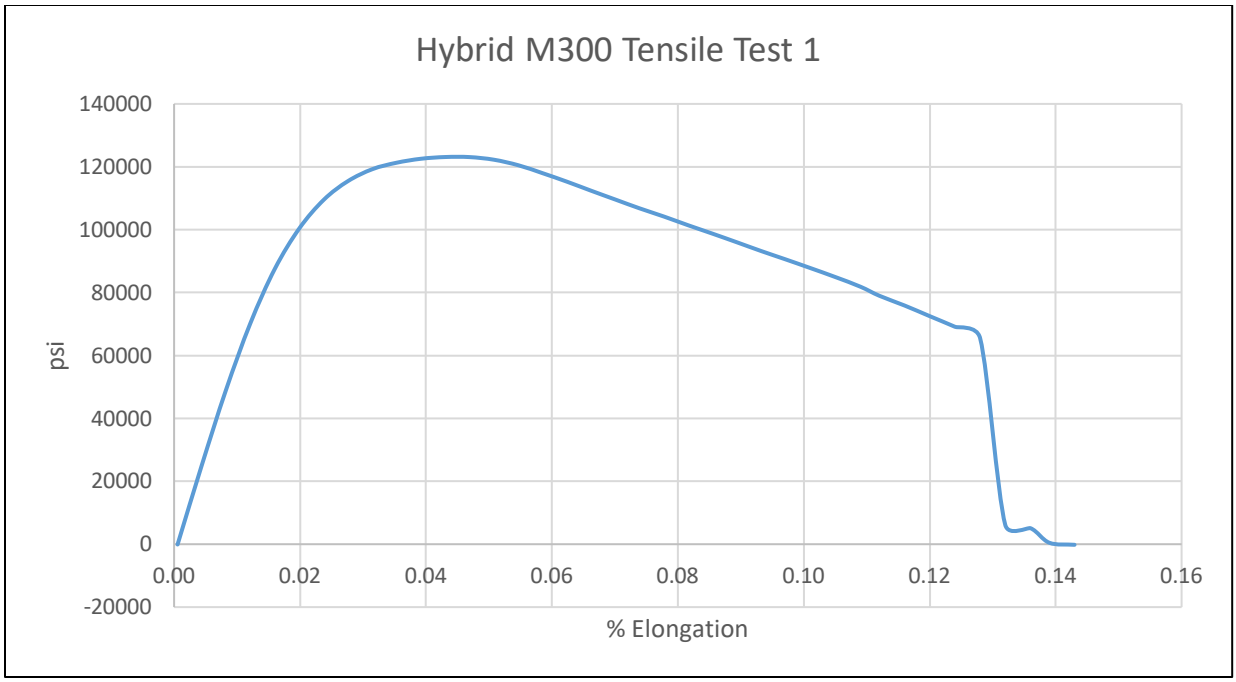
Hybrid M300 Tensile Test 1
140000
120000
100000
80000
60000
40000
20000
0
-20000
psi
0.00
0.02
0.04
0.06
0.08
0.10
0.12
0.14
0.16
% Elongation

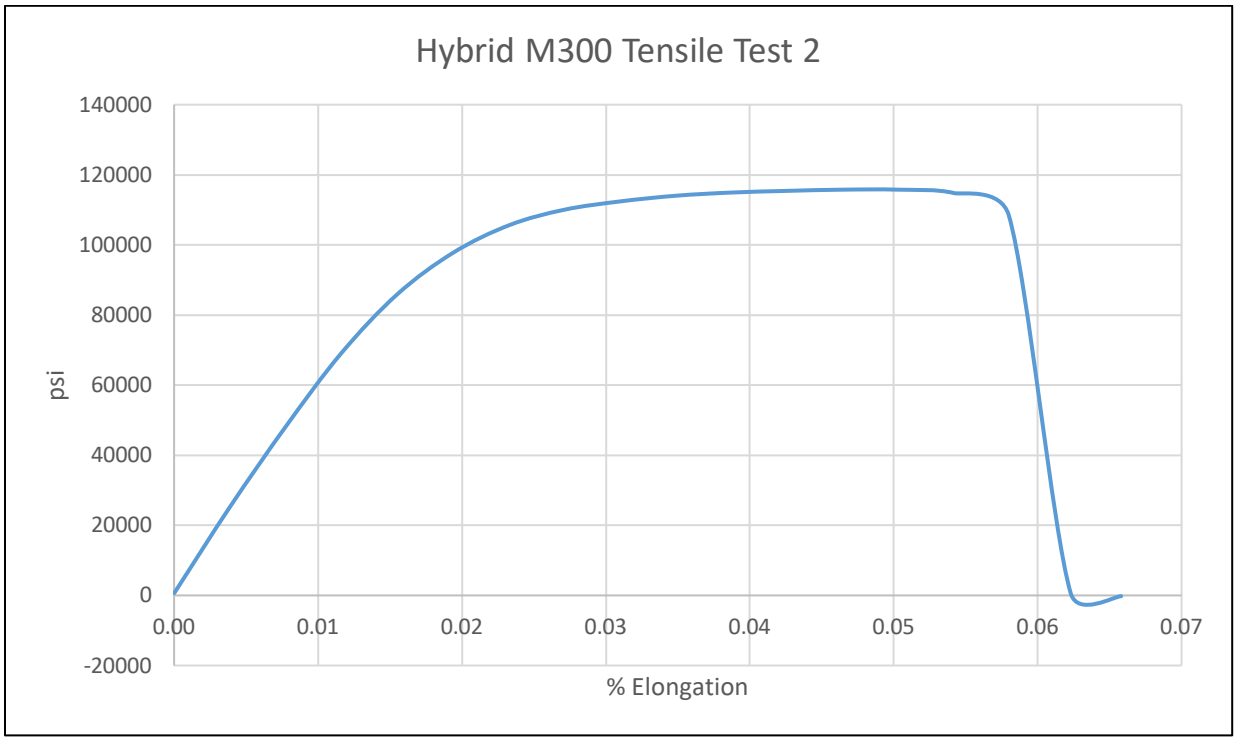
Hybrid M300 Tensile Test 2
140000
120000
100000
80000
60000
40000
20000
0
-20000
psi
0.00
0.01
0.02
0.03
0.04
0.05
0.06
0.07
% Elongation

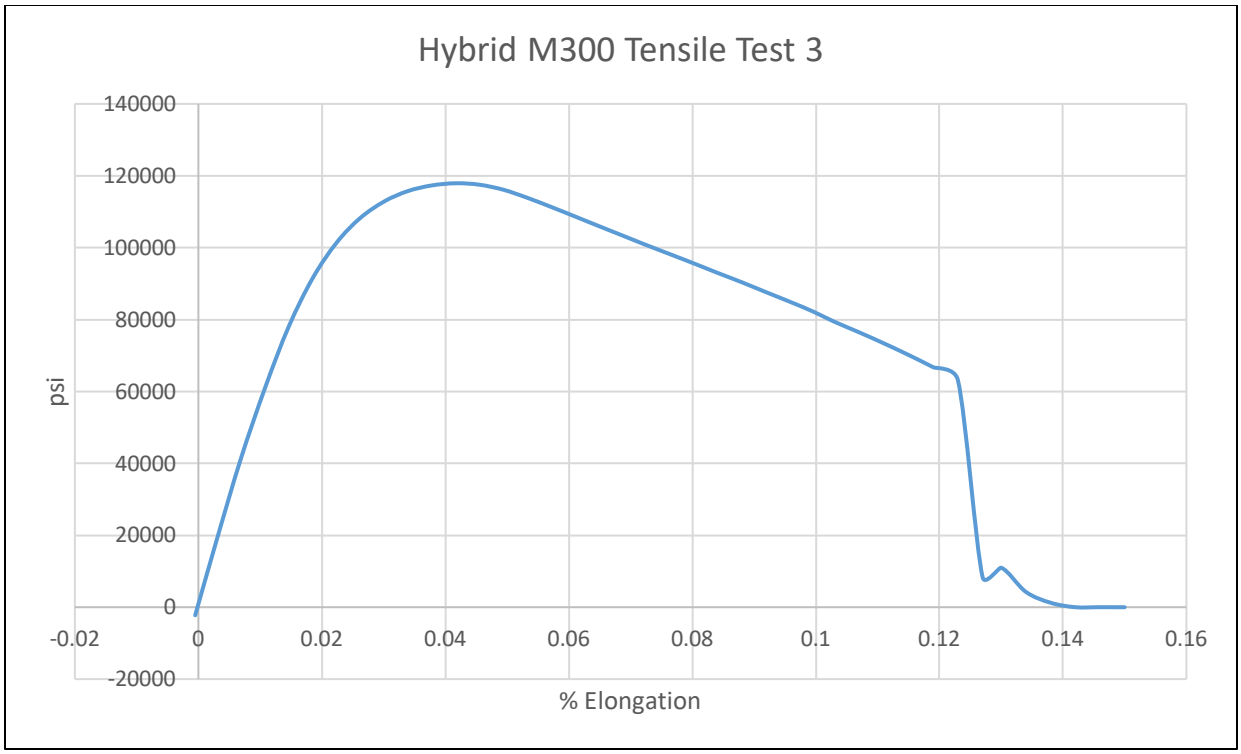
Hybrid M300 Tensile Test 3
140000
120000
100000
80000
60000
40000
20000
0
-20000
psi
-0.02
0
0.02
0.04
0.06
0.08
0.1
0.12
0.14
0.16
% Elongation

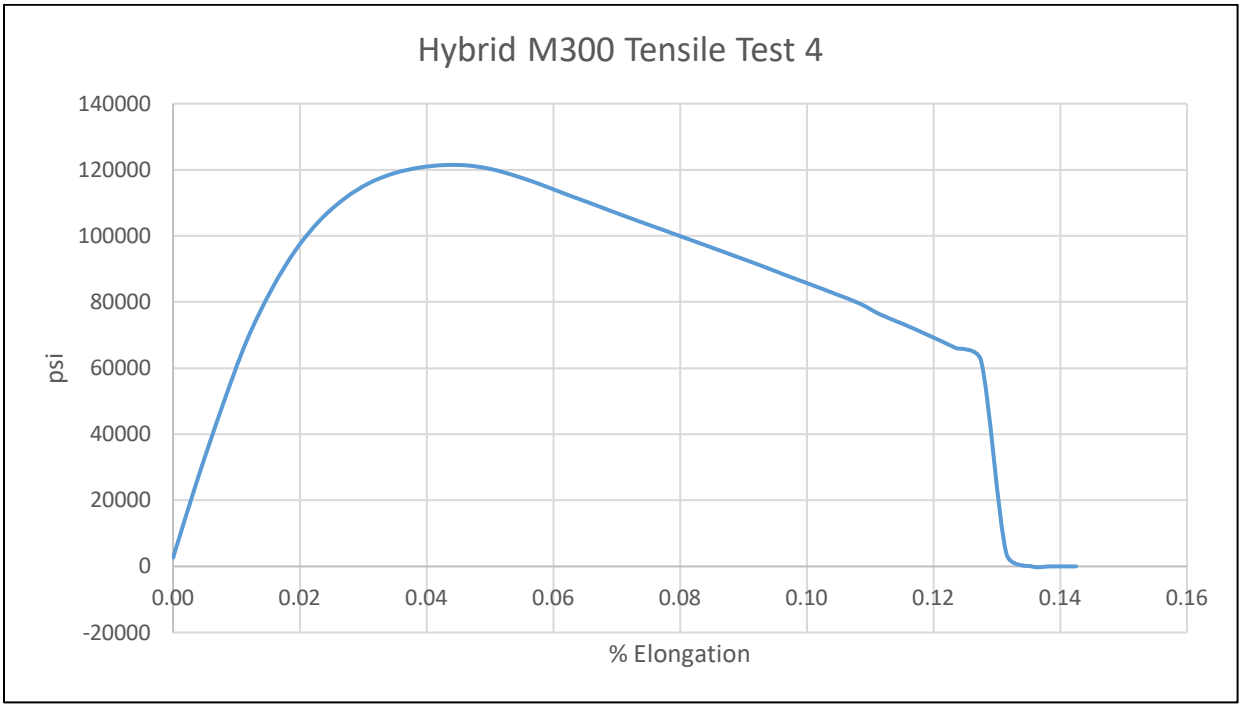
Hybrid M300 Tensile Test 4
140000
120000
100000
80000
60000
40000
20000
0
-20000
psi
0.00
0.02
0.04
0.06
0.08
0.10
0.12
0.14
0.16
% Elongation

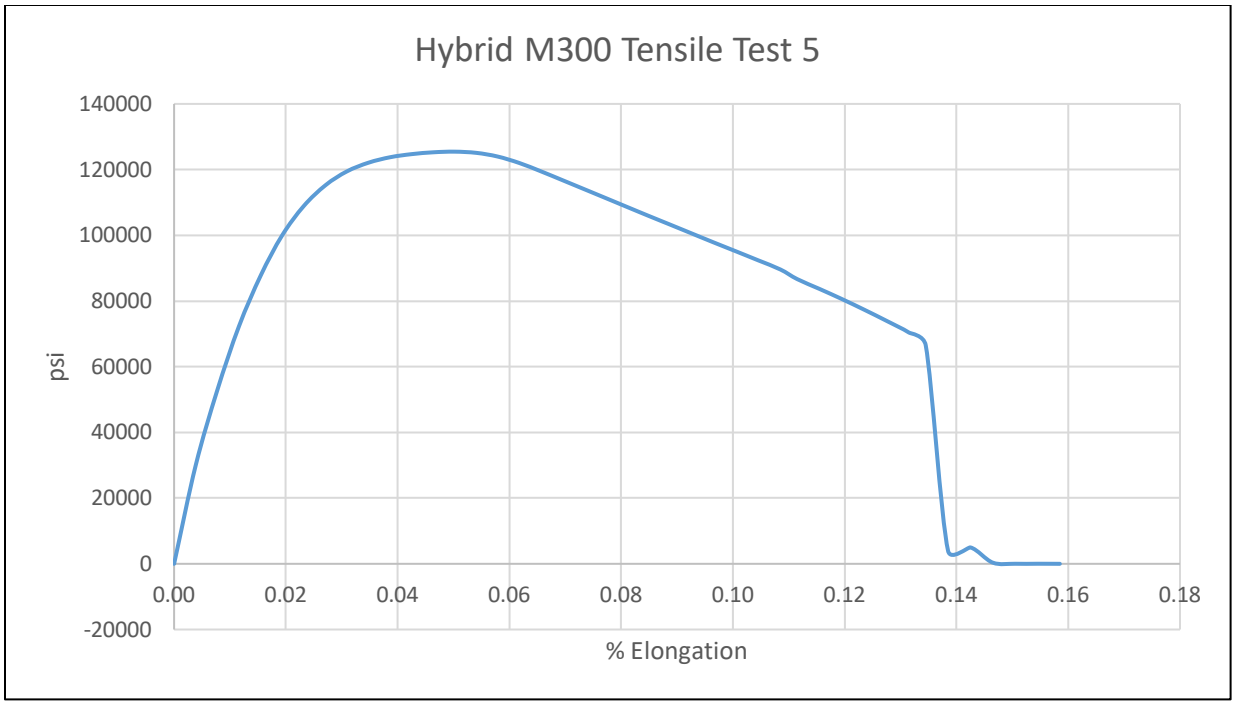
Hybrid M300 Tensile Test 5
140000
120000
100000
80000
60000
40000
20000
0
-20000
psi
0.00
0.02
0.04
0.06
0.08
0.10
0.12
0.14
0.16
0.18
% Elongation

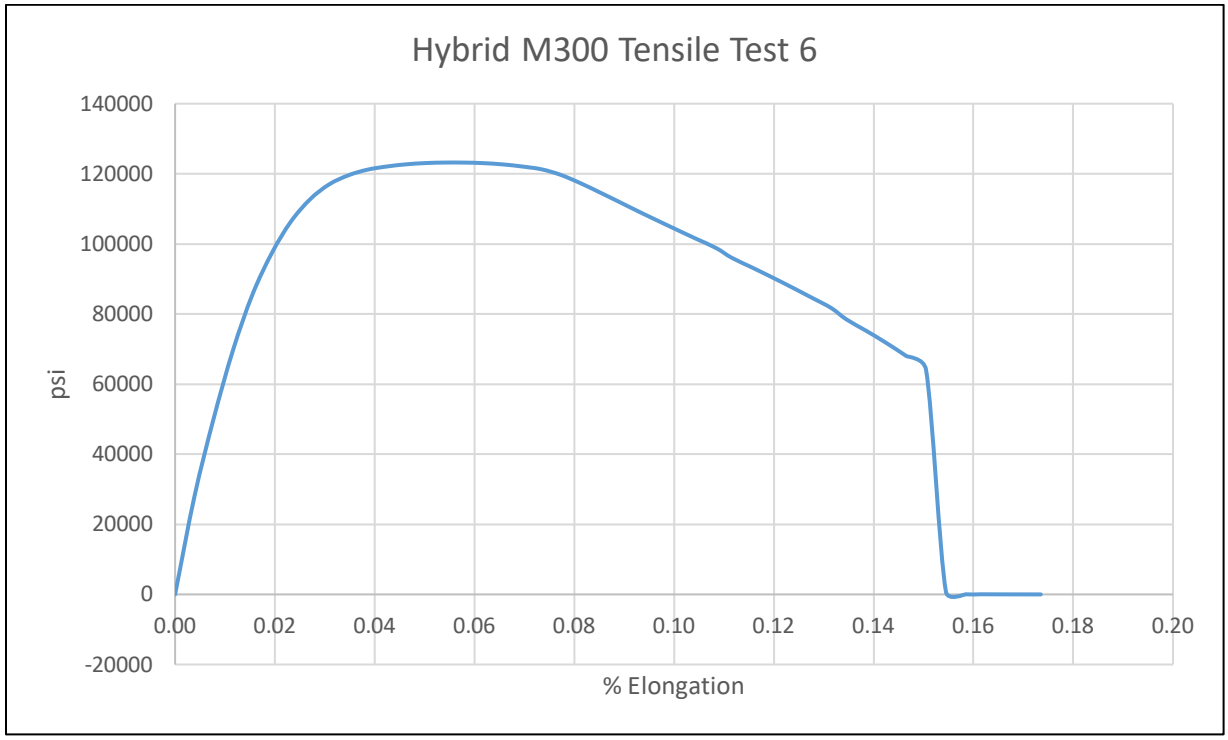
Hybrid M300 Tensile Test 6
140000
120000
100000
80000
60000
40000
20000
0
-20000
psi
0.00
0.02
0.04
0.06
0.08
0.10
0.12
0.14
0.16
0.18
0.20
% Elongation

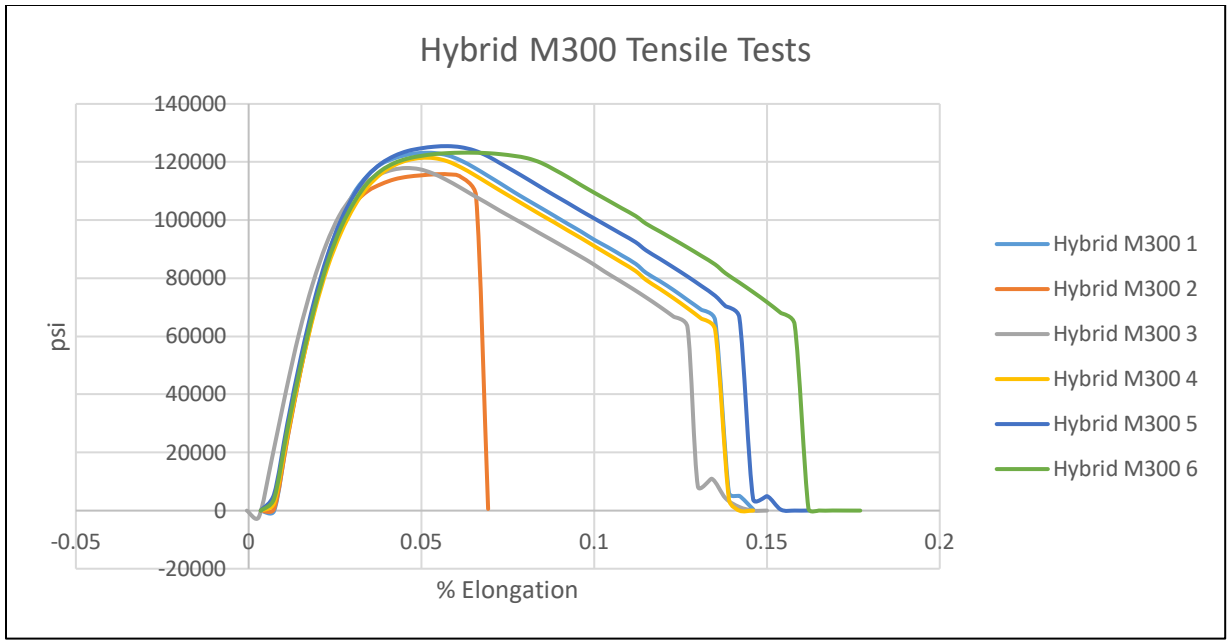
Hybrid M300 Tensile Tests
140000
120000
100000
80000
60000
40000
20000
0
-20000
psi
-0.05
0
0.05
0.1
0.15
0.2
% Elongation
Hybrid M300 1
Hybrid M300 2
Hybrid M300 3
Hybrid M300 4
Hybrid M300 5
Hybrid M300 6

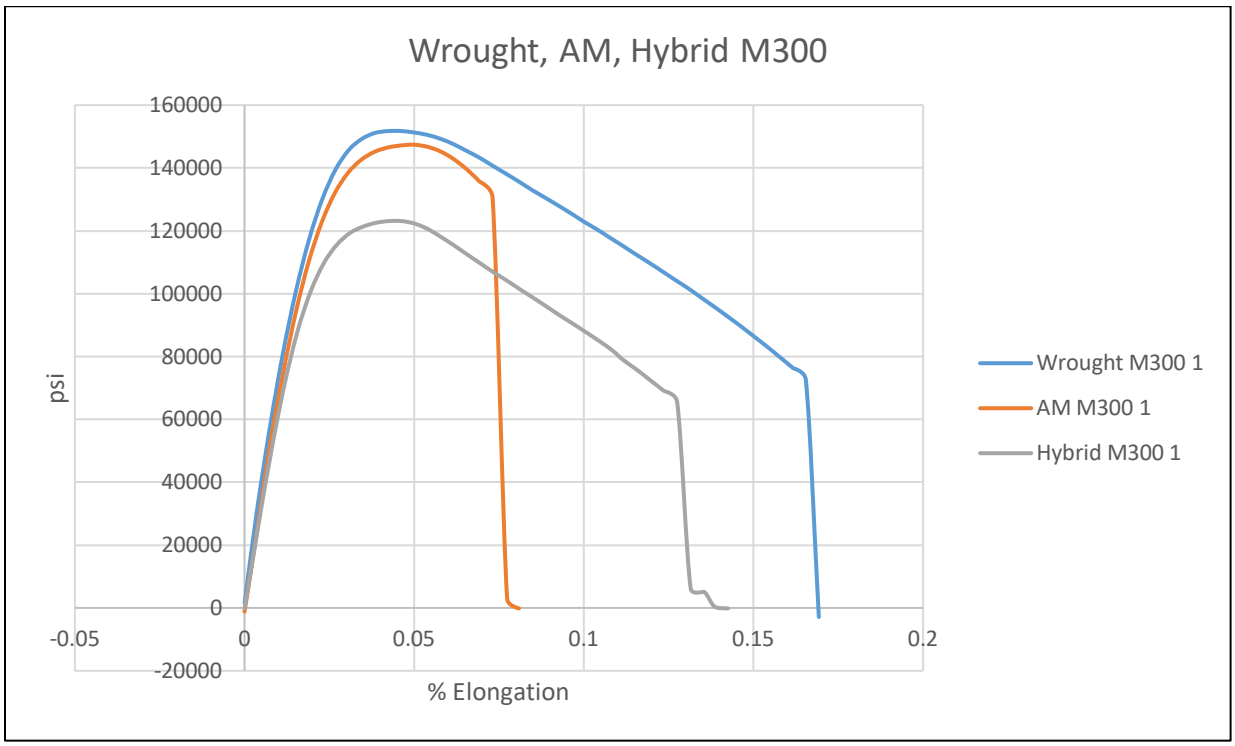
Wrought, AM, Hybrid M300
160000
140000
120000
100000
80000
60000
40000
20000
0
-20000
psi
-0.05
0
0.05
0.1
0.15
0.2
% Elongation
Wrought M300 1
AM M300 1
Hybrid M300 1

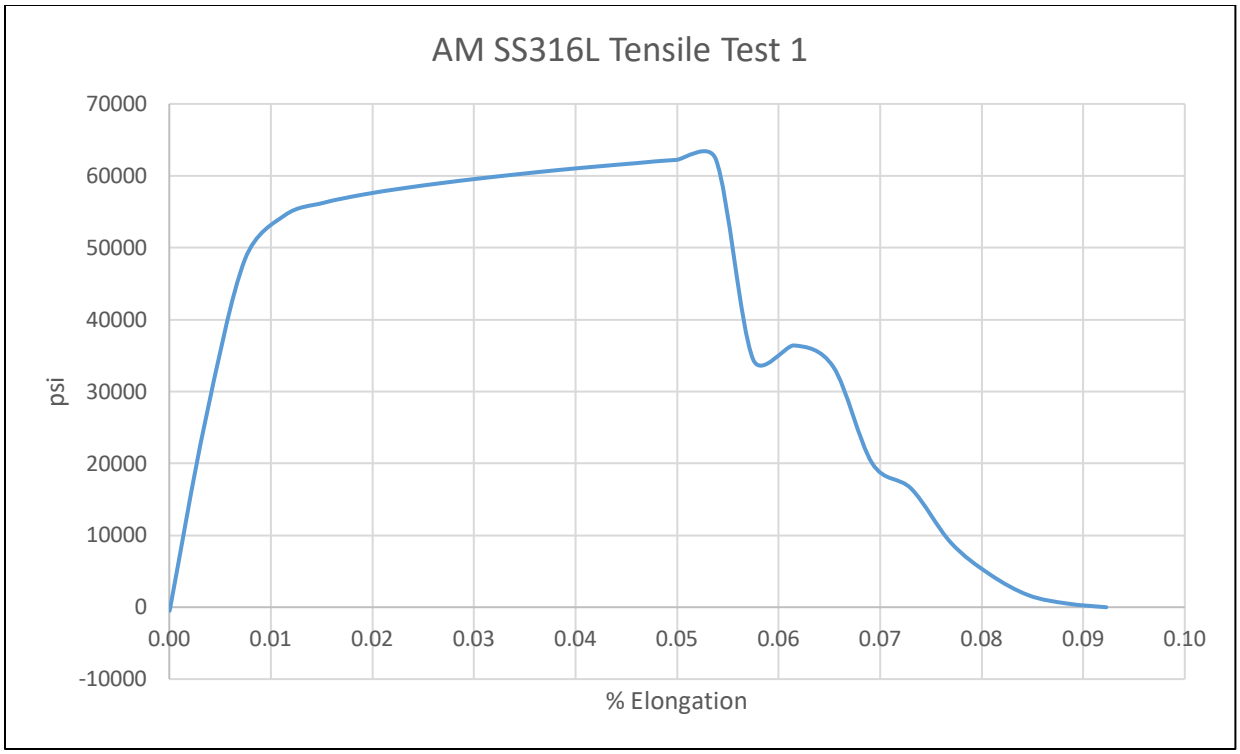
AM SS316L Tensile Test 1
70000
60000
50000
40000
30000
20000
10000
0
-10000
psi
0.00
0.01
0.02
0.03
0.04
0.05
0.06
0.07
0.08
0.09
0.10
% Elongation

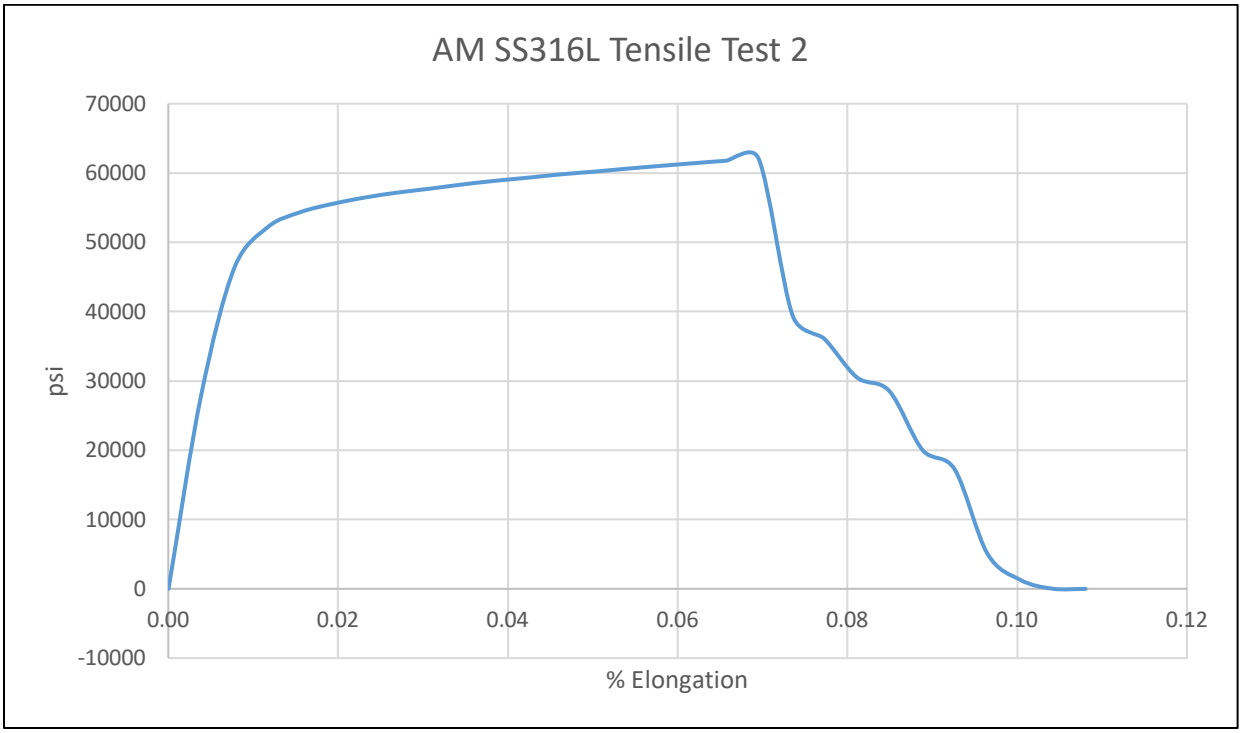
AM SS316L Tensile Test 2
70000
60000
50000
40000
30000
20000
10000
0
-10000
psi
0.00
0.02
0.04
0.06
0.08
0.10
0.12
% Elongation

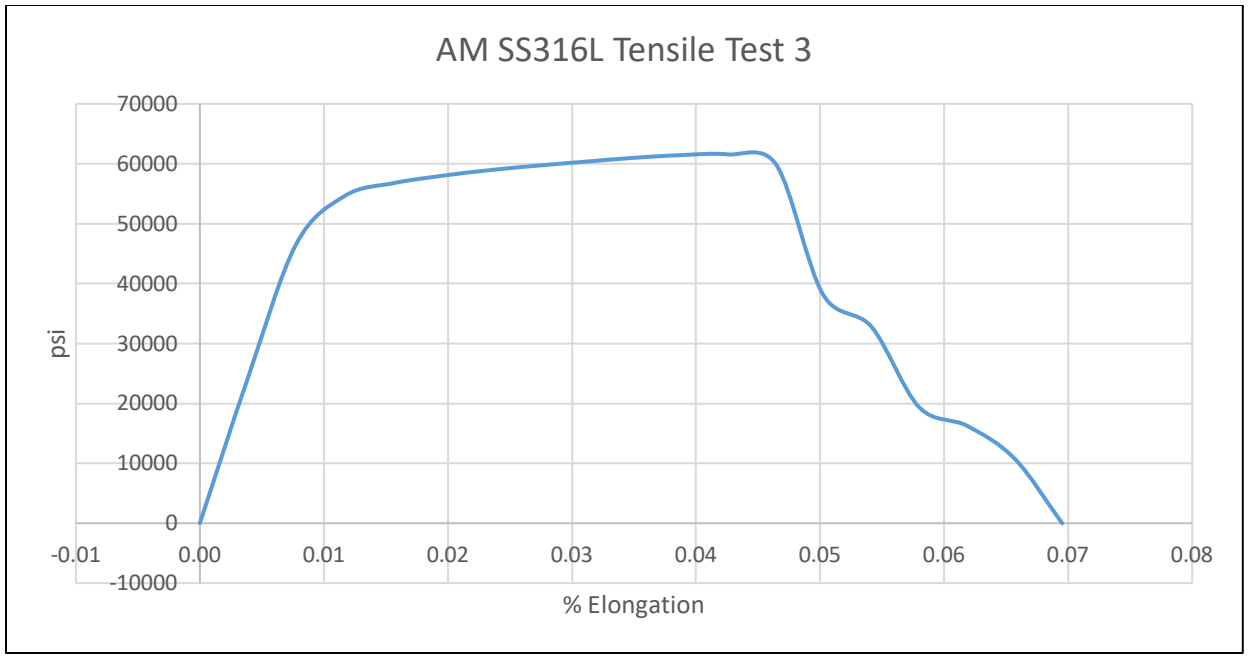
AM SS316L Tensile Test 3
70000
60000
50000
40000
30000
20000
10000
0
-10000
psi
-0.01
0.00
0.01
0.02
0.03
0.04
0.05
0.06
0.07
0.08
% Elongation

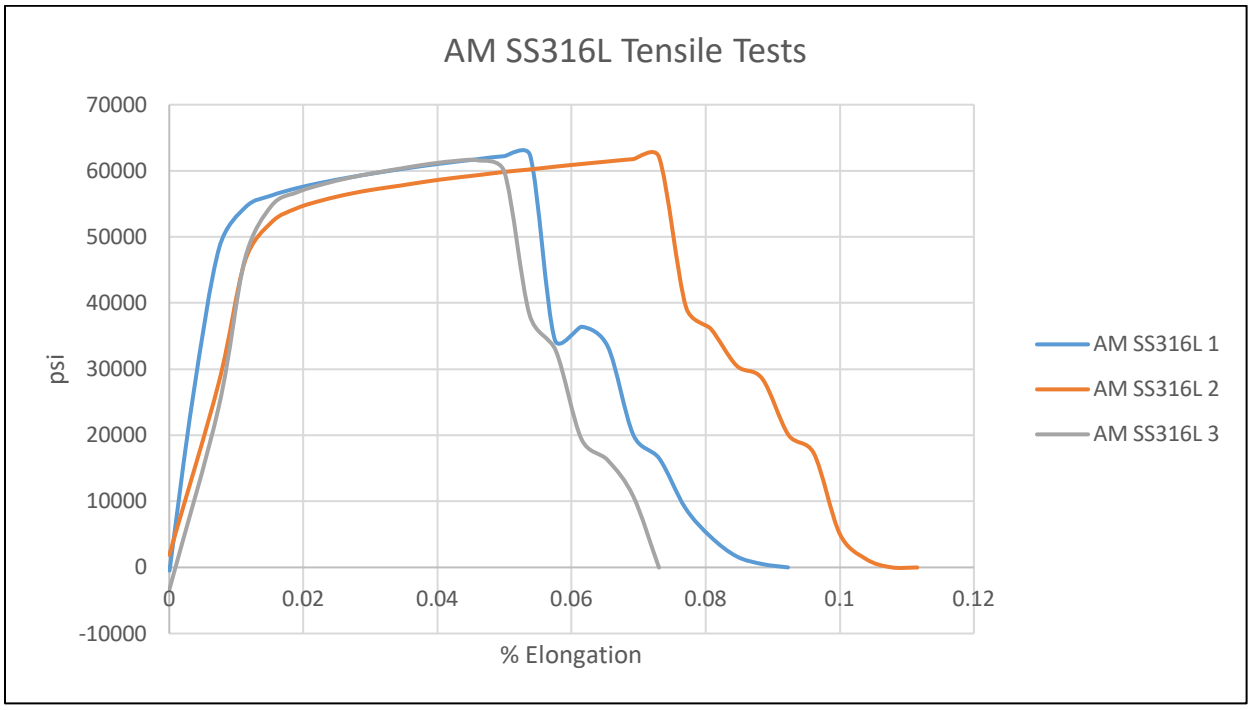
AM SS316L Tensile Tests
70000
60000
50000
40000
30000
20000
10000
0
-10000
psi
0
0.02
0.04
0.06
0.08
0.1
0.12
% Elongation
AM SS316L 1
AM SS316L 2
AM SS316L 3

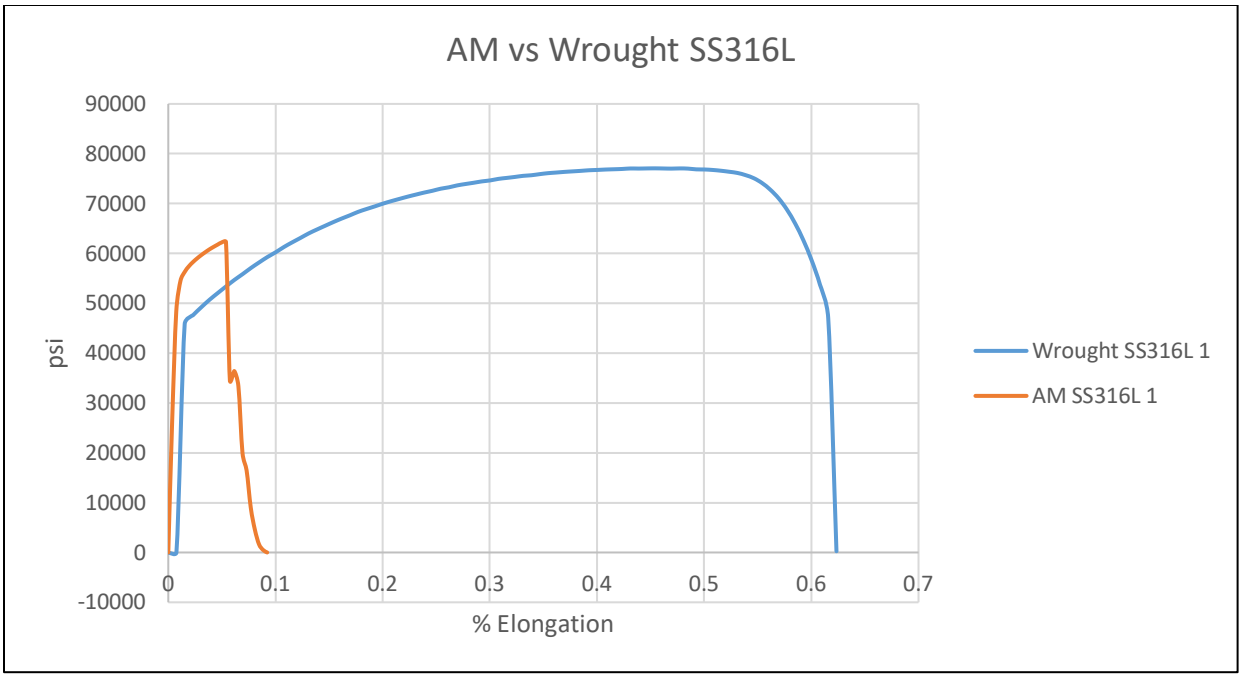
AM vs Wrought SS316L
90000
80000
70000
60000
50000
40000
30000
20000
10000
0
-10000
psi
0
0.1
0.2
0.3
0.4
0.5
0.6
0.7
% Elongation
Wrought SS316L 1
AM SS316L 1

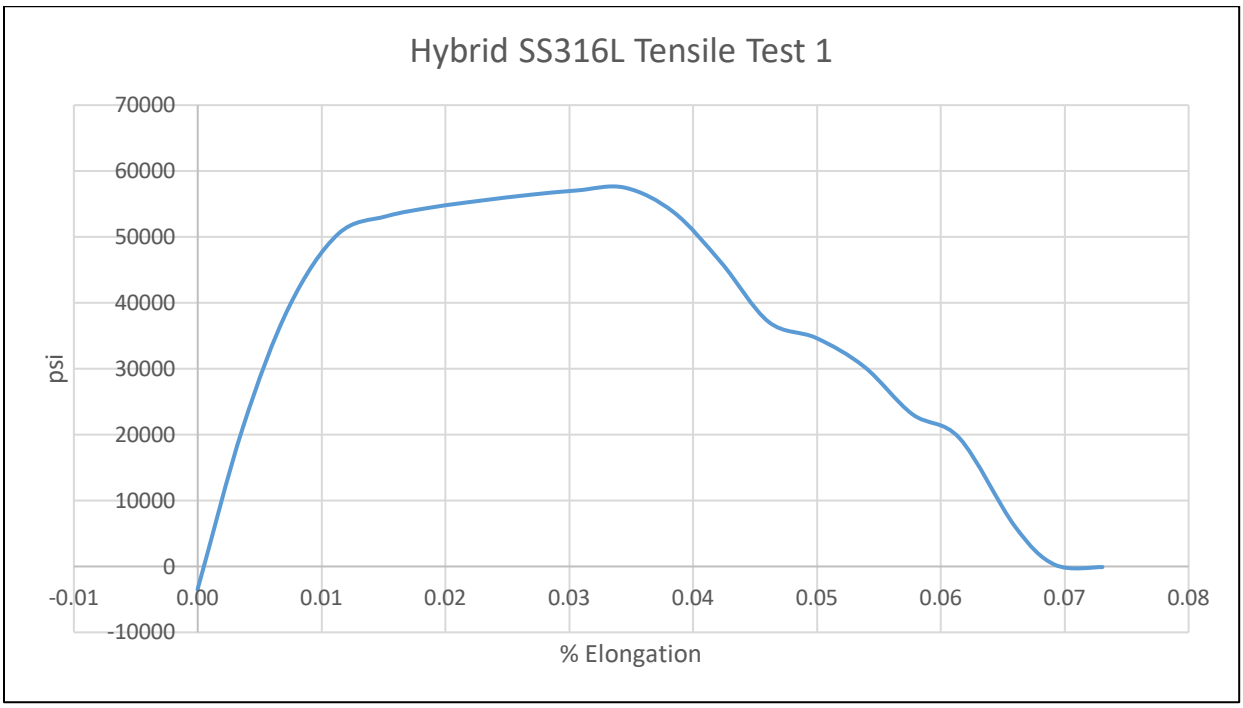
Hybrid SS316L Tensile Test 1
70000
60000
50000
40000
30000
20000
10000
0
-10000
psi
-0.01
0.00
0.01
0.02
0.03
0.04
0.05
0.06
0.07
0.08
% Elongation

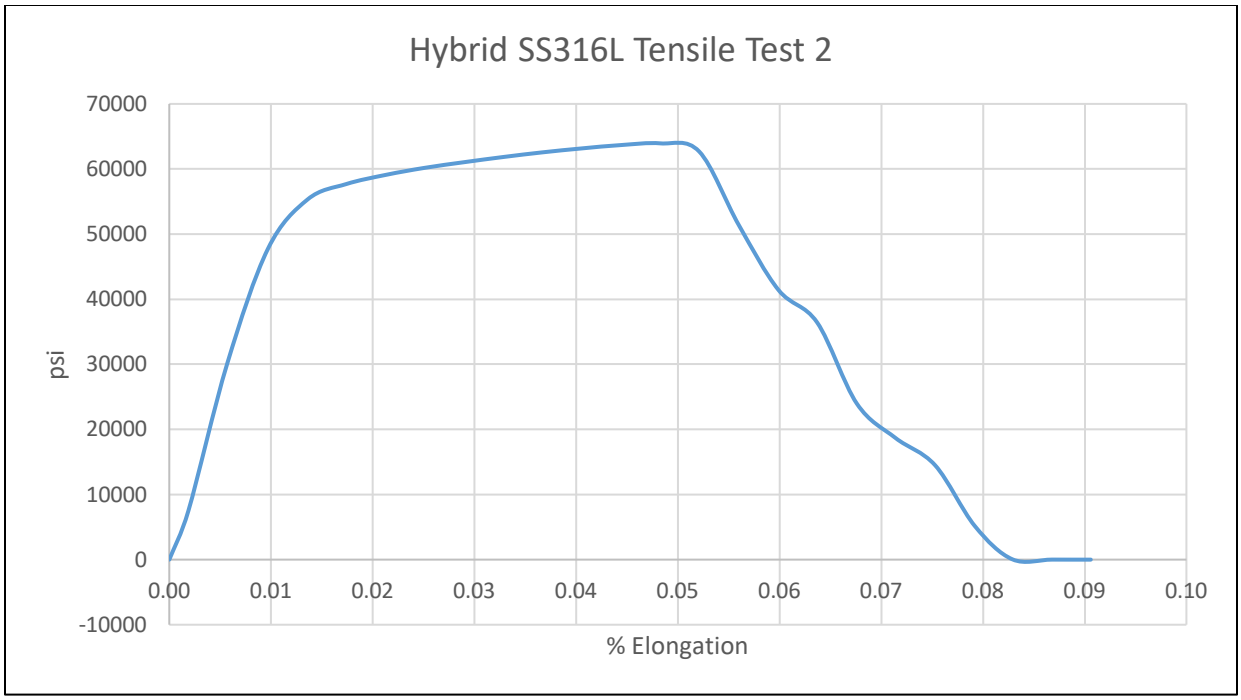
Hybrid SS316L Tensile Test 2
70000
60000
50000
40000
30000
20000
10000
0
-10000
psi
0.00
0.01
0.02
0.03
0.04
0.05
0.06
0.07
0.08
0.09
0.10
% Elongation

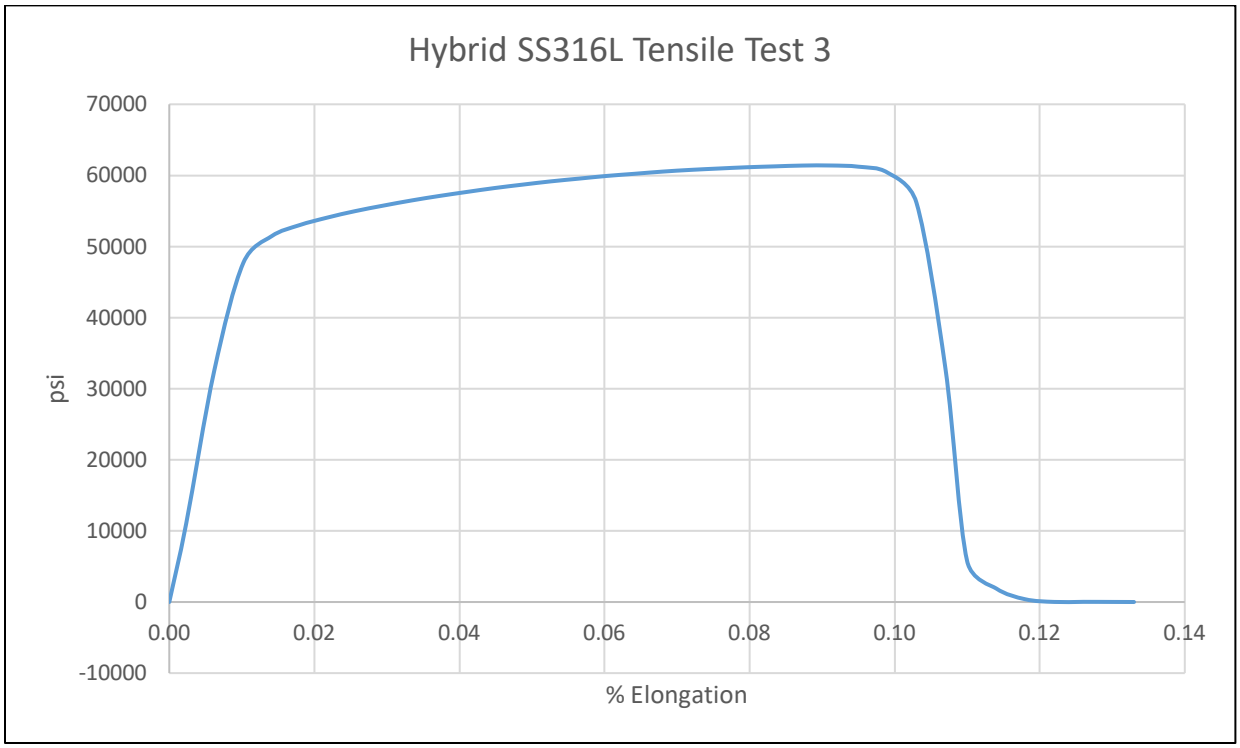
Hybrid SS316L Tensile Test 3
70000
60000
50000
40000
30000
20000
10000
0
-10000
psi
0.00
0.02
0.04
0.06
0.08
0.10
0.12
0.14
% Elongation

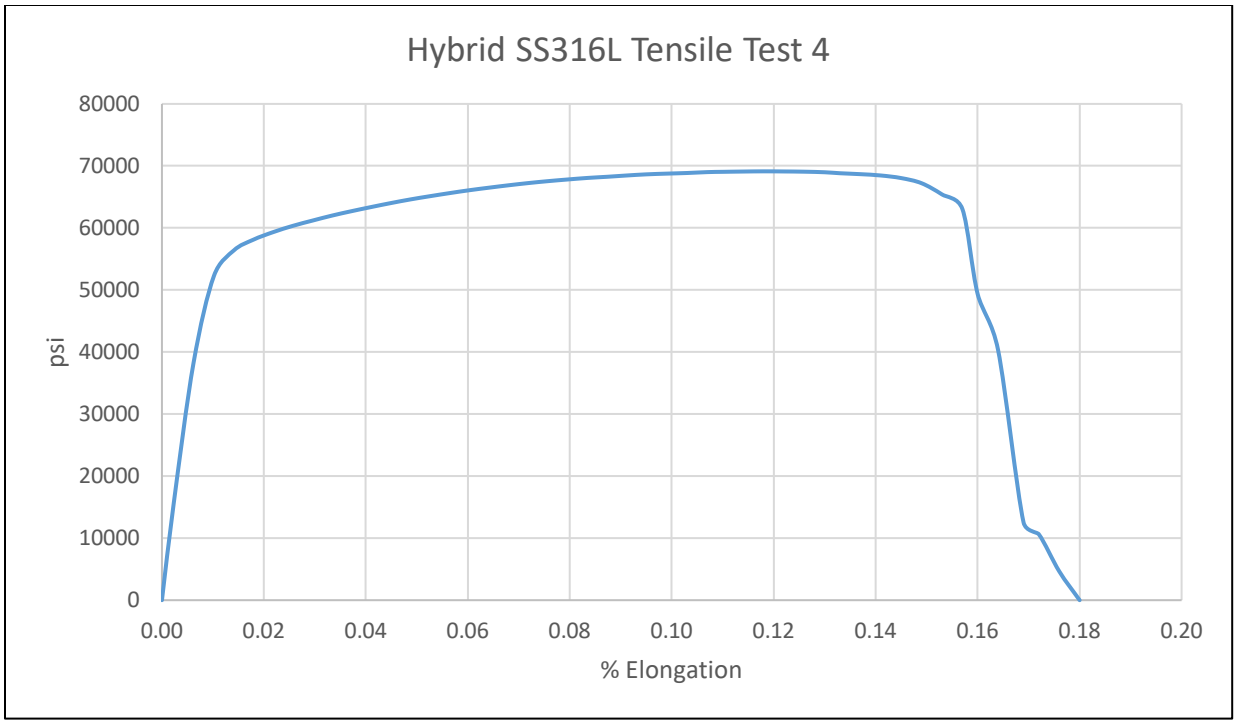
Hybrid SS316L Tensile Test 4
80000
70000
60000
50000
40000
30000
20000
10000
0
psi
0.00
0.02
0.04
0.06
0.08
0.10
0.12
0.14
0.16
0.18
0.20
% Elongation

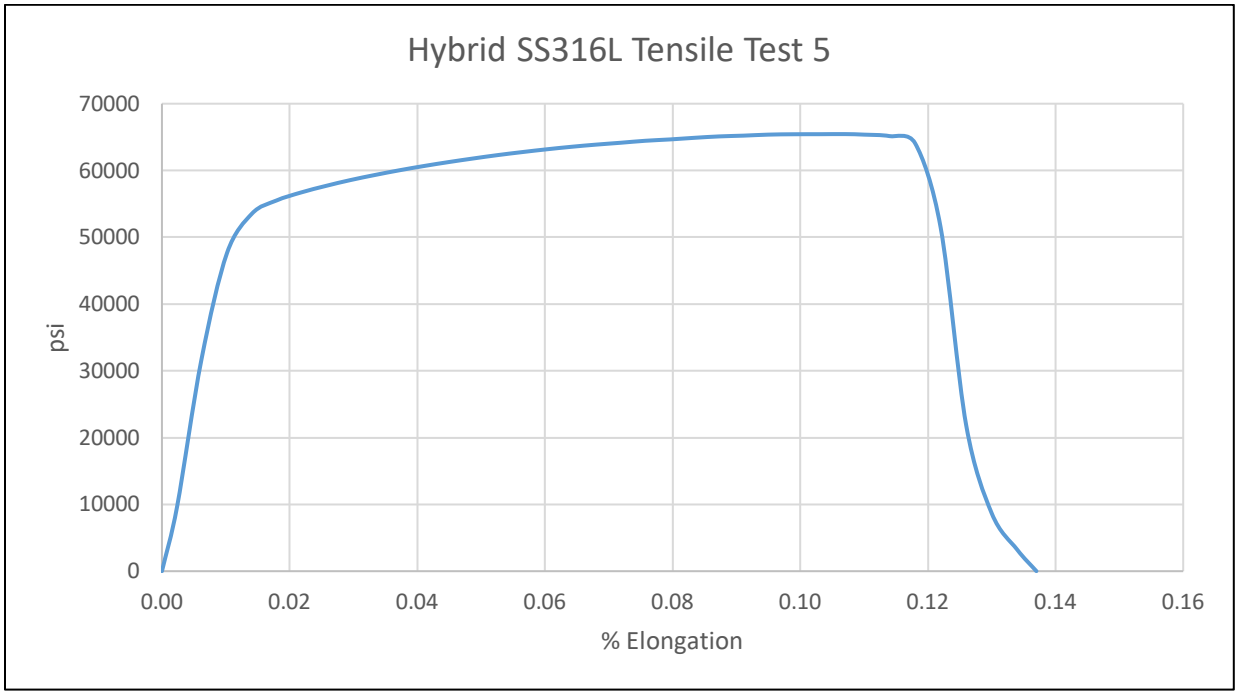
Hybrid SS316L Tensile Test 5
70000
60000
50000
40000
30000
20000
10000
0
psi
0.00
0.02
0.04
0.06
0.08
0.10
0.12
0.14
0.16
% Elongation

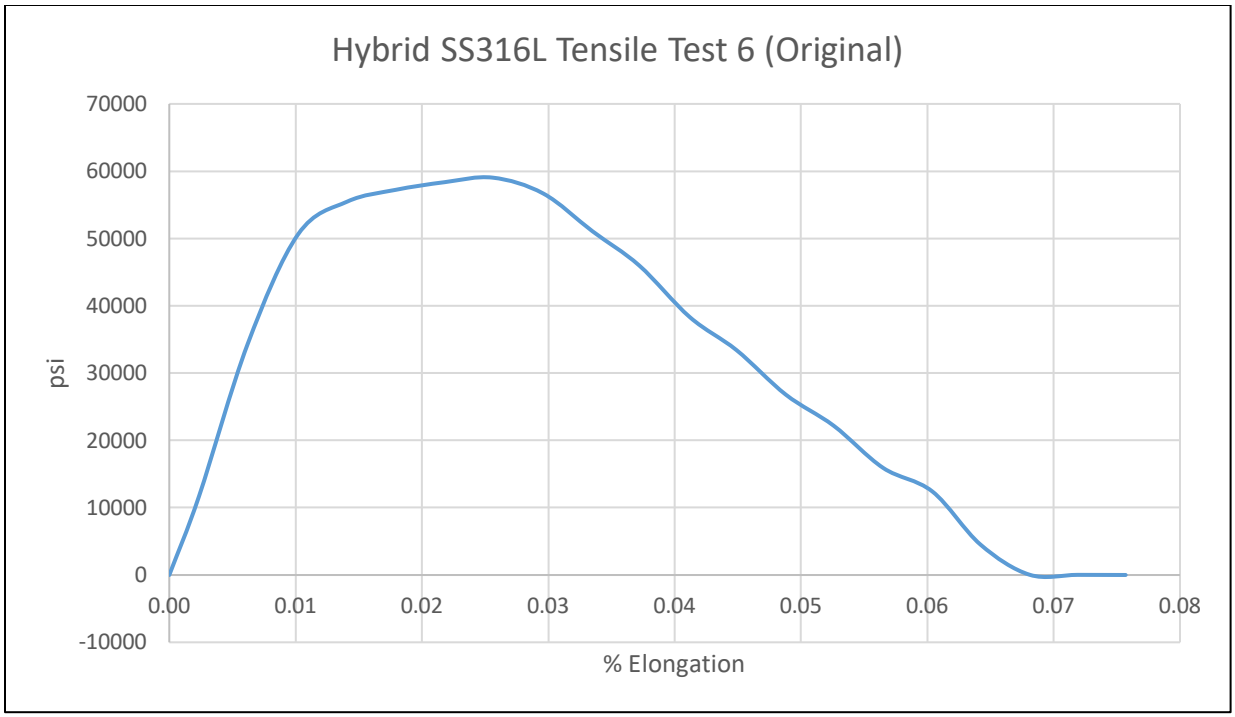
Hybrid SS316L Tensile Test 6 (Original)
70000
60000
50000
40000
30000
20000
10000
0
-10000
psi
0.00
0.01
0.02
0.03
0.04
0.05
0.06
0.07
0.08
% Elongation

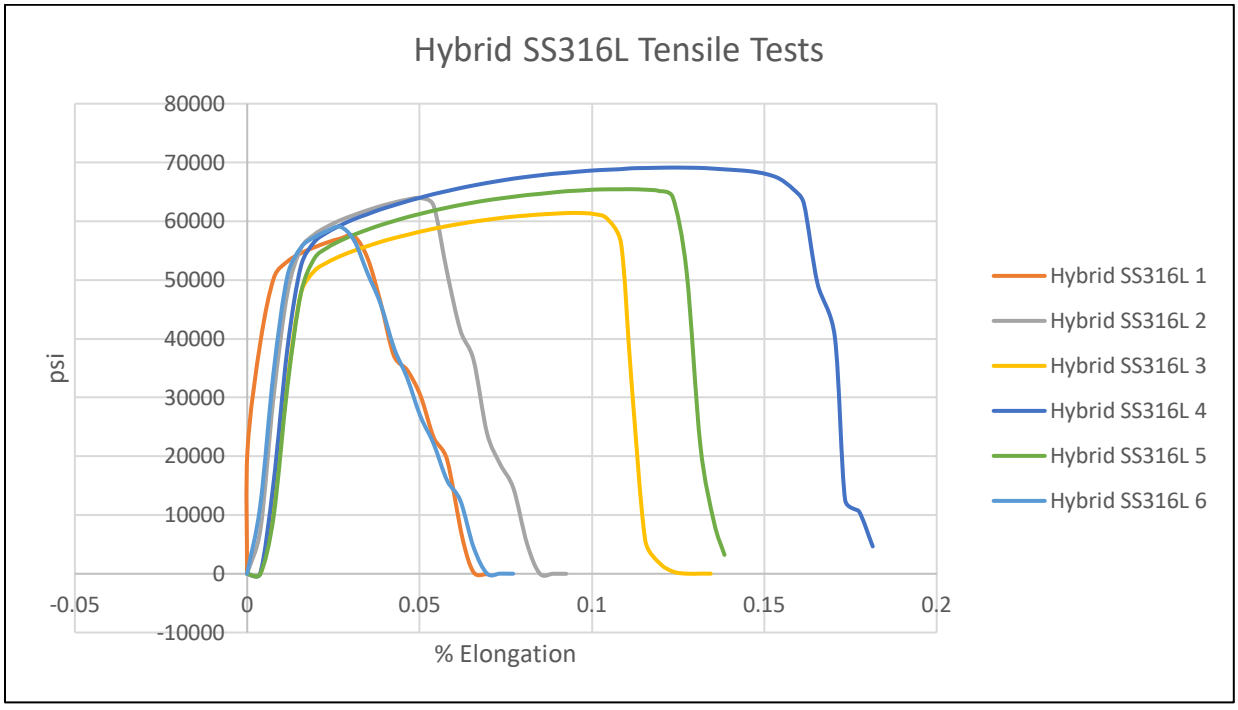
Hybrid SS316L Tensile Tests
80000
70000
60000
50000
40000
30000
20000
10000
0
-10000
psi
-0.05
0
0.05
0.1
0.15
0.2
% Elongation
Hybrid SS316L 1
Hybrid SS316L 2
Hybrid SS316L 3
Hybrid SS316L 4
Hybrid SS316L 5
Hybrid SS316L 6

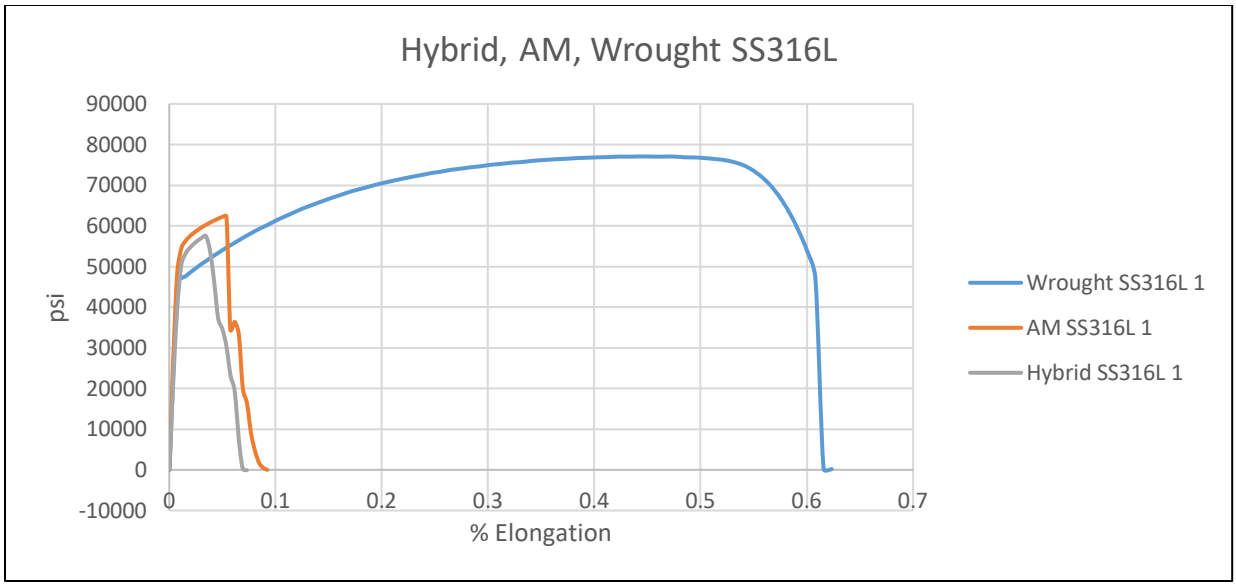

Microscopy Images

DED SS316L @ 32X

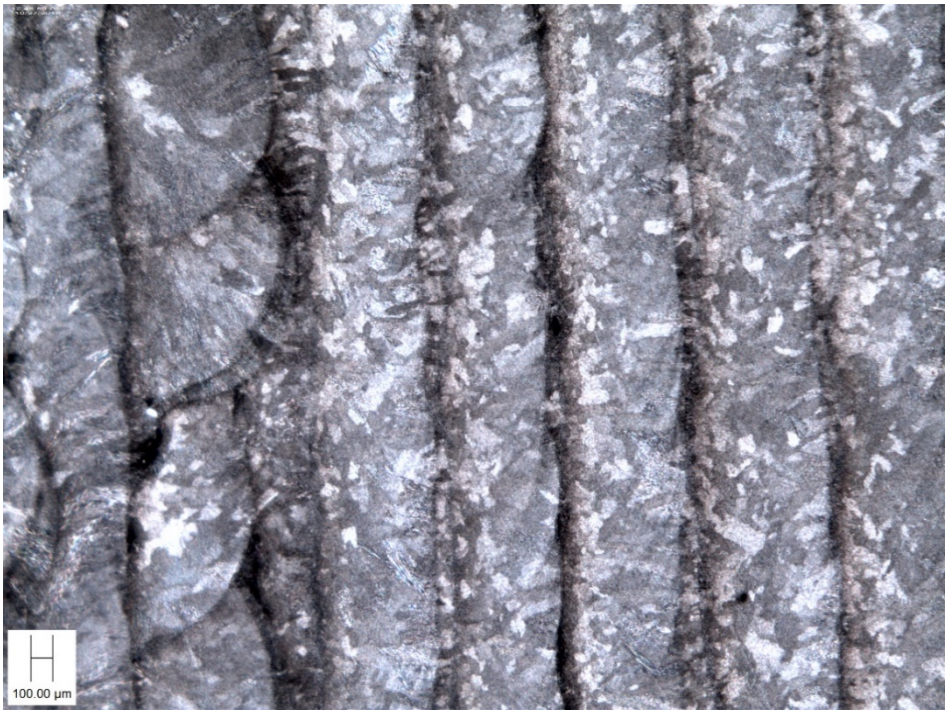

Wrought SS316L @ 32X

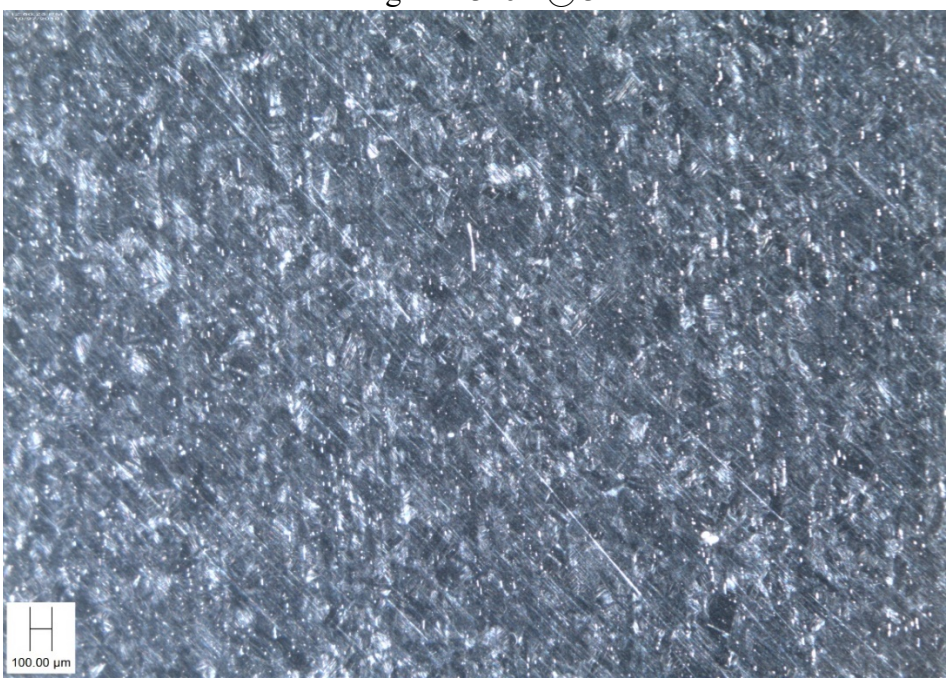

DED SS316L @ 32X